From theory to observational constraints in nonlocal gravity

Dirian, Yves

UNIVERSITÉ DE GENÈVE
Département de physique théorique

FACULTÉ DES SCIENCES
Professeur M. MAGGIORE

From Theory to Observational Constraints in Nonlocal Gravity

THÈSE

présentée à la Faculté des sciences de l'Université de Genève
pour obtenir le grade de Docteur ès sciences, mention physique

par

Yves DIRIAN

de

Blaesheim (France)

Thèse N° 5247

GENÈVE

Atelier d'impression Repromail

2018

UNIVERSITÉ DE GENÈVE
FACULTÉ DES SCIENCES

DOCTORAT ÈS SCIENCES, MENTION PHYSIQUE

Thèse de Monsieur Yves DIRIAN

intitulée :

«From Theory to Observational Constraints in Nonlocal Gravity»

La Faculté des sciences, sur le préavis de Monsieur M. MAGGIORE, professeur ordinaire et directeur de thèse (Département de physique théorique), Monsieur M. KUNZ, professeur associé (Département de physique théorique), Monsieur C. DEFFAYET, professeur (Institut d'astrophysique de Paris et Institut des Hautes Etudes Scientifiques, Paris, France), Madame V. PETTORINO, docteure (Département d'astrophysique, Institut de recherche sur les lois fondamentales de l'Univers, Commissariat à l'Énergie atomique et aux Énergies alternatives (CEA) Saclay, Gif-sur-Yvette, France), autorise l'impression de la présente thèse, sans exprimer d'opinion sur les propositions qui y sont énoncées.

Genève, le 7 août 2018

Thèse - 5247 -

Le Doyen

N.B. - La thèse doit porter la déclaration précédente et remplir les conditions énumérées dans les "Informations relatives aux thèses de doctorat à l'Université de Genève".

à Marie-Louise et René.
à Tara et Violette.

Abstract

Cette thèse aborde une problématique de recherche en physique théorique fondamentale, et plus particulièrement en cosmologie, le problème de l'énergie noire. Dans l'hypothèse où l'énergie noire résulte d'une modification de la relativité générale dans son régime infrarouge, ce travail se concentre sur l'étude de corrections non-locales qui peuvent jouer ce rôle. Ces corrections peuvent typiquement émerger d'une dynamique quantique effective mais aussi dans des théories de dimensions supérieures. En particulier, l'application de l'idée de la « degravitation » mène à deux modèles prototypes où la relativité générale est modifiée par des corrections non-locales, générant une phase d'expansion accélérée dans l'Univers tardif. Nous analysons la structure théorique et phénoménologique de ces deux modèles, avant de les contraindre à l'aide de données cosmologiques complémentaires de haute précision et de comparer leurs performances à celles du modèle standard de la cosmologie dans un cadre bayésien. Finalement, prenant ces théories comme exemples, nous discutons aussi la modification de la propagation des ondes gravitationnelles et les implications d'une telle modification pour les interféromètres de génération future.

Résumé (français)

Cette thèse s'inscrit dans le programme scientifique visant à acquérir une compréhension plus profonde de l'un des problèmes fondamentaux de la physique moderne, le problème de l'énergie noire.

À la fin du vingtième siècle, notre compréhension de la dynamique de l'Univers dans son ensemble fut marquée par une véritable révolution. Des observations de supernovae distantes de Type Ia ont révélé l'évidence d'une phase actuelle d'accéleration de l'expansion de l'Univers. L'explication la plus simple que l'on puisse fournir à ce phénomène, en accord avec les principes de la relativité générale, est l'introduction d'une constant cosmologique Λ dans les équations d'Einstein, modélisant une composante d'énergie noire dominant la densité d'énergie totale de l'Univers. Cette découverte entraîna l'ajout de Λ comme une des pièces maîtresses au modèle standard de la cosmologie contemporaine, dénoté ΛCDM. Depuis ce temps, le rafinement des développements théoriques et l'augmentation des capabilités observationnelles et numériques ont permis d'établir des constraintes de plus en plus fortes sur l'espace des paramètres de ce modèle. Dorénavant, ces contraintes se situent au niveau du pourcent de précision sur de nombreux paramètres, ceux qui élève la cosmologie d'aujourd'hui au rang d'une science de précision, et démontrent en particulier la consistence du modèle ΛCDM étant donné de nombreuses observations complémentaires.

Cependant, le succès de l'introduction d'une constante cosmologique dans les équations d'Einstein pour expliquer la récente accélération cosmique est terni par des objections théoriques quant à sa nature, son origine et sa domination récente. De surcroît, on constate que certaines observations, en nombre cependant restreint, se trouvent être en désaccord étant donné le modèle ΛCDM, bien que les erreurs systématiques doivent encore être prouvées se trouver sous contrôle. La résolution de ces problèmes est l'une des quêtes les plus importantes de la physique fondamentale contemporaine. En effet, de nombreux modèles alternatifs à la constante cosmologique ont été proposé pour expliquer l'accélération cosmique récente. Ces modèles sont, par exemple, basés sur l'addition de nouveaux degrés de liberté associés à l'énergie noire tel qu'un champ scalaire ou métrique, ou une composante plus exotique tel qu'un gaz de Chaplygin. De plus, des explications de l'énergie noire ont aussi été avancées sous la forme de théorie modifiant la relativité générale, en particulier dans son regime infrarouge, motivées par un nombre de dimensions supérieures ou par le fait que les degrés de liberté gravitationels pouvaient avoir une masse. Jusqu'à maintenant, aucune de ces alternatives ne s'est montrée convaincante quant à son pouvoir de prédire de manière consistante l'ensemble étendu des observations cosmologiques actuelles en résolvant également les problèmes théoriques associés à la constante cosmologique.

Cette thèse fait partie intégrante de ce programme de recherche. Ici, nous faisons l'hypothèse que la théorie de la gravité d'Einstein est possiblement modifiée dans son regime infrarouge par des effets non-perturbatifs possiblement associés à une dynamique quantique effective. Pour ce faire, nous supposons que des opérateurs non-locaux sont susceptibles d'être générés dans l'action effective associée à la théorie de la relativité générale. En effet, ce type de corrections sont typiquement générées dans les théories de bosons de jauge, par les fluctuations quantiques du vide de champs légers ou sans masse auxquels ces bosons couplent. De plus, des opérateurs non-locaux potentiellement pertinents dans l'infrarouge peuvent se voir être générés dans l'anomalie conforme, dans les théories de dimensions supérieures ou également par les fluctuations quantiques du vide du champ de gravité lui-même, comme récemment suggéré par des simulations

de gravité quantique sur réseau. Les effets infrarouges induits par des corrections quantiques en gravité sont encore très largement mal compris et pour cette raison nous adoptons une approche plutôt phénoménologique, inspirée par l'application de l'idée de la « degravitation » à la théorie de la gravité massive linéarisée sur l'espace de Minkowski. Notre étude porte sur les aspects théoriques, phénoménologiques et observationnels de deux théories de gravité modifiée développées dans ce cadre.

Après un bref essai d'introduction historique sur la construction du modèle standard de la cosmologie et un résumé des problèmes associés à la constante cosmologique dans le Chapitre 1, nous illustrons comment différents effets peuvent produire des opérateurs non-locaux dans le cadre de la théorie effective des champs dans le Chapitre 2. Nous présentons également plusieurs résultats d'études complémentaires à la nôtre, modifiant la théorie de la relativité générale dans l'infrarouge. Dans le Chapitre 3, nous analysons la structure théorique de deux modèles de gravité non-locale obtenus à travers l'application de l'idée de la degravitation à la théorie de la gravité massive linéarisée sur l'espace de Minkowski. Nous verrons que, sur espace-temps plat, ces deux modèles exposent une structure de propagateur contenant un pôle associé au champ de spin deux non massif de la gravité, alors qu'il renferme également un pôle associé à un champ scalaire sans masse et un autre associé à un champ scalaire de masse m inconnue, ayant un signe opposé dans son terme cinétique. Plus loin, on montre de différentes façons que la structure non-locale de ces théories implique qu'aucun degré de liberté physique n'est associé à ces deux derniers pôles et que, de ce fait, ces théories sont fiables d'un point de vue effectif. Nous verrons également que l'instabilité associée au pôle massif se développe génériquement à des longueurs d'ondes plus grandes que la longueur de « Compton » du champ correspondant, qui doit être de l'ordre de la taille de l'Univers observable sur le plan phénoménologique, c'est-à-dire pour générer une accélération cosmique permetant d'expliquer les observations. À ces échelles, ce n'est plus l'espace temps de Minkowski que l'on doit considérer comme métrique de fond, mais plutôt la solution cosmologique de Friedmann-Lemaître-Robertson-Walker. Pour un modèle en particulier, on démontre que toutes les perturbations linéaires sur ce fond sont globalement stables, à cause de la violente expansion du fond induite par la nature « fantôme » de l'énergie noire effective décrite par le modèle, entraînant une domination de la friction de Hubble sur ses perturbations cosmologiques.

La phénoménologie cosmologique des deux théories non-locales est investiguée en détails dans le Chapitre 4, où on montre que les deux modèles décrivent une énergie noire effective dynamique de caractère « fantôme », i.e. d'équation d'état inférieure à moins un, menant à une phase accélérée d'expansion dans l'Univers tardif. Les perturbations linéaires autour de ce fond cosmologique sont également étudiées dans le secteur scalaire et tensoriel. On montre en particulier que les ondes gravitationelles sont stables et se propagent à la vitesse de la lumière, en accord avec l'observation récente des ondes gravitationnelles associées à la fusion d'étoiles à neutrons binaires et de la contrepartie électromagnétique associée, mais que leur propagation est tout de même altérée par une modification du terme de friction dans l'équation la gouvernant. De plus, nous montrons que les perturbations scalaires sont également stables et nous quantifions leurs déviations par rapport à ΛCDM à l'aide de fonctions indicatrices utiles dans ce cadre. À paramètres cosmologiques fixés, nous verrons que les deux modèles décrivent une croissance de structures plus forte comparée à celle décrite par ΛCDM et également un effet de lentille gravitationnelle plus proéminent. Nous étudions également les perturbations des énergies noires effectives dans les deux modèles et trouvons que les composantes d'énergie noire effectives sont assez « lisses ». Les déviations de ΛCDM étant seulement de l'ordre de quelques à plusieurs pourcents dans les deux modèles, leur phénoménologie apparaît par conséquent pertinente a priori.

Dans le Chapitre 5, nous implémentons ces deux modèles dans une version modifiée du code d'évolution cosmologique linéaire CLASS et exerçons des contraintes observationelles sur ceux-ci. Nous verrons que les deux modèles de gravité non-locale mènent essentiellement à l'inférence des mêmes paramètres cosmologiques de base que ΛCDM, étant donné des mesures de haute résolution du fond diffus cosmique, des supernovae de Type Ia et des oscillations acoustiques des baryons, à l'exception d'une préférence pour une plus grande valeur de la constante de Hubble, par conséquent plus en accord avec les mesures locales. Nous verrons également que le modèle dont l'énergie noire effective est la plus fantôme expose, de manière assez générique, une tension entre les mesures du fond diffus cosmique et des supernovae de Type Ia, le défavorisant par rapport à standard ΛCDM sur des bases de statistique bayesienne que nous exposons en détails. Nous montrons alors que cette tension est résolue par la considération d'une masse absolue des neutrinos variable dans l'ajustement des paramètres, résultant en la prédiction d'une masse absolue non-nulle à deux deviations standards, étant donné le modèle non-local en question. Nous étudions également les contraintes observationnelles fournies par les mesures de croissance de structures à travers les distortions induites dans l'espace des décalages vers le rouge.

Le Chapitre 6 est consacré à l'étude de la modification du terme de friction dans l'équation gouvernant la propagation des ondes gravitationnelles linéaires sur un fond cosmologique. Nous montrons qu'une telle modification altère la notion de distance de luminosité de la source des ondes gravitationelles, et par conséquent la relation distance-décalage vers le rouge obtenue à travers les sirènes standards que celles-ci consistuent. Nous introduisons une paramétrisation utile modélisant une telle déviation et contraignons ces paramètres avec des mesures du fond diffus cosmologique, des supernovae de Type Ia, d'oscillations acoustiques des baryons et de la detection de (mille) sirènes standards étant donné la sensibilité des interféromètres gravitationnels de prochaine génération. Nous trouvons que les contraintes sur ce paramètre sont plus importantes que celles sur la valeur de l'équation d'état de l'énergie noire aujourd'hui d'un facteur quatre, et, par conséquent, que les perspectives de detection de déviations de la relativité générale sont plus optimistes qu'initialement prévues. Nous illustrons également la capacité potentielle de tels interféromères à distinguer un des modèles de gravité non-locale prédemment cité par rapport à ΛCDM, en estimant le nombres de sirènes standards (avec leur contrepartie électromagnétique) qu'ils devraient detecter.

Le Chapitre 7 présente nos conclusions.

Remerciements

Je tiens tout d'abord à remercier mon superviseur de thèse, le professeur Michele Maggiore, pour m'avoir offert l'opportunité de travailler au sein de son groupe pendant ces cinq dernières années, sur une thématique de recherche des plus passionnantes – la tête dans les étoiles, jusqu'aux abysses des plus sombres de notre Univers. Je le remercie pour m'avoir formé au métier de chercheur et d'enseignant, toujours avec un enthousiasme, une bonne humeur, mais aussi une rigueur heureusement contagieuse, en me faisant découvrir les nombreux aspects associés à ces professions et en m'y initiant patiemment. Merci pour avoir eu confiance en moi, pour m'avoir soutenu, pour m'avoir accordé l'autonomie de laquelle j'ai bénéficier dans mes travaux et pour m'avoir fait vivre des expériences de travail extraordinaires, comme notre présentation partagée à Barcelone, l'opportunité d'une visite au Perimeter Institute au Canada ou plusieurs périodes d'échange constructives à l'Université de Heidelberg, dont je salue l'hospitalité au passage.

Je remercie évidemment aussi les membres de ce groupe qui m'ont initialement accueilli, Stefano Foffa et Ermis Mitsou, pour leur sympathie, leur écoute, leur soutien continuel et pour m'avoir fait partager leur expérience et leurs pensées, me permettant ainsi de forger solidement mon charactère scientifique. Dans ces mêmes lignes, je remercie également les doctorants et les chercheurs avec qui j'ai eu le plaisir de collaborer sur des thématiques de recherche diverses, dans des conditions toujours très agréables, Luca Amendola, Alex Barreira, Enis Belgacem, Santiago Casas, David Daverio, Nima Khosravi, Elisabetta Majerotto, Henrik Nersisyan, Valeria Pettorino. En particulier, un grand merci à Martin Kunz, pour sa complicité, sa (son extrême) sympathie et les nombreuses conversations échangées (parfois octroyées) me permettant de mieux comprendre la cosmologie moderne, et également la statistique bayesienne pour laquelle il a su me transmettre une part de sa sensibilité.

Merci également à l'entièreté du groupe de cosmologie de l'Université de Genève pour le cadre de travail stimulant et agréable qu'il offre au quotidien, que ce soit durant les journal-clubs ou les séminaires du vendredi, ou tout simplement durant le traditionnel « lunch » ou la relaxante pose café associée. Merci également aux secrétaires Francine Gennai-Nicole et Cécile Jaggi-Chevalley pour transformer l'enfer administratif en simple formalité, pour leurs bons tuyaux et leur soutien constamment souriant. Merci également aux techniciens en informatique, Andréas Malaspinas, Jacques Rougemont et Yann Sagon, pour leur précieux support, incontournable dans notre lutte continuelle contre les machines – même quand certains d'eux se trouvent sur une plage en Grèce ! Merci à tous les collaborateurs de l'Uni avec qui j'ai pu échanger au quotidien durant ces douces années passées à Genève. Je pense en particulier à Julian Adamek, Jonatan Bohr Brask, Margherita Boselli, Davide Costanzo, Simone Dresti, Ruth Durrer, Pierre Fleury, Gabriele Franciolini, Jacopo Fumagalli, Iaroslav Gaponenko, Pietro Guarato, Leïla Haegel, Fabien Lacasa, Diego Mauro, David Medina, Hugo Meley, Francesco Montanari, Mariele Motta, Jorge Norena, Subodh Patil, Marco Tulio, Davide Racco, Elise Schubert, Iggy Sawicki, Elena Sellentin, Vittorio Tansella, Manuel Vielma, Renan Villarreal, Peter Wittwer, et bien d'autres qui se reconnaîtront.

Naturellement, je dédie un paragraphe de remerciements au 205, aux deux acolytes (presque) parfaits, heureusement parachutés dans ma vie par le destin, mes exemples, mes deux mamamouchis, David Daverio et Ermis Mitsou. Merci pour avoir partagé votre passion débordante qui vous fait travailler jusque tard dans la nuit et courir au bureau tous les matins. Merci pour cette ambiance sonore, parfois musicale. Merci pour nos rires. Merci pour nos engueulades. Merci pour les contre-lunches pizza-South Park. Merci pour les innombrables café-clopes

(double-clopes pour David, parfois sans clope pour Ermis) passés à refaire le monde, l'Univers. Vous savez quoi ? Je fume des roulées pour rendre ces moments volontairement interminables, pour en profiter un maximum. Force et robustness !

Je tiens aussi à remercier les personnes avec qui, au delà du cadre académique, j'ai pu trouver une véritable osmose durant mon séjour de sept ans à Genève. Ceux qui m'ont animé, ceux avec qui j'ai eu la chance et le plaisir de partager ce bout de chemin incroyable, et que j'espère pouvoir toujours recroiser dans un futur aussi proche que lointain. Amaury, Vincent, Flavien, Rémi, Julien, Sergio, Szabolcs. Et ceux qui m'ont donné les clefs. Emm, Gab, Léo, Phil, Tiag, Titouan, Tim et Wally-G. Une pensée particulière à Giulia pour tous les moments de complicité qu'on a pu passer ensemble. Sans vous tous, il est clair que cette aventure n'aurait pas été aussi belle.

Aussi, je remercie bien sûr ceux qui ont toujours été là. Les copains du Blaedi qui se reconnaîtront, merci pour votre soutien certain mais lointain. Merci à la bande de l'UFR de Strasbourg, en particulier à mon bon Jéjé, avec qui ma passion pour la physique théorique est née et n'a toujours fait que grandir. En plus, merci à Anna et Jean-Yves, à Soline et Gaston, à ma marraine Cathy et mon oncle Constant, et à Annette pour avoir fait le voyage jusqu'à ma défense de thèse. Un merci particulier à Thibault (ou Igooor) pour les mêmes raisons, mais aussi pour avoir partagé cette aventure à Ge pendant la première année. Maintenant on remet ça à Zu ! Merci aussi à mon petit Shannon pour m'avoir soutenu et supporté durant mon intense geekerie, et également pour avoir illuminé et enjaillé ma coloc par sa présence et ses salmigondis en tout genre !

Finalement, je remercie du fond du coeur mes parents qui m'ont toujours encouragé et poussé à accomplir mes ambitions, mes rêves. Merci pour leur soutien, pour leur confiance et pour leur amour, c'est d'abord ce qui alimente ma force et mon courage.

Jury de thèse

— Professeur Michele Maggiore, Université de Genève, Genève, Suisse (directeur de thèse).

— Professeur Martin Kunz, Université de Genève, Genève, Suisse.

— Professeur Cédric Deffayet, Institut d'Astrophysique de Paris (IAP) et Institut des Hautes Études scientifiques (IHÉS), Paris, France.

— Docteur Valeria Pettorino, Commissariat à l'Énergie atomique et aux Énergies alternatives (CEA), Saclay, France.

Je tiens à remercier les membres du jury pour avoir accepté d'examiner le présent rapport de thèse, ainsi qu'avoir évalué la soutenance associée.

Contents

Introduction

Contemporary cosmology has undergone fast developments over the past century. These advances were built on fundamental theoretical insights originating from Einstein's theory of General Relativity, that has now been extensively tested on solar system and terrestrial scales. Until now, no significant deviations from General Relativity have been detected in such regimes. On cosmological, far-infrared, scales the theory provides the bedrock of the standard cosmological model whose structure has undergone several mutations over the years, resulting from the synergy between theoretical and observational efforts. This has gradually promoted cosmology to a precision science, where theories can be rigorously tested against increasingly accurate and complementary observations. In particular, observations of the motion of galaxies led to the introduction of a cold dark matter component into the standard model, whose fundamental nature is still not understood. In addition, measurements of distant Type Ia supernovae light-curves provide significant evidence for an accelerated expansion of the Universe at late time, suggesting the presence of a dark energy component dominating the present cosmic energy density. In nowadays standard cosmological model, the dark energy is modelled in the simplest way following general relativistic principles, that is, by the introduction of a cosmological constant Λ into the equations of General Relativity. This provides an essential building block of the standard ΛCDM model, which has been shown to be able to consistently describe a handful of high-resolution complementary cosmological observations.

Nevertheless, such a consideration raises fundamental theoretical questions about the nature, origin and late time domination of the dark energy associated to the cosmological constant, as well as observational puzzles that may however still be subject to unresolved systematics. At the same time, Λ only affects the behavior of General Relativity at large observable scales, so that its associated weaknesses can be translated into our lack of understanding of the infrared dynamics of General Relativity itself. In this thesis, we attempt to provide relevant information for a better understanding of the solution to the fundamental problem of dark energy. We make the hypothesis that the theory of General Relativity is susceptible to be modified in its infrared regime by intrinsic processes becoming relevant at these scales. For accessing this, we focus on modellisations based on a particular class of modified gravity theories, where infrared modifications are realised through the presence of nonlocal terms into Einstein's equations or into the Einstein-Hilbert action.

Chapter 1 starts by briefly outlining the major theoretical and observational advances made in the past, that allowed cosmologists to shape the current standard ΛCDM model. We then describe the current state-of-the-art, summarise its main current observational inconsistencies and emphasize the importance of future cosmological surveys for accessing a better understanding about the physics of the dark energy. We then provide a description of the theoretical objections made against the cosmological constant and provide examples of alternative descriptions of dark energy proposed for resolving these issues.

Chapter 2 illustrates how nonlocal operators are typically generated into an effective field theoretical framework and how these can lead to infrared corrections to gravity. At the classical level, we will see that such corrections arise from explicitly integrating-out interacting fields in generic theories, while at the quantum level, they are typically generated in the gravitational quantum effective action through vacuum polarisation induced by the presence of light or massless fields, through the conformal anomaly or quantum fluctuations of the gravitational field itself, as recently suggested by lattice quantum gravity computations. As will also be discussed, nonlocal corrections can also come from extra-dimensions, and generate a "degravitation" mechanism that makes the interaction between the vacuum and gravity weaker at large scales, therefore providing a possible solution to the "naturalness problem" of Λ.

Chapter 3 presents how the application of the degravitation idea leads to the development of two distinct kinds of modified gravity models, the so-called RT and RR nonlocal gravity models. We also describe peculiarities typically associated to the presence of nonlocal terms into a theory and meticulously analyse the theoretical structure of the two nonlocal models presented.

Chapter 4 reviews the associated phenomenology of both nonlocal models, showing in particular that they lead to interesting self-accelerating solutions characterised by phantom effective dark energies and stable linear perturbations within the cosmological context.

Observational constraints and Bayesian model comparison between the nonlocal models and standard ΛCDM are worked out in Chapter 5. For performing this, we consider data from Cosmic Microwave Background measurements, as well as from observations of distant Type Ia supernovae, Baryon Acoustic Oscillations, Redshift-Space-Distortions and local measurements of the present Hubble constant H_0. In a first part, we present the results obtained in assuming the standard six-dimensional cosmological parametrisation, similar to that adopted within the framework of the standard ΛCDM model. In a second part, we consider an extension of this parametrisation within the framework of the RR model, consisting in allowing the absolute mass of three degenerated massive neutrino species to vary.

In Chapter 6, inspired by the fact that the studied nonlocal models describe a modified propagation for the gravitational waves compared to ΛCDM, we forecast the constraining power of next generation gravitational waves interferometers. These experiments will measure the gravitational waves emitted from binary inspirals with a high precision. We assume that the redshifts of the binaries will be determined accurately, for instance from the detection of an associated electromagnetic counterpart, as for the binary neutron star merger recently detected, or by statistical methods. Together with a measurement of the amplitude of the gravitational waves, this knowledge allows one to build a redshift-distant relation, making these binary inspirals "standard sirens". In turn, this relation provides a useful probe of the expansion history of the Universe and is therefore relevant for constraining deviations from a cosmological constant. Moreover, we will see that this relation is also very useful for constraining modifications of the way gravitational waves propagate as compared for instance to those described by ΛCDM. We parametrise this relation and show that the associated parameter can be measured with a higher accuracy than the ones usually used in the literature. The expectations for testing General Relativity using gravitational waves interferometers are therefore more optimistic than initially expected. We then illustrate such constrains in the framework of the RR nonlocal gravity model, and evaluate the number of sources needed to be detected for distinguishing it from ΛCDM, given the forecast sensitivity of next generation gravitational waves experiments.

Our conclusions are drawn in Chapter 7.

Publication List

This thesis is based on the following publications, developing theoretical and observational aspects of two specific nonlocally modified gravity models:

— Dirian Y., Foffa, S., Khosravi, N., Kunz, M., Maggiore, M., *Cosmological perturbations and structure formation in nonlocal infrared modifications of general relativity*, JCAP 06 033 (2014), arXiv:1403.6068,

— Dirian Y. and Mitsou E., *Stability analysis and future singularity of the $m^2R\Box^{-2}R$ model of non-local gravity*, JCAP 10 065 (2014), arXiv:1408.5058,

— Dirian Y., Foffa, S., Kunz, M., Maggiore M., Pettorino, V.", *Non-local gravity and comparison with observational datasets*, JCAP 04 044 (2015), arXiv:1411.7692,

— Dirian Y., Foffa S., Kunz M., Maggiore M., Pettorino V.", *Non-local gravity and comparison with observational datasets. II. Updated results and Bayesian model comparison with ΛCDM*, JCAP 05 068 (2016), arXiv:1602.03558,

— Dirian Y., *Changing the Bayesian prior: Absolute neutrino mass constraints in nonlocal gravity*, Phys. Rev. D96, 083513 (2017), arxiv:1704.04075,

— Belgacem E., Dirian Y., Foffa, S., Maggiore M., *Nonlocal gravity. Conceptual aspects and cosmological predictions*, JCAP 03 002 (2018), arXiv:1712.07066,

and to the study of gravitational waves propagation in generic classes of modified gravity models described phenomenologically, including a specific nonlocal model of modified gravity as an example:

— Belgacem E., Dirian Y., Foffa, S., Maggiore, M., *The gravitational-wave luminosity distance in modified gravity theories*, Phys. Rev. D97, 104066 (2018), arXiv: 1712.08108,

— Belgacem E., Dirian, Y., Foffa, S., Maggiore, M., *Modified gravitational-wave propagation and standard sirens*, submitted to Phys. Rev. D (2018), arXiv:1805.08731.

The author also contributed to a program aiming to compare a handful of linear Einstein-Boltzmann codes simulating the cosmological evolution of a variety of modified gravity models:

— Bellini E. *et al.*, *Comparison of Einstein-Boltzmann solvers for testing general relativity*, Phys. Rev. D97, 023520 (2018), arXiv:1709.09135,

and contributed to the development of a new computational scheme in the framework of numerical relativity, most suitable for cosmological simulations:

— Daverio D., Dirian Y., Mitsou E., *A numerical relativity scheme for cosmological simulations*, Class. Quant. Grav. 34, 237001 (2017), arXiv:1611.03437.

Chapter 1

A Brief History of the Universe

1.1 The Geometric Properties of the Universe

At the beginning of the twentieth century, A. Einstein revolutionised the concepts of absolute space and time in merging them into a single entity, *spacetime*. In 1905, based on works of H. Lorentz, H. Minkowski, H. Poincaré and others, he established the principles of Special Relativity (Einstein, 1905), whose group representation theory was later used to provide the field algebra of the Standard Model of particle physics (SM). The SM governs the classical and quantum-relativistic dynamics of all the known visible matter that we observe in the present Universe. At the same time, the theory expresses the equivalence between mass and energy through the now world famous formula, $E = mc^2$. Ten years later, his desire to incorporate gravity into the same framework led him to postulate his equivalence principle. It states that, in the presence of an arbitrary gravitational field, no local non-gravitational experiment can distinguish a freely falling non-rotating system, from a system moving uniformly in the absence of gravitational field [see e.g. (Straumann, 1984) for a historical discussion]. Einstein's equivalence principle implies the equivalence between inertial and gravitational masses and essentially formulates itself mathematically as the principle of General Covariance of physical laws. These principles imply that spacetime is a dynamical entity sensitive to any form of energy and provides the foundations of the theory of General Relativity (GR) governing such dynamics (Einstein, 1915, 1916). The corresponding equations are given by,

$$R_{\mu\nu} - \frac{1}{2} g_{\mu\nu} R = \frac{8\pi G}{c^4} T_{\mu\nu} \,.$$

In his works, Einstein supplied the theory with three explicit predictions: the gravitational redshift, the bending of light and the precession of Mercurys' perihelion, which were all shown to be consistent with observations. Other predictions have also been tested since then [see for instance (Will, 2014) for a review] and, until now, none of them has been able to falsify the theory. Most notably, a hundred years after the predictions, the direct detections of gravitational waves (GWs) emitted from binary black hole mergers (Abbott et al., 2016c) [see also (Abbott et al., 2017a) and references therein] and a binary neutron star inspiral (Abbott et al., 2017h), have provided a further remarkable confirmation of GR, in particular confirming that GWs propagate at the speed of light.

All the aforementioned predictions allow to constrain GR on small scales. In 1917, Einstein and his contemporary W. de Sitter got interested in describing the Universe on larger scales, in its most coarse grained and global structure. They adopted the class of solutions in agreement with the cosmological principle, i.e. with homogeneous and isotropic spatial hypersurfaces.

Einstein, motivated by the fact that the relative velocities of stars where observed to be much smaller than the velocity of light, introduced a uniform matter component described by a pressureless perfect fluid and was convinced that the Universe was spatially static. Such an hypothesis forced him to introduce a "universal constant", that he called λ (denoted Λ in modern language), playing the role of a fudge factor into the equations of GR, so as to counteract the effects of the uniform matter distribution on space (Einstein, 1917). Such a fact did not change the yet confirmed predictions of the theory on smaller scale, as λ only modifies its dynamics on large scale, in the far *infrared*. Five years later, A. Friedmann established the so-called Friedmann equations (Friedmann, 1922, 1924) from which derives cosmological solutions where space is expanding. Not much attention was given to his class of metric solutions until 1929, when observations of E. Hubble unveiled the proportionality relation between the line-of-sight velocity component and the radial distances of galaxies (Hubble, 1929). This relation, known as the Hubble law, defines the Hubble constant characterising the expansion of the Universe. In fact, this relation had already been derived theoretically and inferred observationally by G. Lemaître in 1927, who was the first giving a physical meaning to Friedmann's solution (Lemaître, 1927). Works of H. Robertson and A. Walker also provided significant contributions in understanding this solution and, in particular, showed that it is implied by the cosmological principle (Robertson, 1935; Walker, 1937). This solution is today referred to as the Friedmann-Lemaître-Robertson-Walker (FLRW) metric. Einstein was then forced to admit the dynamical nature of the spatial component of the Universe and considered it as an evidence for setting $\lambda = 0$ in his equations. Later, alternative cosmological solutions were also put forward [see e.g. (Zwicky, 1929; Milne, 1935; Bondi and Gold, 1948; Hoyle, 1948)]. These were discredited in 1964 when, based on predictions of G. Gamow, R. Alpher and R. Herman (Gamow, 1948; Alpher and Herman, 1948), the serendipitous discovery of the cosmic microwave background (CMB) by A. Penzias and R. Wilson suggested that the FLRW universe, starting in a hot "big bang", provides the best explanation consistent with observations (Penzias and Wilson, 1965). Such an understanding of the geometric properties of our Universe has marked the foundation of modern cosmology and, in particular, provided the bedrock for the construction of the current standard cosmological model.

1.2 Towards the Modern Standard Model of Cosmology

Nowadays, the standard model of cosmology is composed by four major pillars: the underlying theory of gravity, the assumed symmetries of the Universe on large scales, its global structure (topology) and its matter constituents together with their non-gravitational and gravitational interactions [see e.g. (Uzan, 2009)]. As outlined in the previous section, the first three of them are currently accepted to be provided by Einstein's theory of GR together with solutions which spatially average to the FLRW type.

1.2.1 The Primordial Universe and the Inflationary Paradigm

Regarding the matter components, its visible part is made of particles described by the SM. At early times, the Universe was in a dense, highly energetic radiation dominated phase (RD) composed by a mixture of elementary particles in thermal equilibrium. As the Universe expanded and cooled down, its temperature dropped below a series of relevant scales inducing several phase transitions. Similarly, the cooling of the Universe led to a cascade of other phenomena as for instance at $T \sim 1\,\mathrm{MeV} \sim 10^{10}\,\mathrm{K}$, when the first light elements such as helium, deuterium or lithium nucliei were formed during the big bang nucleosynthesis (Alpher

et al., 1948), as well as when the relic neutrinos decoupled from the primordial plasma and started propagating freely until today, producing the cosmic neutrino background (CνB) [see e.g. (Lesgourgues et al., 2013)]. The Universe was then composed by a plasma of electrons, protons (or charged nuclei) and photons interacting through Thomson scattering whose typical timescale was much smaller than the typical time associated to the expansion, preventing atomic structures to form. Once the Universe get even colder, these timescales became comparable favoring atomic formation and protons (helium nuclei) and electrons could combine into neutral atoms of hydrogen (helium) making the photons decouple from them in a process known as (helium) *recombination*. The Universe then became effectively transparent to photons, which were allowed to propagate freely throughout the Universe until today. This relic radiation provides a snapshot of the last scattering surface at the present time, making up the CMB that Penzias and Wilson discovered in the sky at $T_{\rm CMB} \simeq 3\,{\rm K}$. Other ground-based experiments were realised in the following years [see e.g. (Weinberg, 1972), p. 512 for a list] and all of them established the same conclusions about the consistency of the hot big bang model.

However, the hot big bang paradigm suffered for not addressing several fundamental questions which arose at the time. For instance, it did not provide a mechanism describing why the Universe is so homogeneous and isotropic on large scales.
Indeed, if one considers that the expansion of the Universe was only composed by a dominating radiation component at early times, the comoving radius of a causal patch (the particle horizon, determined by light rays propagating outwards of a given location in a given time interval) is at most bounded by the comoving Hubble radius defining the size of the observable Universe at the final time of the interval. Therefore, in that case, the Hubble horizon provides a maximal region of causal contact within which the homogeneity of a given process taking place on larger scales (such as recombination) can be established. However, as the Universe continues to expand, the Hubble radius increases and will cover regions that were not causally connected at the time when the aforementioned process happened. Therefore, there is no reason why the early times patch-wise homogeneity should result in a (global) large scale homogeneity at late times. This is known as the *horizon problem*.

A solution to that problem is to invoke a pre-recombination period of accelerated expansion. In such a way, the comoving radius of causally connected regions can become infinitely large after a finite amount of time whereas the comoving Hubble radius shrinks down. Once the Hubble horizon then increases again in a subsequent deceleration phase, fluctuations entering the Hubble horizon were causally connected in the past, and large scale homogeneity can be explained. Such a process has been proposed to be realised in an inflationary phase of the Universe (Guth, 1981; Linde, 1982; Starobinsky, 1982; Bardeen et al., 1983), taking place right below the Planck scale at $T \sim 10^{16}\,{\rm GeV}$.

The inflationary paradigm also solves another problem of the hot big bang model: the fact that the spatial curvature of the Universe is so close to vanish at present time. This is essentially a fine-tuning problem which consists in explaining why the total energy density fraction of matter (i.e. non-curvature components) was close to one by tens of orders of magnitude in the early Universe. The problem is that the flatness condition is an unstable solution in a decelerating expansion phase. In an accelerating phase of expansion, the situation is reversed and the flatness condition of the Universe becomes an attractor [see e.g. (Lesgourgues, 2006; Baumann, 2011)]. Moreover, inflation also solves the primordial monopole problem and predicts the origin of the primordial density fluctuations which grew into the cosmic web we observe today in the sky. In this paradigm, it is the quantum fluctuations associated with the internal degree(s)-of-freedom of the theory, typically a scalar field called the inflaton, that gives raise to a nearly scale invariant, gaussian spectrum for adiabatic primordial density fluctuations.

Other theories offered an alternative to inflation, as topological defects such as cosmic strings, textures, global monopoles or domain walls [see e.g. (Liddle and Lyth, 1993) and references therein].

Precision observations of the *COBE* satellite revealed that the CMB has a near-ideal thermal black body spectrum (Mather et al., 1994). Furthermore, *COBE* and *RELIKT-1* CMB missions observed that its temperature distribution respects nearly perfect isotropy over the whole sky: it possesses a relative departure from it at the level of 10^{-5} (Smoot et al., 1992; Wright et al., 1992; Klypin et al., 1992). It was found that the shape of the primordial power spectrum of density fluctuations underlying this nearly isotropic temperature distribution is compatible with the one predicted by inflationary theories.

1.2.2 Galaxy Motion and Flat Rotation Curves

Apart from the important discovery of the CMB and its anisotropies, earlier astronomers were also concerned with another puzzle, the problem of "missing mass" at galactic to galactic cluster scales underlying the existence of a *dark matter* component. Its empirical origin can be tracked back to the beginning of the twentieth century or even before [see (Bertone and Hooper, 2016) for an exhaustive historical review].

In his lectures in 1904 (Kelvin, 1904), Lord Kelvin regarded the Milky Way as a gas composed by stars under the influence of gravity and estimated an upper bound on its total stellar mass density in relating it to the observed velocities of the stars. He was eventually led to formulate the hypothesis that there may be a fraction of extinct or dark bodies invisible to us composing the galaxy. In the few decades that followed, astronomers studying the dynamics of stars in the Milky Way did take the hypothetic presence of invisible matter into account in their analysis.

Later, firmer estimations were derived by F. Zwicky during the 1930s from observations of the Coma galaxy cluster. First, in estimating the mass of the cluster from the ~ 800 galaxies which were observed to compose it, and estimating its effective radius, he was able to compute the potential energy of the cluster. Applying then the virial theorem, he could compute the velocity dispersion of the galaxy distribution. The result that he calculated was smaller than the observed velocity dispersion by an order of magnitude and he concluded that, if his result is correct, the total amount of "dark matter" within the galaxy is much greater than the amount of visible matter (Zwicky, 1933). Similar conclusions were reached by S. Smith, whose estimations led to a larger galactic mass for the Virgo cluster (Smith, 1936). Also later, Zwicky turned the situation the other way around in deriving the total mass of the Coma cluster from the observed galaxy velocity dispersion and predicted the associated the mass-to-light ratio, which featured an astonishing high value compared to that of a local star system (Zwicky, 1937). The reality of this puzzle remained unclear for several decades. Numbers of hypotheses about the systematic understanding of this apparent mass discrepancy were explored, but no solutions were found to be compelling.

In the 1970s, K. Ford and V. Rubin (Rubin and Ford, 1970), and later with N. Thonnard (Rubin et al., 1978, 1980), observed, through the Doppler shift of optical lines, the rotation curves of spiral galaxies: the orbital velocity of the stars or gas in a galaxy as a function of the radius. They noticed that they do not follow the second law of Kepler, which states that objects farther to the center have smaller rotational velocity, as for instance for the planets of our solar system. Instead, they observed that the rotation curve for galaxies flattens at a given threshold, as the radius to the galactic center is increased (see Fig. 1.1 for an illustration). Such results imply that for the galaxy to be stable, its mass profile should linearly increase as a function of the radius, so as to compensate for the constant orbital velocity. This mass excess at large

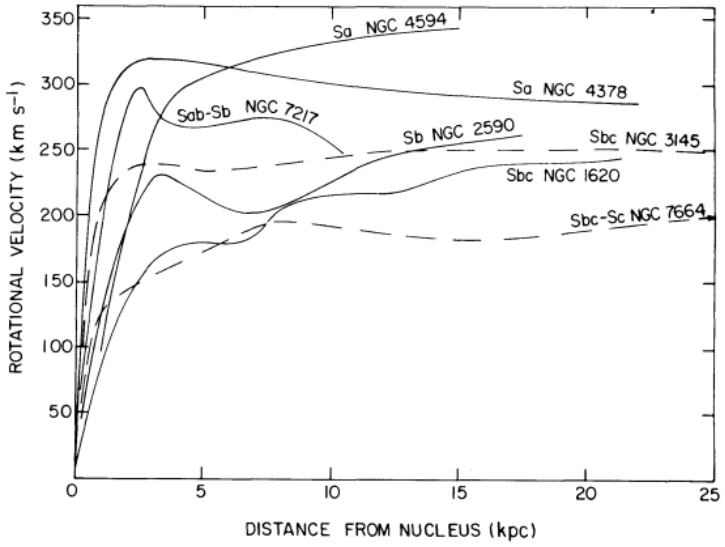

Figure 1.1 – Rotational velocities as a function of the distance from the nucleus, for seven galaxies from the New General Catalog. From (Rubin et al., 1978).

radii revealed, under the assumption of Newtonian gravity, that the total mass of the galaxy is larger than the stellar mass observed to compose it, suggesting evidence for the presence of an invisible and massive matter component. Observations have also been performed in the 21cm lines of extragalactic hydrogen allowing to probe larger radii and they reached the same conclusions [see e.g. (Whitehurst and Roberts, 1972)].

It was then shown that dark matter was likely to be distributed in extended haloes surrounding galaxies and could account for the virial mass discrepancy in clusters of galaxies mentioned hereabove (Einasto et al., 1974; Ostriker et al., 1974).

1.2.3 What is Dark Matter?

Since then, the search for the exact nature of the dark matter became a major challenge in particle and astroparticle physics and cosmology. Several hypotheses were put forward soon after the observations of flat galactic rotation curves. Although the general trend was to postulate a new form of matter to account for this effect, M. Milgrom (Milgrom, 1983) suggested instead to do so in modifying Newton's laws in a theory of Modified Newtonian Dynamics (MOND), that he formalised further with J. Beckenstein (Bekenstein and Milgrom, 1984), whose relativistic generalisation is known as the Tensor-Vector-Scalar gravity (TeVeS) (Bekenstein, 2004).

From the former perspective, the microscopic structure of dark matter and its eventual interactions with other visible particles needs to be identified. Some proposals in that direction included already known structures such as baryons or light massive neutrinos later referred to as "hot dark matter" (Bond et al., 1980; Doroshkevich et al., 1980b; Schramm and Steigman, 1981; Zeldovich et al., 1982; Bond and Szalay, 1983).

However, these simplest hypothesis were rapidly found to be unsatisfactory. Indeed, considering the critical density of the Universe today being made of purely baryonic matter was shown to be in conflict with predictions of big bang nucleosynthesis on the deuterium abundance. Such a high baryonic density would have involved a too large fraction of deuterium to be burned into helium, whereas observations of deuterium abundance rather suggested a critical density fraction of about 5 percent at the time (Reeves et al., 1973; Gott et al., 1974).

Constraints from improved estimates of the small-scale anisotropy of the CMB also served to rule out baryonic matter models (Uson and Wilkinson, 1984). Hot dark matter models were considered to be flawed as well, as they predict erroneous scenarios for the formation of galaxies and galaxy clusters in N-body numerical simulations (White et al., 1983). Other possibilities invoking new types of particles of more speculative origin have also been proposed.

Examples are provided by models of so-called warm dark matter, which exhibit a smaller free-streaming scale than hot dark matter models and are therefore in better agreement with clustering scenarios (Dodelson and Widrow, 1994). The microscopic structure of such a component was shown to be possibly realised, for instance, by gravitinos in the context of supergravity (Pagels and Primack, 1982; Bond et al., 1982) or by right-handed sterile neutrinos (Olive and Turner, 1982). Furthermore, cold dark matter (CDM) candidates have also been extensively proposed and studied. Notable possibilities are provided by new particles such as axions, motivated by SM particle physics in that they give a solution of the strong-CP problem of QCD (Weinberg, 1978; Wilczek, 1978; Ipser and Sikivie, 1983) or more generic weakly interacting massive particles (WIMPs) (Gary and Michael, 1985) such as photinos or neutralinos in the context of the minimal supersymmetric extension of the SM (Ellis et al., 1984; Jungman et al., 1996a). Mixed models of hot plus cold dark matter have also been shown to provide promising candidates for explaining the observations (Schaefer et al., 1989).

Other hypotheses not requiring the need of new particles to be invoked have also been put forward, speculating that dark matter could be made of massive astrophysical compact halo objects (MACHOs) such as primordial black holes (Carr and Hawking, 1974), in particular detectable through microlensing (Irwin et al., 1989).

From these benchmarks, it progressively became popular to admit that dark matter is more likely to be described by quite cold, weakly interacting massive particles (Peebles, 1982; Blumenthal et al., 1984; Davis et al., 1985) and led to the emergence of the inflationary CDM paradigm, also called the standard CDM model. In that picture, the Universe is described by an early phase of cosmic acceleration, where primordial density fluctuations are generated from quantum fluctuations of internal degrees of freedom. As such, inflationary scenarios predict a flat Universe with a Gaussian, scale invariant spectrum of adiabatic perturbations later inherited by a CDM component. Its distribution subsequently seeds perturbations of the baryon, electron, photon primordial plasma through gravitational interaction. These perturbations manifest themselves into temperature fluctuations in the CMB released at recombination and, at the same time, in a hierarchical growth of the presently observed structures. The combination of both CMB and large scale structure data is therefore complementary for constraining such scenarios.

1.2.4 Structure Formation with Cold Dark Matter

In the 1980s, the statistical properties of the distributions of galaxies and galaxy clusters became a valuable tool to study the formation of large-scale structures (Peebles, 1967; Doroshkevich, 1970; Peebles, 1973; Kirshner et al., 1979; Klypin and Kopylov, 1983). Technological developments at that time allowed increasingly large and precise galaxy surveys such as for example *CfA* (Tonry and Davis, 1979), *APM* (Maddox et al., 1990), *IRAS* (Strauss et al., 1990) or *SRSS* (Park et al., 1992) which, in conjuction with increasing numerical computational power, allowed to robustly constrain cosmological models in making extensive use of N-body techniques (Doroshkevich et al., 1980a; Efstathiou and Eastwood, 1981; Davis et al., 1982; Davis and Peebles, 1983; White et al., 1983; Fry and Melott, 1985).

In particular, nonlinear structure formation properties of pure CDM models were studied and compared with galaxy clustering observations on small and intermediary scales in (Davis

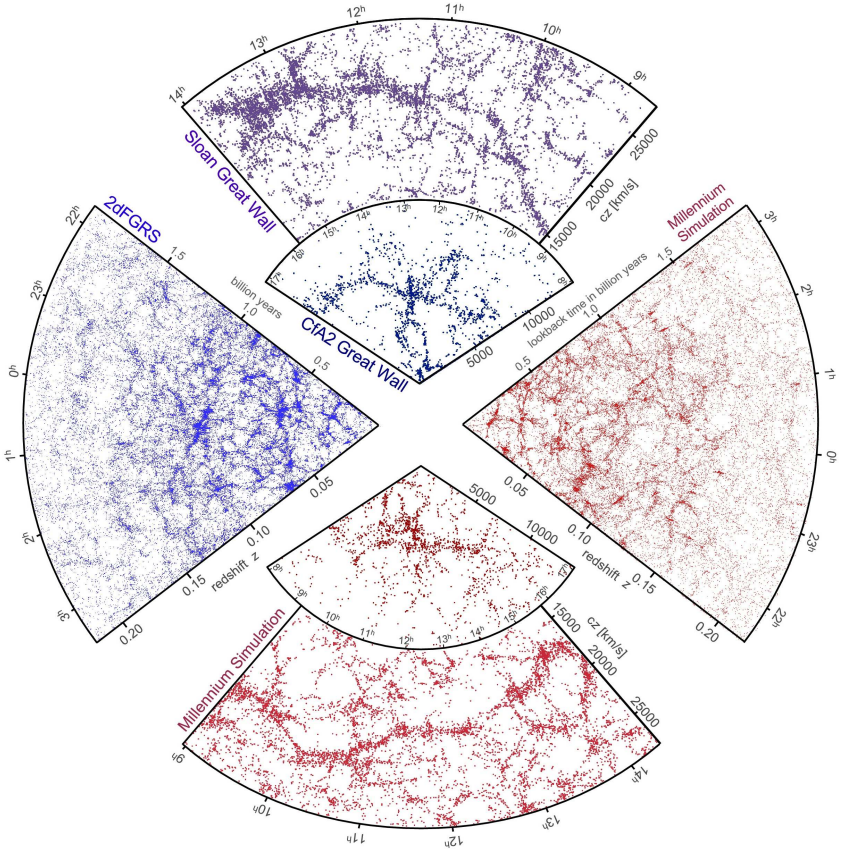

Figure 1.2 – Two-dimensional projection of the galaxy distribution obtained from the spectroscopic redshifs surveys *CfA2, 2dF* and *SDSS* (upper left half) and assigned to dark matter halos from mock catalogues constructed from the *Millenium* N-body simulation (lower right half). From (Springel et al., 2006).

et al., 1985). In the latter, the authors compared the two- and three-point correlation functions of simulated mass distributions with the ones derived from observed galaxies, as well as their peculiar velocity distribution. They found that the pure CDM model is inconsistent with the observations, unless one introduces a *bias* (Kaiser, 1984), converting the distribution of the overall simulated CDM mass fluctuations into that of the supposedly seen galaxies and bringing the standard model in agreement with the data at the scales considered [see also (White et al., 1987a) for a more extended study]. This underlines that the understanding of the large-scale galaxy bias is essential in large-scale structure formation studies and this remains a major subject of research interests today [see e.g. (Desjacques et al., 2016) for a review].

Based on the results of (Davis et al., 1985), the same authors extended their simulation on larger scales using the biasing prescription from (Bardeen et al., 1986), worked out from statistical studies of Gaussian random fields. They found that, given the same parametrisation, the model was able to resolve the distribution of structures on scales larger than $10\,\mathrm{Mpc}\,h^{-1}$, providing even stronger support for the flat CDM model, and implying that no large-scale processes other than the gravitational attraction is required for large-scale structures to form (White et al., 1987b). Further investigations in the same spirit, but involving maps of the galaxy distribution out to even larger scales, were later carried out. Observational constraints then showed strong evidence for an excess of power on these very larger scales (tens of $\mathrm{Mpc}\,h^{-1}$)

within the data, as compared to that predicted by the standard CDM model (Maddox et al., 1990; Park et al., 1992; Saunders et al., 1991; Vogeley et al., 1992; Ueda et al., 1993). It has then been argued that this excess of power could be accommodated by a flat model with a nonzero (positive) cosmological constant Λ, whose present energy density fraction represents 80 percent of the total density fraction of the Universe today (Efstathiou et al., 1990). Moreover, this would also bring the model in agreement with predictions of inflation and make it compatible with CMB observations made at the time.

The specification of a cosmological model allowing one to translate the amplitude of CMB temperature fluctuations into that of matter density fluctuations at the present epoch, the measurement of CMB anisotropies from the *COBE DMR* experiment provided a normalisation for the present matter power spectrum. As such, in combining CMB and galaxy surveys data, stronger constraints have been put on the CDM model and further inconsistencies were uncovered (Efstathiou et al., 1992). In addition, similar constraints were carried out in (Kofman et al., 1993), which suggested that the addition of the cosmological constant Λ to the CDM model is consistent with the data, for an amount of present matter density fraction of ~ 25 percent [see also (Ostriker and Steinhardt, 1995)].

Furthermore, the use of different techniques revealed other tensions in the model as well. For example, constraints from the abundance of clusters as a function of their mass (Bahcall and Cen, 1993), the overabundance of baryonic matter in rich galaxy clusters (White et al., 1993), or the prediction of bounds to the cosmological age of the Universe from determinations of the age of old globular clusters and stars (Demarque et al., 1991), were all favorable to a Universe of low matter density, including or not a cosmological constant. Open Universe models were also shown to provide a good fit to large scale structure data, once the power spectrum amplitude has been normalised to the *COBE* value (Kamionkowski and Spergel, 1994), although evading the "theoretical imperatives" of the inflationary paradigm. So-called mixed dark matter models, including both a cold and a hot dark matter components, presented attractive structure formation properties as well [see e.g. (Klypin et al., 1993; Holtzman and Primack, 1993; Schaefer and Shafi, 1993)] [1]. However, methods based on the reconstruction of the mass density field from the large scale peculiar velocity distribution have also been worked out (Bertschinger et al., 1990), and were shown to be able to constrain the amplitude of mass fluctuations in the CDM model, finding further agreement with the value provided by *COBE* (Seljak and Bertschinger, 1994). Other techniques have also been developed for testing the presence for a cosmological constant at late times, as for example gravitational lensing of quasars or distant galaxies (Turner, 1990). Local measurements of the Hubble constant at that time were quite poor, as they could easily vary by a factor of two [see for instance (Fukugita et al., 1993; Sandage and Tammann, 1975)].

In the mid-1990s, there was no clear evidence for privileging a given model over an other. Although the inflationary CDM model was considered as an elegant and attractive theory, because of its reduced number of parameters, the aforementioned internal inconsistencies raised some skepticism about its overall ability for explaining combined sets of refined observations. At that time, the standard model was therefore rather considered as a base model for developing observational techniques, or a substrate on top of which one could add further theoretically well-motivated structures to study, leading to a family of CDM based models (Dodelson et al., 1996; Liddle and Lyth, 1993). Such structures involving different predictions for various observable

1. From such a structure formation point of view, other phenomena affecting the generation of primordial fluctuations have also been proposed and shown to potentially leave observables features into the data. Examples are provided by topological defects such as cosmic strings or textures [see e.g. (Kibble, 1976; Gooding et al., 1991; Durrer et al., 1994; Shellard, 1995)].

quantities, they could therefore be readily detected by increasingly diverse experiments, precise measurements and the refinement of the associated methodology.

1.2.5 Supernovae Ia: Dark Energy for Accelerating Expansion

The strongest evidence against the CDM paradigm came from observations of distant Type Ia supernovae (SNIa) made in the late 1990s. Two different groups, The High-Z Supernova Search Team led by A. Riess (Riess et al., 1998) and Supernova Cosmology Project led by S. Perlmutter (Perlmutter et al., 1999), selected about one hundred distant SNIa in total, previously observed at redshifts $0.1 \lesssim z \lesssim 0.8$, in order to robustly constrain cosmological parameters.

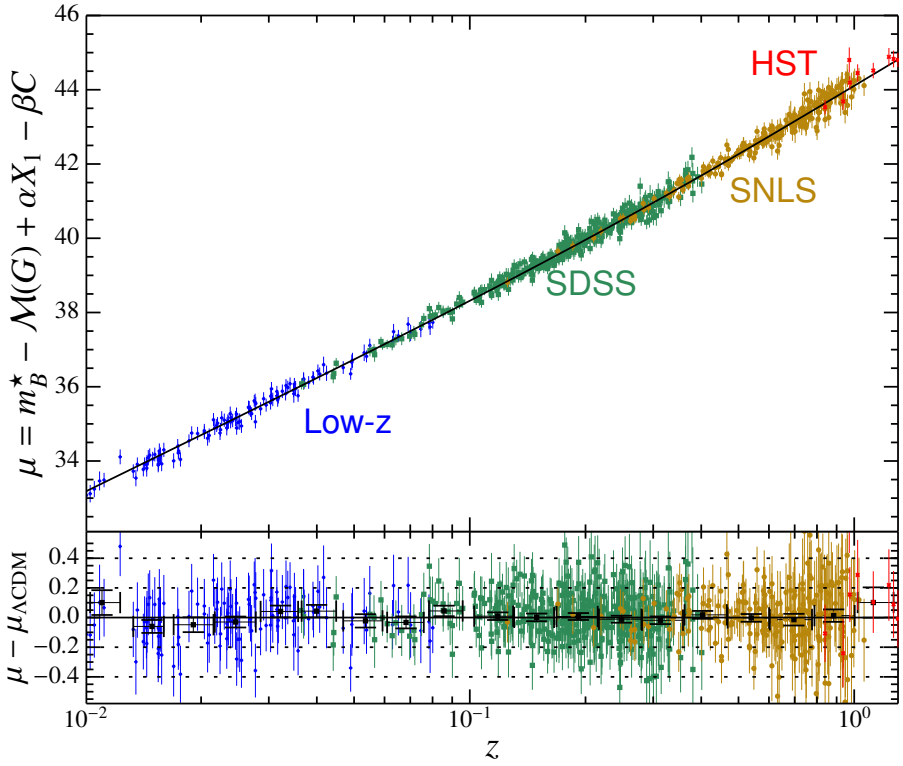

Figure 1.3 – Hubble diagram of the *SDSS-II/SNLS3 Joint Light-curve Analysis* (*JLA*) (upper panel) and its residuals compared to the corresponding best-fit ΛCDM cosmology. From (Betoule et al., 2014).

SNIa are the product of thermonuclear explosions of white dwarfs after the accretion of matter from nearby objects, such as a companion star. They are very bright, that is, detectable at high redshifts ($z \sim 1$) and are therefore of prime interest for late time cosmology. Since their explosion is closely related to the Chandrasekhar mass, their absolute magnitude distribution narrowly peaks at a fixed value of the order $M \simeq -19.5$, and in this sense, they are referred to as "standard candles". However, depending on the nature of the accreting material and on their environment, this magnitude can acquire a quite high dispersion, so they are not perfectly "standard". In fact, SNIa are "standardisable" because there is an observed correlation between their peak brightness, the shape of their light-curve (i.e. the higher the peak the slower the light curve declines after the peak) and their color, so that their absolute magnitude can be corrected in using color-brightness and light-curve shape-brightness relations [see e.g.

(Hillebrandt and Niemeyer, 2000; Goobar and Leibundgut, 2011)], and this makes the absolute magnitude a nuisance parameter. The knowledge of the apparent magnitude and redshift then provides a measure of the luminosity distance to the source and is represented as the Hubble diagram (see for example Fig. 1.3). The luminosity distance being sensitive to the cosmological parameters, SNIa provide tight constraints from the establishment of a distance ladder (Goobar and Perlmutter, 1995).

The team of Riess placed constraints on the flat standard CDM model and showed that it was ruled out at 7 to 9 standard deviations given two different methodologies, whereas Perlmutter *et al.* found it to be ruled out at 99.7 percent (3σ) confidence level. This is not only implying that the cosmological constant density fraction is nonzero at present time, but in fact that it is dominating the energy budget of the Universe at a level of 70 percent. From this, it follows that the background expansion of our Universe is in fact *accelerating*, if one assumes the latter to be flat. This discovery unambiguously appealed for the cosmological constant λ (or Λ in more modern notations), earlier discarded by Einstein, to be reintroduced into the model for it to be consistent with observations. Such observations led to the birth of a new paradigm in cosmology, described by the Lambda-cold dark matter (ΛCDM) model. The energy component associated to the acceleration of the Universe is called the *dark energy*.

The idea that the cosmological constant Λ could be replaced by alternative components explaining cosmic acceleration, as for instance by a "smooth" component [see e.g. (Turner and White, 1997; Coble et al., 1997)], i.e. a mostly time-varying vacuum energy, such as a quintessence field (Ratra and Peebles, 1988; Wetterich, 1988; Caldwell et al., 1998; Sahni and Starobinsky, 2000), was already considered at the time. In that case, the dark energy fluid is characterised by an equation of state $p = w\rho$, different from the ΛCDM value of $w = -1$, and possibly varying in time as well. Constraints on a constant dark energy equation of state have been shown to be provided by CMB and SNIa observations in (White, 1998), and updated in (Perlmutter et al., 1999), showing that the consistency of the prediction of ΛCDM given these data. The accuracy on the cosmological parameters remained however quite restricted at the time but this situation changed drastically in the following years.

1.3 Precision Cosmology Era

1.3.1 Resolving the CMB Temperature Spectrum

The *COBE* satellite observed the CMB temperature anisotropies over the whole sky reaching $\ell = 26$ in multipole space, corresponding to an angular resolution of 7 degrees, and was therefore only able to resolve its angular power spectrum at low multipoles, i.e. at large angular scales (see Fig. 1.4 for a map of the CMB over the full sky). In that region, the shape of the anisotropies power spectrum is dominated by the Sachs-Wolf effect (SW) (Sachs and Wolfe, 1967), that is sensitive to the amplitudes of the linear gravitational potential at decoupling (ordinary SW) and to their time variation integrated along the line-of-sight from last scattering (integrated SW, ISW). As the gravitational potential is constant during the matter dominated era (at least in linear theory), the former contributes at decoupling and basically reflects the initial conditions provided from early Universe physics, whereas the latter is mostly affected by eventual dominating energy components other than matter at mid-to-late times, e.g. dark energy or spatial curvature [2]. However, at those scales, the constraining power of CMB measurements is intrinsically limited by *cosmic variance*, because one can only naturally access one realisation of the sky. This is especially important at very low multipoles ($\ell \lesssim 10$), where the cosmic variance

2. Note that an exotic energy component at early times could also involve an early ISW effet.

is maximal because of the restricted number of $(2\ell + 1)$ projected spherical modes labeled by $-\ell \leq m \leq \ell$. This fact considerably reduces the statistical sampling compared to that obtained on smaller angular scales.

Since *COBE*, CMB science has undergone fast developments due to increasingly accurate theoretical predictions, numerical simulations and precise measurements. Indeed, in looking at higher multipoles, cosmic variance is reduced and the shape of the power spectrum can be better resolved. Its shape was expected to be more complex at smaller scales, reflecting dynamical features of the photon, baryons, electron plasma at decoupling (Sachs and Wolfe, 1967; Silk, 1968; Sunyaev and Zeldovich, 1970; Doroshkevich et al., 1978). For example, the

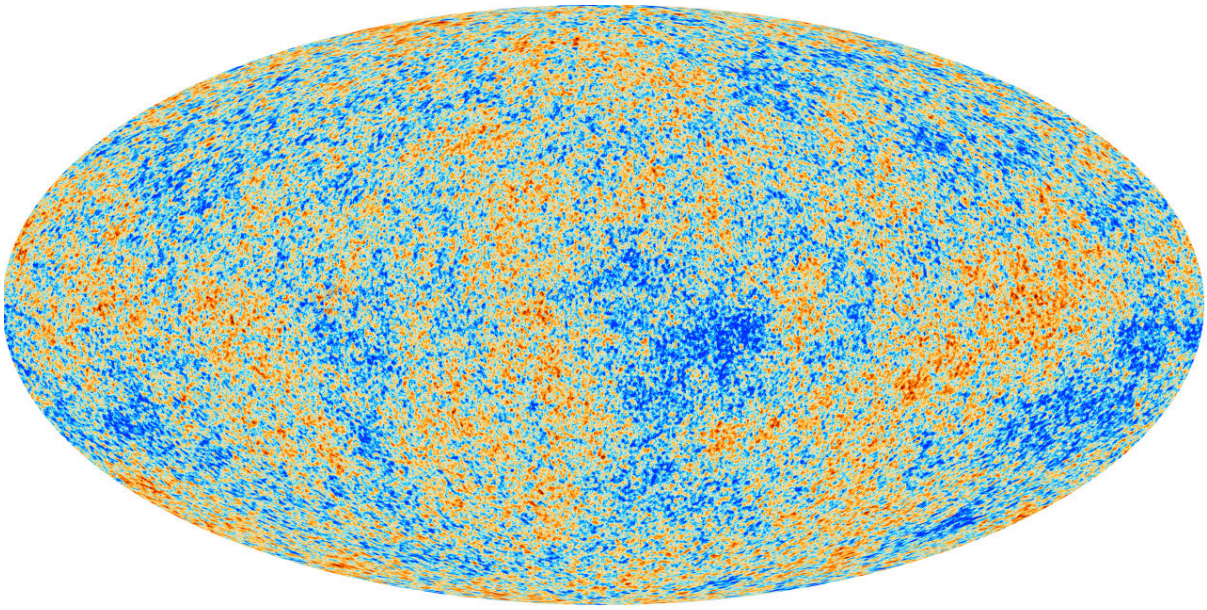

Figure 1.4 – The temperature anisotropies of the Cosmic Microwave Background (CMB) as observed by *Planck* (Ade et al., 2014c). Image Credit: ESA, *Planck* Collaboration (ESA).

photons scattering off electrons and baryons (tied together by electrostatic interaction) in the plasma through Compton effect, tend to mix cold and hot regions on scales smaller than their diffusion length. Such an effect exponentially damps the amplitude of temperature anisotropies below that scale. As the process of recombination is not instantaneous, but took place in a finite amount of time, the diffusion length of the photon increased as the ionization fraction (i.e. the ratio of the number of electron to that of hydrogen nuclei) decreased, which implies that smaller scales undergo more damping than larger ones. This produces a characteristic damping tail in the power spectrum of CMB temperature anisotropies at high multipoles, whose cut-off characterises the finite thickness of the surface of last scattering [see e.g. (Hu and White, 1997a)]. Such a process is referred to as the *Silk damping* (Silk, 1968). A similar damping process arises during the period of reionisation, when the first objects started to form in the early Universe and were able to reionised the neutral hydrogen atoms which recombined at decoupling. These combined effects result in an exponential suppression $\sim e^{-2\tau_{\rm re}}$ of the temperature power spectrum at scales smaller than the horizon, controlled by the Thomson optical depth to reionisation $\tau_{\rm re}$.

Moreover, at the epoch of radiation-matter equality, CDM density perturbations dominate

the evolution of the gravitational potential, forming wells which deepen with time. Because of gravitational instability, the photon-baryon plasma inherits the scale invariant density fluctuations configuration from CDM in falling into potential wells and starting to form overdense regions. As the plasma is a relativistic gas, its effective pressure counteracts the gravitational force at a distance given by the *sound horizon*. Below this scale, the fluctuations of the plasma oscillate, giving raise to an oscillating pattern of standing sound waves. At the time of recombination, some standing wave modes were therefore at their maximum/minimum (induced by compression/decompression) while some others were vanishing. Such a phenomenon gives rise to an imprint of harmonic acoustic oscillations in the temperature anisotropies power spectrum of the CMB, forming peaks and troughs at characteristic scales. These are typically referred to as the Baryonic Acoustic Oscillations (BAO) of the CMB (Sunyaev and Zeldovich, 1970), whose first peak in increasing scales corresponds to the sound horizon size at recombination (see Fig. 1.5 for an illustration).

A precise theoretical understanding of these features, and, more generally, on the physics of the CMB, therefore allows one to access precious information about the physics of the early Universe and its overall expansion history. In turn, such measurements provide powerful constraints on the underlying cosmological model (Bond et al., 1994; White et al., 1994). This has been illustrated by forecast constraints given future CMB experiments at the time, that have shown that the observation of the CMB temperature spectrum prove to encode information on a large set cosmological parameters such as the geometry of the Universe, the baryon density, the Hubble constant, the cosmological constant, the number of light neutrinos, the ionisation history, and the amplitudes and spectral indices of the primordial scalar and tensor perturbation spectra, and in particular allows to measure some of them to percent precision (Jungman et al., 1996b,c; Zaldarriaga et al., 1997; Bond et al., 1997; Bond et al., 1998).

From a practical point of view, computing predictions from CMB physics is not an easy task as it requires to solve simultaneously for the evolution of the various matter components through their fluid or Blotzmann equations, together with the general relativistic dynamics of spacetime governed by Einsteins' equations. However, in the early Universe matter density and metric fluctuations over the FLRW background are very small and one can compute robust predictions from the system linearised to first order in perturbation theory [see e.g. (Lifshitz, 1946; Peebles and Yu, 1970; Ma and Bertschinger, 1995)]. This computation is especially made easier by the fact that Fourier modes evolve independently at linear level. However, solving for such a linear system still requires the use of numerical computations. This has led to the development of the first linear Einstein-Boltzmann solvers, especially made efficient by using the line-of-sight method in CMBFAST (Seljak and Zaldarriaga, 1996), which sped up the computations by orders of magnitude.

1.3.2 Flat Universe: Cosmic Variance, Geometrical Degeneracy and Cosmic Complementarity

Observations with higher resolution have been able to uncover the acoustic structure of the CMB power spectrum [see e.g. (Scott. et al., 1996; Netterfield et al., 1997; Melchiorri et al., 2000)]. In particular, the *BOOMERanG* (de Bernardis et al., 2000), and *MAXIMA* (Hanany et al., 2000), balloon-borne experiments measured the CMB with a resolution of $\simeq 0.2$ degree, over a range of hundreds of multipoles. This allowed them to report a high signal-to-noise detection of the first acoustic peak in 2000. An accurate detection of the location of the first peak allows one to put stringent constraints on the so-called acoustic-distance scale ratio at recombination, the ratio of the comoving sound horizon size at decoupling to the angular

diameter distance to decoupling. This quantity sensitively depends on variations in the energy density parameter controlling the amount of total matter, spatial curvature and dark energy. The latter experiments concluded the Universe to be spatially flat and that the primordial power spectrum is compatible with a scale invariant one, supporting the inflationary paradigm. However, their results on the amount of spatial curvature were shown to be unstable under different prior assumptions (de Bernardis et al., 2000; Lange et al., 2001). This fact indicates that their inferences were partially dominated by their prior knowledge and, as a consequence, witnesses a lack of constraining power from the data.

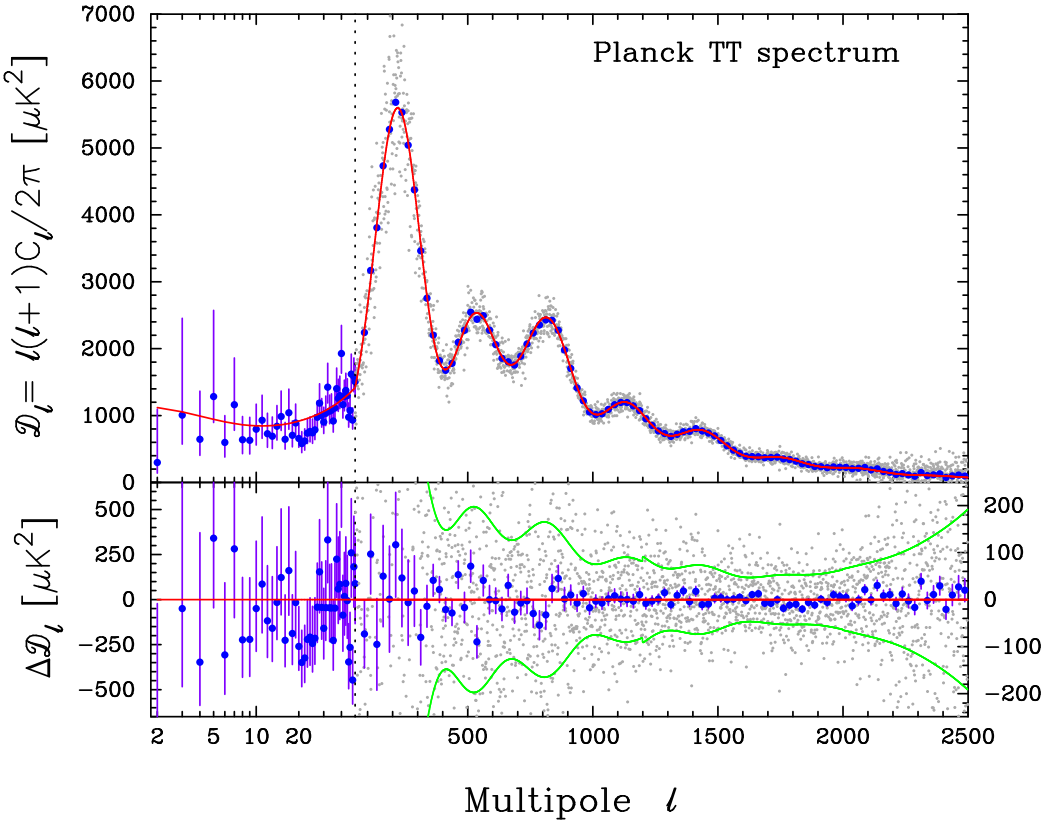

Figure 1.5 – The grey dots show the CMB temperature anisotropies power spectrum measured by *Planck* 2013 multipole-by-multipole and blue dots show their average on $\Delta\ell \approx 31$ bands. The red curve in the upper panel is the best-fit base ΛCDM theoretical spectrum fitted to the *Planck* likelihood. The lower panel shows the corresponding residuals. The error bars on blue dots show $\pm 1\sigma$ uncertainties, while the green lines shows the $\pm 1\sigma$ errors on the individual power spectrum estimates at high multipoles. From (Ade et al., 2014d).

The reason to this fact is that there is a "geometrical degeneracy" into the temperature anisotropy power spectrum of the CMB, implying that simultaneous changes of the total matter, curvature and dark energy density fractions, can lead to the same angular power spectra, and in particular to the same acoustic scale. This practically works up to different late time ISW contributions affecting low multipoles, that are however poorly detectable as this region is dominated by cosmic variance (Hu et al., 1997; Bond et al., 1997; Efstathiou and Bond, 1999). The way for getting rid of this degeneracy is to use CMB temperature-independent data such as from the observations of SNIa or galaxy surveys [see e.g. (Bond et al., 2000; Jaffe et al., 2001)], in a complementary perspective (Tegmark et al., 1998; Eisenstein et al., 1998, 1999)

(see Fig. 1.6 for an illustration). Galaxy weak lensing and CMB weak lensing surveys also provide complementary constraints on the FLRW background-related cosmological parameters, in particular because they measure the total mass distribution and do not depend of the dark matter-to-galaxy biais (Hu and Tegmark, 1999; Hu, 2002).

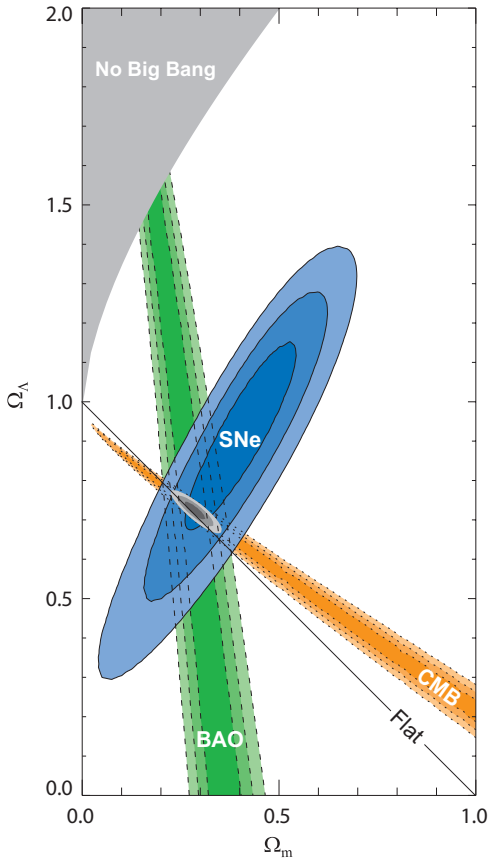

Figure 1.6 – Cosmic complementarity in the Ω_Λ–Ω_M plane between CMB, SNIa and BAO observations. From (Kowalski et al., 2008).

1.3.3 CMB Polarisation

Other degeneracies were also observed to be present in the CMB temperature spectrum. Most notably, at large scales, it was shown that the different ISW contributions resulting from a change of cosmological parameters intervening into the geometrical degeneracy, in particular the dark energy density fraction, can be compensated with the adjustment of the primordial tensor-to-scalar amplitudes ratio, the scalar spectral index and the optical depth to reionisation (Zaldarriaga et al., 1997). At small scales, a variation of the optical depth can be compensated by a change in the primordial scalar amplitude A_s, so as to preserve the damping tail of the CMB temperature power spectrum, that only efficiently constrains the combination $A_s\, e^{-2\tau_{\rm re}}$.

In that case, it is the measurement of CMB polarisation auto- and temperature-polarisation cross-spectra that provide complementary constraints to the temperature spectrum. For instance, earlier reionisation increases the amplitude of polarisation, creating a bump at large scales, while decreases its amplitude at small scales (Zaldarriaga, 1997). This provides constraints on $\tau_{\rm re}$ which consequently partially reverberates on the background cosmological pa-

rameters. The first detection of CMB polarisation was reported by the *Degree Angular Scale Interferometer* (*DASI*) in 2002 (Kovac et al., 2002), and was found to be in agreement with prediction of the standard ΛCDM model. From a technical point of view, CMB polarisation was shown to be conveniently decomposed into E- and B-mode contributions for both theoretical and observational purposes (Kamionkowski et al., 1997a; Hu and White, 1997c). In particular, B-modes cannot be generated from scalar perturbations and therefore provide information on primordial gravitational waves and vorticity (Seljak and Zaldarriaga, 1997; Kamionkowski et al., 1997b; Zaldarriaga and Seljak, 1997; Hu and White, 1997b), given that one gets systematic errors induced by foregrounds, e.g. polarised dust and synchrotron emission, under control. As such, a complete statistical characterisation of CMB anisotropies requires four correlation functions, the temperature, E- and B-modes auto-correlations and the temperature-E mode cross-correlation, as cross-correlations including B-modes vanish for parity reasons.

Inflationary theories also find constraints through the measurement of the B-modes auto-correlations, as different theories predict different gravitational wave primordial spectra (Turner et al., 1993; Lyth, 1997), although the detection of such effects require a good understanding of the gravitational lensing of CMB polarisation, as it can convert E-modes into B-modes (Zaldarriaga and Seljak, 1998). The importance of such an understanding is also supported by the fact that CMB lensing gives raise to non-gaussianities into the temperature and polarisation spectra (Bernardeau, 1998; Zaldarriaga and Seljak, 1999; Okamoto and Hu, 2003), while typical inflationary models generate primordial fluctuations with a Gaussian spectrum [see e.g. (Gangui et al., 1994; Acquaviva et al., 2003)]. In particular, being able to isolate the non-gaussianities induced by lensing provides a way to test simplest inflationary theories (Komatsu and Spergel, 2001), such as single field models which are characterised by consistency relations relating the three-point correlation function in the squeezed-limit to the spectral tilt of the spectrum of the two-point function (Maldacena, 2003).

1.3.4 *WMAP* for Six Cosmological Parameters

In 2003, the *Wilkinson Microwave Anisotropy Probe* (*WMAP*) space mission (Bennett et al., 2003), provided full sky maps of the CMB allowing a very precise determination of the temperature anisotropies spectrum. In turn, these applied unprecedented tight constraints on the cosmological parameters of the standard inflationary ΛCDM model (Spergel et al., 2003), which allowed to shape its overall structure much more precisely. Indeed, *WMAP* also detected the temperature-polarisation cross-correlation (Kogut et al., 2003), that showed evidence for reionisation at redshift $z_{\rm re} \simeq 20$, in accordance with bounds from the observation of the Gunn-Peterson trough in the absorption line of distant quasars (Becker et al., 2001). The ΛCDM model was therefore supplemented with an extra parameter, the optical depth to reionisation $\tau_{\rm re}$, and shown to describe well *WMAP* observations with only six cosmological parameters (Spergel et al., 2003),

$$\theta_{\rm base} = (\omega_{\rm b}, \omega_{\rm cdm}, H_0, A_s, n_s, \tau_{\rm re}) \ ,$$

where the $\omega_{\rm b}$, $\omega_{\rm cdm}$, are the physical energy densities of baryons and CDM, respectively, H_0 is the Hubble parameter, A_s is the amplitude and n_s the tilt of the power spectrum for primordial scalar fluctuations. Constraining the above parameter space, but also extensions of it, was made possible by the use of the efficient linear Einstein-Boltzmann code CMBFAST (Seljak and Zaldarriaga, 1996), allowing to compute robust predictions from the model, together with a Monte Carlo Markov Chain (MCMC) algorithm described in (Verde et al., 2003), for performing Bayesian cosmological parameter inference. The consideration of additional external constraints

from various astronomical data such as local measurements of H_0, weak lensing, galaxy velocity fields and number counts of clusters also found agreement with the *WMAP*-ΛCDM predictions [see (Spergel et al., 2003) for details]. In particular, joint likelihood analyses including data from smaller angular scale CMB experiments, distant SNIa, local measurements of H_0 and large scale structure where shown to be able to constrain the geometry of the Universe, the running of the scalar spectral index as well as the nature of the dark energy. They found a striking consistency for a flat Universe, whose late time cosmic acceleration is modelled by a cosmological constant Λ, and whose primordial fluctuations are encoded in a nearly scale invariant Gaussian power spectrum as those provided by inflationary scenarios. Further constraints from combined *Sloan Digital Sky Survey* (*SDSS*) spectroscopic galaxy redshift survey and *WMAP* were also carried out and were shown to provide the very same conclusions (Tegmark et al., 2004a,b).

The increasingly precise measurement of cosmological probes such as the CMB by *WMAP* or the galaxy distribution by *SDSS* made modern cosmology enter into its precision era, as these were able to place constraints on a handful of cosmological parameters at the level of a few percents.

1.3.5 Baryon Acoustic Oscillations in Galaxy Surveys

An additional very relevant probe complementary to CMB observations, in particular for dark energy physics, is the measurement of the BAO peaks in the power spectrum of the late time galaxy distribution. The distribution of galaxies in the sky inherits the imprint of acoustic oscillations of the primoridial plasma. This is realised by the decoupling of the baryons from the photons some time after recombination, at the end of the so-called *drag epoch*. The baryon drag leads to alternating height of the peaks amplitude of the CMB (see Fig. 1.5), and translates the acoustic oscillations of the primordial plasma into an acoustic feature in the baryon distribution. Together with cold dark matter, such a distribution seeds the growth of structures and leads to a Baryon Acoustic Peak into the real space two-point correlation function of the late time galaxy distribution, and manifests itself in BAO peaks in the corresponding power spectrum (Peebles and Yu, 1970; Bond and Efstathiou, 1984; Hu and Sugiyama, 1996; Eisenstein and Hu, 1998). The possibility of observing such feature in the distribution of high redshift quasars has also been evoked earlier (Shanks et al., 1987) [see (Bassett and Hlozek, 2009) for a review]. Although largely resulting from linear structure formation physics, the observation of this feature is however quite delicate in practice, as it is affected by Silk damping (Silk, 1968), redshift-space distortions induced by peculiar velocities (Kaiser, 1987; Hamilton, 1997), a possibly scale-depent biais and other mild nonlinear effects induced by structure formation (Meiksin and White, 1999), that alter the broadening of the peak structure, therefore making it more difficult to detect.

The first detection of the BAO peak was reported by the spectroscopic *SDSS* in 2005 (Eisenstein et al., 2005), at an effective redshift $z = 0.35$. The physical scale of the oscillations is determined by the baryon and CDM densities and its measurement allows to access a typical acoustic-distance scale ratio, similar to the one provided by the CMB. As such, the observation of the BAO peaks provides a *standard ruler* once it is calibrated on CMB measurements (Eisenstein et al., 1998; Eisenstein, 2003), or on local measurements from SNIa (Cuesta et al., 2015; Cuesta et al., 2015). The decomposition of the BAO feature in the directions transverse and longitudinal to the line-of-sight allows the separate measurements of the angular diameter distance and expansion rate (Hubble parameter) respectively, rendered dimensionless by the comoving sound horizon at the epoch of baryon drag. Such a decomposition therefore allows to place useful constraints on the expansion history of the Universe, and therefore on its geometry

and on the nature of the dark energy. In particular, the inferred quantities provide a so-called Alcock-Paczynski test (Alcock and Paczynski, 1979) for the quantity $D_A(z)H(z)$, which gives precious information about the geometrical structure of the Universe at the redshift of observation, independently of assumptions on the prior evolution. Moreover, observing the BAO features in the distribution of galaxies and distant quasars at several redshifts allows for the construction of a distance ladder which probes the expansion history of the Universe over an extended redshift range.

Several works have considered such measurements for constraining the nature of the dark energy through simple equation of state parametrisations (Blake and Glazebrook, 2003; Hu and Haiman, 2003; Seo and Eisenstein, 2003; Matsubara, 2004), but also modelled as a perfect fluid or a scalar field (Amendola et al., 2005), and other alternative scenarios such as decaying photons (Bassett, 2004; Bassett and Kunz, 2004).

1.3.6 Growth of Structures and Weak Lensing

Redshift-Space Distortions

The observation of the distribution of galaxies in the sky in particular allows one to access their redshift and their position on the celestial sphere. Converting these notions into real space needs the input of a background geometry, and therefore of a cosmological model. Moreover, the position of the galaxies in redshift-space is also influenced by their peculiar velocities with respect to the Hubble flow. As such, the peculiar motion of galaxies induces redshift-space distortions (RSD) (Jackson, 1972; Kaiser, 1987) [see e.g. (Strauss and Willick, 1995; Hamilton, 1997; Percival et al., 2011) for reviews], that can be used as a tool to probe the growth of structures. Because redhift-space distortions are only induced in the direction longitudinal to the line-of-sight, they induce an anisotropic clustering pattern which can be used to determine a combination of the amplitude of growth and the linear biais between the galaxy and dark matter distribution [see e.g. (Tadros et al., 1999; Percival and White, 2009)]. To our knowledge, the first high-significance measurements of these features that were shown to provide robust cosmological constraints have been reported in 2001 by the *Two-Degree-Field Galaxy Redshift Survey* (*2dFGRS*) (Hatton and Cole, 1999; Peacock et al., 2001). As these distortions are correlated with the Alcock-Paczynski effect, their consideration and associated controlled treatment is unavoidable for a reliable measurement of the BAO feature. Ultimately, these measurements constrain the linear growth of structure described by the underlying theory of gravity, and can for instance be used to discriminate a modification in the response of the gravitational potential to matter described by the theory, or deviations in its expansion history (Ballinger et al., 1996).

In particular, the standard ΛCDM model gives raise to consistency relationships between expansion rate and growth, that can be used to test eventual modifications of gravity (Ishak et al., 2006; Guzzo et al., 2008; Song and Koyama, 2009). Structure formation data were therefore extensively used for constraining modified gravity models possessing self-accelerating solutions. Examples are provided by studies in the framework of the DGP braneworld (Koyama and Maartens, 2006; Ishak et al., 2006; Kunz and Sapone, 2007; Song and Percival, 2009) (see Sec. 2.4 for more details on the model), or in theories involving an arbitrary function of the Ricci curvature scalar $f(R)$, for modifying the Einstein-Hilbert action (Song et al., 2007) [see also (Carroll et al., 2004, 2005), where this class of models was originally proposed].

Weak Lensing

Galaxies. The light emitted by point source galaxies travel to the observer under the gravitational influence of the stacked inhomogeneous total matter distribution along the photon path. This gives raise to small distortions (shear) and magnification (convergence) effects in the shapes of the observed galaxies, and provides a powerful method for evaluating the projected mass distribution when analysed statistically. This phenomenon is referred to as weak gravitational lensing or cosmic shear (Gunn, 1967) [see e.g. (Bartelmann and Schneider, 2001; Munshi et al., 2008; Kilbinger, 2015) for reviews]. The first precise cosmic shear measurements of the *Canada-France-Hawaii Telescope* (*CFHTLens*), were shown to provide useful constraints on the cosmological parameters of the ΛCDM model, and on its possible deviations with from the point of view of the nature of the dark energy it describes (Hoekstra et al., 2006; Semboloni et al., 2006). The cosmic shear is only sensitive to the total mass distribution in the Universe and therefore does not need the modellisation of the bias between the galaxy and CDM distributions. Consequently, weak lensing surveys provide complementary constraints to the ones of BAO and RSD observations and, in turn, proves to be of particular relevance for testing deviations from Einstein gravity [see e.g. (Yoo, 2009; Song et al., 2011)].

In particular, at the time, weak lensing constraints on modified gravity models were considered in the framework of the DGP model (Knox et al., 2006), and together with $f(R)$ and TeVeS theories in (Schmidt, 2008).
They were also used in more phenomenological approaches using specific parametrisations for appreciating the deviations to GR at the level of linear perturbations, conveniently constrained using combined weak lensing and growth data (Hu and Tegmark, 1999; Sealfon et al., 2005; Caldwell et al., 2007; Hu and Sawicki, 2007; Huterer and Linder, 2007; Zhang et al., 2007; Amendola et al., 2008b; Sapone and Kunz, 2009).

CMB. The effects of weak lensing on the CMB have also been shown to be non-negligible (Blanchard and Schneider, 1987; Cole and Efstathiou, 1989; Linder, 1990; Seljak, 1996) [see e.g. (Lewis and Challinor, 2006) for a review], as they smooth-out the acoustic oscillations in the temperature, polarisation spectra and temperature-polarisation cross-spectra by several percents. Moreover, weak lensing convert E-modes into B-modes, which introduces a degeneracy with those generated from primordial GWs. However, it also generates a small-scale non-Gaussian trispectrum that can be utilised for breaking cosmological parameter degeneracies present into CMB primary anisotropies, such as the geometric degeneracy and the one present in the damping tail of the CMB between the amplitude of primordial fluctuations and the optical depth to reionsiation. It therefore provides further information about late time structure formation physics, where the manifestation of dark energy becomes important.

1.3.7 Other Probes Relevant for Dark Energy

Here above, we briefly outlined various observations proving to be relevant in understanding the cosmic expansion history, and in particular dark energy, as these will be used in the following study. We refer the reader to (Weinberg et al., 2013) for a far more exhaustive account. Of course, the physics of various other phenomena are relevant as well for understanding the dark energy more precisely and we provide a selected list of them here.

As already discussed above, the emergence of dark energy at late time causes the gravitational potential, which is constant to a good approximation during the matter era, to vary in time. This induces a late time ISW effect which affects the large-scale power of CMB

temperature and polarisation anisotropies (Kofman and Starobinskii, 1985). Although such effect is difficult to detect, because it takes place in regions dominated by cosmic variance, the cross-correlation between CMB and large-scale galaxy surveys (Crittenden, 1996; Boughn et al., 1998), was proven to give significant information on this effect, and therefore on the dark energy dominating at late time (Peiris and Spergel, 2000; Cabre et al., 2006; Giannantonio et al., 2008).

Observations of the X-rays emitted from intracluster gas provide estimations of the redshift dependence of the underlying baryonic mass fraction, which is sensitive to the angular diameter distance to the cluster assumed in the modellisation. These can therefore provide a distance-redshift relation for inferring cosmological parameters (Sasaki, 1996; Pen, 1997). Such observations from the *Chandra* space telescope, observing faint X-ray emitting sources, has been shown to be able to place constrains on base cosmological parameters, as well as on the equation of state of dark energy (Allen et al., 2002, 2004; Allen et al., 2008).
Such observations also allow to access the cluster abundance as a function of redshift, which is also probed thought the thermal Sunyaev-Zeldovich (SZ) effect (Sunyaev and Zeldovich, 1972), induced by the CMB photons being heated up in propagating through the hot intracluster gas. Both of these observations provide complementary constraints, especially useful for constraining dark energy related cosmological parameters (Haiman et al., 2000; Grego et al., 2001; Verde et al., 2002; Komatsu and Seljak, 2002; Majumdar and Mohr, 2004), although affected by the ignorance of an hydrostatic bias (Komatsu and Seljak, 2001).

1.3.8 The Standard (dark) ΛCDM Model: Current Status

Over the years, the aforementioned features were uncovered with increasingly exquisite precision from cosmological observations, placing powerful and robust constraints on the six-dimensional parameter space of the standard ΛCDM model (1.1), and various extensions of it.

Linear Einstein-Boltzmann Solvers. Such a task was especially rendered possible by the development of more and more accurate linear Einstein-Boltzmann solvers through the years such as CMBEASY (Doran, 2005), or CAMB (Lewis et al., 2000), and more recently CLASS (Blas et al., 2011). The two last ones are frequently updated and define nowadays standard for linear cosmological solvers. Once interfaced with MCMC codes such as COSMOMC (Hu et al., 2015) or MONTEPYTHON (Audren et al., 2013), these allow one to place accurate constraints on the parameter space of the considered cosmological model.

Cosmic Microwave Background. Most notably, the *WMAP* CMB experiments provided refined analyses over a nine-year period (Spergel et al., 2007; Komatsu et al., 2009; Komatsu et al., 2011; Hinshaw et al., 2013), which were complemented with small scales ground-based CMB experiments such as the *Atacama Cosmology Telescope* (*ACT*) (Sievers et al., 2013), which reported the first CMB lensing detection through measurement of the CMB temperature trispectrum in 2011 (Das et al., 2011), and the *South Pole Telescope* (*SPT*) (Reichardt et al., 2012), that also provided CMB lensing data (van Engelen et al., 2012).

These were closely followed by the results of the *ESA Planck* spatial mission whose satellite was launched in 2009, and allowed to release accurate CMB measurements, in particular of the temperature, trispectrum-extracted lensing spectra and catalogue of SZ sources from the "nominal mission" in 2013 (Ade et al., 2014c), and was already shown to provide tight constraints on the extended ΛCDM parameter space (Ade et al., 2014d). In 2015, *Planck* released the "full mission" low-ℓ temperature and polarisation (cross-) spectra, the "cross-half-mission"

high-ℓ spectra, as well as an update of its lensing spectrum and SZ cluster counts catalogue (Adam et al., 2016), allowing to reach the most accurate percent-level precision measurements of cosmological parameters of the *base* ΛCDM model (Ade et al., 2015d). A refined analysis of *Planck* polarisation data has been provided in (Aghanim et al., 2016b), while the final full-mission *Planck* measurements were recently presented in (Aghanim et al., 2018). Moreover, a pre-*Planck* CMB analysis including updated *WMAP* and *ACT/SPT* data were performed in (Calabrese et al., 2013, 2017).

Finally, the ground-based CMB observatories *POLARBEAR* (Ade et al., 2017) and the *Background Imaging of Cosmic Extragalactic Polarization* (*BICEP*), together with the *Keck Array* (Takahashi et al., 2010), have been conceived for specifically focusing on B-modes polarisation measurements. At the end of 2013, the *BICEP2/Keck* collaboration reported a large excess of B-modes in the multipole range where the signal from inflationary GWs is expected to peak (Ade et al., 2014b). However, further investigations based on a joint analysis of their results with the ones from *Planck*, showed that this peak was largely induced by foreground dust emission, and that the data displayed no statistical evidence for inflationary gravitational waves (Ade et al., 2015a). A more recent reanalysis of these data in (Gott and Colley, 2017), has equivalently shown no statistical evidence for B-modes generated from inflationary GWs.

Overall, these CMB observations were shown to be well described by the six-parameter base ΛCDM model, being consistent within each surveys and when these are joined together. An exception is however given in the case of the *Planck* 2015 results, where their primary CMB constraints where shown to be in tension with the *Planck* SZ cluster counts (Ade et al., 2015d, 2016), although this is still subject to debate because of a major uncertainty in the overall mass calibration typically controlled by an unknown hydrostatic mass bias parameter [see e.g. (Hurier and Lacasa, 2017; Salvati et al., 2017; Bolliet et al., 2017) for a recent account].

Distant SNIa. Others observations were also developed beside those of CMB. In particular, distant SNIa have been extensively observed by various scientific programs. For example, at high redshift (up to $z \sim 1$) by the *Supernova Legacy Survey* (*SNLS*) (Astier et al., 2006) and by the *ESSENCE* survey (Wood-Vasey et al., 2007) which, together with distant SNIa observed by the *Hubble Telescope* (Knop et al., 2003) [see also (Suzuki et al., 2012)], were gathered into the *Union* compilation (Kowalski et al., 2008), later updated in the *Union2* compilation in (Amanullah et al., 2010), or by the *pan-STARRS* project (Rest et al., 2014) or the ore recent *Pantheon* sample (Scolnic et al., 2017). Intermediate redshift SNIa ($0.05 \lesssim z \lesssim 0.4$) were observed by the *SDSS-II* supernova survey (Holtzman et al., 2008), which were later joined to the *SNLS* sample to form the *SNLS/SDSS Joint Lightcurve Analysis* (*JLA*) (Betoule et al., 2014). Low-redshift SNIa measurements ($z < 0.1$) have been performed by the *Harvard-Smithsonian Center for Astrophysics* (*CfA*) surveys (Hicken et al., 2009), the *Carnegie* supernova project (Contreras et al., 2010), the *Lick Observatory Supernova Search* (Ganeshalingam et al., 2013) or the *Nearby Supernova Factory* (Aldering et al., 2002) [see also (Betoule et al., 2014) for more references]. These provide over a thousand of distant SNIa measured to high accuracy, which can consequently be used to set constraints on the expansion history of the Universe. Here also, no significant deviations from ΛCDM were found up-to-date.

Baryon Acoustic Oscillations and Growth Rate. Detections of the BAO feature in the real-space correlation function or the Fourier-space power spectrum have also been reported. Examples are provided by the isotropic constraints provided by the *6dF* galaxy survey at $z_{\rm eff} = 0.106$ (Beutler et al., 2011), *SDSS* main-galaxy sample *DR7* at $z_{\rm eff} = 0.15$ (Ross et al., 2015)

and or the *Baryon Oscillation Spectroscopic Survey BOSS LOWZ* at $z_{\rm eff} = 0.32$ (Anderson et al., 2014), and anisotropic constraints from *BOSS CMASS* at $z_{\rm eff} = 0.57$ (Anderson et al., 2014). These were in particular joined with CMB observations such as those of *Planck* in (Ade et al., 2015d), and were shown to drastically improve CMB the constraints, in that they serve to break the geometrical degeneracy present into the acoustic structure of the CMB. In particular, they impose tight constraint on the geometry of the Universe and show high consistency with a flat Universe. BAO measurements such as those of the *PAU* survey (Benitez et al., 2009), also prove to be useful for such a purpose.

In conjunction to these BAO measurements, RSD data have also been collected. A selected sample of them is given for instance by *6dF* galaxy-redshift survey (Beutler et al., 2012), the *SDSS Luminous Red Galaxies* (*LRG*) (Oka et al., 2014), *SDSS MGS* (Howlett et al., 2014), *BOSS LOWZ* (Chuang et al., 2016), *BOSS CMASS* (Samushia et al., 2014; Alam et al., 2016), *WiggleZ* (Blake et al., 2012) and *VIPERS* (de la Torre et al., 2013), and have been proven to be consistent with *Planck* 2015 data as well (Ade et al., 2015d,e).

Galaxy clustering and weak lensing data from the *Dark Energy Survey Year 1* (Abbott et al., 2017j), were also recently released and found consistency with the *Planck* 2015 ΛCDM predictions.

Cosmic Shear. Non-CMB data also arise from cosmic shear surveys such as *CFHTLenS* (Heymans et al., 2012) or the *Kilo-Degree Survey KiDS-450* (Kuijken et al., 2015), which have in particular shown a preference for lower growth of structure as compared to the one inferred from *Planck* 2015 CMB data given the ΛCDM model. However, systematic issues first need to be addressed, and have recently been pointed out into (Troxel et al., 2018), where it was found that taking into account the survey boundary and masks effects into the shape noise term of the cosmic shear analytic covariance matrix, improves agreement between the *KiDS-450* cosmic shear constraints and the results of *Planck*.

Local Measurements of H_0. Another crucial ingredient for constraining the cosmological model is provided by the direct measurements of the present Hubble constant H_0. Indeed, evaluating H_0 independently from other experiments as CMB, BAO or SNIa surveys, allows one to break associated degeneracies present in extensions of it, and can lead to a better determination of the nature of the dark energy, or of the neutrino mass for instance. When applied to *Planck* CMB data alone in the case of the base ΛCDM model, these measurements can be used for testing the consistency of the model.

Local H_0 measurements relies on the observation of well-understood objects in the sky, such as stars known as Cepheid variables or maser galaxies, allowing one to access reliable distance indicators (Freedman and Feng, 1999) [see also (Jackson, 2007; Freedman and Madore, 2010) for reviews]. Such measurements have in particular been performed by the *Hubble Space Telescope* (*HST*) Key Project, which have led to a final estimate of $H_0 = 72 \pm 8\,{\rm km\,s^{-1}\,Mpc^{-1}}$ (Freedman et al., 2001). Since then, multiple programs are aiming to measure H_0, as for instance the *Supernova and H_0 for the Equation of State* (*SH0ES*) (Riess et al., 2009) or the *Megamaser Cosmology Project* (*MCP*) (Reid et al., 2013).

Various data analysis from local measurements have provided different constraints on H_0, as for instance the new and extended analysis of the *HST* data of (Riess et al., 2011) led to $H_0 = 73.8 \pm 2.4\,{\rm km\,s^{-1}\,Mpc^{-1}}$ or $H_0 = 73.0 \pm 2.4\,{\rm km\,s^{-1}\,Mpc^{-1}}$, after recalibration to NGC 4258 (Humphreys et al., 2013), while (Freedman et al., 2012) sets $H_0 = 74.3 \pm 2.1\,{\rm km\,s^{-1}\,Mpc^{-1}}$. More recently, the analysis of (Efstathiou, 2014), sets $H_0 = 70.6 \pm 3.3\,{\rm km\,s^{-1}\,Mpc^{-1}}$ (note that this

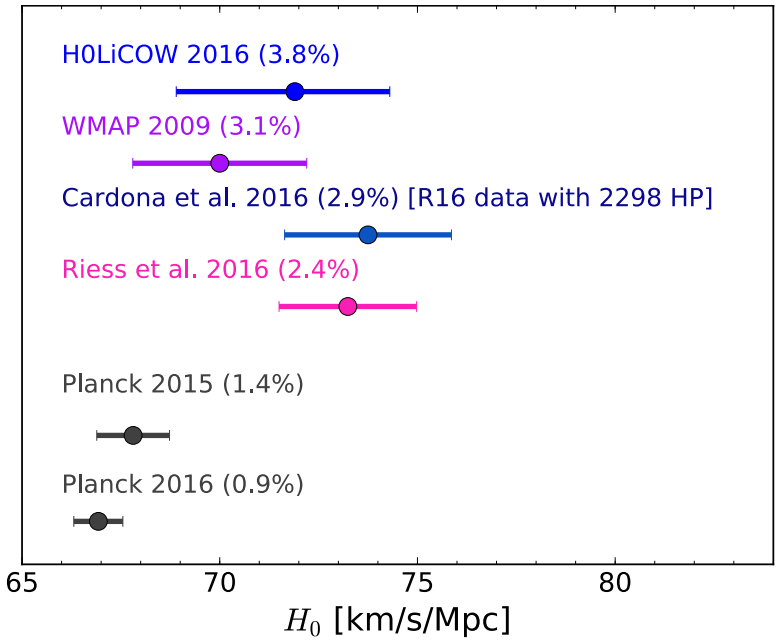

Figure 1.7 – From top to bottom: H_0 values measured from the *H0LiCOW* collaboration (Bonvin et al., 2017), inferred from *WMAP* (Hinshaw et al., 2013), from the "baseline analysis" of the data from (Riess et al., 2016) (R16) in (Cardona et al., 2017), from the actual value of (Riess et al., 2016), from the indirect measurement of *Planck* 2015 (Ade et al., 2015d) and from the updated *Planck* data of (Aghanim et al., 2016b). Image courtesy of (Cardona et al., 2017).

value becomes $H_0 = 72.5 \pm 2.5\,\mathrm{km\,s^{-1}\,Mpc^{-1}}$ if other assumptions are made into the analysis), whereas the work of (Riess et al., 2018), sets a higher value of $73.48 \pm 1.66\,\mathrm{km\,s^{-1}\,Mpc^{-1}}$ [see also Refs. (Humphreys et al., 2013; Riess et al., 2016)]. Furthermore, a determination of H_0 based on the re-analysis of the data used in (Riess et al., 2016), through Bayesian hyper-parameters has been performed in (Cardona et al., 2017), that found $H_0 = 73.75 \pm 2.11\,\mathrm{km\,s^{-1}\,Mpc^{-1}}$. Measurements from other methods such as gravitational lensing time delay were also carried out by the *H0LiCOW* collaboration (Bonvin et al., 2017) and provide $H_0 = 71.9^{+2.4}_{-3.0}\,\mathrm{km\,s^{-1}\,Mpc^{-1}}$.

Intriguingly, the *Planck* 2015 CMB results infer $H_0 = 67.51 \pm 0.64\,\mathrm{km\,s^{-1}\,Mpc^{-1}}$ (Ade et al., 2015d), given the joined temperature, polarisation and lensing spectra, a value which is even further decreased to $H_0 = 66.93 \pm 0.62\,\mathrm{km\,s^{-1}\,Mpc^{-1}}$, in the more recent analysis of (Aghanim et al., 2016b), updating the polarisation data but excluding lensing data from the constraint. The latter inferred measurement displays a tension with the value found by (Riess et al., 2018) at 3.7σ, while is in tension at 3.1σ with the result of (Cardona et al., 2017) (see Fig. 1.7 for an illustration). The final full-mission *Planck* analysis (Aghanim et al., 2018) finds $H_0 = 67.36 \pm 0.54\,\mathrm{km\,s^{-1}\,Mpc^{-1}}$, with a discrepancy at a level of 3.6σ with respect to the value of (Riess et al., 2018). Furthermore, large scale surveys also prove to be decisive with respect to such a determination. In particular, the recent *BOSS DR12* analysis provides $H_0 = 67.6 \pm 0.5\,\mathrm{km\,s^{-1}\,Mpc^{-1}}$, when combined with *Planck* (Alam et al., 2016), and *DES* yields $H_0 = 67.2^{+1.2}_{-1.0}\,\mathrm{km\,s^{-1}\,Mpc^{-1}}$, in combination with other BAO experiments but independently from CMB measurements (Abbott et al., 2017j). These also display tension with current local determinations of H_0. This discrepancy is still subject to current debate, as it could be an indicator of unresolved systematics as well as of new physics [see e.g. (Amendola et al., 2013; Bernal et al., 2016)], especially favorable for phantom dynamical dark energy as we will illustrate

later.

Future Galaxy Redshift Surveys and S4 CMB Experiments. Constraints from future ground-based surveys such as the *Square Kilometre Array* (*SKA*) (Dewdney et al., 2009; Yahya et al., 2015), the *The Large Synoptic Survey Telescope* (*LSST*) (LSST Science Collaboration et al., 2009), or the *Dark Energy Spectroscopic Instrument* (*DESI*) (Levi et al., 2013; DESI Collaboration et al., 2016a,b), but also from the space-based mission *Euclid* (Amendola et al., 2013), also prove to be of particular relevance. These missions will be able to observe tomographic galaxy clustering, cosmic shear and clusters counts which form complementary probes for collecting useful cosmological information, in particular on the expansion and structure formation history of the Universe. So-called ground-based CMB *Stage 4* (*S4*) experiments will also be deployed in the near future and will provide cosmological constraints from several probes such as CMB temperature and polarisation spectra, CMB lensing, SZ cluster number counts and other anisotropies (Abazajian et al., 2016).

1.3.9 The Importance of Future Gravitational Wave Experiments

A cosmological probe of a completely different nature than those discussed above, which has become very important recently, is provided by the measurement of GWs from compact binary mergers, or from the stochastic GW background in the Universe. Indeed, surveys probing the CMB, galaxy surveys, distant or close-by SNIa only allow to access cosmological or gravitational information through the detection of photons, i.e. light. Recently, the fantastic observations of the GWs from binary compact objects such as black-hole mergers by the *LIGO/Virgo* collaboration (Abbott et al., 2016a,b, 2017a,b,c), as well as from the binary neutron star merger GW170817 (Abbott et al., 2017i), together with its associated γ-ray burst (Goldstein et al., 2017; Savchenko et al., 2017; Abbott et al., 2017g), and the further studies of this electromagnetic counterpart (Abbott et al., 2017f), have opened the way for multi-messenger gravitational-wave astrophysics and cosmology. In particular, the latter measurement has allowed to put stringent constraints on the propagation speed of GWs, whose relative deviation from the speed of light is found to be of the order of 10^{-15} (Abbott et al., 2017g). In turn, such a constraint has significantly reduced the number of viable modified gravity theories (Creminelli and Vernizzi, 2017; Sakstein and Jain, 2017; Ezquiaga and Zumalacárregui, 2017; Baker et al., 2017). Moreover, as we will discuss in more details in Chapter 6, these experiments already allow one to extract information about the expansion history of the Universe. A reason for this is because binary mergers are *standard sirens* (Schutz, 1986, 2001; Holz and Hughes, 2005), which is the GW analogue of standard candles such as SNIa. Nowadays cosmological constraints still remain quite poor, as the number of detected objects and associated redshift range are quite restricted. However, with the appearance of next-generation ground-based GWs interferometers such as the *Einstein Telescope* (*ET*) (Sathyaprakash et al., 2012), the *Cosmic Explorer* (Abbott et al., 2017e), or the space-based *Laser Interferometer Space Antenna* (*LISA*) (Audley et al., 2017), which is expected to be launched in 2034, cosmological prospects appear much more optimistic. As we will see in Chapter 6, this not only allows to probe the expansion history of the Universe, but also potential features in the propagation of the GWs.

1.4 What is the Cause of Cosmic Acceleration?

As outlined above, until now, modelling the observed late time cosmic acceleration by a cosmological constant in Einstein's equations explains numbers of complementary cosmological

observations, without any well-established discrepancy. A straightforward conclusion to this fact could be that Λ is a new fundamental constant of nature, on the same footing than the Planck mass M_p, the Planck constant $\hbar$, the speed of light c, the elementary charge e, the electric vacuum permeability μ_0, etc. However, it is believed that this is not the case, as is suggested by several theoretical objections.

1.4.1 The Cosmological Constant Problem(s)

When viewed on the right hand side of Einstein's equations,

$$G_{\mu\nu} = 8\pi G\, T_{\mu\nu} - g_{\mu\nu}\Lambda\,, \tag{1.1}$$

the cosmological constant can be interpreted as the energy density of vacuum $T_{\mu\nu} = 0$, such as $T^{\rm vac}_{\mu\nu} \equiv -\Lambda/(8\pi G) g_{\mu\nu}$, so that $\rho_\Lambda = \Lambda/(8\pi G)$. In a quantum field theory on Minkowski space, e.g. for a massive scalar field, the "bare" vacuum energy density λ can be implemented as,

$$S[\phi] = \int \mathrm{d}^4x \left[\frac{1}{2}\phi\big(\Box - m^2\big)\phi - \lambda\right]. \tag{1.2}$$

Once quantised, vacuum fluctuations of the free field correct the bare vacuum energy density as [see e.g. (Maggiore, 2005)],

$$\lambda_{\rm corr} = \frac{1}{2}\int \frac{\mathrm{d}^3p}{(2\pi)^3} E_{\vec{p}}\,, \tag{1.3}$$

where $E_{\vec{p}} \equiv (\vec{p}^2 + m^2)^{1/2}$, which, once regularised by a ultraviolet cutoff $\lambda_{\rm cut}$, diverges as $\sim \lambda^4_{\rm cut}$, for large momenta. Such a correction arises from every single field of the SM, where the contributions from bosonic fields have the opposite sign than the ones from fermionic fields. On energy scales where the quantum theory of the SM has proven to agree well with observations, such as at the (conservative) electroweak scale $M_{\rm EW} \sim G_{\rm F}^{-1/2} \simeq 10^{11}\,\mathrm{eV}$, where $G_{\rm F}$ is the Fermi constant, this amounts to a correction of the order $\lambda_{\rm corr} \simeq 10^{44}\,\mathrm{eV}^4$, to the bare vacuum energy density λ. On the other hand, the vacuum energy density inferred from gravitational considerations, i.e. cosmological observations, is found to be of the order of $\rho_\Lambda \simeq 10^{-11}\,\mathrm{eV}^4$. This means that, if one promotes the vacuum energy density generated by quantum fields to the vacuum energy density of the semi-classical gravitational theory (where gravity can supposedly still be treated classically), i.e. for the renormalised values $\lambda^{\rm ren} \equiv \rho^{\rm ren}_\Lambda$, this amounts to fudge the bare vacuum energy λ to a number of digits of the order of 55, for reproducing the observed value of ρ_Λ. From an effective field theory point of view, this a *fine-tuning* problem, underlying the fact that the cosmological constant Λ is not *natural* under quantum corrections, in the sense of ('t Hooft, 1980). This is the essence of the *cosmological constant problem* [see e.g. (Weinberg, 1989, 2000; Padmanabhan, 2003; Peebles and Ratra, 2003; Carroll, 2003; Antoniadis et al., 2007; Bianchi and Rovelli, 2010)].

This problem is well-defined in the case where one believes that the vacuum energy induced by quantum fields on Minkowski space can readily be transported to cosmological scales without hindrance. However, such a consideration implies that the vacuum energy associated to λ gravitates, and in turn that the flat space solution for the metric $g_{\mu\nu} = \eta_{\mu\nu}$, is not the solution of interest any more but, in an idealised situation, would rather be of the de Sitter (or FLRW) type. In that framework, the associated quantum corrections are known to give raise to strong infrared instabilities, indicating the potential presence of relevant non-perturbative effects possibly altering the vacuum energy density in a non-trivial way [see e.g. (Antoniadis

and Mottola, 1991; Tsamis and Woodard, 1997; Antoniadis et al., 2007)][3]. The cosmological constant problem is therefore intimately related to our lack of understanding of the quantum theory of gravity, for which perturbative methods have been shown to provide only little reach for describing the overall quantum dynamics of GR.

Nevertheless, when taken at face value, the fine-tuning problem of the cosmological constant has been attempted to be solved in several ways. A notable example is provided by supersymmetric theories [see e.g. (Martin, 1997) for an introduction and (Fuks, 2013) for a review], in which each of the SM fields possesses a corresponding "superpartner" of different statistics, so that their contributions to the vacuum energy automatically cancel each other. Another example corresponds to the hypothesis assuming that gravity is asymptotically safe, that is, that the theory features a non-trivial UV fixed point, away from which associated quantum corrections are under control, and can effectively suppress the vacuum energy (Weinberg, 1980) [see also (Falls, 2016) for a more recent discussion]. This idea is effectively founded on the fact that non-perturbative effects regularise the quantum theory by themselves [see for example (Percacci, 2007) for a review].

Another related puzzle of the cosmological constant is that its small value leads to the *coincidence problem*, which can be stated as follows. Given the standard ΛCDM model, the present cosmological observations lead to an inferred value of the dark energy density fraction Ω_Λ of the order of $\Omega_\Lambda \simeq 0.7$, while the one associated to the total matter in the Universe today is inferred to be $\Omega_M \simeq 0.3$. This implies that, for reproducing nowadays cosmological observations, given the ΛCDM model, one should have $\Omega_\Lambda \sim \Omega_M$, which, as the total matter density fraction redshifts as $\sim a^{-3}$, is only the case in a "brief" moment of the cosmological history. This means that the model describes the present epoch as a special moment in the Universe's history, where the $\Omega_\Lambda \sim \Omega_M$–"coincidence" is satisfied. This goes against the cosmological principle stating that the Universe is homogeneous and isotropic in space and time on its largest scales, and therefore can be interpreted as problematic [see however (Bianchi and Rovelli, 2010) for an alternative view on this].

The smallness of Λ and its associated coincidence problem were shown to be possibly addressed by anthropic arguments, supporting the fact that if such conditions were not established, observers like us would never have been present for measuring these values (Weinberg, 1989; Efstathiou, 1995). In what follows, we will not consider how anthropic arguments can provide an explanation to the cosmological constant problem, but rather describe a selection of rigorous theoretical models that have been proposed over the years to address the issue, as this is also the framework of the study of this thesis.

1.4.2 Modelling Dark Energy by Evading Lovelock's Theorem

The search for an alternative to the cosmological constant Λ for describing the observed late time cosmic acceleration is a major topic in nowadays research in cosmology. Its origin goes back before the actual discovery of the cosmic acceleration, given the number of earlier analyses suggesting the need for a cosmological constant. In fact, the idea of modifying the cosmological "constant" by allowing it to vary in time was already mentioned in the 1930s in (Bronstein, 1933), for providing an explanation to the cosmic expansion based on assumed energy non-conservation processes induced in star nuclei. Since then, several phenomenological studies of such a smooth dark energy component producing an accelerated expansion were performed

3. Non-perturbative infrared renormalisation effects from gravitation fluctuations were recently shown to be non-trivial on flat space and in the framework of the so-called "variable gravity" (Wetterich, 2017).

[see for example (Steinhardt, 1996; Silveira and Waga, 1997; Turner and White, 1997; Hu and Eisenstein, 1999; Chevallier and Polarski, 2001; Linder, 2003)], and more concrete theoretical models have been put forward for potentially providing an explanation of its origin, and at the same time resolving the intrinsic problems associated to Λ.

Diverse ways for realising the late time cosmic acceleration without a cosmological constant exist, and a major part of them have a common tenet in that they evade the Lovelock theorem (Lovelock, 1971, 1972), which was developed on the earlier works of (Vermeil, 1917; Cartan, 1922; Weyl, 1922). This theorem states that the only covariantly conserved rank-two tensor including only derivatives of the metric $g_{\mu\nu}$ up to two in four dimensions is proportional to the Einstein tensor or to the metric itself, i.e. a cosmological constant. Modifying Einstein's theory of GR therefore amounts to either breaking diffeomorphism invariance, including higher derivatives of the metric or nonlocal operators acting on it, considering higher dimensions or introducing explicit extra degrees of freedom beside the two modes of the massless spin-two field described by the metric.

One might find useful to classify the various attempts to explain late time cosmic acceleration in theories that are describing a genuine dark energy component and those modifying Einstein's theory of GR, although a clear distinction between these two classes can sometimes be a subjective matter (Joyce et al., 2016). Reviews surveying different classes of models of dynamical dark energy are provided for instance in (Copeland et al., 2006; Padmanabhan, 2006; Silvestri and Trodden, 2009; Caldwell and Kamionkowski, 2009; Tsujikawa, 2010; Ruiz-Lapuente, 2010; Joyce et al., 2015) [see also (Amendola and Tsujikawa, 2010) for a standard textbook], whereas reviews on modifications of gravity relevant for late time cosmic acceleration are provided by e.g. (Nojiri and Odintsov, 2011; Clifton et al., 2012; Berti et al., 2015; Koyama, 2016).

Other alternative to explain the late time cosmic acceleration have also been proposed without the need of modifying GR or including additional species. Examples of them are given by a possible backreaction of inhomogeneities on the cosmological averaged background [see e.g. (Buchert and Räsänen, 2012) for a review], the variation of fundamental constants such as the fine-structure constant (Uzan, 2005, 2007), or the speed of light (Albrecht and Magueijo, 1999; Magueijo, 2003).

Scalar-Tensor Theories. Notable examples including extra degrees of freedom are most commonly represented by the presence of an additional minimally coupled canonical scalar field, generating the late time cosmic acceleration in rolling down its potential, much as cosmic inflation is driven by an inflaton field. This idea was already evoked in the late 1980s (Weiss, 1987; Ratra and Peebles, 1988; Wetterich, 1988) and is nowadays known as *quintessence* [see e.g. (Caldwell et al., 1998; Ferreira and Joyce, 1997, 1998; Copeland et al., 1998; Wang et al., 2000; Sahni and Starobinsky, 2000; Binetruy, 2000), (Tsujikawa, 2013) for a review and (Durrive et al., 2018) for recent observational constraints]. These models have been shown to be able to produce a tracker behavior (Zlatev et al., 1999), generating a dynamical dark energy density fraction $\Omega_{\rm de}(z)$ that reproduces the cosmic coincidence $\Omega_{\rm de} \sim \Omega_M$ at late time, for an extended range of initial conditions for the scalar field. Such theories provide a solution to the coincidence problem but typically translate the unnaturalness of Λ into the unnaturalness of the scalar fields' potential (Weinberg, 1989). Nevertheless, quintessence-like behavior in cosmic axion theories, i.e. effective models of pseudo-Nambu-Goldstone bosons, were also found (Coble et al., 1997), and represent a remarkable candidate evading the naturalness problem, as the potential they describe is symmetry-protected from large radiative corrections. Moreover, such soft modes can find a fundamental explanation in string theory (Choi, 2000; Kim and Nilles, 2003). Coupled

quintessence models where the scalar is coupled to matter fields were developed in (Amendola, 2000) [see in particular (Barros et al., 2018) for recent observational constraints considerations], and led to the concept of a coupled quintessence field controlling the amplitude of the neutrino mass and generating the late time cosmic acceleration (Fardon et al., 2004; Peccei, 2005; Wetterich, 2007; Amendola et al., 2008a). In the same spirit as quintessence, scalar field models with non-linear derivative self-interactions, dubbed K–essence, were developed in (Armendariz-Picon et al., 2001), and include in particular ghost condensates (Arkani-Hamed et al., 2004) or so-called Cuscuton models (Afshordi et al., 2007a,b). Alternatives to quintessence describing an "exotic" extra matter component as well for producing the late time cosmic acceleration are given by the so-called Chaplygin gas models, which have also been motivated by findings in string theories [see e.g. (Kamenshchik et al., 2001; Gorini et al., 2004)].

Scalar tensor theories also include particular modifications of the Einstein-Hilbert action where the corresponding Ricci curvature scalar is promoted to an arbitrary function of it, by an $f(R)$ term (Carroll et al., 2004, 2005; Song et al., 2007). This fact could appear quite counter intuitive at the first glance, but such theories can be shown to be equivalent to scalar-tenosr ones when certain conditions are satisfied [see e.g. (Sotiriou, 2006) and references therein].

These scalar-tensor models are particular classes of the more general scalar-tensor theory developed by G. Horndeski (Horndeski, 1974), which contains higher derivative terms into the action, but lead to equations of motion that are second order, such as to avoid the introduction of other additional degrees of freedom carrying an Ostrogradski ghost. Furthermore, a remarkable class of models belonging to this theory when linearised on flat space is provided by *Galileons*, where the scalar sector is characterised by an internal shift symmetry (Nicolis et al., 2009), and whose covariant generalisation (Deffayet et al., 2009; Deffayet et al., 2009, 2011), has been shown to be provide interesting self-accelerating solutions (Chow and Khoury, 2009; Gannouji and Sami, 2010; De Felice and Tsujikawa, 2010; Barreira et al., 2012). Horndeski theory has recently been generalised in theories going Beyond Horndeski (Gleyzes et al., 2015a), where the resulting equations of motion are found to be higher order, but a "kinetic degeneracy" in the model prevents the appearance of additional degrees of freedom. A further generalisation of Beyond Horndeski theories has been presented in (Langlois and Noui, 2016), which includes more general degenerate higher derivatives scalar-tensor theories. All these theories are included in the effective field theory of dark energy (Gleyzes et al., 2013, 2015b), whose construction is inspired by the effective field theory of inflation (Cheung et al., 2008).

Models based on an extra scalar degree-of-freedom typically give raise to a fifth force that need to be screened at small scales, in order to evade strong constraints from solar system experiments. Quintessence models where such a screening is explicitly realised are provided by chameleon models (Khoury and Weltman, 2004; Brax et al., 2004). In these models, the scalar field is non-minimally coupled to matter, so that it acquires a mass proportional to the local matter density, and its effect is screened in overdense regions. Another notable screening mechanism is realised in so-called symmetron models (Hinterbichler and Khoury, 2010; Hinterbichler et al., 2011), where the scalar field has a (non-)trivial vacuum expectation value in (under)overdense regions. This value controlling the coupling to matter, the fifth force induced by the scalar field is suppressed in high density regions. Moreover, screening induced by strong kinetic non-linearities of the scalar field induced by derivative self-interactions that become dominant in high density regions has also been shown to be present scalar-tensor theories (Babichev et al., 2009), though the so-called K–mouflage mechanism, equivalent to the Vainshtein mechanism in massive gravity (Vainshtein, 1972) (see the next paragraph for more details on this), that was also shown to be at play in Galileon models (Nicolis et al., 2009).

Massive Gravity and Bi-gravity. Another important example of attempts at explaining the late time accelerated expansion, and at the same time to solve the cosmological constant problem, is the theory of massive gravity [see (Hinterbichler, 2012; de Rham, 2014) for reviews]. In this theory, the graviton has a mass that makes the force mediated between two static sources of the Yukawa type, i.e. changing the behavior of the theory of GR in its infrared regime, and therefore possibly able to describe cosmic acceleration. Moreover, from a quantum field theoretical point of view, the mass of the graviton is expected to receive controlled quantum corrections as it is naturally protected by the diffeomorphism symmetry. The construction of this theory has received a lot of attention during the last decades. From a theoretical point of view, its origin goes back to 1939, when M. Fierz and W. Pauli (Pauli and Fierz, 1939) first elaborated a consistent theory describing a free massive spin-two field propagating over Minkowski space. The question asking whether or not it is possible to add nonlinear corrections to this model so as to construct a "massive GR", then arose quite naturally. In fact, in the early 1970s, it was shown by H. van Dam, M. Veltman, V.I. Zakharov (vDVZ) and Y. Isawaki (van Dam and Veltman, 1970; Zahkarov, 1970; Isawaki, 1970) that, once the spin-two field is coupled to a source, the massless limit of Fierz-Pauli's linear theory does not reproduce the initially massless one, i.e. linearised GR, and was consequently in disagreement with solar system observations. Nevertheless two years later, A.I. Vainshtein (Vainshtein, 1972) found a solution to this problem by showing that once kinetic nonlinear corrections are taken in consideration, they provide further information on the domain of validity of the linear approximation. In particular, Vainshtein showed that the more the graviton mass goes to zero, the more the space-time region where the approximation is valid shrinks. This therefore discredited the physical relevance of the vDVZ discontinuity and motivated further consideration of nonlinear corrections. Nevertheless, the same year, G. Boulware and S. Deser (Boulware and Deser, (1972) showed that once nonlinear corrections are included to the linear model over flat space, the theory generically ends up with an additional degree of freedom which is a ghost. The recent works of C. de Rham, G. Gabadadze and A. Tolley (de Rham and Gabadadze, 2010; de Rham et al., 2011), have shown that a healthy nonlinear model can be built through a perturbative approach in avoiding the Boulware-Deser ghost. Not much later, (Hassan and Rosen, 2012a) addressed the ghost issue at the non-perturbative level which allowed them to write down a consistent nonlinear theory of massive gravity. A quite artificial aspect of such a theory is that it requires the presence of an additional metric, a so-called non-dynamical "reference" metric, whose choice is arbitrary. However, one can consider that this metric is dynamical as well, and construct the theory of bi-metric massive gravity (Hassan and Rosen, 2012b). The cosmological consequences of these models where vastly investigated in the last years, and some of them where found to provide self accelerating solutions potentially able to explain the late time cosmic acceleration. We refer the reader to the relevant literature for details about the current status of these theories, to which a quite up-to-date detailed description can be found in e.g. (Hinterbichler, 2016).

Extra-dimensions. A particularly interesting model modifying the behavior of gravity on infrared scales is the Dvali-Gabadadze-Porrati (DGP) braneworld model (Dvali et al., 2000; Dvali and Gabadadze, 2001), which was shown to possess self-accelerating solutions (Deffayet, 2001; Deffayet et al., 2002). This model evades Lovelock's theorem in that it is defined on a spacetime of dimension higher than four, that is, gravity is taking place on a five-dimensional (bulk) spacetime and is in turn only induced on a four dimensional brane where the field of the SM are confined. Furthermore, the induced graviton propagator on the four dimensional brane signals the presence of nonlocal operators taking place in the theory. More details about the

model will be provided below [see Sec. 2.4].

This thesis incorporates itself in the framework of studies aiming to investigate alternative effects influencing the infrared behavior of gravity. In particular, we will consider nonlocal modifications to the theory of GR that can hypothetically be present in the associated quantum effective action, and be relevant for describing the observed late time cosmic acceleration. The following report closely follows the studies performed in (Dirian et al., 2014; Dirian and Mitsou, 2014; Dirian et al., 2015, 2016; Dirian, 2017; Bellini et al., 2018; Belgacem et al., 2018b, 2017, 2018c), but also contains original material. Modifications of gravity through the presence of nonlocal terms have recently attracted a lot of interest for modifying GR in its infrared regime. For a more detailed discussion of such models, we refer the reader to our Sec. 2.4.

1.5 Conventions & Notations

Here we report the notational conventions used throughout the thesis.

We work in the natural units : $\hbar = c = 1$, the Planck mass is denoted by M_p and Newton's constant as G. In these units, the Planck mass reads $M_p = 1.221 \times 10^{19}\,\text{GeV} \simeq 6.1870 \times 10^{34}\,\text{m}^{-1}$ and the Hubble scale is given by $H_0^{-1} \simeq 9.26 \times 10^{25} h^{-1}\,\text{m}$. Generically, megaparsecs convert to meters as $1\,\text{Mpc} \simeq 3.0857 \times 10^{22}\,\text{m}$ and the astromonical unit is $1\,\text{a.u.} \simeq 1.4960 \times 10^{11}\,\text{m}$.

We exclusively work in $3+1$ spacetime dimensions, where our conventions for differential geometric quantities are the same as the ones of the book of C. Misner, K. Thorne and J. Wheeler (Misner et al., 1973), so that the signature of the metric is taken to be $(-+++)$ and therefore the Minkowski metric is $\eta_{\mu\nu} = \text{diag}(-,+,+,+)$. The Greek indexes will run over $0,1,2,3$, while the Latin ones only over the spatial dimensions $1,2,3$, unless specified otherwise and we use the Einstein summation convention.

In a local coordinate system, the Christoffel symbols for the Levi-Civita connection are given by,

$$\Gamma^{\rho}_{\mu\nu} = \frac{1}{2} g^{\rho\sigma} (\partial_\mu g_{\nu\sigma} + \partial_\nu g_{\mu\sigma} - \partial_\sigma g_{\mu\nu})\,, \tag{1.4}$$

whereas the Riemann tensor takes the form,

$$R^{\alpha}{}_{\beta\mu\nu} = \partial_\mu \Gamma^{\alpha}{}_{\nu\beta} - \partial_\nu \Gamma^{\alpha}{}_{\mu\beta} + \Gamma^{\alpha}{}_{\mu\rho}\Gamma^{\rho}{}_{\nu\beta} - \Gamma^{\alpha}{}_{\nu\rho}\Gamma^{\rho}{}_{\mu\beta}\,.$$

The associated Ricci curvature tensor reads $R_{\beta\nu} = R^{\alpha}{}_{\beta\alpha\nu}$, the associated Ricci scalar is $R = g^{\mu\nu} R_{\mu\nu}$ and the corresponding Einstein tensor is,

$$G_{\mu\nu} = R_{\mu\nu} - \frac{1}{2} g_{\mu\nu} R\,. \tag{1.5}$$

We denote the curved spacetime d'Alembert operator as $\Box \equiv g^{\mu\nu}\nabla_\mu\nabla_\nu$, while the flat space spatial Laplacian is written as $\Delta \equiv \delta^{ij}\partial_i\partial_j$.

Our convention for the spacetime Fourier transformations follow,

$$f(x) = \int \frac{\mathrm{d}^4 k}{(2\pi)^4}\, e^{ikx} \tilde{f}(k)\,, \qquad \tilde{f}(k) = \int \mathrm{d}^4 x\; e^{-ikx} f(x)\,,$$

and therefore the spatial Fourier transform we adopt,

$$f(\vec{x}) = \int \frac{\mathrm{d}^3 k}{(2\pi)^3}\, e^{i\vec{k}\cdot\vec{x}} \tilde{f}(\vec{k})\,, \qquad \tilde{f}(k) = \int \mathrm{d}^3 x\; e^{-i\vec{k}\cdot\vec{x}} f(\vec{x})\,.$$

Chapter 2

Nonlocal Modifications to Gravity

We review basic concepts about nonlocal modifications to gravity and in particular, the modifications that are relevant for cosmology, i.e. modifying the theory in its infrared regime. We first introduce what is meant by "nonlocal" into our field theoretical framework and present related subtleties and caveats. We then introduce mechanisms which generate nonlocal corrections to the dynamics of GR from first principles, in a top-down approach, before to present various bottom-up proposals that have been made in a more phenomenological framework.

The concept of nonlocality is broad in physics and possesses different meanings depending on the framework that one addresses. Nonlocality in the present context applies to field theory and can be defined by the negation of the definition of a local field theory.
A classical field theory is *local* if its Lagrangian density $\mathcal{L}$ at a given spacetime coordinate x^μ is exclusively a functional of the fields and their derivatives (in finite number) at that coordinate.

As a consequence, nonlocal field theories are generically characterized by the presence of an infinite number of derivatives or non-polynominal operators in their Lagrangian.

2.1 Classically Induced Nonlocality: Open Systems

One of the simplest example of nonlocality that arises in classical field theory is well illustrated by a system of two coupled massive scalar fields, where one of them is integrated out in using its own equation of motion. Starting from the action,

$$S = \int \mathrm{d}^4x \, \left[\frac{1}{2}\phi\big(\Box - m_\phi^2\big)\phi + \frac{1}{2}\psi\big(\Box - m_\psi^2\big)\psi - \lambda\phi\psi\right], \tag{2.1}$$

one can derive the equation of motion for ψ which yields $\big(-\Box + m_\psi^2\big)\psi = -\lambda\phi$. Its solutions can generically be expressed as,

$$\psi(x) = \psi^{(h)}(x) - \lambda \int \mathrm{d}^4x' \; G_\psi(x - x')\phi(x')\,, \tag{2.2}$$

where $\psi^{(h)}$ is a homogeneous solution satisfying $\big(-\Box + m_\psi^2\big)\psi^{(h)} = 0$ and $G_\psi(x-x')$ characterizes a generic Green's function for the Klein-Gordon operator, i.e. respecting the condition,

$$\big(-\Box + m_\psi^2\big)G_\psi(x - x') = \delta(x - x')\,, \tag{2.3}$$

which can be solved in going to Fourier space,

$$\big((k^0)^2 - E_k^2\big)\tilde{G}_\psi(k) = -1, \tag{2.4}$$

where we have defined $E_k \equiv \sqrt{\vec{k}^2 + m^2}$. The solution is obtained by inverting the corresponding operator and applying the inverse Fourier transformation. This needs to be done in the sense of distributions since the denominator vanishes on-shell, i.e. it induces two simple poles at $\pm E_k$ once one integrates over k^0. The method consists in integrating the distribution over a closed contour in the complex plane, chosen so that it passes around the poles on the real axis. Equivalently, one can use the so-called $i\epsilon$ prescription during the inversion, amounting to shift the poles in various directions. The way one closes the half contour then depends on the sign of $x^0 - x'^0$. The contour is chosen to run clockwise into the lower plane when x'^0 is on the past lightcone of x^0 ($x^0 - x'^0 > 0$) and counterclockwise into the upper plane when x'^0 is on the future lightcone of x^0 ($x^0 - x'^0 < 0$) [see e.g. (Itzykson and Zuber, 1980)]. The three typical choices relevant for the present discussion are (see Fig. 2.1):

— $k^0 \longrightarrow k^0 + i\epsilon$: *retarded* Green's function $G(x - x') \equiv G_{ret}(x - x')$ vanishes for $x^0 < x'^0$.
— $k^0 \longrightarrow k^0 - i\epsilon$: *advanced* Green's function $G(x - x') \equiv G_{adv}(x - x')$ vanishes for $x^0 > x'^0$.
— $k^0 \longrightarrow (k^0)^2 + i\epsilon$: *Feynman* Green's function $G(x - x') \equiv G_F(x - x')$.

In particular they respect $G_{ret}(x - x') = G_{adv}(x' - x)$ and $G_F(x - x') = G_F(x' - x)$, so only the latter is symmetric. Their expressions can be written as,

$$G_{ret}(x - x') = \theta\big(x^0 - y^0\big) \int \frac{\mathrm{d}^3k}{(2\pi)^3} \frac{e^{i\vec{k}(\vec{x}-\vec{y})}}{E_k} \sin\big(E_k(x^0 - y^0)\big)\,, \tag{2.5}$$

$$G_{adv}(x - x') = -\theta\big(y^0 - x^0\big) \int \frac{\mathrm{d}^3k}{(2\pi)^3} \frac{e^{i\vec{k}(\vec{x}-\vec{y})}}{E_k} \sin\big(E_k(x^0 - y^0)\big)\,, \tag{2.6}$$

$$G_F(x - x') = \int \frac{\mathrm{d}^3k}{(2\pi)^3} \frac{1}{2E_k} \big(\theta(x^0 - y^0)e^{ik(x-y)} + \theta(y^0 - x^0)e^{-ik(x-y)}\big)\,, \tag{2.7}$$

and can be interpreted as the fact that the Feynman propagator evolves positive energies forward in time and negative ones backwards, while the retarded (advanced) propagator evolves both forward (backward) in time. The retarded Green's function implements causality at classical level and the Feynman one implements it at quantum level in the *in-out* formalism.
We are only interested in the classical evolution of the above system therefore we choose the Green's function to be of the retarded kind,

$$\psi(x) = \psi^{(h)}(x) - \lambda \int \mathrm{d}^4x'\; G_{\psi,ret}(x - x')\phi(x')\,, \tag{2.8}$$

with,

$$G_{\psi,ret}(x - x') = -\lim_{\epsilon\to 0^+} \int \frac{\mathrm{d}^4k}{(2\pi)^4} \frac{e^{ik(x-x')}}{(k^0 + i\epsilon)^2 - \vec{k}^2 - m_\psi^2}\,. \tag{2.9}$$

The initial conditions fix the fields' homogeneous solution and, together with the choice of Green's function, uniquely determines the solution. Inserting (2.8) into the action (2.1), it becomes,

$$S = \int \mathrm{d}^4x \left[\frac{1}{2}\phi(x)\big(\Box - m_\phi^2\big)\phi(x) + \frac{\lambda^2}{2}\phi(x) \int \mathrm{d}^4x'\; G_{\psi,ret}(x - x')\phi(x') - \frac{\lambda}{2}\psi^{(h)}(x)\phi(x)\right], \tag{2.10}$$

which is nonlocal in the sense defined above, i.e. the knowledge of the Lagrange density at a given event x^μ depends on the whole history of the field $\phi(x)$ in the past lightcone of that event.

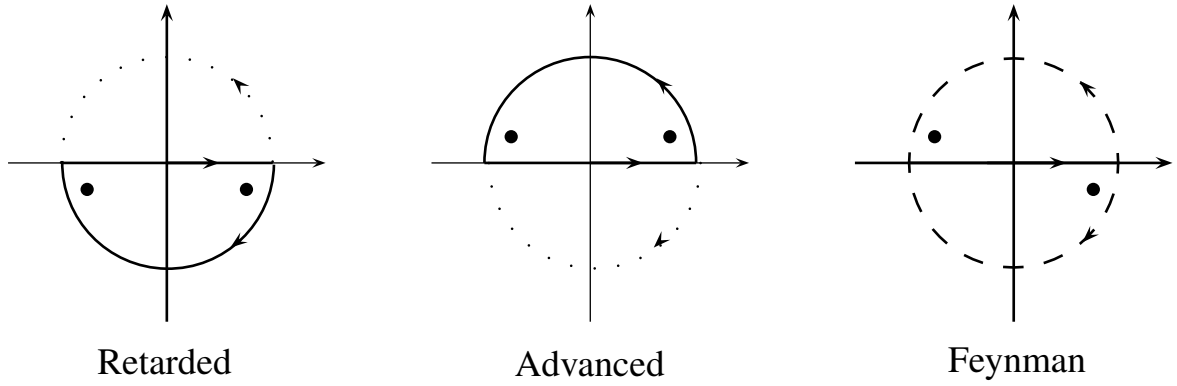

Figure 2.1 – Different prescriptions for solving Eq. (2.4). Axes represent the k_0 complex plane with the horizontal being real. Points are the poles at $\pm E_k$ shifted through the $i\epsilon$ prescription described in the text. In the case of the retarded (advanced) propagator only the lower (upper) half-contour contributes, whereas for the Feynman propagator both do contribute.

Despite of having enforced causality by choosing the retarded propagator when solving for ψ, this action does not lead to a causal behavior for the ϕ. Indeed, by computing its Euler-Lagrange equations of motion, under variation, the nonlocal term automatically symmetrises,

$$(\Box - m_\phi^2)\phi(x) + \frac{\lambda^2}{2}\int \mathrm{d}^4y \, \big[G_{\psi,ret}(x-y) + G_{\psi,adv}(x-y)\big]\phi(y) - \frac{\lambda}{2}\psi^{(h)}(x) = 0\,, \tag{2.11}$$

and the appearance of the advanced Green's function makes the classical evolution of ϕ acausal. At classical level, as the dynamics of the system is determined by the underlying Euler-Lagrange equations of motion, one could have inserted the solution for ψ (2.8), into the equation of motion for ϕ,

$$(\Box - m_\phi^2)\phi(x) = \lambda\psi\,, \tag{2.12}$$

so as to get a causal evolution for the latter. Nevertheless, for classical systems, a rigorous way of deriving such causal equations of motion from an action is given by the variational principle for non-conservative systems (Galley, 2013). At quantum level, the causal dynamics for the expectation values of quantum fields relates upon the use of the Schwinger-Keldysh, or *in-in*, formalism (Schwinger, 1961; Keldysh, 1964) closely related to the influence functional formalism of Feynman and Vernon (Feynman and Vernon, 1963) [see also (Jordan, 1986)]. The procedure outlined in (Galley, 2013), consists in doubling the degrees of freedom of the original theory $\{\phi, \psi\}$. One set will evolve forward in time, say $\{\phi_1, \psi_1\}$, while the second $\{\phi_2, \psi_2\}$ evolves

backwards. The action can be written,

$$S = \int_{-\infty}^{+\infty} \mathrm{d}x^0 \int \mathrm{d}^3x \left[\frac{1}{2}\phi_1(\Box - m_\phi^2)\phi_1 + \frac{1}{2}\psi_1(\Box - m_\psi^2)\psi_1 - \lambda\phi_1\psi_1\right] + \int_{+\infty}^{-\infty} \mathrm{d}x^0 \int \mathrm{d}^3x \left[\frac{1}{2}\phi_2(\Box - m_\phi^2)\phi_2 + \frac{1}{2}\psi_2(\Box - m_\psi^2)\psi_2 - \lambda\phi_2\psi_2\right] \tag{2.13}$$

$$= \int_{-\infty}^{+\infty} \mathrm{d}x^0 \int \mathrm{d}^3x \left[\frac{1}{2}\phi_1(\Box - m_\phi^2)\phi_1 + \frac{1}{2}\psi_1(\Box - m_\psi^2)\psi_1 - \frac{1}{2}\phi_2(\Box - m_\phi^2)\phi_2 - \frac{1}{2}\psi_2(\Box - m_\psi^2)\psi_2 - \lambda\phi_1\psi_1 + \lambda\phi_2\psi_2\right]. \tag{2.14}$$

where the initial conditions for the set $\{\phi_2, \psi_2\}$ is identified with the final ones of $\{\phi_1, \psi_1\}$ such that the action becomes an initial value problem rather than a boundary one. At the end of the computation, one applies the physical limit $\phi_{1,2} \to \phi$ and $\psi_{1,2} \to \psi$, to make contact with the original theory. At this point, it is convenient to introduce the variables defined by $\phi_\pm \equiv \phi_1 \pm \phi_2$ and $\psi_\pm \equiv \psi_1 \pm \psi_2$, for which the physical limit leads the "$-$" fields to vanish. Under this field redefinition the above action takes the form,

$$S = \int \mathrm{d}^4x \left[\frac{1}{2}\phi_-(\Box - m_\phi^2)\phi_+ + \frac{1}{2}\psi_-(\Box - m_\psi^2)\psi_+ - \frac{\lambda}{2}(\phi_+\psi_- + \phi_-\psi_+)\right]. \tag{2.15}$$

The equations of motion of $\phi_\pm$ and $\psi_\pm$ are respectively given by,

$$(\Box - m_\phi^2)\phi_\pm = \lambda\psi_\pm\,, \tag{2.16}$$

$$(\Box - m_\psi^2)\psi_\pm = \lambda\phi_\pm\,. \tag{2.17}$$

Now, according to the causality prescription required above, the "+" fields evolving forward in time are automatically solved with a retarded Green's function, while the "$-$" fields with an advanced one. One obtains,

$$\psi_+(x) = \psi_+^{(h)}(x) + \lambda \int \mathrm{d}^4x'\; G_{\psi,ret}(x - x')\phi_+(x')\,, \tag{2.18}$$

$$\psi_-(x) = \lambda \int \mathrm{d}^4x'\; G_{\psi,adv}(x - x')\phi_-(x')\,, \tag{2.19}$$

with,

$$\psi_+^{(h)}(x) = \int \frac{\mathrm{d}^4k}{(2\pi)^4}\left(a_{k,+}e^{-ikx} + a_{k,+}^* e^{ikx}\right)\theta(k^0)\delta(k^2 + m^2)\,. \tag{2.20}$$

where $a_{k,+}$ are complex numbers. Similar expression can be computed for $\phi_\pm$. The homogeneous solution for ψ_- is zero since the latter has to vanish at final time, as it equals $\psi_1 - \psi_2$. One can now put the corresponding expression of ψ_+ into the action (2.15),

$$S = \int \mathrm{d}^4x \left[\frac{1}{2}\phi_-(\Box - m_\phi^2)\phi_+ - \frac{\lambda}{2}\phi_-\psi_+^{(h)} - \frac{\lambda^2}{2}\int \mathrm{d}^4x'\phi_-(x)G_{\psi,ret}(x - x')\phi_+(x')\right]. \tag{2.21}$$

The equation of motion derived with respect to ϕ_- therefore leads to the effective equation of motion for the open subsystem composed only by ϕ_+,

$$(\Box - m_\phi^2)\phi(x) = \frac{\lambda}{2}\psi^{(h)}(x) + \lambda^2 \int \mathrm{d}^4x' G_{\psi,ret}(x - x')\phi(x'), \tag{2.22}$$

where the physical limit $\phi_+ \to 2\phi$ has been applied. This procedure justifies therefore unambiguously the use of the retarded Green's function in the resulting effective action and equation of motion. Moreover, this shows that the system made of ϕ only is non-conservative as it is non symmetric under time reversal, i.e. it is now an *open system* through which the dynamics of ψ only manifests itself in the nonlocal $G_{\psi,ret}$ operator, and its homogeneous solution $\psi^{(h)}$ that one can interpret as an external force (Galley, 2013). Observe that using such a technique can allow for the presence of friction terms of the form $\phi^+\partial_0\phi^-$ into the action, that in the usual case reduce to a total derivative $\phi\partial_0\phi \to \partial_0(\phi^2)/2$, and vanish under the integral.

This example shows how nonlocality can be obtained classically, by simply integrating out fields that are interacting with others. The resulting theory describes the non-conservative dynamics of the remaining subsystem, that is an "open" system. The evolution of the latter is nonlocal, i.e. the Lagrange density of the theory (or equivalently its equations of motion) at a given spacetime point x^μ depends on the fields' configuration on a finite patch of spacetime, not only on the infinitesimal neighborhood of x^μ. Using the variational principle for non-conservative systems, one can obtain the causal classical evolution of the corresponding subsystem. Observe also that turning all the Green's function in Eq. (2.11) to the retarded type, the causal equations of motion of Eq. (2.22) are recovered. This means that, instead of going through the machinery outlined here, one could just apply the standard variational principle and, at the end, turn all the Green's function appearing to be of the retarded kind. Such an *ad hoc* prescription has been extensively considered by various authors in nonlocal gravity studies [see e.g. (Soussa and Woodard, 2003; Tsamis and Woodard, 2014) and references therein].

2.2 Nonlocality Induced by Quantum Effects

Quantum corrections induced on the classical dynamics do also typically generate nonlocal operators, for example when massless or light degrees of freedom are integrated out, or also by quantum fluctuations of the vacuum on a curved spacetime. In this section, we review some basis of the quantum effective action on Minkowski spacetime and provide examples illustrating how nonlocal operators come into play in this context.

2.2.1 Effective Action

The quantum effective action encodes in principle all the information of a quantum field theory. It allows one to access a semi-classical expansion in quantum loops suppressed by powers of $\hbar$, providing back-reaction effects to the classical dynamics induced by quantum effects of perturbative [1] and non-perturbative nature [see e.g. (Itzykson and Zuber, 1980; Zinn-Justin, 2002) for standard textbooks]. These correct the classical dynamics of a given field theory characterised by an action $S[\phi]$; where we denote collectively by ϕ the various fields involved in the theory. This expansion is provided in a well controlled manner, as it includes only proper vertices, also called 1-particle irreducible (1PI) Feynman diagrams. This is especially relevant for computing how bare parameters are dressed up by quantum corrections. Its extrema correspond not to the classical solution as for the regular action $S[\phi]$, but to the evolution of the vacuum expectation values of the fields ϕ. Its definition relies on the functional path integral

1. The perturbative notion here refers to an expansion in the coupling constants of the theory.

formalism which is based on the generating functional of n-points Green's function,

$$Z[J] = \langle 0|T\exp\Big(-i\int \mathrm{d}^4x\ J(x)\phi(x)\Big)|0\rangle \tag{2.23}$$

$$= \int \mathcal{D}\phi\ \exp\Big(iS[\phi] - i\int \mathrm{d}^4x\ J(x)\phi(x)\Big)\,, \tag{2.24}$$

where the vacuum expectation value is taken between two asymptotic *in* and *out* Poincaré invariant vacua of the theory, $\langle 0|\phi|0\rangle \equiv \langle 0_{out}|\phi|0_{in}\rangle$. The T-operator orders the fields in decreasing time and is naturally implemented in the construction of the path integral. Within this framework, it is convenient to switch to imaginary time through Wick rotation $x^0 \to ix^0$, so that the metric becomes Euclidean and hyperbolic operators are turned into elliptic ones, which generically makes the problem more tractable. The generating functional then becomes,

$$Z[J] = \int \mathcal{D}\phi\ \exp\Big(-S[\phi] + \int \mathrm{d}^4x\ J(x)\phi(x)\Big)\,, \tag{2.25}$$

and generates the n-point Green's functions as,

$$Z[J=0]^{-1}\ \frac{\delta^N}{\delta J_1\delta J_2\ldots\delta J_N}Z[J]\Big|_{J=0} = \langle 0|T\big\{\phi_1\phi_2\ldots\phi_N\big\}|0\rangle\,, \tag{2.26}$$

where we use the shorthand notation $J_i \equiv J(x_i)$, $\phi_i \equiv \phi(x_i)$. The denominator in front removes the divergent vacuum-to-vacuum contributions (vacuum bubbles). Moreover, assuming an action that splits into a quadratic and an interacting part,

$$S[\phi] = \frac{1}{2}\phi_1 K_{12}\phi_2 + S_{int}(\phi)\,, \tag{2.27}$$

where we used the compact notation that we generalize throughout,

$$\phi_1 K_{12}\phi_2 \equiv \int \mathrm{d}^4x_1 \int \mathrm{d}^4x_2\ \phi(x_1)K(x_1,x_2)\phi(x_2)\,, \tag{2.28}$$

with $K(x_1,x_2)$ a local operator that does not depend on the fields, the generating functional can be written as,

$$Z[J] = \int \mathcal{D}\phi\ \exp\Big(-\frac{1}{2}\phi_1 K_{12}\phi_2 - S_{int}(\phi) + J_1\phi_1\Big) \tag{2.29}$$

$$= \int \mathcal{D}\phi\ \sum_{k=0}^{\infty}\frac{\big(-S_{int}(\phi)\big)^k}{k!}\exp\Big(-\frac{1}{2}\phi_1 K_{12}\phi_2 + J_1\phi_1\Big) \tag{2.30}$$

$$= \int \mathcal{D}\phi\ \sum_{k=0}^{\infty}\frac{\big(-S_{int}(\delta/\delta J)\big)^k}{k!}\exp\Big(-\frac{1}{2}\phi_1 K_{12}\phi_2 + J_1\phi_1\Big) \tag{2.31}$$

and dragging the infinite sum outside of the integral,

$$Z[J] = \sum_{k=0}^{\infty}\frac{\big(-S_{int}(\delta/\delta J)\big)^k}{k!}\int \mathcal{D}\phi\ \exp\Big(-\frac{1}{2}\phi_1 K_{12}\phi_2 + J_1\phi_1\Big) \tag{2.32}$$

$$\equiv \exp\Big(-S_{int}\Big(\frac{\delta}{\delta J}\Big)\Big)Z_0[J]\,. \tag{2.33}$$

The first exponential term is only a formal notation and should be rather seen as its infinite power series. We have also defined the Gaussian integral $Z_0[J]$, which can be evaluated by shifting ϕ by its saddle point value at $\phi_1 = K_{12}^{-1} J_2 \equiv \Delta_{12} J_2$, that is, by substituting $\phi_1 \to \phi_1 + \Delta_{12} J_2$, where Δ_{12} is the *free propagator* taken to be of the Feynman type. One gets,

$$Z_0[J] = \int \mathcal{D}\phi \ \exp\Big(-\frac{1}{2}\phi_1 K_{12}\phi_2 + \frac{1}{2} J_1 \Delta_{12} J_2 \Big) \tag{2.34}$$

$$= \big(\det K\big)^{-1/2} \ e^{\frac{1}{2} J_1 \Delta_{12} J_2} \tag{2.35}$$

where the irrelevant (although infinite) normalisation factor can be dropped in imposing $Z_0[J = 0] = 1$. Finally we can rewrite the generating functional in the compact form,

$$Z[J] = e^{-S_{int}\left(\delta/\delta J\right)} e^{\frac{1}{2} J_1 \Delta_{12} J_2} \,. \tag{2.36}$$

From this expression, one can access to a systematic perturbative expansion in powers of the coupling constant of the theory once the interacting action S_{int} is specified. Considering a given number n of external fields, through the n-point Green's function (2.26), one can then easily access its perturbative expression through an expansion which represents itself nicely in terms of Feynman diagrams. This functional still contains disconnected contributions (where the external points are not linked by propagators) which can be removed by defining the generating functional of the connected n-point Green's function,

$$W[J] = \log Z[J] \,, \tag{2.37}$$

with,

$$\frac{\delta^N}{\delta J_1 \delta J_2 \dots \delta J_N} W[J]\bigg|_{J=0} = \langle 0|T\phi_1\phi_2 \dots \phi_N|0\rangle_c \,, \tag{2.38}$$

and in particular,

$$\frac{\delta W[J]}{\delta J(x)}\bigg|_{J=0} = \langle 0|\phi(x)|0\rangle \equiv \langle \phi(x)\rangle \,, \tag{2.39}$$

is the vacuum expectation value of ϕ in the full theory. The generating functional of proper vertices we are interested in is defined as the Legendre transform of $W[J]$,

$$\Gamma[\varphi] = \int \mathrm{d}^4x \ J(x)\varphi(x) - W\big[J[\varphi]\big] \,, \quad \text{with} \quad \frac{\delta\Gamma}{\delta\varphi(x)} = J(x) \,, \quad \text{and} \quad \frac{\delta W}{\delta J(x)} = \varphi(x) \,, \tag{2.40}$$

One notes that $\varphi(x)|_{J=0} = \langle\phi(x)\rangle$. The generating functional Γ can be treated perturbatively in powers of $\hbar$. A convenient way for deriving it consists in applying the background field method which leads to an implicit expression for Γ, that can then be solved iteratively in the number of φ-derivatives acting on Γ. From the definition of $W[J]$ [2],

$$e^{\frac{1}{\hbar}W[J]} = \int \mathcal{D}\phi \ e^{-\frac{1}{\hbar}\left(S[\phi] - J\phi\right)} \,, \tag{2.41}$$

and multiplying both sides by $e^{-J\varphi}$ and using Eq. (2.40) yields,

$$e^{-\frac{1}{\hbar}\Gamma[\varphi]} = \int \mathcal{D}\phi \ \exp\bigg(-\frac{1}{\hbar}\big(S[\phi] - \frac{\delta\Gamma}{\delta\varphi}(\phi - \varphi)\big)\bigg) \,. \tag{2.42}$$

2. From now on until the end of this section we display $\hbar$.

Performing the saddle point approximation,

$$\left.\frac{\delta S[\phi]}{\delta\phi}\right|_{\phi=\phi_c} = \frac{\delta\Gamma[\varphi]}{\delta\varphi} \tag{2.43}$$

and expanding the exponent in the integrand around that solution $\phi \to \phi_c + \hbar^{1/2}\phi$, leads to,

$$\begin{aligned}\Gamma[\varphi] = S[\phi_c] - \frac{\delta\Gamma}{\delta\varphi}(\phi_c - \varphi) \\ - \hbar \log\left[\int \mathcal{D}\phi \ \exp\left(-\frac{1}{2}S^{(2),\phi_c}_{12}\phi_1\phi_2\right)\left(1 - \frac{\hbar}{3!}S^{(3),\phi_c}_{123}\phi_1\phi_2\phi_3 + \mathcal{O}(\hbar)\right)\right],\end{aligned} \tag{2.44}$$

where we have written,

$$S^{(N),\phi_c}_{12\ldots N} \equiv \frac{\delta^{(N)}S[\phi_c]}{\delta\phi_1\phi_2\ldots\phi_N}\,. \tag{2.45}$$

Solving then perturbatively for ϕ_c in terms of φ from the saddle point expansion in Eq. (2.37), using the last relation of Eq. (2.40) and working recursively on the derivatives of Γ leads to the generating functional of proper vertices,

$$\Gamma[\varphi] = S[\varphi] + \frac{\hbar}{2}\ \mathrm{Tr}\log\left[\frac{S^{(2),\varphi}}{S^{(2),0}}\right] + \frac{\hbar^2}{8}$$

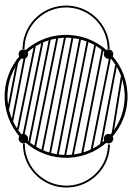

$$- \frac{\hbar^2}{12}$$

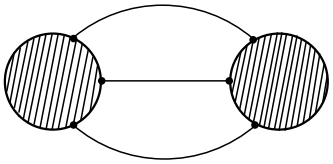

$$+ \mathcal{O}(\hbar^3)\,, \tag{2.46}$$

with,

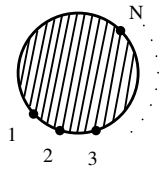

$$= S^{(N),\varphi}_{12\ldots N}\,, \qquad \text{and} \qquad$$

$$= \Delta^{\varphi}_{12} \equiv \left(S^{(2),\varphi}_{12}\right)^{-1}, \tag{2.47}$$

and where the division by $S^{(2),0}$ is equivalent to normal ordering, i.e. cancels the divergent contribution from vacuum energy. $\Gamma[\varphi]$ is sometimes called the quantum effective action, as it corrects the classical dynamics given by the action S by quantum effects. This expansion generically contains a finite part and a part that diverges in the ultraviolet regime (UV), at every loop order. Furthermore, if the theory contains massless fields, it also diverges in the infrared (IR). The UV divergences need to be regularized by counter-terms introduced in the original "bare" action, while the IR ones can sometimes by cured at the level of scattering amplitudes in including inelastic processes (as for instance bremsstrahlung in the case of Coulomb scattering) or can signal the presence of new physics as in QCD. Regularisation methods are for instance provided by lattice, dimensional or Pauli-Villars regularisation, or also Schwinger proper time and zeta regularisation. Finite parts with operator structure already present in S rescale the corresponding bare parameters and fields of the theory, they provide an energy scale dependence to the renormalised parameters which therefore run as this energy scale is modified. Other operators can be generated as well, together with their associated couplings and divergences, new terms should then be added to the classical action for curing the latter. Theories in which all divergences can be cured with a finite number of regulated operators are renormalisable.

We now illustrate by an example how new operators in a theory can be generated by quantum corrections, and in particular, that these operators can be nonlocal, i.e. susceptible of modifying the behavior of the theory in both its UV and IR regime. In the latter case, they are therefore relevant within a cosmological context.

2.2.2 Vacuum Polarisation Effects

Vacuum Induced Quantum Corrections to Light

In the framework of Quantum Electrodynamics (QED), the effective theory of a classical electromagnetic field interacting with vacuum quantum fluctuations of the electron-positron field via pair production, i.e. by taking into account the polarisability of the vacuum, is provided by the Euler-Heisenberg theory (Heisenberg and Euler, 1936). It can be obtained in computing the effective action for a classical electromagnetic field interacting with fermionic loops as we outline below. The generating functional for QED is given by,

$$Z[j,\eta,\bar{\eta}] = \int \mathcal{D}A_\mu \mathcal{D}\psi \mathcal{D}\bar{\psi}\ \exp\left[i \int \mathrm{d}^4x\ \left(-\frac{1}{4}F^{\mu\nu}F_{\mu\nu} + \bar{\psi}\big(i\not{D} - m\big)\psi - j_\mu A^\mu - i\bar{\eta}\psi - \eta\bar{\psi}\right)\right], \tag{2.48}$$

where $\not{D} \equiv \gamma^\mu(\partial_\mu - ieA_\mu)$, η and $\bar{\eta}$ are Grassmann numbers, and the gauge fixing term has been omitted since it is irrelevant for the present discussion. As we are interested in the dynamics of A_μ only, we consider rather the case where the fermionic sources are put to zero, $\eta = \bar{\eta} = 0$. In that case, the integral over ψ and $\bar{\psi}$ is Gaussian and can be carried out explicitly leading to,

$$Z[j,\eta=0,\bar{\eta}=0] = \int \mathcal{D}A_\mu\ \exp\left(iS_{\text{eff}}[A_\mu] - i\int \mathrm{d}^4x\ j_\mu A^\mu\right), \tag{2.49}$$

where,

$$S_{\text{eff}}[A_\mu] = \int \mathrm{d}^4x\ \left[-\frac{1}{4}F^{\mu\nu}F_{\mu\nu}\right] - i\,\mathrm{Tr}\log\left(\frac{i\not{D} - m}{i\not{\partial} - m}\right). \tag{2.50}$$

Observe that this action is a truncation of the quantum effective action (2.46) at one-loop order, where the fermions external legs have been removed because of the absence of fermionic sources. In the case one is interested in the low-energy regime of the theory, that is, when the energy of the electromagnetic field is much lower than the mass of the fermions, this one-loop effective action reduced to the Wilson effective action. Expanding up to quadratic order in the fields one gets [see e.g. (Parker, 1985; Dalvit and Mazzitelli, 1994; Dobado and Maroto, 1999)],

$$S_{\text{eff}}[A_\mu] = \int \mathrm{d}^4x\ \left[-\frac{1}{4}F^{\mu\nu}\left(1 + \frac{e^2(\Box)}{8\pi^2}\right)F_{\mu\nu} + \mathcal{O}(F^4)\right], \tag{2.51}$$

where,

$$e^2(\Box) = e^2(\mu)\int_0^1 (1-t^2)\log\left[\frac{m^2 - (1-t^2)\Box/4}{\mu^2}\right], \tag{2.52}$$

with μ the renormalisation scale, $e(\mu)$ the associated renormalised charge and we recognise the running of the coupling constant. The form factor induced by quantum averaging is nonlocal, as it is non-polynomial in the d'Alembert differential operator. Considering the UV regime,

where the mass of the fermions are light with respect to the typical energy scale, i.e. $m^2 \ll -\Box$, it becomes,

$$e^2(\Box) = 1 - \frac{e^2(\mu)}{12\pi^2} \log\left(\frac{-\Box}{\mu^2}\right), \tag{2.53}$$

where the log of the d'Alembertian is defined as,

$$\log\left(\frac{-\Box}{\mu^2}\right) = \int_0^\infty \mathrm{d}m^2 \left[\frac{1}{m^2+\mu^2} - \frac{1}{m^2-\Box}\right]. \tag{2.54}$$

This shows how vacuum fluctuation of light fields leads to the presence of nonlocalities arising in the corresponding form factors, due to the presence of particle creation. By taking the opposite low-energy limit where the fermionic mass is assumed to be large $m^2 \gg -\Box$, the form factor becomes an infinite series of local terms,

$$e^2(\Box) \simeq 1 + \frac{4\,e^2(\mu)}{15(4\pi)^2}\frac{\Box}{m^2}, \tag{2.55}$$

reflecting the decoupling of heavier particles, as stated by the Appelquist-Carazzone theorem (Appelquist and Carazzone, 1975) [3]. Adding higher order terms in the effective action (2.51) in that regime leads to the Euler-Heisenberg effective action to second order in e^2,

$$S_{\text{eff}}[A_\mu] = \int \mathrm{d}^4x \left[-\frac{1}{4}F^{\mu\nu}F_{\mu\nu} - \frac{e^2(\mu)}{15(4\pi)^2}\frac{1}{m^2}F^{\mu\nu}\Box F_{\mu\nu} \right. \tag{2.56}$$

$$\left. \frac{e^4(\mu)}{90(4\pi)^2}\frac{1}{m^4}\left(\left(F^{\mu\nu}F_{\mu\nu}\right)^2 + \frac{7}{4}(F^{\mu\nu}\tilde{F}_{\mu\nu})^2\right)\right], \tag{2.57}$$

where $\tilde{F}^{\mu\nu} \equiv \epsilon^{\mu\nu\alpha\beta}F_{\alpha\beta}/2$ is the Hodge dual of the Maxwell stress tensor.

As we shall outline next, similar effects arise when one considers the response of a classical gravitational field to quantum vacuum fluctuations of a quantised massive scalar field.

Vacuum-induced Quantum Corrections to Gravity

In a similar spirit as in the above example, when treated perturbatively, quantum fluctuations of the metric and of any matter field on curved spacetime induce higher order curvature invariants such as $R^2, R_{\mu\nu}R^{\mu\nu}, \ldots$, to the Einstein-Hilbert action (Stelle, 1978; Barvinsky and Vilkovisky, 1990). Such higher-derivative corrections indicate the presence of an Ostrograsky ghost (Ostrogradsky, 1850), which consequently ruins the unitarity of the theory at perturbative level. However, this ghost has mass of the order of the Planck mass M_p, so that it is sensible to use the resulting theory as a low energy effective field theory with UV cutoff $\Lambda = M_p$. However when considered in such regimes, quantum gravitational effects induced by these local operators are generically very small [see e.g. (Donoghue, 1994)]. Above that scale the theory requires an appropriate UV completion.

The same semi-classical procedure as in the above QED example can be applied in the case of a massive scalar field evolving on a curved background [see e.g. (Birrell and Davies,

3. In this case, the decoupling of heavy particles is explicit in the mass-dependent subtraction scheme (Manohar, 1997).

1984; Buchbinder et al., 1992; Mukhanov and Winitzki, 2007) for standard textbooks, see also (Barvinsky and Mukhanov, 2002)],

$$S_M[\phi] = -\frac{1}{2}\int \mathrm{d}^4x\sqrt{-g}\,\left[g^{\mu\nu}\partial_\mu\phi\partial_\nu\phi + m^2\phi^2 + \xi R\phi^2\right], \tag{2.58}$$

where ξ is a dimensionless constant for which the value $\xi = 1/6$, makes the coupling conformal, i.e. the overall action becomes conformally invariant when the mass is set to zero. The relevant generating functional in that case reads,

$$Z[J] = \int \mathcal{D}g_{\mu\nu}\mathcal{D}\phi\ \exp\!\left[i\int \mathrm{d}^4x\sqrt{-g}\left(\frac{1}{16\pi G}\big(R-2\Lambda\big) + \frac{1}{2}\phi\big(\Box - m^2 - \xi R\big)\phi - iJ^{\mu\nu}g_{\mu\nu}\right)\right],$$

and the classical evolution is given by,

$$R_{\mu\nu} - \frac{1}{2}g_{\mu\nu}R + g_{\mu\nu}\Lambda = 8\pi G\, T_{\mu\nu}\,, \tag{2.59}$$

where,

$$T_{\mu\nu}(x) = -\frac{2}{\sqrt{-g}}\frac{\delta S_M}{\delta g^{\mu\nu}(x)}\,. \tag{2.60}$$

Carrying the integration over the Gaussian functional integral leads to the effective action,

$$S_{\text{eff}}[g_{\mu\nu}] = \frac{1}{16\pi G}\int \mathrm{d}^4x\sqrt{-g}\,\big(R-2\Lambda\big) + \frac{i}{2}\,\mathrm{Tr}\log\big(\Box - m^2 - \xi R\big)\,. \tag{2.61}$$

Defining,

$$\Gamma^{(1)}[g_{\mu\nu}] \equiv \frac{1}{2}\,\mathrm{Tr}\log\big(\Box - m^2 - \xi R\big)\,, \tag{2.62}$$

we can write,

$$e^{i\Gamma^{(1)}[g_{\mu\nu}]} = \int \mathcal{D}\phi\ \exp\big(iS_M[\phi]\big)\,,$$

from which one can derive,

$$-\frac{2}{\sqrt{-g}}\frac{\delta\Gamma^{(1)}}{\delta g^{\mu\nu}(x)} = -\frac{2}{\sqrt{-g}}\frac{\int\mathcal{D}\phi\ \big[\delta S_M/\delta g^{\mu\nu}(x)\big]\exp\big(iS_M[\phi]\big)}{\int\mathcal{D}\phi\ \exp\big(iS_M[\phi]\big)}\,, \tag{2.63}$$

$$= \frac{\int\mathcal{D}\phi\ T_{\mu\nu}(x)\ \exp\big(iS_M[\phi]\big)}{\int\mathcal{D}\phi\ \exp\big(iS_M[\phi]\big)}\,, \tag{2.64}$$

$$= \frac{\langle 0,\mathrm{out}|\,T_{\mu\nu}(x)|0,\mathrm{in}\rangle}{\langle 0,\mathrm{out}|0,\mathrm{in}\rangle} \equiv \langle T_{\mu\nu}(x)\rangle_{\mathrm{in-out}}\,. \tag{2.65}$$

Observe that here the computation is done in the context of the in-out formalism, appropriate for computing scattering amplitudes. This typically leads to a complex vacuum expectation value for the energy momentum tensor $\langle T_{\mu\nu}\rangle_{\mathrm{in-out}}$ and therefore does not make much sense once it enters into Einsteins' equations. Instead, for obtaining a real vacuum expectation value, the correct formalism to use is rather the in-in or closed time path formalism already mentioned in Sec. 2.1. In this framework, the Feynman Green's functions are turned into retarded ones

making the overall evolution of the system causal [4]. In such a framework, Eq. (2.61) leads to a semi-classical dynamics for the metric,

$$R_{\mu\nu} - \frac{1}{2}g_{\mu\nu}R + g_{\mu\nu}\Lambda = 8\pi G \left\langle T_{\mu\nu} \right\rangle_{\text{in}-\text{in}} , \tag{2.66}$$

The computation of the one-loop vacuum effective action $\Gamma^{(1)}$ can be done using the Schwinger-De Witt heat kernel technique [see e.g. Ref. (Vassilevich, 2003) for a review] and the finite part of the resulting one-loop contribution takes the form (Avramidi, 1986; Barvinsky and Vilkovisky, 1987; Gorbar and Shapiro, 2003a; Codello and Jain, 2016),

$$\begin{aligned}\Gamma^{(1)} = &- \frac{1}{2(4\pi)^2}\int \mathrm{d}^4x\sqrt{-g}\left\{\frac{m^4}{2}\left[\log\left(\frac{4\pi\mu^2}{m^2}\right)+\frac{3}{2}\right] + m^2\left(\xi-\frac{1}{6}\right)\left[\log\left(\frac{4\pi\mu^2}{m^2}\right)+1\right]R \right.\\ &\left. + C_{\mu\nu\rho\sigma}\left[\frac{1}{60}\log\left(\frac{4\pi\mu^2}{m^2}\right)+k_W(\Box)\right]C^{\mu\nu\rho\sigma} + R\left[\frac{1}{2}\left(\xi-\frac{1}{6}\right)^2\log\left(\frac{4\pi\mu^2}{m^2}\right)+k_R(\Box)\right]R\right\}.\end{aligned}$$

where the form factors $k_{W,R}$ are nonlocal and have quite complicated expressions that we do not report here, but can be found for instance in (Gorbar and Shapiro, 2003a). In the same limits as those considered in the above QED example, the form factors acquire similar structures. In the case where the scalar is massless $m = 0$, the form factors recombine with the finite parts and read,

$$k_W(\Box) = -\frac{1}{60}\log\left(\frac{-\Box}{4\pi\mu^2}\right), \qquad k_R(\Box) = -\frac{1}{2}\left(\xi-\frac{1}{6}\right)^2\log\left(\frac{-\Box}{4\pi\mu^2}\right), \tag{2.67}$$

while at finite mass but still in the UV regime $-\Box \gg m^2$, they take the form (Codello and Jain, 2016),

$$k_{W,R}(\Box) \sim a_1\log\left(\frac{-\Box}{m^2}\right) + a_2\left(\frac{m^2}{-\Box}\right) + a_3\left(\frac{m^2}{-\Box}\right)\log\left(\frac{-\Box}{m^2}\right) + a_4\left(\frac{m^2}{-\Box}\right)^2 + \dots \tag{2.68}$$

where the a_i's are real numbers. At low energies one also finds the expected higher derivative structure,

$$k_W(\Box) \sim k_R(\Box) \sim \frac{-\Box}{m^2}\,. \tag{2.69}$$

The same kind of corrections are also observed for massive spinor and vector fields (Gorbar and Shapiro, 2003b). These quantum induced corrections are suppressed by the Planck scale M_p^2 in the effective action, therefore they are expected to be irrelevant in the late-time cosmological context were the typical energy scale of the Universe is much lower, $H_0 \sim 10^{-61}M_p$. However, at early time when the Universe was energetic enough, for instance in the course of an inflationary period, these corrections can have significant effects on the expansion rate (Espriu et al., 2005).

One can conclude that gravitational corrections induced by quantum fluctuations of massive fields have generically a nonlocal structure. In the high energy limit with respect to the masses of the particles at play, such corrections involve non-polynomial derivative operators, characterising a genuine nonlocality, induced by long distance propagation of light particle in loop processes. In the opposite low energy limit, the decoupling of heavy massive particles

4. Note that the use of such a formalism necessitates also to introduce an extra correction to the measure of the generating functionals' integral, so as to guarantee a correct unitary, real and causal evolution of the system (DeWitt, 1967).

leads to an infinite series of higher-order derivative (local) terms suppressed by powers of m^2. The structure of the form factors in either cases is very similar to that in QED, when quantum fluctuations of the electron-positron field correct the classical dynamics of an interaction electromagnetic field.

However, being suppressed by powers of the Planck mass M_p, they become relevant only close to that scale, where perturbative methods break down as well. These effects are therefore of none cosmological relevance and cannot be linked to dark energy physics. As we outline below, another semi-classical effect induced by quantum corrections to the classical gravitational dynamics giving raise to nonlocalities is provided by the conformal anomaly.

2.2.3 Conformal Anomaly

According to Noether's theorem, any symmetry generator gives raise to a conserved current. When a theory is globally invariant under coordinate dilatation $x^\mu \to e^\alpha x^\mu$, the conservation of the current $j^\mu_D = x_\mu T^{\mu\nu}$ implies the vanishing of the trace of the energy-momentum tensor of the theory, $T^\mu_\mu = 0$,[5]. In the presence of a curved background, vacuum quantum fluctuations induce the so-called conformal anomaly, i.e. finite quantum corrections to the trace of the vacuum expectation value of the renormalised energy-momentum tensor break the conformal symmetry (Capper and Duff, 1974). Such an anomaly carries information about the nonlocal structure of the gravitational effective action and, in particular, about the quantum corrected dynamics of its conformal sector.

In computing vacuum fluctuations of a massless, conformally coupled scalar field [Eq. (2.58) with $m = 0$, $\xi = 1/6$], the divergence one needs to cure into the renormalised effective action reads [see e.g. (Deser et al., 1976; Birrell and Davies, 1984; Riegert, 1984; Barvinsky et al., 1995) for derivations],

$$\Gamma^{(1)}_{\rm div} = \frac{1}{2}(4\pi)^{-(4-\epsilon)/2}\left(\frac{\mu}{m}\right)^\epsilon \Gamma\left(\frac{2}{\epsilon}\right)\int {\rm d}^{4-\epsilon}x\sqrt{-g}\,\left(\frac{1}{120}C^2 - \frac{1}{360}E\right), \tag{2.70}$$

in using dimensional regularisation, where,

$$\Gamma\left(\frac{2}{\epsilon}\right) = \frac{2}{\epsilon} - \gamma_E + \mathcal{O}(\epsilon)\,, \tag{2.71}$$

with $\gamma_E \simeq 0.577$ the Euler-Mascheroni constant, E is the Gauss-Bonnet term,

$$E \equiv R_{\mu\nu\rho\sigma}R^{\mu\nu\rho\sigma} - 4R_{\mu\nu}R^{\mu\nu} + R^2\,, \tag{2.72}$$

and C^2 the square of the Weyl tensor,

$$C^2 \equiv R_{\mu\nu\rho\sigma}R^{\mu\nu\rho\sigma} - 2R_{\mu\nu}R^{\mu\nu} + \frac{1}{3}R^2\,. \tag{2.73}$$

Computing the corresponding energy-momentun tensor and using the relations,

$$-\frac{2}{\sqrt{-g}}g^{\mu\nu}\frac{\delta}{\delta g^{\mu\nu}}\int {\rm d}^{4-\epsilon}x\sqrt{-g}\;C^{\mu\nu\rho\sigma}C_{\mu\nu\rho\sigma} = -\epsilon\left(C^{\mu\nu\rho\sigma}C_{\mu\nu\rho\sigma} - \frac{2}{3}\Box R\right), \tag{2.74}$$

$$-\frac{2}{\sqrt{-g}}g^{\mu\nu}\frac{\delta}{\delta g^{\mu\nu}}\int {\rm d}^{4-\epsilon}x\sqrt{-g}\;E = -\epsilon E\,, \tag{2.75}$$

5. Subtleties associated to the construction of such a current can be understood in solving the QED example in Ex. 3.4 of (Maggiore, 2005).

the divergent contribution to the vacuum expectation value of the energy-momentum tensor becomes finite as $\epsilon \to 0$,

$$\langle T^{\mu}_{\mu} \rangle_{\rm div} = -\frac{2}{\sqrt{-g}} g^{\mu\nu} \frac{\delta \Gamma^{(1)}_{\rm div}}{\delta g^{\mu\nu}} \tag{2.76}$$

$$= -\frac{1}{(4\pi)^2} \left[\frac{1}{120} \left(C^2 - \frac{2}{3} \Box R \right) - \frac{1}{360} E \right], \tag{2.77}$$

and therefore the renormalised counterpart acquires a non-vanishing trace $\langle T^{\mu}_{\mu} \rangle_{\rm ren} = -\langle T^{\mu}_{\mu} \rangle_{\rm div}$. This is the origin of the trace, or conformal anomaly. It can be seen as a reminiscent of the fact that the Weyl tensor and the Gauss-Bonnet terms are not scale invariant in dimensions other than four. This anomaly persists in the case where more complicated geometrical structures (tensor functions of the metric) are added to the original action and cannot be entirely removed. However, there is still some freedom in modifying the action so as to modify the form of the trace anomaly. Indeed, adding the conformally invariant $\sqrt{-g}\ R^2$ term into the action, and noticing that,

$$-\frac{2}{\sqrt{-g}} g^{\mu\nu} \frac{\delta}{\delta g^{\mu\nu}} \int {\rm d}^4x \sqrt{-g}\ R^2 = -12 \Box R \,, \tag{2.78}$$

the coefficient of the $\sim \Box R$ term in Eq. (2.77) can therefore be adjusted at will. It is convenient to choose it as,

$$\langle T^{\mu}_{\mu} \rangle_{\rm ren} = -\frac{1}{(4\pi)^2} \left[\frac{1}{120} C^2 - \frac{1}{360} \left(E - \frac{2}{3} \Box R \right) \right], \tag{2.79}$$

so that under conformal decomposition $g_{\mu\nu} = e^{2\sigma} \bar{g}_{\mu\nu}$, the various quantities transform as,

$$\sqrt{-g}\, C^2 = \sqrt{-\bar{g}}\, \bar{C}^2 \,, \tag{2.80}$$

$$\sqrt{-g} \left(E - \frac{2}{3} \Box R \right) = \sqrt{-\bar{g}} \left(\bar{E} - \frac{2}{3} \bar{\Box} \bar{R} \right) + 4 \sqrt{-\bar{g}}\, \bar{\Delta}_4 \sigma \,. \tag{2.81}$$

where Δ_4 is the Paneitz operator (Paneitz, 2008),

$$\Delta_4 \equiv \Box^2 + 2 R^{\mu\nu} \nabla_\mu \nabla_\nu - \frac{2}{3} R \Box + \frac{1}{3} g^{\mu\nu} \nabla_\mu R \nabla_\nu \,. \tag{2.82}$$

which is conformally covariant,

$$\sqrt{-g}\ \Delta_4 = \sqrt{-\bar{g}}\ \bar{\Delta}_4 \,. \tag{2.83}$$

Now, by focusing on the conformal sector, i.e. by taking the metric $\bar{g}_{\mu\nu}$ to be fixed, Eq. (2.65) implies that,

$$\frac{\delta \Gamma^{(1)}}{\delta \sigma} = \sqrt{-g}\ \langle T^{\mu}_{\mu} \rangle_{\rm ren} \,, \tag{2.84}$$

which can be integrated with respect to σ to give,

$$\Gamma^{(1)} = \frac{1}{120} \int {\rm d}^4x \sqrt{-\bar{g}}\ \bar{C}^2 \sigma - \frac{1}{360} \int {\rm d}^4x \sqrt{-\bar{g}} \left[\left(\bar{E} - \frac{2}{3} \bar{\Box} \bar{R} \right) \sigma + 2 \sigma \bar{\Delta}_4 \sigma \right], \tag{2.85}$$

where we discarded the irrelevant overall numerical factor. In solving Eq. (2.81) for σ and replacing it back into the action leads to,

$$\Gamma^{(1)} = \Gamma_{anom}[g] - \Gamma_{anom}[\bar{g}]\,, \tag{2.86}$$

with,

$$\Gamma_{anom}[g] = \frac{1}{8}\int \mathrm{d}^4x\sqrt{-g}\,\left(E - \frac{2}{3}\Box R\right)\Delta_4^{-1}\left[2\alpha\, C^2 + \beta\left(E - \frac{2}{3}\Box R\right)\right], \tag{2.87}$$

where the coefficients $\alpha = 1/120$ and $\beta = 1/360$, in the single massless scalar case that we are considering here. In the case where several fields are integrated out, these coefficients are modified by the corresponding number of scalar, spinor and vector fields. One can see that the anomalous effective action (2.87) has a genuinely nonlocal structure, due to the long range character of the massless fields quantum fluctuations. The anomaly induces the conformal factor of the spacetime metric to become dynamical (Antoniadis et al., 1997). This has been considered to play a relevant role in the understanding of the dark energy (Antoniadis et al., 2007; Mottola, 2010), and uncover other potentially detectable effects such as gravitational waves induced by scalar excitations (Mottola, 2017).

2.3 Nonlocality Versus Gauge Symmetry in Massive Theories

In this section, we provide examples showing that (abelian) gauge theories whose gauge symmetry is explicitly broken by a mass term can be recast in a nonlocal form, so that their symmetry is recovered. This underlines an interesting interplay between locality and gauge symmetry. We first apply such a procedure on the Proca action describing massive electrodynamics while we continue in applying the same method in Fierz-Pauli massive gravity.

2.3.1 Massive Electrodynamics

The theory describing massive spin-1 particles is provided by the Proca Lagrangian (Proca, (1936),

$$\mathcal{L}_{\mathrm{proca}}[A] = -\frac{1}{4}F^{\mu\nu}F_{\mu\nu} - \frac{1}{2}m^2A^\mu A_\mu - A_\mu j^\mu. \tag{2.88}$$

In the massless limit $m \to 0$, the theory acquires a $U(1)$ gauge symmetry,

$$A_\mu \longrightarrow A_\mu - \partial_\mu\theta\,, \tag{2.89}$$

where θ is an arbitrary smooth scalar fields. In the absence of sources, a residual gauge freedom remains and this symmetry can be used to eliminate two components of the massless field A_μ. For example the radiation, or Coulomb gauge conditions are provided by,

$$A^0 = \partial_i A^i = 0\,, \tag{2.90}$$

which implies the Lorentz gauge $\partial_\mu A^\mu = 0$. In that case, the theory therefore governs the dynamics of two modes being the helicity ± 1 of the photon. When a source is present, the residual gauge condition is lost and a third component of the field is non-vanishing and, although non-dynamical, plays the role of the Coulomb potential induced by that source.
In the presence of a mass, this gauge symmetry is explicitly broken and can no longer be used to

fix spurious degrees of freedom. However, according the representation theory of the Poincaré group, a massive spin-1 particles is described by three degrees of freedom being the two transverse helicity ± 1 modes, similarly to the massless case, together with an additional longitudinal helicity-0 mode. The vanishing of the forth component of the field A_μ is in fact enforced from a condition that arises dynamically. Indeed, computing the Euler-Lagrange equations for the Lagrangian (2.88) one finds,

$$\partial_\mu\big(\partial^\mu A^\nu - \partial^\nu A^\mu\big) - m^2 A^\nu = j^\nu \,, \tag{2.91}$$

and applying ∂_ν one finds,

$$m^2 \partial_\nu A^\nu = -\partial_\nu j^\nu \,. \tag{2.92}$$

Therefore, if the current is conserved or is identically zero $\partial_\nu j^\nu = 0$, the Lorentz condition emerges dynamically. In that case, going to the center of mass of the particle, its four-momentum vector reads $k^\mu = \big(m, \vec{0}\big)$ and the condition (2.92) in Fourier space leads to $A^0 = 0$. In that case, the equations of motion (2.91) take the Klein-Gordon form for each component of the spatial vector field A^i,

$$(\Box - m^2) A^i = 0 \,, \tag{2.93}$$

in accordance with the representation theory of the Poincaré group.

In the massive case however, a *new* gauge invariant theory can be constructed. This can be realised in using the so-called Stueckelberg formalism (Stueckelberg, 1938) consisting in introducing supplementary degrees of freedom so as to restore the broken symmetry. This is done by considering the new Lagrangian,

$$\mathcal{L}_{\text{proca}}[A] \to \mathcal{L}_{\text{stueck}}[A, \phi] \,, \tag{2.94}$$

obtained by performing the substitution,

$$A_\mu \to A_\mu + \frac{1}{m}\partial_\mu \phi \,, \tag{2.95}$$

where the scalar field ϕ, the so-called *Stueckelberg field*, has canonical dimension of mass. Observe that, since this introduction follows the pattern of the original gauge transformation of the massless theory, $F_{\mu\nu}$ is invariant. Writing down the explicit form of the new Lagrangian, the extra terms arise only from the mass and the source term,

$$\mathcal{L}_{\text{stueck}}[A, \phi] = -\frac{1}{4}F^{\mu\nu}F_{\mu\nu} - \frac{1}{2}m^2 A^\mu A_\mu - \frac{1}{2}\partial_\mu\phi\partial^\mu\phi - m A_\mu \partial^\mu \phi - A_\mu j^\mu + \frac{1}{m}\phi\partial_\mu j^\mu, \tag{2.96}$$

where we have integrated by part the source term involving ϕ and until now we assume nothing about whether or not the current is conserved. This gives rise to a theory that contains now more (five) field components, but has the advantage of being gauge symmetric. Indeed, according that the fields transform simultaneously under $U(1)$ as,

$$A_\mu \to A_\mu - \partial_\mu \theta \quad , \quad \phi \to \phi + m\theta, \tag{2.97}$$

the Lagrangian density do not change since the combination (2.95) is trivially invariant. Essentially, the new field introduced plays to role of the Goldstone boson of the emergent spontaneous symmetry breaking pattern, non-linearly realising the spontaneously broken $U(1)$ symmetry. This is an example of the Stueckelberg trick and shows that one can, by construction, always

restore a gauge symmetry by introducing new field degrees of freedom. Now, consider the corresponding equation of motion for A_μ and ϕ,

$$\partial_\mu F^{\mu\nu} = m^2 \left(A^\nu + \frac{1}{m}\partial^\nu \phi \right) + j^\nu \,, \tag{2.98}$$

$$\partial_\mu \left(A^\mu + \frac{1}{m}\partial^\mu \phi \right) = -\frac{1}{m^2}\partial_\mu j^\mu \,. \tag{2.99}$$

The latter can be solved formally in writing (Dvali et al., 2007) [see also (Hinterbichler, 2012) for a review],

$$\phi = -\frac{\Box^{-1}}{m}\left(\partial_\mu j^\mu - m\partial_\mu A^\mu\right), \tag{2.100}$$

and replacing ϕ by this expression in the equation of motion for A^μ, (2.98), one obtains,

$$\mathcal{L}_{\text{stueck}}[A] = -\frac{1}{4}F^{\mu\nu}\left(1 - \frac{m^2}{\Box}\right)F_{\mu\nu} - A^\mu \tilde{j}_\mu \,, \tag{2.101}$$

where we dropped an $\mathcal{O}(j^2)$ term and the current has been redefined as,

$$\tilde{j}^\mu \equiv \left(\eta^{\mu\nu} - \frac{\partial^\mu \partial^\nu}{\Box}\right) j_\nu \,, \tag{2.102}$$

which reflects the gauge symmetry restoration. The equations of motion for A_μ read,

$$\left(1 - \frac{m^2}{\Box}\right)\partial_\nu F^{\mu\nu} = \tilde{j}^\mu \,. \tag{2.103}$$

Such a procedure shows that one can recover a gauge symmetry explicitly broken by a mass term by paying the price of nonlocality. In fixing the Lorentz gauge condition, one recovers the local Klein-Gordon equations of motion for A_μ, sourced by a transverse current $\tilde{j}^\mu$. At high energy compared to the mass scale, the nonlocal term becomes negligible $-m^2/\Box \ll 1$ and one recovers the behavior of a massless photon. In the infrared, this term becomes relevant and suppresses the electrostatic potential, as expected for a massive particles with a Yukawa-type potential. The operator in front of $\partial_\nu F^{\mu\nu}$ can be seen as a high-pass filter and, in the case of a semi-classical approach as the one presented in the massless case in Sec. 2.2.2, one can see it as de-electrifying the vacuum,

$$\partial_\nu F^{\mu\nu} = \frac{\Box}{\Box - m^2}\langle 0|\tilde{j}^\mu|0\rangle \,. \tag{2.104}$$

This is the essence of the degravitation idea (Arkani-Hamed et al., 2002; Dvali et al., 2002) [see also (Barvinsky, 2004; Dvali et al., 2007; Patil, 2009)], which states that such an operator can be used to make the quantum vacuum energy gravitate less at low energies than at higher ones, so as to provide an explanation of why the cosmological constant is so small, whereas the vacuum energy at small scales is huge. Such an effect therefore supposes a running of Newton's constant $G \equiv G(-\Box)$. In the following, we show how the very same procedure applies in the linearised theory of massive gravity.

2.3.2 Pauli-Fierz Massive Gravity

The Pauli-Fierz action of linear theory for a massive spin-2 field over Minkowski spacetime coupled to a source $T^{\mu\nu}$ is given by (Pauli and Fierz, 1939),

$$S_{\rm FP}+S_{\rm int}=\frac{1}{2}\int {\rm d}^4x\,\left[h_{\mu\nu}\mathcal{E}^{\mu\nu,\rho\sigma}h_{\rho\sigma}-m^2(h_{\mu\nu}h^{\mu\nu}-h^2)+\kappa h_{\mu\nu}T^{\mu\nu}\right]\,, \tag{2.105}$$

where the metric perturbation $h_{\mu\nu}\equiv g_{\mu\nu}-\eta_{\mu\nu}$, with $|h_{\mu\nu}|\ll 1$, and $h\equiv h^{\mu\nu}\eta_{\mu\nu}$, is coupled to the matter fields $T^{\mu\nu}$, through the coupling constant $\kappa\equiv\sqrt{32\pi G}\sim M_p^{-1}$, and the Lichnerowicz operator $\mathcal{E}^{\mu\nu,\rho\sigma}$, is defined as,

$$\begin{aligned}\mathcal{E}^{\mu\nu,\rho\sigma} \;\equiv\; & \frac{1}{2}(\eta^{\mu\rho}\eta^{\nu\sigma}+\eta^{\mu\sigma}\eta^{\nu\rho}-2\eta^{\mu\nu}\eta^{\rho\sigma})\Box+(\eta^{\rho\sigma}\partial^\mu\partial^\nu+\eta^{\mu\nu}\partial^\rho\partial^\sigma)\\ & -\frac{1}{2}\left(\eta^{\mu\rho}\partial^\sigma\partial^\nu+\eta^{\nu\rho}\partial^\sigma\partial^\mu+\eta^{\mu\sigma}\partial^\rho\partial^\nu+\eta^{\nu\sigma}\partial^\rho\partial^\mu\right)\,.\end{aligned} \tag{2.106}$$

The relative coefficient between the two members of the mass term is the only one avoiding the presence of an extra ghost [see (Hinterbichler, 2012; de Rham, 2014) for reviews]. The equations of motion read,

$$\Box h^{\mu\nu}-\eta^{\mu\nu}\Box h+\eta^{\mu\nu}\partial_\rho\partial_\sigma h^{\rho\sigma}+\partial^\mu\partial^\nu h-\partial_\rho\partial^\nu h^{\mu\rho}-\partial_\rho\partial^\mu h^{\nu\rho}-m^2\left(h^{\mu\nu}-\eta^{\mu\nu}h\right)=-\frac{\kappa}{2}T^{\mu\nu}\,, \tag{2.107}$$

to which the application of ∂_μ leads to the dynamical constraint,

$$\partial_\mu(h^{\mu\nu}-\eta^{\mu\nu}h)=\frac{\kappa}{2m^2}\partial_\mu T^{\mu\nu}\,, \tag{2.108}$$

which vanishes when the energy-momentum tensor is conserved at linear level $\partial_\nu T^{\mu\nu}=0$. Taking instead the trace of Eq. (2.107) leads to,

$$3m^2h=-\frac{\kappa}{2}T\,. \tag{2.109}$$

For the massless theory, the gauge symmetry is provided by infinitesimal diffeomorphisms $x^\mu\to x^\mu+\xi^\mu$ that induces,

$$h_{\mu\nu}(x)\longrightarrow h_{\mu\nu}-(\partial_\mu\xi_\nu+\partial_\nu\xi_\mu)\,. \tag{2.110}$$

Using the same procedure as in the previous example, we restore the latter symmetry in the massive theory by introducing a Stückelberg vector field A^μ through,

$$h_{\mu\nu}\to h_{\mu\nu}+\frac{1}{m}(\partial_\mu A_\nu+\partial_\nu A_\mu)\,, \tag{2.111}$$

which transforms as $A_\mu\to A_\mu+m\xi_\mu$, so that the action is left invariant. It becomes,

$$\begin{aligned}S_{\rm FP}+S_{\rm int} \;=\; & \int {\rm d}^4x\,\left[\frac{1}{2}h_{\mu\nu}\mathcal{E}^{\mu\nu,\rho\sigma}h_{\rho\sigma}-\frac{m^2}{2}(h_{\mu\nu}h^{\mu\nu}-h^2)-\frac{1}{2}F_{\mu\nu}F^{\mu\nu}\right]\\ & +\int {\rm d}^4x\,\left[\frac{\kappa}{2}h_{\mu\nu}T^{\mu\nu}+2mA_\nu j^\nu\right]\,,\end{aligned} \tag{2.112}$$

where $F_{\mu\nu}\equiv\partial_\mu A_\nu-\partial_\nu A_\mu$ and,

$$j^\nu\equiv\partial_\mu(h^{\mu\nu}-\eta^{\mu\nu}h)\,. \tag{2.113}$$

We then use the equations of motion of A_μ,

$$\partial_\mu F^{\mu\nu} = -mj^\nu \,, \tag{2.114}$$

together with the condition,

$$\partial_\nu j^\nu = 0 \,, \tag{2.115}$$

obtained by applying ∂_ν to eq. (2.114), for integrating it out the Stückelberg field (Porrati, 2002). For doing so we separate A^ν into its transverse and longitudinal parts,

$$A^\nu = A^\nu_T - \partial^\nu \alpha \,, \tag{2.116}$$

where $\partial_\nu A^\nu_T = 0$, and we have $\Box A^\nu_T = -mj^\nu$. Thus, Eq. (2.115) allows us to fix the transverse part to $A^\nu_T = -m\Box^{-1}j^\nu$, while the longitudinal part α remains arbitrary. The most general solution of eq. (2.114) is given by (Dvali, 2006; Dvali et al., 2007),

$$A^\nu = -m\Box^{-1}j^\nu - \partial^\nu \alpha \,, \tag{2.117}$$

The transformation properties of the field α under linearised diffeomorphisms can be obtained by observing that $\Box\alpha = -\partial_\mu A^\mu$. Since under linearised diffeomorphisms $A^\mu \to A^\mu + m\xi^\mu$, it reads,

$$\Box\alpha \to \Box\alpha - m\partial_\mu \xi^\mu \,. \tag{2.118}$$

Observe that the transformation property of $(\Box\alpha)/m$, is the same as that of $h/2$. It is therefore convenient to trade α for a new field N (Jaccard et al., 2013),

$$N \equiv \frac{h}{2} - \frac{\Box\alpha}{m} \,, \tag{2.119}$$

which is invariant under linearised diffeomorphisms and where α is fixed to some given value, e.g. $\alpha = 0$. Performing the replacement (2.117) in the action (2.112) and trading α for N we find,

$$S = \int \mathrm{d}^4x \, \left[\frac{1}{2}h_{\mu\nu}\left(1 - \frac{m^2}{\Box}\right)\mathcal{E}^{\mu\nu,\rho\sigma}h_{\rho\sigma} - 2m^2 N\frac{1}{\Box}\partial_\mu\partial_\nu(h^{\mu\nu} - \eta^{\mu\nu}h) + \frac{\kappa}{2}h_{\mu\nu}T^{\mu\nu}\right] \,, \tag{2.120}$$

where the scalar field N enters the action as a Lagrange multiplier. This action is the nonlocal formulation of Fierz-Pauli massive gravity, where invariance under linearised diffeomorphism is restored. Observe that the kinetic term features the same structure as in nonlocal massive electrodynamics (2.101). However, it also presents an additional term enforcing the constraint,

$$\partial_\mu\partial_\nu(h^{\mu\nu} - \eta^{\mu\nu}h) = 0 \,. \tag{2.121}$$

which is also a consequence of the local theory, as seen from (2.109). At the fully covariant level the latter reads $g_{\mu\nu}R^{\mu\nu} = 0$, in the presence of any sources. This conditions clearly leads to an unacceptable physical theory and expresses the presence of the van Dam, Veltman, Zakharov (vDVZ) discontinuity (Zahkarov, 1970; van Dam and Veltman, 1970) at linearised level, which manifest itself also at fully nonlinear level in that case, since for GR one has $R = -8\pi GT$ (Porrati, 2002).

2.4 Infrared Nonlocal Modifications to Gravity

Along with the ones mentioned in the previous sections, other approaches involving nonlocalities motivated by different mechanisms have been developed as well for modifying GR in its low energy regime. Here, we non-exhaustively provide a list of some models which we proposed into that framework, presenting their structure, their main characteristics and their current status in a cosmological context.

DGP Braneworld

Inspired by higher dimensional theories aiming to provide a solution to the hierarchy problem (Antoniadis et al., 1998; Arkani-Hamed et al., 1998; Randall and Sundrum, 1999; Gregory et al., 2000; Kogan and Ross, 2000; Parikh and Solodukhin, 2001), the Dvali-Gabadadze-Porrati (DGP) model (Dvali et al., 2000; Dvali and Gabadadze, 2001) attracted a lot of interest at the beginning of the twenty-first century. Aiming to modify the behavior of Einstein's gravity on infrared scales, the model describes the gravity induced on a $3+1$ dimensional brane from gravity present on a higher, $4+1$ dimensional infinite ambient space, while matter fields are confined on the brane. The action reads,

$$S_{\rm DGP} = \frac{M_5^3}{2}\int \mathrm{d}^5X\sqrt{-G}\;R(G) + \frac{M_p^2}{2}\int \mathrm{d}^4x\sqrt{-g}\;R(g) + S_M\big[g,\psi\big]\,, \tag{2.122}$$

where M_5, M_p are the five and four dimensional Planck constants and X^A, x^μ (where A runs from 0 to 4) are the coordinate systems on the bulk and the brane, respectively. The brane metric $g_{\mu\nu}(x)$ is induced by the bulk one G_{AB}. In a particular gauge where the brane is fixed at $X^5 = 0$ and the four other bulk coordinates coincide with the ones of the brane, this relation reads,

$$g_{\mu\nu} = G_{\mu\nu}(x, X^5 = 0)\,. \tag{2.123}$$

In that case, the propagator intervening into the computation of the classical potential between static masses on the brane implies [see e.g. (Deffayet et al., 2002)],

$$\tilde{G}_{\rm DGP}(k) = \frac{-i}{M_p^2k^2 + 2M_5^3k}\,, \tag{2.124}$$

which translates into real space as a nonlocal quadratic form $-\Box + M_{\rm DGP}\sqrt{-\Box}$, with the so-called DGP scale, $M_{\rm DGP} = 2M_5^3/M_p^2$. The Källén-Lehmann spectral density computed from this quadratic form describes a continuum of massless to infinitely massive gravitons [see e.g. (Hinterbichler, 2012)]. Above the DGP scale, the k^2 term dominates the propagator (2.124) and the $1/r$ Newtonian potential is recovered (modulo small corrections), whereas in the infrared the potential scales as $1/r^2$, so that the gravitational force weakens. Such a decrease is produced by the four dimensional gravitons leaking out into the extra dimension below $M_{\rm DGP}$. The model was shown to possess self-accelerating solutions (Deffayet, 2001; Deffayet et al., 2002) and therefore is of potential relevance in a cosmological context. However, longitudinal gravitational degrees of freedom acquire a negative kinetic term on the self-accelerating solution, leading to the presence of ghost instabilities that render the model physically unacceptable (Luty et al., 2003; Nicolis and Rattazzi, 2004; Charmousis et al., 2006; Gorbunov et al., 2006; Izumi et al., 2007; Koyama, 2007).

Other modified gravity models featuring a nonlocal character where also introduced. Some of them were inspired by first principle while other ones were introduced into a more phenomenological context for addressing the cosmological constant problem and cosmic acceleration. We review some of them in the subsequent sections.

First Attempt at Nonlocal Modifications of Gravity

An early nonlocal modification to the theory of GR was given by C. Wetterich (Wetterich, 1998) on purely theoretical grounds. This model, although modifying the dynamics of GR at

large scales, was not motivated for explaining cosmic acceleration, as it was not yet discovered at the time. Instead, the theory was motivated by the fact that the linearised action for gravitational fluctuations around Euclidean flat space is not bounded from below, and implies that no generating functional with standard covariant measure can be well-defined. The corresponding action reads,

$$S_{\rm nl} = \frac{1}{16\pi G}\int \mathrm{d}^4x\sqrt{-g}\,\left[R - \frac{\tau^2}{2}R\frac{1}{\Box-\xi R}R\right], \tag{2.125}$$

where τ, ξ are real numbers. For $\tau^2 \geq 0$, the action for small fluctuations becomes positive semi-definite, while in four dimensions for $\tau \geq 2/3$, flat space provides its absolute minimum. From the cosmological perspective, it has been shown later on that this model is irrelevant for explaining cosmic acceleration (Koivisto, 2008a).

Implementation of Degravitation

Nonlocal models where then proposed as solutions to solve the cosmological constant and to provide an alternative to cosmic acceleration. The degravitation idea outlined at the end of Sec. 2.3.1, was implemented into an action by A. Barvinsky (Barvinsky, 2003). Starting from the covariantisation of the Einstein-Hilbert action over flat space that has been rewritten in a nonlocal form,

$$S = \int \mathrm{d}^4x\sqrt{-g}\,\left[G^{\mu\nu}\Box^{-1}R_{\mu\nu} + \mathcal{O}\left(R^3_{\mu\nu}\right)\right]. \tag{2.126}$$

As such the degravitation mechanism can be obtained from the replacement,

$$\frac{1}{\Box} \longrightarrow \frac{1+\mathcal{F}\left(L^2\Box\right)}{\Box}, \tag{2.127}$$

where the function $\mathcal{F}$ respects $\mathcal{F}(X \gg 1) \ll 1$ and $\mathcal{F}(X \to 0) \gg 1$, so as to be relevant for late time cosmology, and L is the characteristic length scale where the infrared modification takes place. The equation of motion takes the form,

$$\left[1+\mathcal{F}\left(L^2\Box\right)\right]G_{\mu\nu} + \mathcal{O}\left(R^2_{\mu\nu}\right) = 8\pi G\,T_{\mu\nu}\,, \tag{2.128}$$

where the Bianchi identities are satisfied, i.e. the energy-momentum tensor of matter is conserved, as the action (2.126) is diffeomorphism invariant. Formally, the commutator $\left[\nabla_\mu, \Box^{-1}\right]$ gives raise to an infinite number of powers of curvature terms which are compensated by the covariant derivative of the $\mathcal{O}\big(R^2_{\mu\nu}\big)$ term and higher orders. To our knowledge, no cosmological considerations have been made for such a model, whose infinite curvature expansion makes it seemingly difficult to handle in the presence of a FLRW background.

Deser-Woodard Model

A model which stimulated much interest in recent years has been proposed by S. Deser and R. Woodard (Deser and Woodard, 2007), so as to modify gravity in what could seen as a minimal nonlocal version of $f(R)$ theories. They suggested a modified Einstein-Hilbert action of the form,

$$S_{\rm DW} = \frac{1}{16\pi G}\int \mathrm{d}^4x\sqrt{-g}\;R\left[1+f\left(\frac{1}{\Box}R\right)\right], \tag{2.129}$$

where f is a dimensionless free function [6]. The introduction of this model was inspired by the fact that such terms can be generated by quantum loop effects, as we have seen in Sec. 2.2.2, and motivated in that it could provide an explanation for cosmic acceleration. Objectively, as $f(R)$ theories, this model has no predictive power as long as the function f is arbitrary. It has been proposed that the form of this function is fixed so as to reproduce a ΛCDM background cosmology (Deffayet and Woodard, 2009), but also other choices where explored (Koivisto, 2008a). In the former case, the model has the same number of parameters than ΛCDM and the distortion function reads,

$$\bar{f}(\zeta) = -2\int_{\zeta}^{\infty} \mathrm{d}\zeta_1\, \zeta_1 \phi(\zeta_1) - 6\Omega_\Lambda \int_{\zeta}^{\infty} \mathrm{d}\zeta_1\, \frac{\zeta_1^2}{h(\zeta_1)\, I(\zeta_1)} \int_{\zeta_1}^{\infty} \mathrm{d}\zeta_2\, \frac{I(\zeta_2)}{h(\zeta_2)\,\zeta_2^4} \\ +2\int_{\zeta}^{\infty} \mathrm{d}\zeta_1\, \frac{\zeta_1^2}{h(\zeta_1)\, I(\zeta_1)} \int_{\zeta_1}^{\infty} \mathrm{d}\zeta_2\, \frac{r(\zeta_2)\,\phi(\zeta_2)}{\zeta_2^5}\,, \tag{2.130}$$

where ζ and r are given by $\zeta \equiv 1+z$ and,

$$r \equiv \bar{R}/H_0^2\,, \tag{2.131}$$

with $\bar{R}$ the background Ricci scalar, and the functions $\phi(\zeta)$ and $I(\zeta)$ read,

$$\phi(\zeta) = -6\Omega_\Lambda \int_{\zeta}^{\infty} \mathrm{d}\zeta_1 \frac{1}{h(\zeta_1)} \int_{\zeta_1}^{\infty} \mathrm{d}\zeta_2 \frac{1}{h(\zeta_2)\,\zeta_2^4}, \qquad I(\zeta) = \int_{\zeta}^{\infty} \mathrm{d}\zeta_1 \frac{r(\zeta_1)}{\zeta_1^4 h(\zeta_1)}\,. \tag{2.132}$$

Furthermore, the dimensionless Hubble function $h \equiv \mathcal{H}/H_0$ appearing into the above is the one of the cosmology one wants to recover, i.e. ΛCDM in the present case. The function $\bar{f}\big(\bar{\Box}^{-1}\bar{R}\big)$ is then recovered in inverting the following relation,

$$\bar{\Box}^{-1}\bar{R}(\zeta) = -\int_{\zeta}^{\infty} \frac{\mathrm{d}\zeta_1 \zeta_1^2}{h(\zeta_1)} \int_{\zeta_1}^{\infty} \mathrm{d}\zeta_2 \frac{r(\zeta_2)}{\zeta_2^4 h(\zeta_2)} = -\int_{\zeta}^{\infty} \frac{\mathrm{d}\zeta_1 \zeta_1^2}{h(\zeta_1)} I(\zeta_1)\,. \tag{2.133}$$

The same reconstruction technique has also been shown to apply for non-standard ΛCDM cosmologies (Park and Shafieloo, 2017). To some general extent, this theory is free of ghost instabilites (Koivisto, 2008b; Deser and Woodard, 2013a).

In the case where the background is fixed to ΛCDM in the nonlocal model, its distinction from the latter resides in its linear and nonlinear perturbation features. The effect of linear perturbations on the growth of structures has first been studied in (Dodelson and Park, 2014), which arrived at the conclusion that current data redshift space distortion data rule out the model at a level of 8σ, due to a strong excess of growth. However, a further analysis revealed that the model was in fact viable for explaining the data in the same context (Nersisyan et al., 2017b) and actually described a lower growth of structures than ΛCDM. This discrepancy has been due to an error in the numerical computation code of the former group, as recognised in (Park, 2018). A more quantitative analysis of the observational performance of this model with respect to ΛCDM is currently under way (Amendola et al., 2018).

RT and RR Models

Since then, the exploration of possible nonlocal modifications to gravity has turned into an expedition. Several phenomenological nonlocally modified gravity theories have flourished and many model have been studied in a cosmological context. For instance, the quadratic action

6. Notice that Eq. (2.125) with $\xi = 0$ is a special case of this theory.

of nonlocal massive gravity of Eq. (2.120) has been considered without the constraining term controlled by N, since it is the latter that flaws the theory on physical grounds. In this case, the equations of motion take the form,

$$\left(1-\frac{m^2}{\Box}\right)\mathcal{E}^{\mu\nu,\rho\sigma}h_{\rho\sigma}=-16\pi G\,T^{\mu\nu}\,, \tag{2.134}$$

where $h_{\mu\nu}$ has been rescaled by κ so as to become dimensionless. Under canonical covariantisation $\mathcal{E}^{\mu\nu,\rho\sigma}h_{\rho\sigma}\to-2G^{\mu\nu}$, but enforcing $\Box_\eta=\partial^2\to\Box_g\equiv g^{\mu\nu}\nabla_\mu\nabla_\nu$, violates energy momentum conservation, since $\left[\nabla_\mu,\Box_g^{-1}\right]\neq 0$. One way out of this situation is to add higher curvature terms so as to compensate for this discrepancy, in the same way as in Eq. (2.128), or to extract the transverse part of the corresponding expression (Porrati, 2002; Jaccard et al., 2013) [see also (Modesto and Tsujikawa, 2013)] by writing,

$$G_{\mu\nu}-m^2\big(\Box_g^{-1}G_{\mu\nu}\big)^{\mathrm{T}}=8\pi G\,T_{\mu\nu}\,, \tag{2.135}$$

where $^{\mathrm{T}}$ denotes the covariant transverse extraction defined in Eq. (3.4). Cosmological, FLRW background solutions of this model were investigated into (Foffa et al., 2014b), where it was shown to be flawed by a growing mode present in the RD and MD era, spoiling the viability of the cosmological evolution. Instead, the following theory does not exhibit these unwanted features (Maggiore, 2014; Foffa et al., 2014b),

$$G_{\mu\nu}-\frac{1}{3}m^2\big(g_{\mu\nu}\Box_g^{-1}R\big)^{\mathrm{T}}=8\pi G\,T_{\mu\nu}\,. \tag{2.136}$$

At the fully nonlinear level, the transverse part extraction presents difficulties for being implemented into an action. Nevertheless, in linearising the theory over Minkowski space one can find,

$$S=\frac{1}{2}\int\mathrm{d}^4x\left[h_{\mu\nu}\mathcal{E}^{\mu\nu\rho\sigma}h_{\rho\sigma}-\frac{2}{3}m^2h_{\mu\nu}P^{\mu\nu}P^{\rho\sigma}h_{\rho\sigma}\right], \tag{2.137}$$

where $P^{\mu\nu}$ is the linear transverse projector defined in Eq. (3.9). Remarking that $P^{\mu\nu}h_{\mu\nu}$ canonically covariantises to $\sim\Box^{-1}R$, one can write the following action (Maggiore and Mancarella, 2014),

$$S=\int\mathrm{d}^4x\sqrt{-g}\,\left[R-\frac{1}{6}m^2R\frac{1}{\Box^2}R\right]. \tag{2.138}$$

This model has therefore the same equations of motion as the one of Eq. (2.136), once linearised over flat space, but its corresponding nonlinear corrections are generically different, as well as the dynamics it induces for non-trivial backgrounds, as we will see below.

$$S=\int\mathrm{d}^4x\sqrt{-g}\,\left[R-\frac{1}{6}m^2R\frac{1}{\Box^2}R\right]. \tag{2.139}$$

The nonlocal modified gravity models (2.136), (2.139) have been shown to provide a viable cosmological background evolution and, in particular, both exhibit late time self-accelerating solutions induced by a phantom dark energy component, i.e. with $w_{\mathrm{de}}<-1$. The theoretical structure and cosmological implications of these two models are the main subject of this thesis and will be presented in great details in the subsequent chapters.

An extended model where the $\Box$ operator in Eq. (2.139), is promoted to the operator $\Box \to \Box - \xi R$, which is conformally covariant for the value $\xi = 1/6$ (Mitsou, 2015; Cusin et al., 2016a),

$$S = \int \mathrm{d}^4x\sqrt{-g}\,\left[R - \frac{1}{6}m^2 R\frac{1}{(-\Box + \xi R)^2}R\right], \tag{2.140}$$

has also been shown to provide interesting FLRW background cosmologies. In particular, when ξ is left as a free parameter, such a model interpolates between the one in Eq. (2.139) ($\xi = 0$) and ΛCDM ($\xi \to +\infty$), as can be seen directly from the above action. A more sophisticated version of the RR class of models is given in (Narain and Li, 2018), which has the structure of an ultraviolet renormalisable theory, including similar nonlocalities at leading order in curvature.

Tensor Nonlocalities

Studies focusing on nonlocal structures similar to (2.139), but involving curvature tensors such as the Ricci and Weyl tensors instead of the Ricci scalar have also been studied. Notice that, in that case, studying the dynamics that such terms induce on an FLRW background is sufficient since the Weyl tensor,

$$C_{\mu\nu\rho\sigma} = R_{\mu\nu\rho\sigma} - \left(g_{\mu[\rho}R_{\sigma]\nu} - g_{\nu[\rho}R_{\sigma]\mu}\right) + \frac{1}{3}g_{\mu[\rho}g_{\sigma]\nu}R\,, \tag{2.141}$$

is the trace-free part of the Riemann one, and vanishes on the FLRW solution. Therefore, a basis of curvature operators convenient for cosmological phenomenological studies is provided by $\{R, R_{\mu\nu}, C_{\mu\nu\rho\sigma}\}$. Terms involving the Ricci tensor have been studied in (Ferreira and Maroto, 2013) through an action of the form,

$$S = \frac{1}{16\pi G}\int \mathrm{d}^4x\sqrt{-g}\,\left[R - \alpha R^{\mu\nu}\frac{1}{\Box}R_{\mu\nu}\right], \tag{2.142}$$

where α is a constant number, while more general structures involving the Weyl tensor where considered in (Cusin et al., 2016b),

$$S = \frac{1}{16\pi G}\int \mathrm{d}^4x\sqrt{-g}\,\left[R - \mu_1 R\frac{1}{\Box^2}R - \mu_2 C_{\mu\nu\rho\sigma}\frac{1}{\Box^2}C^{\mu\nu\rho\sigma} - \mu_3 R_{\mu\nu}\frac{1}{\Box^2}R^{\mu\nu}\right]. \tag{2.143}$$

where the μ_i's have dimension of mass-squared. Nonlocal models involving more complex structures for the Green's function invoked were considered into (Nersisyan et al., 2017a), where the action under interest reads,

$$S = \frac{1}{16\pi G}\int \mathrm{d}^4x\sqrt{-g}\,\left[R - \frac{1}{6}M^2 R_{\mu\nu}\triangle^{-1}R^{\mu\nu}\right], \tag{2.144}$$

with,

$$\triangle \equiv m^4 + \alpha_1\Box + \alpha_2\Box^2 + \beta_1 R_{\mu\nu}\nabla^\mu\nabla^\nu + \beta_2 R\Box + \gamma\big(\nabla_\mu R_{\mu\nu}\big)\nabla^\nu\,, \tag{2.145}$$

where $m, \alpha_1, \alpha_2, \beta_1, \beta_2, \gamma$ are constant.

These developments have led to the same conclusions while examining the $\sim R_{\mu\nu}\Box^{-n}R^{\mu\nu}$ terms with $n = 1, 2$, from a cosmological perspective. They concluded that these terms generically lead to the presence of a growing mode in the radiation era that prevents a viable cosmological evolution, unless the nonlocal terms in the actions are largely suppressed, a fact that however makes the model quite unnatural. Nevertheless was noticed that in setting $\alpha_1 = \alpha_2 = 0$

in Eq. (2.145), the resulting model (2.144) could in principle provide viable cosmological solutions, behaving as a cosmological constant at late time (Nersisyan et al., 2017a). Furthermore, although the contribution of the Weyl tensor vanishes on the FLRW background, its influence sets in at the perturbative level. In (Cusin et al., 2016b), it was found that this term modifies the tensor sector of the theory in a non-trivial way, but that these perturbations are unstable at late time, grow faster for increasing frequency modes and therefore do violate bounds on the primordial GW spectral density.

Another model involving tensor nonlocalities has been presented in (Cusin et al., 2016b) by the action,

$$S = \frac{1}{16\pi G}\int \mathrm{d}^4x\sqrt{-g}\,\left(R - \frac{1}{6}m^2 R\frac{1}{\Delta_4}R\right), \tag{2.146}$$

where the Paneitz operator Δ_4 is defined in Eq. (2.82). Cosmological consequences of this model were worked out in the Appendix A of (Belgacem et al., 2018b) where it has been found that the speed of the gravitational waves was significantly smaller (at order of tens of percents) than the speed of light. In view of the recent observations of a neutron star binary coalescence (Abbott et al., 2017h), combined with the observation of the γ-ray burst counterpart, providing a strong constraint for the speed of GW $c_{\rm gw}$, being equal to the speed of light c to one part in 10^{15} (Abbott et al., 2017i), this model is ruled out on firm grounds. However, as we will discuss in more detail below, the RT (2.136) and RR model (2.139), do not suffer from such discrepancy as they feature $c_{\rm gw} = c$.

A Lattice Quantum Gravity Inspiration

A nonlocal gravity model inspired by non-perturbative quantum gravity computations based on Regge's lattice formulation (Hamber and Williams, 1995, 2005) has also been studied (Amendola et al., 2017a). Quantum gravity computations on the lattice suggests the running of gravitational couplings due to renormalisation group relevant effects induced by weak graviton vacuum polarisation. The running of Newton's constant is suggested to arise from the presence of a non-trivial non-perturbative UV fixed point at G_c. Away from this fixed point, the running of the coupling is thought to behaves as,

$$S = \int \mathrm{d}^4x\sqrt{-g}\,\left[1 - c_\xi\left(\frac{1}{\xi^2\Box}\right)^{1/(2\nu)} + \mathcal{O}\big((\xi^2\Box)^{-1/\nu}\big)\right]R\,, \tag{2.147}$$

where ν is the critical exponent $\beta'(G_c) = -1/\nu$ and, together with $c_\zeta \sim \mathcal{O}(1)$, is a finite number determined from the theory. Typically, $\nu^{-1} \in [1, 4]$ (see above references and therein). Instead, $\xi \sim m$ is a mass scale of the infrared modification. It is not predicted by the theory and requires some more physical input motivated by theoretical assumptions/modeling or observations. The latter characterises the behavior of the correlations length away from G_c as,

$$\xi^{-1} \sim \Lambda_{\rm UV}\exp\left(-\int^G \frac{\mathrm{d}G'}{\beta(G')}\right) \overset{G\to G_c}{=} \Lambda_{\rm UV}|G - G_c|^\nu\,, \tag{2.148}$$

where $\Lambda_{\rm UV}$ is the UV cutoff that is fixed by the lattice spacing. Such effects are therefore of particular relevance for late time cosmology. Cosmological considerations have been made in (Hamber and Toriumi, 2011), where a slightly enhanced growth of structures and non-trivial gravitational slip were found. The authors of (Amendola et al., 2017a) considered the case

where $\nu = 1/4$ and studied the action,

$$S = \frac{1}{16\pi G}\int \mathrm{d}^4x\sqrt{-g}\,\left(1 - \frac{M^4}{6}\frac{1}{\Box^2}\right)R\,. \tag{2.149}$$

They found that for $\xi \sim H_0^{-1}$, the cosmology of this models is very similar to that of Eq. (2.139) at late times, in that it gives raise to a phantom effective dark energy that produces a cosmologically viable phase of accelerated expansion. Another, similar model was derived from a very orthogonal direction into the context of bimetric gravity.

Another intriguing aspect that recently arose in background independent lattice quantum gravity calculations, using Monte Carlo simulations in Causal Dynamical Triangulation, is the "first-hand evidence for the presence of nonlocal terms which could affect the gravitational dynamics at cosmic scales" (Knorr and Saueressig, 2018). Indeed, using the technique presented in the latter reference, one can infer the relevance of several couplings in the quantum effective action of gravity from correlation functions on the lattice. In particular, these techniques reveals the existence of a mass-type operator of the nonlocal form for which the correction,

$$\Gamma^{\mathrm{nonloc}} = -\frac{b^2}{96\pi G}\int \mathrm{d}^4x\sqrt{g}\,\mathcal{R}\mathcal{F}(\Box)\mathcal{R}\,, \tag{2.150}$$

where b is a parameter with dimension of mass and,

$$\mathcal{R} \equiv R + \frac{1}{2}{}^{(3)}R\,, \qquad \mathcal{F}(\Box) \equiv \Box^{-2}\,, \tag{2.151}$$

provides a representative of the class of the relevant terms. Such nonlocal infrared relevant terms have also been motivated in QCD from lattice computations (Boucaud et al., 2001; Capri et al., 2005; Dudal et al., 2008), where it is in particular shown that the non-perturbative gluon propagator in the IR is reproduced by nonlocal terms of the form,

$$\Gamma = -\frac{m^2}{2}\mathrm{Tr}\int \mathrm{d}^4x\; F_{\mu\nu}\frac{1}{\Box}F^{\mu\nu}\,, \tag{2.152}$$

where $F_{\mu\nu} = F^a_{\mu\nu}T^a$, $\Box^{ab} = D^{ac}_\mu D^{\mu,cb}$ and $D^{ab}_\mu = \delta^{ab}\partial_\mu - g f^{abc}A^c_\mu$, giving an effective mass m to the gluon. Quite interestingly, these terms are similar to the form of the nonlocal correction to gravity in the RR model (2.139). Indeed, in focusing on the conformal sector of the metric in writing $g_{\mu\nu} = e^{2\sigma}\eta_{\mu\nu}$, we have that $R = -6\Box\sigma + \mathcal{O}(\sigma^2)$, and therefore the term,

$$R\frac{1}{\Box^2}R = 36\sigma^2 + \mathcal{O}(\sigma^3)\,, \tag{2.153}$$

provides a mass to the conformal mode of the graviton (Maggiore, 2015; Belgacem et al., 2018b).

Nonlocally coupled bimetric gravity

The authors of (Vardanyan et al., 2018) considered a theory of two dynamical metrics interacting through a term inspired by the simplest version of the Deser-Woordard model, i.e. with $f(X) \sim X$, and introduced the action,

$$\begin{aligned} S =& \frac{M_p^2}{2}\int \mathrm{d}^4x\sqrt{-g}\;R + \frac{M_f^2}{2}\int \mathrm{d}^4x\sqrt{-f}\;R_f - \frac{M_p^2}{2}\int \mathrm{d}^4x\sqrt{-g}\;\alpha\left(R_f\frac{1}{\Box}R + R\frac{1}{\Box}R_f\right) \\ &+ S_M[g,\psi]\,, \end{aligned} \tag{2.154}$$

where matter is only coupled to $g_{\mu\nu}$ and M_p, M_f are the couplings, R, R_f the Ricci scalars and $\Box, \Box_f$ the d'Alembertian operators for the metrics $g_{\mu\nu}, f_{\mu\nu}$, respectively, whereas α is a constant number. Interestingly, in this model the Bianchi constraints impose that the Ricci scalar for the metric $f_{\mu\nu}$ is constant over spacetime, $R_f = m^2$. Settings this condition into the action (2.154) implies,

$$S = \frac{1}{16\pi G}\int \mathrm{d}^4x\sqrt{-g}\,\left(1+\frac{m^2}{\Box}\right)R + S_M[g,\psi]\,, \tag{2.155}$$

with a very similar structure than the action in Eq. (2.139). Background cosmological consequences are very the same for both models as well.

Resummed Nonlocal Gravity Model

The similarities between the two theories given by (2.139) and (2.154), in terms of their actions and FLRW background cosmological features appeals for them to be combined into some sort of resummation. Indeed, working at an effective field theoretic level, low energy corrections typically arise in an expansion suppressed by powers of $\sim -\Box/m^2$, that typically signals the decoupling of heavier particles, and converges to zero as one goes in the far infrared. This is typically the case for general relativistic quantum corrections in its low energy expansion in powers of curvature, where the latter are suppressed by powers of the Planck mass M_p. Instead, allowing for the presence nonlocal terms to appear, one can then compensate the curvature mass dimensions with a nonlocal operator, e.g. $\Box^{-1}$, and even turn it to an arbitrary negative power. This means that the inclusion of any powers of operators $\sim \Box^{-1}$ is allowed from the effective field theory point of view. Such models where already considered into the context of string-inspired higher derivative theories of gravity (Capozziello et al., 2009). Furthermore, these terms are typically non-negligible in the infrared, so that they can give raise to a divergent series. In the view where one can write $X = \Box^{-1}R$, the model (2.139) features a correction $\sim -m^2X^2$ while the ones in (2.155) is corrected by $\sim +m^2X$. They can therefore be implemented in a resummed version reading,

$$S = \frac{1}{16\pi G}\int \mathrm{d}^4x\sqrt{-g}\,\left[R+\Lambda^2\log\left(1+\frac{1}{\Box}R\right)\right], \tag{2.156}$$

or also into a non-analytic structure such as,

$$S = \frac{1}{16\pi G}\int \mathrm{d}^4x\sqrt{-g}\,\left[R-\Lambda^2\big(e^{-R/\Box}-1\big)\right], \tag{2.157}$$

whose behavior is to suppress the effect of Λ^2 in the UV ($-\Box^2 \gg 1$), while making it effective in the far infrared.

Summary

From the previous analysis, we have seen that nonlocal corrections are typically emerging into the quantum effective action from different perspectives.

In a perturbative framework, they arise framework in the high energy limit when the theory contains light particles, or generically when it contains light particles, such as gravitons or photons, which also lead to the emergence of the conformal anomaly. However, these corrections are mostly susceptible to affect the UV behavior of the theory, while they are irrelevant in the IR, and therefore for cosmological applications.

Nonlocal corrections of IR relevance from first principles are rather motivated by extra-dimensions, in which the gravitons leak at large scales, or by non-perturbative quantum gravity effects away from a non-trivial UV fixed point, which however still remain quite poorly understood.

On more phenomenological grounds, we have presented various simplified models that have already been proposed and embedded into a cosmological context for testing their capabilities of explaining cosmic acceleration. We have seen that such a task is in general difficult to achieve, as the phenomenological imperatives constrain the theory of being free of growing modes at background and (linear) perturbation level, and to describe gravitational waves propagating at the speed of light at the present epoch. In this sense, the models mentioned above provide good candidates to inspire more fundamental studies, where such effect could be properly derived from first principles.

Chapter 3

Aspects of Nonlocal Infrared Modifications to General Relativity

In the previous chapter, we have seen that infrared corrections to the dynamics of GR can be produced by different effects such quantum vacuum fluctuations of light matter, extra dimensions or non-perturbative effects, such as those arising from gravitational vacuum polarisation. There exists two strategies for understanding if these effects can be relevant for infrared gravitational physics. Either one guesses a given mechanism potentially able to do so, and works it out *ab initio*, or one investigates the cosmological consequences of various terms selected in through a more *ad hoc*, effective field theoretical approach. Understanding which corrections generate viable cosmologies can then provide inspirations for bridging the gap with a fundamental understanding.

Subsequently, we present two phenomenological modified gravity models that have been proposed by M. Maggiore (Maggiore, 2014) and M. Maggiore and M. Mancarella (Maggiore and Mancarella, 2014) some years ago, for the second point of view. We introduce the theoretical structure of the models, describe the physical degrees of freedom they contain, clarify some subtleties associated with the presence of nonlocal operators into an action and perform a degrees of freedom count and stability analysis from different perspectives. The phenomenology of these models within a cosmological context is presented in the next chapter.

3.1 The RT Model

As briefly outlined in the previous chapter (see Sec. 2.4), variations of the nonlocal formulation of Fierz-Pauli massive gravity lead to interesting phenomenological models exhibiting self-accelerating solutions on an FLRW background. We review their origin in this section.

Consider the linearised action of Eq. (2.120), without the constraining term proportional to the Lagrange multiplier N, so that condition Eq. (2.121) is no longer realised. In that case, the action reads [1],

$$S = \frac{1}{2}\int d^4x \ \left[h_{\mu\nu}\left(1-\frac{m^2}{\Box}\right)\mathcal{E}^{\mu\nu,\rho\sigma}h_{\rho\sigma} + \kappa h_{\mu\nu}T^{\mu\nu}\right] . \tag{3.1}$$

Investigating the degrees of freedom content of this theory, one finds that it carries 5+1 degrees of freedom, as one could have expected. Indeed, this expression derives from the nonlocal version of

1. Observe that the canonical covariantisation of this action would lead to an action of the form (2.155), where the sign of the mass squared has been changed.

the linearised theory for a massive spin-2 field, where the scalar condition $\big(\partial_\mu\partial_\nu - \eta_{\mu\nu}\Box\big)h^{\mu\nu} = 0$, has been removed [2]. Beside of the four components of $h_{\mu\nu}$ that are annihilated by infinitesimal diffeomorphism invariance $x_\mu \to x_\mu + \xi_\mu$, inducing,

$$h_{\mu\nu} \longrightarrow h_{\mu\nu} - (\partial_\mu\xi_\nu + \partial_\nu\xi_\mu)\ , \tag{3.2}$$

the lack of this scalar condition makes it impossible to remove a fifth one for getting the $10-5=5$ degrees of freedom of a massive spin-2, and introduces one supplementary degree-of-freedom into the theory. In (Jaccard et al., 2013), this was shown to be a scalar mode of mass m^2 which manifests itself in a mixture of a scalar and the helicity-0 mode of the massive spin-2 field. This additional mode has the wrong sign in front of its propagator, i.e. it is a tachyonic ghost. However, as we will discuss below, there is no genuine degrees of freedom associated with such a propagator, and therefore no corresponding particles to be put on the external lines of scattering processes [see e.g. (Foffa et al., 2014a) along these lines]. As outlined in Sec. 2.4, a covariantisation of the equations of motion deriving from this action is provided by,

$$G_{\mu\nu} - m^2\big(\Box^{-1}G_{\mu\nu}\big)^{\rm T} = 8\pi G\, T_{\mu\nu}\ , \tag{3.3}$$

where the transverse part extraction $^{\rm T}$ of a symmetric tensor $W_{\mu\nu}$ is defined as,

$$W^{\rm T}_{\mu\nu} = W_{\mu\nu} - \nabla_\mu W_\nu - \nabla_\nu W_\mu\ , \tag{3.4}$$

with W_ν, a vector field defined by the nonlocal relation,

$$\nabla_\mu W^{\mu\nu} = \Box W^\nu + \nabla_\mu\nabla^\nu W^\mu\ . \tag{3.5}$$

It was shown in (Foffa et al., 2014b), that this model exhibits runaway solutions during the radiation domination era that spoils its cosmological viability. In particular, it was realised that this growing modes originated from the Ricci tensor contribution included in the $m^2(\Box_g^{-1}G_{\mu\nu})^{\rm T}$ term of Eq. (3.3), basically because its non-zero values in RD makes its convolution with $\Box_g^{-1}$ excessively grow. However, since $R|_{\rm FRW}/H^2 \simeq 0$ during the RD epoch, the following model do not have these problematic features,

$$G_{\mu\nu} - \frac{1}{3}m^2\big(g_{\mu\nu}\Box^{-1}R\big)^{\rm T} = 8\pi G\, T_{\mu\nu}\ , \tag{3.6}$$

where the factor $1/3$ is a convenient normalisation for the mass m^2. In the following, we will refer to this model as the "RT" model. The extraction of the transverse part (3.4) makes it difficult to be derived from an action as will be more clearly seen below. However, the linearisation of this equations over flat space reads,

$$\mathcal{E}^{\mu\nu\rho\sigma}h_{\rho\sigma} - \frac{2}{3}m^2P^{\mu\nu}P^{\rho\sigma}h_{\rho\sigma} = -\frac{\kappa}{2}T^{\mu\nu}\ , \tag{3.7}$$

2. Notice here that the procedure consisting in integrating out the Stückelberg fields from Eq. (2.112), does not remove any degrees of freedom from the theory. Indeed, the Stückelberg fields are precisely introduced as redundant, pure gauge fields for restoring an explicitly broken gauge symmetry. If one does not fix this gauge freedom in any way, as is the case when integrating them out, there is no apparent reason why this procedure would removes degrees of freedom of the theory. This was erroneously interpreted in (Dvali, 2006; Dvali et al., 2007), which only focused on the tensorial structure of the propagator of (3.1), that reproduces the one of linearised GR as $m \to 0$. However, in the massive case the conservation of the source in Fourier space $k_\mu\tilde{T}^{\mu\nu}(k) = 0$, where $k_\mu = \big(-\omega, 0, 0, k\big)$ with $\omega = \sqrt{k^2+m^2}$, introduces mass dependent terms that couple the helicity-0 and helicity-1 modes to the source (Jaccard et al., 2013).

where $\mathcal{E}^{\mu\nu\rho\sigma}$ is defined in Eq. (2.106). This equation can be integrated into the following action,

$$S = \int \mathrm{d}^4x \left[\frac{1}{2}h_{\mu\nu}\mathcal{E}^{\mu\nu\rho\sigma}h_{\rho\sigma} - \frac{1}{3}m^2 h_{\mu\nu}P^{\mu\nu}P^{\rho\sigma}h_{\rho\sigma} + \frac{\kappa}{2}h_{\mu\nu}T^{\mu\nu}\right], \tag{3.8}$$

where $P_{\mu\nu}$ is the transverse projector defined as,

$$P^{\mu\nu} \equiv \eta^{\mu\nu} - \frac{\partial^\mu\partial^\nu}{\Box}\,. \tag{3.9}$$

As expected from local Lagrange densities, the degrees of freedom content of the theory is read from its propagator. In inserting a term fixing the Lorentz gauge at the level of the action,

$$S_{gf} = -\int \mathrm{d}^4x \left(\partial^\nu h_{\mu\nu} - \frac{1}{2}\eta_{\mu\nu}\partial^\nu h\right)\left(\partial_\rho h^{\mu\rho} - \frac{1}{2}\eta^{\mu\rho}\partial_\rho h\right), \tag{3.10}$$

which effectively sets,

$$\partial^\nu h_{\mu\nu} - \frac{1}{2}\eta_{\mu\nu}\partial^\nu h = 0\,, \tag{3.11}$$

in Eq. (3.7), yields a gauge fixed action of the form,

$$S = \frac{1}{2}\int \mathrm{d}^4x\ h_{\mu\nu}\left[\mathcal{E}^{\mu\nu\rho\sigma} + \Gamma^{\mu\nu\rho\sigma} - \frac{2}{3}m^2P^{\mu\nu}P^{\rho\sigma}\right]h_{\rho\sigma}\,, \tag{3.12}$$

$$\equiv \frac{1}{2}\int \mathrm{d}^4x\ h_{\mu\nu}Q^{\mu\nu\rho\sigma}h_{\rho\sigma}\,, \tag{3.13}$$

where,

$$\Gamma^{\mu\nu\rho\sigma} \equiv \frac{1}{2}\left(\eta^{\mu\rho}\partial^\nu\partial^\sigma + \eta^{\nu\sigma}\partial^\mu\partial^\rho + \eta^{\nu\rho}\partial^\mu\partial^\sigma + \eta^{\mu\sigma}\partial^\nu\partial^\rho\right) - \left(\eta^{\mu\nu}\partial^\rho\partial^\sigma + \eta^{\rho\sigma}\partial^\mu\partial^\nu\right) + \frac{1}{2}\eta^{\mu\nu}\eta^{\rho\sigma}\Box\,.$$

One can then invert the corresponding quadratic form $Q^{\mu\nu\rho\sigma}$ in Fourier space and one finds,

$$\Delta^{\mu\nu\rho\sigma}(k) = -\frac{1}{2k^2}\left[(\eta^{\mu\rho}\eta^{\nu\sigma} + \eta^{\mu\sigma}\eta^{\nu\rho}) - \eta^{\mu\nu}\eta^{\rho\sigma}\right] - \frac{1}{6}\left[\frac{1}{k^2} + \frac{1}{-k^2+m^2}\right]\bar{P}^{\mu\nu}\bar{P}^{\rho\sigma}\,, \tag{3.14}$$

where we have defined,

$$\bar{P}^{\mu\nu} \equiv \eta^{\mu\nu} + 2\frac{k^\mu k^\nu}{k^2}\,. \tag{3.15}$$

Therefore, from a naive inspection of the propagator, one concludes that the theory contains a massless spin-2 particle, a massless scalar and a massive one which has the wrong sign in front of its kinetic term, i.e. a *ghost*. Such pathologies are very frequent in the context of nonlocal theories and should be interpreted in a correct way. Below, we will address a discussion on the extent to which such pathologies are fatal for the fate of the theory.

3.1.1 No vDVZ Discontinuity, No Quantum Theory

Before we focus on the interpretation of the ghost pole present into (3.14), first observe that the form of the propagator makes explicit the fact that the theory has no vDVZ discontinuity

on flat space. Indeed, at a classical level where the propagator is chosen so as to be of the retarded kind $k^2 \to k^2 = -(k^0 + i\epsilon)^2 - \vec{k}^2$, the massless limit $m^2 \to 0$ implies,

$$\lim_{\epsilon\to 0^+} \frac{1}{k^2} + \frac{1}{-k^2+m^2} \longrightarrow 0\,, \tag{3.16}$$

so that the propagator of the healthy massless scalar cancels with the one of the ghost. Observe that this is however not true in a quantum context where the propagator needs to be taken of the Feynman kind. For a healthy scalar, the Feynman prescription reads $(k^0)^2 \to (k^0)^2 + i\epsilon$ so as to make the path integral converge $iS[\phi] \sim -\epsilon\phi^2$. However, in the case of a ghost one obtains the opposite sign $+\epsilon\phi^2_{\rm ghost}$, the path integral diverges and the unitarity of the quantum theory is lost. Instead, if one makes the opposite, anti-causal choice $(k^0)^2 \to (k^0)^2 - i\epsilon$ for the ghost, unitary is preserved but then the theory propagates negatives energies forward in time, and positive energies backwards in time. In the former case the propagators cancel each other as in the classical case, while in the latter one has,

$$\lim_{\epsilon\to 0^+}\lim_{m\to 0}\left(-\frac{i}{k^2-i\epsilon} - \frac{i}{-k^2+m^2-i\epsilon}\right) = \lim_{\epsilon\to 0^+}\frac{2\epsilon}{k^4-\epsilon^2} = 2\pi\delta(k^2)\,, \tag{3.17}$$

which equals the real part of the Feynman propagator for massless particles. This shows that either the vDVZ discontinuity is maintained at the quantum level, but then unitarity is lost or, alternatively, unitarity can be preserve but then an anomalous vDVZ discontinuity appears together with the propagation of negative energy particles forward in time. From these considerations, we conclude that putting the theory (3.8) into a path integral is meaningless, i.e. it cannot be quantised, and that is, this theory shall be considered to make sense at a classical level only.

3.1.2 Interlude: Apparent Ghost in Nonlocal Theories and Auxiliary Initial Conditions

Let us now address the ghost problem for nonlocal theories. The general idea is that both of the extra scalar poles appearing into the Green's function (3.14) are not genuine degrees of freedom of the theory, in that their initial conditions are constrained by virtue of the nonlocal structure of the action from which they derive.

Let us provide a simple example illustrating how the presence of nonlocalities into an action can give raise to such poles. Consider a massless scalar field coupled to a source on flat space,

$$S = \int \mathrm{d}^4x\, \left[\frac{1}{2}\phi\Box\phi - \phi J\right]. \tag{3.18}$$

Now we can insert the identity operator $\Box\Box^{-1} = 1$, into this action such as, after integration by parts,

$$S = \int \mathrm{d}^4x\, \left[\frac{1}{2}\big(\Box\phi\big)\Box^{-1}\big(\Box\phi\big) - \phi J\right]. \tag{3.19}$$

We can then introduce a new *auxiliary* field ψ as,

$$S = \int \mathrm{d}^4x\, \left[-\frac{1}{2}\psi\Box\psi + \psi\Box\phi - \phi J\right], \tag{3.20}$$

so that in computing its equation of motion and solving for ψ one gets, $\psi = \Box^{-1}\Box\phi = \phi + \psi^{(h)}$, where $\psi^{(h)}$ is a homogeneous solution, $\Box\psi^{(h)} = 0$,[3]. In putting this solution back into the action, one recovers the original action (3.18). Instead, introducing a new field $\psi = \bar{\psi} + \phi$, diagonalises the action,

$$S = \int \mathrm{d}^4x \left[-\frac{1}{2}\bar{\psi}\Box\bar{\psi} + \frac{1}{2}\phi\Box\phi - \phi J \right], \tag{3.21}$$

where one can see that the localised formulation of the (artificially made) nonlocal action (3.19), leads to the presence of a ghost pole into the propagator. However, it is clear from the original action (3.18), that such a pole does in fact not exist, i.e. that it is an artifact of the localisation procedure[4]. Actually, (3.21) is consistent with (3.18), since the ghost is completely decoupled from the rest of the fields ϕ, J and therefore cannot influence them in any way. Within the path integral formalism, this translates into the fact that no such fields can be sourced by the presence of a term ψJ_ψ, into the generating functional of the theory. The presence of such a term is forbidden by the fact that ψ is only an *auxiliary* field, introduced for mathematical convenience. Consequently, if ψ does not interact with any fields, its contribution factors out from any n-point functions,

$$\frac{\langle 0, \mathrm{out}|\ldots|0,\ \mathrm{in}\rangle}{\langle 0, \mathrm{out}|0,\ \mathrm{in}\rangle} = \frac{\int \mathcal{D}\phi\mathcal{D}\psi\ \ldots\ e^{iS[\phi]+iS[\psi]-J\phi}}{\int \mathcal{D}\phi\mathcal{D}\psi\ e^{iS[\phi]+iS[\psi]}} \tag{3.22}$$

$$= \frac{\int \mathcal{D}\phi\ \ldots\ e^{iS[\phi]-J\phi}}{\int \mathcal{D}\phi\ e^{iS[\phi]}}\,, \tag{3.23}$$

i.e. the fields contribution decouples from the theory. Instead, if the ghost couples to ϕ, $S[\psi] \to S[\psi] + S_{\mathrm{int}}[\psi, \phi]$ in (3.22), it can still not appear on the external legs, but can manifest itself into internal lines as virtual particles. Interpreted classically, this means that the homogeneous solution associated to the auxiliary fields introduced in localising the action are constrain to vanish (Koshelev, 2009; Koivisto, 2010; Barvinsky, 2012; Deser and Woodard, 2013b; Maggiore, 2014; Foffa et al., 2014a,b; Maggiore and Mancarella, 2014; Dirian and Mitsou, 2014). In a general context, at the quantum level, this implies that there is no creation and annihilation associated with such fields. However, it is not clear how auxiliary fields can never be produced in resonances whose rate, by virtue of the optical theorem, is related to the imaginary part induced from loop quantum corrections to the masses of physical fields. In gauge theories, such process is protected by gauge invariance and the S-matrix acquires a block diagonal form that prevents unphysical states to be generated out of physical ones. Such a structure is characterised by the presence of the BRST symmetry (Zinn-Justin, 2002), that ensures unitarity to be preserved in any processes, and therefore forbidding the resonances of ghosts. A specific underlying structure for nonlocal theories has however not yet been presented. Given that fact, again, nonlocal theories should be considered only at a classical level, resulting from some form of quantum averaging process giving raise to non-perturbative effects. Therefore, the additional propagators they contain, associated with the presence of nonlocal operators into the action, are seen as associated to auxiliary fields that do not reflect any physical reality. In this view, a local representation of the corresponding theory, if it exists, is only a convenient mathematical reformulation of the problem, where the homogeneous solution for the auxiliary fields need to be fixed to zero.

3. A technical remarks here is that one generically has the identity $\Box\Box^{-1} = 1$, i.e. $\Box^{-1}$ is always a right inverse for $\Box$, however it is a left inverse only up to an homogeneous solution $f^{(h)}$, i.e. $\Box^{-1}\Box = f^{(h)}$.

4. A similar example has been given into (Foffa et al., 2014a) within the framework of GR linearised over flat space.

Observe however that vanishing homogeneous solutions for the auxiliary fields does not necessarily imply the vanishing of their initial conditions. A simple example illustrating this fact is provided in considering the nonlocal correction to the Einstein-Hilbert action reading,

$$\Delta S = \int \mathrm{d}^4x\sqrt{-g}\; R\frac{1}{\Box}R\,. \tag{3.24}$$

Such a nonlocal correction can be localised by invoking an auxiliary scalar field U as,

$$\Delta S = \int \mathrm{d}^4x\sqrt{-g}\; \left[RU + \chi(\Box U - R)\right]. \tag{3.25}$$

where χ is a Lagrange multiplier imposing the constraint $\Box U = R$, which can be formally solved by writing $U = \Box^{-1}R + U^{\mathrm{hom}}$, with the homogeneous solution $\Box U^{\mathrm{hom}} = 0$. Putting then this solution for U into the action (3.25) reproduces the action (3.24), provided the homogeneous solution U^{hom}, is put to zero. Now, for the sake of the argument, consider the metric in synchronous gauge,

$$\mathrm{d}s^2 = -\mathrm{d}t^2 + h_{ij}\mathrm{d}x^i\mathrm{d}x^j\,. \tag{3.26}$$

In that case we have,

$$R = -\Box\log h + \mathcal{O}(\partial_\mu)\,, \tag{3.27}$$

where h is the determinant of the 3-metric h_{ij}, and we neglect terms containing derivative number lower than two, as they do not affect our conclusion [the entire expression for this quantity can be found in (Deser and Woodard, 2013a)]. Therefore, we can write the constraint imposed by χ as, $\Box U = -\Box\log h$ whose general solution reads,

$$U(t,\vec{x}) = -\log\gamma(t,\vec{x}) + U^{\mathrm{hom}}(t,\vec{x})\,, \tag{3.28}$$

where again U^{hom}, needs to be fixed to zero. Therefore, we see that, at initial time, the presence of an operator of the form $\Box(\dots)$, into the source of the auxiliary field provides non-trivial initial conditions to it. Moreover, these initial conditions are not free to choose, as they are related to the ones of the determinant of the three metric (themselves constrained by the Hamiltonian constraint). This needs to be contrasted with the situation where no such operator appear into the source which we denote, say, S. In that case, the general solution with vanishing initial homogeneous part reads, $U = \Box^{-1}S$, where the Green's function needs to be taken of the retarded kind for causality reasons,

$$U(t,\vec{x}) = (\Box^{-1}S)(t,\vec{x}) = \int_{-\infty}^{t}\mathrm{d}t'\int\mathrm{d}^3\vec{x}'\sqrt{-g}\; G_{\mathrm{ret}}\big(t-t';\vec{x}-\vec{x}'\big)S(t',\vec{x}')\,. \tag{3.29}$$

It is only in the case where the nonlocal effect starts at the initial time $t = t_0$, that we then have $G_{\mathrm{ret}}\big(t_0 - t';\vec{x}-\vec{x}'\big) = 0$, for $t' < t_0$, so that the initial conditions for the auxiliary field vanish. In the case where the nonlocal terms is non-negligible into the past, or if the source of the auxiliary field propagating with $\Box$, contains an operator of the generic form $\Box(\dots)$, their initial condition are generically non-vanishing.

In the following, we present a computation allowing to rewrite the nonlocal action (3.8) and a local way, integrating-in such auxiliary fields. In order for this procedure to maintain causality, we make use of the formalism for dissipative systems presented in Sec. 2.1, from nonlocal to local formulation. Ultimately, we will see that this procedure is actually quite pedant, and that more straightforward and simple ways can be used to obtain the very same result, we review it however for completeness.

3.1.3 Localisation using Dissipative Systems Techniques

We consider here the gauge fixed linearised action over flat space for the RT model (3.12), as the resulting nonlocal action obtained from the techniques displayed in Sec. 2.1. In this view, we introduce the fields $h^{\pm}_{\mu\nu} \equiv h^1_{\mu\nu} \pm h^2_{\mu\nu}$, so that one can write,

$$S = \frac{1}{2}\int \mathrm{d}^4x\ h^-_{\mu\nu}\left[\mathcal{E}^{\mu\nu\rho\sigma} + \Gamma^{\mu\nu\rho\sigma} - \frac{2}{3}m^2 P^{\mu\nu}_{\rm ret}P^{\rho\sigma}_{\rm ret}\right]h^+_{\rho\sigma}\,, \tag{3.30}$$

$$\equiv \frac{1}{2}\int \mathrm{d}^4x\ h^-_{\mu\nu}Q^{\mu\nu\rho\sigma}h^+_{\rho\sigma}, \tag{3.31}$$

with $P^{\mu\nu}_{\rm ret}$, the transverse projector (3.9) where the Green's function used is of the retarded type. A causal evolution for $h^+_{\mu\nu}$ can then be obtained by varying the action with respect to $h^-_{\mu\nu}$ and taking the physical limit $h^1_{\mu\nu} \to h^2_{\mu\nu}$. The above action can be obtained from,

$$S = \frac{1}{2}\int \mathrm{d}^4x\ \left[- H^-_{\mu\nu}\Delta^{\mu\nu\rho\sigma}H^+_{\rho\sigma} + H^-_{\mu\nu}h^{\mu\nu}_+ + H^+_{\mu\nu}h^{\mu\nu}_-\right], \tag{3.32}$$

in integrating out the auxiliary field $H^+_{\mu\nu}$, using the equation of motion of $H^-_{\mu\nu}$ and putting the homogeneous solution to zero (we will do so throughout the procedure). Here $\Delta^{\mu\nu\rho\sigma} \equiv \Delta^{\mu\nu\rho\sigma}_{ret}(x)$ is the quadratic form (3.14) in coordinate space, whose Green's functions are fixed to be the retarded ones and characterises the variational procedure that is used. The resulting action is still nonlocal, so we iterate the process. In Eq. (3.32), we know that the quadratic form (3.13) contains that of a massless spin-2, which can therefore be inverted independently. Writing,

$$\begin{aligned} S = \frac{1}{2}\int \mathrm{d}^4x\ K^-_{\mu\nu}\left[\mathcal{E}^{\mu\nu\rho\sigma} + \Gamma^{\mu\nu\rho\sigma}\right]K^+_{\rho\sigma} + \frac{1}{6}H^-_{\mu\nu}\Big(- \Box^{-1}_{ret} + \big(\Box + m^2\big)^{-1}_{ret}\Big)\bar{P}^{\mu\nu}_{ret}\bar{P}^{\rho\sigma}_{ret}H^+_{\rho\sigma} \\ + K^-_{\mu\nu}H^{\mu\nu}_+ + K^+_{\mu\nu}H^{\mu\nu}_- + H^-_{\mu\nu}h^{\mu\nu}_+ + H^+_{\mu\nu}h^{\mu\nu}_-\,, \end{aligned} \tag{3.33}$$

the next step is therefore to work on the remaining nonlocal scalar terms. Integrating-in two scalars so as to invert their propagators one gets,

$$\begin{aligned} S = \frac{1}{2}\int \mathrm{d}^4x\ \Bigg[K^-_{\mu\nu}\Big(\mathcal{E}^{\mu\nu\rho\sigma} + \Gamma^{\mu\nu\rho\sigma}\Big)K^+_{\rho\sigma} + K^-_{\mu\nu}H^{\mu\nu}_+ + K^+_{\mu\nu}H^{\mu\nu}_- + H^-_{\mu\nu}h^{\mu\nu}_+ + H^+_{\mu\nu}h^{\mu\nu}_- \\ + \frac{1}{6}\Big(\phi^-\Box\phi^+ - \psi^-(\Box + m^2)\psi^+ + (\phi^- + \psi^-)\bar{P}^{\mu\nu}_{ret}H^+_{\mu\nu} + (\phi^+ + \psi^+)\bar{P}^{\mu\nu}_{ret}H^-_{\mu\nu}\Big)\Bigg]. \end{aligned} \tag{3.34}$$

The last Green's function contained in $\bar{P}^{\mu\nu}_{ret}$ can be obtained via Lagrange multipliers imposing the constraints,

$$\chi^{\pm} = \bar{P}^{\mu\nu}_{ret}H^{\pm}_{\mu\nu} \quad \overset{hom=0}{\Longleftrightarrow} \quad \Box\chi^{\pm} = \big(\Box\eta^{\mu\nu} + 2\partial^\mu\partial^\nu\big)H^{\pm}_{\mu\nu}\,. \tag{3.35}$$

Therefore one arrives at,

$$\begin{aligned} S = \frac{1}{2}\int \mathrm{d}^4x\ \Bigg\{K^-_{\mu\nu}\Big(\mathcal{E}^{\mu\nu\rho\sigma} + \Gamma^{\mu\nu\rho\sigma}\Big)K^+_{\rho\sigma} + K^-_{\mu\nu}H^{\mu\nu}_+ + K^+_{\mu\nu}H^{\mu\nu}_- + H^-_{\mu\nu}h^{\mu\nu}_+ + H^+_{\mu\nu}h^{\mu\nu}_- \\ + \frac{1}{6}\Bigg[\phi^-\Box\phi^+ - \psi^-(\Box + m^2)\psi^+ + (\phi^- + \psi^-)\chi^+ + (\phi^+ + \psi^+)\chi^- \\ + \theta^-\Big(\Box\chi^+ - \big(\Box\eta^{\mu\nu} + 2\partial^\mu\partial^\nu\big)H^+_{\mu\nu}\Big) + \theta^+\Big(\Box\chi^- - \big(\Box\eta^{\mu\nu} + 2\partial^\mu\partial^\nu\big)H^-_{\mu\nu}\Big)\Bigg]\Bigg\}, \end{aligned} \tag{3.36}$$

The above action can be obtained from,

$$S = \int \mathrm{d}^4x \left\{ \frac{1}{2} K^{\mu\nu} \Big(\mathcal{E}^{\mu\nu\rho\sigma} + \Gamma^{\mu\nu\rho\sigma} \Big) K_{\rho\sigma} + H_{\mu\nu} \big(h^{\mu\nu} + K_{\mu\nu} \big) \right. \\ \left. + \frac{1}{6} \Big[-\frac{1}{2} \partial_\mu \phi \partial^\mu \phi + \frac{1}{2} \partial_\mu \psi \partial^\mu \psi - \frac{1}{2} m^2 \psi^2 + (\phi + \psi)\chi + \theta \Big(\Box \chi - \big(\Box \eta^{\mu\nu} + 2\partial^\mu \partial^\nu \big) H_{\mu\nu} \Big) \Big] \right\}, \tag{3.37}$$

Furthermore, one can integrate out $K_{\mu\nu}$ through the equation of motion for $H_{\mu\nu}$ since it is a Lagrange multiplier. One gets the constraint,

$$K_{\mu\nu} = -h_{\mu\nu} + \frac{1}{6} \big(\Box \eta^{\mu\nu} + 2\partial^\mu \partial^\nu \big) \theta \,, \tag{3.38}$$

and the integration leads to,

$$S = \int \mathrm{d}^4x \left\{ \frac{1}{2} \left[h_{\mu\nu} \Big(\mathcal{E}^{\mu\nu\rho\sigma} + \Gamma^{\mu\nu\rho\sigma} \Big) h_{\rho\sigma} - \frac{2}{3} \big(\partial_\mu \partial_\nu - \Box \eta_{\mu\nu} \big) h^{\mu\nu} \Box \theta - \frac{1}{6} \theta \Box^3 \theta \right] \right. \\ \left. + \frac{1}{6} \Big(-\frac{1}{2} \partial_a \phi \partial^a \phi + \frac{1}{2} \partial_a \psi \partial^a \psi - \frac{1}{2} m^2 \psi^2 + (\phi + \psi)\chi + \theta \Box \chi \Big] \right\}. \tag{3.39}$$

Now, as the equation of motion of χ leads to the constraint $\Box\theta = -(\phi + \psi)$, one can integrate over $\Box\theta$ and obtains,

$$S = \int d^4x \, \left[\frac{1}{2} h_{\mu\nu} \mathcal{E}^{\mu\nu\rho\sigma} h_{\rho\sigma} + \frac{1}{3} \big(\partial_\mu \partial_\nu - \Box \eta_{\mu\nu} \big) h^{\mu\nu} (\phi + \psi) \right. \\ \left. - \frac{1}{6} \Big(-\partial_\mu \psi \partial^\mu \psi + \frac{1}{2} m^2 \psi^2 - \partial_\mu \psi \partial^\mu \phi \Big) \right] \,. \tag{3.40}$$

where we discarded the gauge fixing term $\Gamma^{\mu\nu\rho\sigma}$ for convenience. This is the corresponding *localised* action of the nonlocal equations of motion (3.7) that we started with. To see this more clearly, we replace ϕ by $\xi = \phi + \psi$ and the latter becomes,

$$S = \int d^4x \, \left[\frac{1}{2} h_{\mu\nu} \mathcal{E}^{\mu\nu\rho\sigma} h_{\rho\sigma} + \frac{1}{3} \big(\partial_\mu \partial_\nu - \Box \eta_{\mu\nu} \big) h^{\mu\nu} \xi - \frac{1}{6} \Big(\psi \Box \xi + \frac{1}{2} m^2 \psi^2 \Big) - \frac{\kappa}{2} h_{\mu\nu} T^{\mu\nu} \right], \tag{3.41}$$

where we have coupled $h_{\mu\nu}$ to matter. We can now compute the equation of motion for ξ, ψ and $h_{\mu\nu}$ respectively,

$$\Box \psi = 2(\partial_\mu \partial_\nu - \eta_{\mu\nu} \Box) h^{\mu\nu} \,, \tag{3.42}$$

$$\Box \xi = -m^2 \psi \,, \tag{3.43}$$

$$\mathcal{E}^{\mu\nu\rho\sigma} h_{\rho\sigma} + \frac{1}{3} (\partial^\mu \partial^\nu - \eta^{\mu\nu} \Box) \xi = \frac{\kappa}{2} T^{\mu\nu} \,, \tag{3.44}$$

and focus on the subsystem including $h_{\mu\nu}$ only, i.e. to express its equation of motion in a nonlocal way. To do so, one expresses ξ in terms of the latter. Discarding the homogeneous solutions one gets,

$$\xi = -m^2 \frac{2}{\Box^2} \big(\partial^\rho \partial^\sigma - \eta^{\rho\sigma} \Box \big) h_{\rho\sigma} \,, \tag{3.45}$$

and putting this into the equation of motion for the metric perturbation leads to,

$$\mathcal{E}^{\mu\nu\rho\sigma} h_{\rho\sigma} - \frac{2}{3} m^2 P^{\mu\nu} P^{\rho\sigma} h_{\rho\sigma} = \frac{\kappa}{2} T^{\mu\nu} \,, \tag{3.46}$$

which is the equation of motion (3.7), that we started with. Observe also that (3.41) can be diagonalised in performing the replacement,

$$\bar{h}_{\mu\nu} = h_{\mu\nu} + \frac{1}{3}\left(\eta_{\mu\nu} + 2\frac{\partial_\mu\partial_\nu}{\Box}\right)\xi\,, \tag{3.47}$$

in the action (3.41), which then becomes,

$$S = \int \mathrm{d}^4x\,\left[\frac{1}{2}\bar{h}_{\mu\nu}\mathcal{E}^{\mu\nu\rho\sigma}\bar{h}_{\rho\sigma} + \frac{1}{6}\left(-\psi\Box\xi + \frac{1}{2}\xi\Box\xi - \frac{1}{2}m^2\psi^2\right)\right.$$
$$\left. - \frac{\kappa}{2}\bar{h}_{\mu\nu}T^{\mu\nu} + \frac{1}{6}\xi\left(\eta_{\mu\nu} + 2\frac{\partial_\mu\partial_\nu}{\Box}\right)T^{\mu\nu}\right], \tag{3.48}$$

and going back to $\phi = \xi - \psi$ instead of ξ one obtains,

$$S = \int d^4x\,\left[\frac{1}{2}\bar{h}_{\mu\nu}\mathcal{E}^{\mu\nu\rho\sigma}\bar{h}_{\rho\sigma} + \frac{1}{6}\left(\frac{1}{2}\phi\Box\phi - \frac{1}{2}\psi\Box\psi - \frac{1}{2}m^2\psi^2\right)\right.$$
$$\left. - \frac{\kappa}{2}\bar{h}_{\mu\nu}T^{\mu\nu} + \frac{\kappa}{12}(\phi+\psi)\left(\eta_{\mu\nu} + 2\frac{\partial_\mu\partial_\nu}{\Box}\right)T^{\mu\nu}\right], \tag{3.49}$$

independently of whether or not the gauge fixing term is kept into (3.40). This shows in particular that the structure of the propagators found in (3.14) is recovered directly into the action, when auxiliary fields are integrated-in so as it is local. One should however note that such a localisation procedure is not always possible [see e.g. (Mitsou, 2015)]. From the above action, it is clear that the ghost field is ψ, which is carried by ξ and is present as well into the "Jordan frame" action (3.41). This action admits a rather trivial canonical covariantisation that we show now and that leads to the so-called "RR" model.

3.2 Covariantization: The RR model

The canonical covariant form of the linear action (3.41) is provided by,

$$S = \frac{1}{16\pi G}\int \mathrm{d}^4x\sqrt{-g}\,\left[R\tilde{\xi} - \frac{1}{2}\left(\psi\Box\tilde{\xi} + \frac{1}{12}m^2\psi^2\right)\right] + S_M[\psi, g]\,, \tag{3.50}$$

where we extracted $\kappa \equiv (32\pi G)^{1/2}$ from $h_{\mu\nu}$, ξ and ψ so that they are dimensionless and redefined,

$$\xi \longrightarrow \tilde{\xi} = 1 + \frac{\xi}{6}\,. \tag{3.51}$$

The equations of motion for ψ yields,

$$\psi = -\frac{6}{m^2}\Box\tilde{\xi}\,. \tag{3.52}$$

which once inserted back into (3.50) leads to,

$$S = \frac{1}{16\pi G}\int \mathrm{d}^4x\sqrt{-g}\,\left[R\tilde{\xi} + \frac{1}{2\tilde{m}^2}\left(\Box\tilde{\xi}\right)^2\right] + S_M[\psi, g]\,, \tag{3.53}$$

where we have defined $\tilde{m} \equiv \alpha m$, $\alpha \equiv \sqrt{1/3}$. Computing the equation of motion for $\tilde{\xi}$ one obtains,

$$\Box^2 \tilde{\xi} = -\tilde{m}^2 R\,, \tag{3.54}$$

which is solved by,

$$\tilde{\xi} = \left(1 - \frac{\tilde{m}^2}{\Box^2} R\right), \tag{3.55}$$

where the first term comes from the homogeneous solution of $\tilde{\xi}$ which from (3.51), is equal to 1 since the one of ξ is vanishing (as it is an auxiliary field). Integrating-out $\tilde{\xi}$ from the action leads to the following nonlocal model,

$$S = \frac{1}{16\pi G} \int \mathrm{d}^4x\sqrt{-g}\, \left[R - \frac{1}{2}\tilde{m}^2 R \frac{1}{\Box^2} R\right] + S_M[\psi, g]\,. \tag{3.56}$$

where,

$$\big(\Box^{-1} R\big)(x) = \int \mathrm{d}^4y \sqrt{-g(y)} G(x,y) R(y)\,, \qquad \Box_x G(x,y) = \frac{1}{\sqrt{-g(x)}}\delta^{(4)}(x-y)\,, \tag{3.57}$$

and $G(x,y)$ is a generic Green's function. Observe that, as is clear from the procedure we followed, this action has the same linearisation over Minkowski space than the RT model (3.6), given in Eq. (3.8). However, at nonlinear level they differ significantly in their higher corrections $\mathcal{O}(h^n_{\mu\nu})$ with $n > 2$, as well as their dynamics on a different background, as we will see below in the case of FLRW. The corresponding equations of motion are obtained using,

$$\delta R = \big(R_{\mu\nu} - \nabla_\mu\nabla_\nu + g_{\mu\nu}\Box_g\big)\delta g^{\mu\nu}\,, \tag{3.58}$$

$$\big(\delta\Box\big)\phi = \left(\nabla_\mu\nabla_\nu\phi + \nabla_\mu\phi\nabla_\nu - \frac{1}{2}g_{\mu\nu}\nabla_\rho\nabla^\rho\right)\delta g^{\mu\nu}\,, \tag{3.59}$$

and read,

$$\left(1 - \frac{\tilde{m}^2}{\Box^2}R\right)G_{\mu\nu} + \tilde{m}^2\Bigg[\big(\nabla_\mu\nabla_\nu - g_{\mu\nu}\Box_g\big)\frac{1}{\Box^2}R + \frac{1}{4}g_{\mu\nu}\left(\frac{1}{\Box}R\right)^2 - \frac{1}{2}\big(g_{\mu\rho}g_{\nu\sigma} + g_{\mu\sigma}g_{\nu\rho} - g_{\mu\nu}g_{\rho\sigma}\big)\left(\nabla^\rho\frac{1}{\Box}R\right)\left(\nabla^\sigma\frac{1}{\Box^2}R\right)\Bigg] = 8\pi G\, T_{\mu\nu}\,, \tag{3.60}$$

where the Green's function is chosen to be of the retarded type,

$$G(x,y) \equiv G_{\rm ret}(x,y)\,. \tag{3.61}$$

This condition is not sufficient for solving (3.57), as one still needs to specify initial conditions. Invoking some local coordinates x^μ (e.g. synchronous), where ∂_0 is timelike and stating that the nonlocal effects start at an initial time t_0, one must impose that,

$$G(x,y)|_{x^0=t^0} = 0\,, \qquad \partial_0 G(x,y)|_{x^0=t_0} = 0\,, \tag{3.62}$$

which is equivalent of fixing the homogeneous solution together with the Green's function type when solving, $\Box\phi = R$. From general covariance, one can immediately check that Eq. (3.60),

respects the Bianchi identities. This is easily checked in applying ∇^μ to the latter equation and using the relation $\left[\nabla_\mu, \nabla_\nu\right]\nabla^\mu = R_{\mu\nu}\nabla^\mu$.

We recall that this theory only makes sense in a classical context, where the Green's function are systematically all switched to their retarded cousins. As we will discuss below, together with the RT model (3.6), the RR model gives raise to a late time phase of cosmic acceleration without the need of a cosmological constant. Before getting to this, we address another method for counting the degrees of freedom into the theory, which will highlight further the fact that only massless tensor modes are propagating into the theories provided by Eqs. (3.6) and (3.56).

3.2.1 Degrees of Freedom Count and Stability

The strategy used here for counting the number of degrees of freedom is inspired by the one used in (Deser and Woodard, 2013a) [see also (Dirian and Mitsou, 2014)] for establishing the degrees of freedom count and dynamical stability of the $f(\Box^{-1}R)$ model present in Sec. 2.4. Take the metric in synchronous gauge that we recall here,

$$\mathrm{d}s^2 = -\mathrm{d}t^2 + h_{ij}\mathrm{d}x^i\mathrm{d}x^j\,, \tag{3.63}$$

chosen as the coordinate system where the initial conditions of the Green's function (3.62) are realised. In GR the dynamical equations are provided by the equations of motion for g_{ij},

$$G_{ij} = \frac{1}{2}\ddot{h}_{ij} - \frac{1}{2}h_{ij}\partial_t^2\log h + \mathcal{O}(\partial_t^2)\,, \qquad h \equiv h_{ij}\,, \tag{3.64}$$

while the equations of motion for g_{00} and g_{i0} are the Hamiltonian and momentum constraints respectively, constraining the initial conditions $h_{ij}(t_0)$, $\dot{h}_{ij}(t_0)$. The latter reduce the number of independent initial conditions of h_{ij} and therefore determines the degrees of freedom of the theory. Therefore, if the correction to the (0μ) component of the equations of motion (3.60) vanishes, the RR model has the same number of degrees of freedom as GR. The terms $\partial_t^n\Box^{-m}R$ with $n = 0, 1$ and $m = 1, 2$ are zero when $t = t_0$, because of the properties of the Green's function chosen. Moreover, the operator $(\nabla_0\nabla_\mu - g_{0\mu}\Box)$ does not contain second-order time derivative when evaluated on the metric (3.63) and we can conclude that the nonlocal correction to the (0μ) components of Eq. (3.60) vanishes. This means that the RR model propagates only two degrees of freedom, which are the ones of a massless spin-2 field.

Concerning the stability of these modes, as investigating the stability of the dynamics of GR is a very non-trivial task [see e.g. (Christodoulou and Klainerman, 1993) for a rigorous treatment in the flat case], we study whether some necessary stability conditions are fulfilled. An obvious such condition is that the nonlocal correction of the (ij) component of Eq (3.60) does not significantly alter the dynamics of the propagating modes, e.g. that the overall sign of the kinetic term (3.64) does not change, such as the degrees of freedom of the theory do not turn ghostlike [5]. Expressing the Ricci scalar as,

$$R = -\Box\log h + \mathcal{O}(\partial_t)\,, \tag{3.65}$$

so that $\Box^{-1}R$ only contains the fields h_{ij} and their first time derivatives. However, the latter are inside an integral on time since the Green's functions are retarded, so one needs two time derivatives acting on $\Box^{-1}R$ to obtain second-order derivatives of h_{ij}. Thus, the only terms that can contain two time derivative in the (ij) component of Eq. (3.60) are those proportional to

5. Notice that only the first term matters in (3.64), as the second one is constrained by the Hamiltonian constraint.

G_{ij}, or those with at least to derivative acting on $\Box^{-1}R$. As a consequence, only the first two terms are concerned, and since we can write the second one as,

$$(\nabla_i\nabla_j - h_{ij}\Box)\Box^{-2}R = \nabla_i\nabla_j\Box^{-2}R - h_{ij}\Box^{-1}R\,, \tag{3.66}$$

only the first one matters. Therefore the kinetic part of the dynamical equation reads,

$$\frac{1}{2}\left(1 - \frac{\tilde{m}^2}{\Box^2}R\right)\left(\ddot{h}_{ij} - h_{ij}\partial_t^2\log h\right) + \mathcal{O}(\partial_t) = 8\pi G\, T_{ij}\,. \tag{3.67}$$

Thus, if the term $(1 - \tilde{m}^2\Box^{-2}R)$ becomes negative, then graviton becomes a ghost. The fact that the theory does not feature a vDVZ discontinuity and that, for cosmological purposes, the mass should be of the order of the horizon $\sim H_0$, the term $\tilde{m}^2\Box^{-2}R \ll 1$ is very suppressed at solar system scales. One must therefore study the behavior of this term into the cosmological context. As has been shown in (Dirian and Mitsou, 2014), this term remains positive during the whole past history of the Universe, and therefore the corresponding degrees of freedom are stable. It only approaches dangerously zero into the very far future. This proves the stability of gravitational waves in cosmological linear perturbation theory for both, the RT and the RR model, as could have been already anticipated from the linearised action Eq. (3.8), together with the conditions that no degrees of freedom are associated with the scalar pole of the corresponding propagator.

3.3 Local RR in Einstein Frame

In the case of the RR model, one can also draw the same considerations about the number of degrees of freedom and stability thereof, but at the fully nonlinear level. This can be done in expressing the localised action for the RR action (4.13) into Einstein frame, where the kinetic term for gravity $\sqrt{-g}R$ is decoupled for the scalar sector. In order to do so, for realistic scenarios $\xi > 0$, we defined a new field by $\xi \equiv e^{\frac{\alpha\varphi}{M}}$, and the action becomes,

$$S = \int \mathrm{d}^4x\sqrt{-g}\left[M^2 e^{\frac{\alpha\varphi}{M}}R + \frac{1}{2\tilde{m}^2}e^{\frac{2\alpha\varphi}{M}}\left(\Box\varphi + \frac{1}{3M}\nabla_\mu\varphi\nabla^\mu\varphi\right)^2\right], \tag{3.68}$$

where one has defined $M \equiv (16\pi G)^{-1}$. We can then go to the Einstein frame,

$$g_{\mu\nu} = e^{-\frac{\alpha\varphi}{M}}\tilde{g}_{\mu\nu}\,, \tag{3.69}$$

where the action reads,

$$S = \int \mathrm{d}^4x\sqrt{-\tilde{g}}\left[M^2\tilde{R} - \frac{1}{2}\tilde{\nabla}_\mu\varphi\tilde{\nabla}^\mu\varphi + \frac{1}{2m^2}e^{\frac{2\alpha\varphi}{M}}\left(\tilde{\Box}\varphi\right)^2\right], \tag{3.70}$$

where we have dropped a total derivative term [6]. Furthermore, the initial conditions of the field are,

$$\varphi(t_0) = \dot{\varphi}(t_0) = \ddot{\varphi}(t_0) = \dddot{\varphi}(t_0) = 0\,. \tag{3.71}$$

6. Note that, by the fact that $\xi \equiv e^{\frac{\varphi}{3M}}$, the canonical normalisation of φ only makes sense for $m \neq 0$, so here the GR limit $m \to 0$ should rather be understood as $\varphi \to 0$, $m \to 0$.

Since these are fixed, the RR model has the same degrees of freedom as GR. Finally, let us integrate-in a second auxiliary field ψ into Eq. (3.72), so as to lower the derivative order of the system,

$$S = \int \mathrm{d}^4x\sqrt{-\tilde{g}}\left[M^2\tilde{R} - \frac{1}{2}\tilde{\nabla}_\mu\varphi\tilde{\nabla}^\mu\varphi + \tilde{\nabla}_\mu\varphi\tilde{\nabla}^\mu\psi - \frac{m^2}{2}e^{-\frac{2\alpha\varphi}{M}}\psi^2\right], \tag{3.72}$$

and diagonalise the scalar sector $\varphi = \phi + \psi$ to obtain the canonical form,

$$S = \int \mathrm{d}^4x\sqrt{-\tilde{g}}\left[M^2\tilde{R} - \frac{1}{2}\tilde{\nabla}_\mu\varphi\tilde{\nabla}^\mu\varphi + \frac{1}{2}\tilde{\nabla}_\mu\psi\tilde{\nabla}^\mu\psi - \frac{1}{2}m^2\psi^2e^{-\frac{2\alpha(\phi+\psi)}{M}}\right], \tag{3.73}$$

with initial conditions reading,

$$\phi(t_0) = \dot{\phi}(t_0) = \psi(t_0) = \dot{\psi}(t_0) = 0\,. \tag{3.74}$$

As a consequence, one retrieves the kinetic structure read from the propagator (3.14) at the covariant level, including a physical graviton and two auxiliary scalars, one of which is massless while the other one is a massive ghost.

3.4 Stability re-Analysis and Future Singularity

From Eq. (3.73) we can extend the stability analysis perfomed in Sec. 3.2.1. From this equation we see that the Einstein-Hilbert term has the good sign and therefore that all modes of the metric $\tilde{g}_{\mu\nu}$ are well behaved. The deviation of GR is characterised by an extra, auxiliary scalar sector to which the metric couples, whose initial conditions are constrained to vanish. In effect, for linear perturbations around flat space without a source, $\bar{g} = \eta$, $\bar{\phi} = \bar{\psi} = 0$, the auxiliary fields are fixed to zero on the initial hypersurface and stay constant, as they do not interact with anything. However, if nonlinearities or interactions with a source are taken into account, the scalar degrees of freedom will get excited, and in particular, the infrared perturbations of ψ will involve runaway solutions diverging as $\sim \exp(\sqrt{m^2 - |k|^2}t)$ for $|k| < m$, affecting the dynamics of the whole system. On phenomenological, cosmological grounds, the mass of the m should be of the order of the Hubble constant today H_0, so as to influence only the far infrared regime of GR, that is, its dynamics at very large time and spatial scales. Consequently, the unstable modes are at very large scales $|k| < H_0$, mostly pushed behind the horizon, and solar system scales are safe.

Spherically Symmetric Solution

Such a conclusion is supported by the works of Refs. (Kehagias and Maggiore, 2014; Maggiore and Mancarella, 2014), which showed that the static spherically symmetric solution goes smoothly to the one of GR as $m \to 0$ and that the corrections to the Newtonian potential induced at small scales compared to the mass $r \ll m^{-1}$ are negligible. Indeed, for a static spherically symmetric solution of the form,

$$\mathrm{d}s^2 = -A(r)\mathrm{d}t^2 + B(r)\mathrm{d}r^2 + r^2\left(\mathrm{d}\theta^2 + \sin^2\theta\mathrm{d}\phi^2\right), \tag{3.75}$$

the Newtonian limit $r \gg r_S$, where r_S is the Schwartzchild radius, leads to,

$$A(r) = 1 - \frac{r_S}{r}\left[1 + \frac{1}{3}(1 - \cos mr)\right] \tag{3.76}$$

$$B(r) = 1 + \frac{r_S}{r}\left[1 - \frac{1}{3}(1 - \cos mr - mr\sin mr)\right] \tag{3.77}$$

so that the corrections to GR are of the order $\mathcal{O}(m^2r^2)$. For a mass $\sim H_0$ and a radius of $r = 1$ a.u., one finds the negligible amount $m^2r^2 \sim 10^{-30}$.

Big Rip from Phantom Dark Energy

On infrared scales however, linear perturbation theory on Minkowski space predicts the appearance of instabilities on infrared scales $\gtrsim H_0$. However, on such scales, the Hubble flow is non-negligible and one has to consider a cosmological background instead. We specialise therefore the RR model to flat homogeneous and isotropic FLRW background,

$$\mathrm{d}s^2 = -\mathrm{d}t^2 + a^2(t)\,\mathrm{d}\vec{x}^2\,, \qquad H \equiv \partial_t \log a\,, \tag{3.78}$$

and use the same definitions and localisation procedure as is used in (Dirian et al., 2014). The equations of motion for the two scalars a given by,

$$U = -\Box^{-1}R\,, \qquad S = -\Box^{-1}U = \Box^{-2}R\,, \tag{3.79}$$

where we consider vanishing initial conditions. We set the scale factor today $a_0 = 1$ and introduce the dimensionless variables $V \equiv H_0^2 S$, $h \equiv H/H_0$ and use the number of e-folds as time coordinates $x = \log a$, where ∂_x is denoted by a prime. The first Friedmann equation then reads,

$$h^2 = \frac{\Omega + (\gamma/4)U^2}{1 + \gamma(-3V' - 3V + U'V'/2)}\,, \tag{3.80}$$

which can be solve given the equations of motion for the auxiliary scalars,

$$U'' + (3+\zeta)U' = 6(2+\zeta)\,, \tag{3.81}$$

$$V'' + (3+\zeta)V' = h^{-2}U\,, \tag{3.82}$$

where,

$$\Omega \equiv \Omega_R e^{-4x} + \Omega_M e^{-3x}\,, \tag{3.83}$$

$$\zeta \equiv \frac{h'}{h} = \frac{1}{2(1-3\gamma V)}\left[h^{-2}\Omega' + 3\gamma\left(h^{-2}U + U'V' - 4V'\right)\right]. \tag{3.84}$$

In Eq. (3.84), the amount of effective dark energy is controlled by the parameter $\gamma \equiv m^2/(9H_0^2)$ and is fixed so as to close the Universe at present time. $h(x=0) = 1$. Typical cosmological studies need $\gamma \sim 10^{-2}$ [see e.g. (Dirian et al., 2014)]. We also define the total equation of state $w \equiv \rho/p$, where ρ and p are the effective energy density and pressure, respectively. It is defined through the Friedmann equations in the form of the once of GR,

$$H^2 = 8\pi G\,\rho\,, \qquad 2\dot{H} + 3H^2 = -8\pi G\,p\,, \tag{3.85}$$

where the modified contribution of the RR model has been included into the source terms, so that they represent the *effective dark energy* density and pressure. One has the relation,

$$w = -\frac{2}{3}\zeta - 1\,. \tag{3.86}$$

The bevahior of the total effective equation of state is shown in Fi. 3.1. We can see that, after the usual MD and RD phase at $w = 1/3$ and $w = 0$, respectively, the equation of state drops

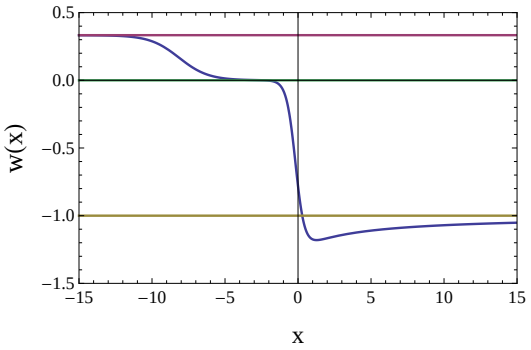

Figure 3.1 – The total equation of state parameter $w(x)$. The three plateaux correspond to the values for RD (purple), MD (green) and for the case of a cosmological constant (yellow).

below $w < -1$, during the present and future dark energy domination period. This behavior is the one of a so-called *phantom dark energy*, and its phenomenology was first considered into (Caldwell, 2002; Caldwell et al., 2003) [see also the more recent (Albarran et al., 2017)]. In the latter references, it was realised that such a type of dark energy generically leads a future singularity at finite time, a "Big Rip" at $t_{\rm rip}$ where the scale factor becomes infinite,

$$\lim_{t\to t_{\rm rip}^-} a(t) = \infty\,. \tag{3.87}$$

For constant w, such a fact can be computed from the continuity and the first Friedmann equation,

$$\dot\rho + 3H(1+w) = 0\,, \qquad \dot a = a\sqrt{\frac{8\pi G}{3}\rho}\,, \tag{3.88}$$

where the first provide $\rho = \rho_0 a^{-3(1+w)}$ and in inserting this into the second one gets,

$$\dot a = H_0 a^{-\frac{3}{2}(1+w)+1}\,, \tag{3.89}$$

that integrates to,

$$a(t) = \left[-\frac{3}{2}H_0(1+w)(t-t_{\rm rip})\right]^{\frac{2}{3(1+w)}}\,, \tag{3.90}$$

where $t_{\rm rip}$ is the integration constant. As $1+w<0$, the term in brackets is positive while the exponent is negative, resulting in a Big Rip at $t_{\rm rip}$. Proceeding perturbatively, one can find the equivalent expression for the RR cosmology in the far future limit $x \gg 1$. In that case, one can get (Dirian and Mitsou, 2014),

$$a(t) = \exp\left[\frac{T^2}{(t_{\rm rip}-t)^2}\right]. \tag{3.91}$$

It should be kept in mind that as $w<-1$, the Hubble parameter is growing in the future, and therefore the Ricci curvature scale R grows as well. This means that close to the singularity, this effective field theoretic description will not be valid anymore and therefore cannot be trusted. As is also explicitly shown in (Dirian and Mitsou, 2014), such a background expansion leads

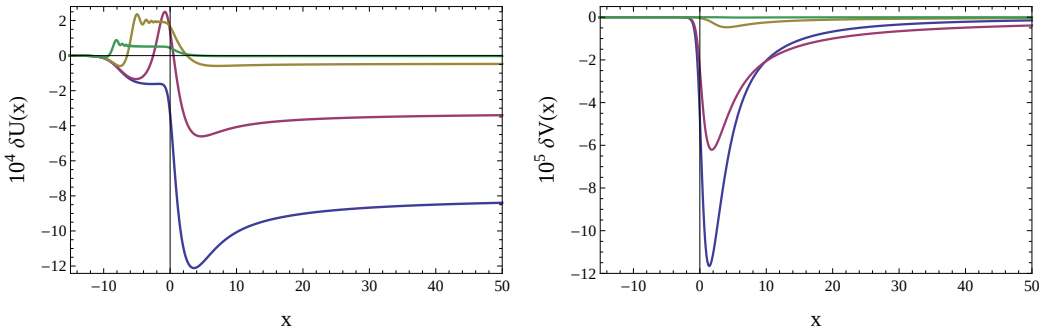

Figure 3.2 – The linear perturbations of U and V as a function of x for the modes $\kappa = 5 \times 10^{-3}$ (blue), $\kappa = 5 \times 10^{-2}$ (purple), $\kappa = 5 \times 10^{-1}$ (brown), $\kappa = 5$ (green).

to a domination of the Hubble friction at late times. At the present epoch, the perturbations associated to the auxiliary fields δU, δV start to grow as the dark energy era sets in, as expected for perturbations with a wrong sign for the kinetic term. However those fields are rapidly tamed by the violent background expansion, and so do not represent instabilities. The behavior of these perturbations can be seen in Fig. 3.2 for three different values of $\kappa \equiv k/k_{\rm eq}$ where $k_{\rm eq} = a_{\rm eq}H_{\rm eq}$, where the $_{\rm eq}$ quantities are evaluated at radiation-matter equality.

Summary

In this chapter, we started by examining the theoretical structure of the so-called RT model defined by the equation of motions in Eq. (3.6). It was show that its flat space propagator contains one pole associated to a massless spin-2 field, beside of one massless scalar and a massive one having a wrong sign in front of its kinetic term (3.14). This wrong sign is responsible for the lack of vDVZ discontinuity into the model at classical level, whereas in a quantum mechanical context, either the theory is continuous but unitarity is lost, or unitarity is preserved but an anomalous discontinuity then appears (3.17). This led us to the conclusion that this model can only be considered in a classical context and most probably results from some quantum averaging process. We then addressed a discussion supported by an illustrative example aiming to explain why the aforementioned scalar poles are not genuine degrees of freedom in the nonlocal theory, but should rather be though as associated to additional auxiliary fields whose homogeneous solutions are constrained. In Sec. 3.1.3, we then showed how the structure kinetic structure of the propagator can be recovered into the action when additional, auxiliary fields are introduced (3.41), and becomes local. We did so in using the variational principle for dissipative system presented in Sec. 2.1, so as to preserve causality throughout the procedure. The local action suggested a straightforward covariantisation that led to a different model than RT at full nonlinear level, the so-called RR model (3.56). We then analysed the degrees of freedom and stability of the RR model using different methods (see Secs. 3.2.1 and 3.4). In particular, we showed that the presence of the ghost pole is irrelevant for classical UV physics, and that the theory matches the prediction of GR at solar system scales. This is due to the fact that the associated instability is supposed to develop on far infrared scales, where the flat solution is not phenomenologically valid anymore. We saw that the cosmological FLRW solution for the RR model features a future singularity at finite time, a “Big Rip”, due to the phantom nature of the effective dark energy described by the model. Such a singularity originates from a violent phase of accelerated expansion taking place at late time, that makes the Hubble friction

dominate the kinetics of the scalar perturbations. Therefore, on the cosmological solution, no instabilities associated to an unstable pole appears at the linear perturbation level in the RR model. Concerning the RT model, such a stability analysis has not yet been presented, but, as we will see below, this model meets difficulties in explaining a primordial inflationary phase, on which ground it is a priori hard to believe it to be responsible for the generation of the presently observed cosmic acceleration.

In the next chapter, we present in details the phenomenology associated with the RR and RT models within a cosmological context.

Chapter 4

Phenomenology of the RT and RR Models

We expose the cosmological phenomenology of the RT and RR models that we recall here. The RT model is defined by the equation of motion (see Sec. 3.1 for details),

$$G_{\mu\nu} - \frac{1}{3}m^2\big(g_{\mu\nu}\Box^{-1}R\big)^{\mathrm{T}} = 8\pi G\, T_{\mu\nu}\,, \tag{4.1}$$

where the $^{\mathrm{T}}$ operator denotes the covariant extraction of the transverse part defined in Eq. (3.4), while the RR model is defined by the action (see Sec. 3.2),

$$S = \frac{1}{16\pi G}\int \mathrm{d}^4x\sqrt{-g}\,\left[R - \frac{1}{6}m^2 R\frac{1}{\Box^2}R\right] + S_M[\psi, g]\,. \tag{4.2}$$

In these expressions, the operator $\Box^{-1}$ is a formal notation for a Green's function of the curved-space d'Alembert operator $\Box \equiv g^{\mu\nu}\nabla_\mu\nabla_\nu$, $S_M[\psi, g]$ is the action of matter field collectively denoted as ψ and,

$$T_{\mu\nu}(x) = -\frac{2}{\sqrt{-g}}\frac{\delta S_M[\psi, g]}{\delta g^{\mu\nu}(x)}\,, \tag{4.3}$$

is the associated energy-momentum tensor. Subsequently, we specialise these models to a cosmological context in writing the metric $g_{\mu\nu}$ in a FLRW background form. After presenting the modified Friedmann equations, we then study the dark energy phenomenology associated to both models at the background level, when the system is evolved forward in time starting deep in RD. We will see that these models provide viable background cosmological solutions, which is a quite non-trivial fact. In particular, we will see that both models lead to an effective, dynamical phantom dark energy emerging at late time, producing cosmic acceleration. We then address the issue of possible modification of the RD initial conditions by effects induced from an earlier evolution phase, such as during inflation. Then, we turn to the study of linear perturbations on this cosmological background and provide details on the dynamics of the system, in particular, showing how it deviates from the one of ΛCDM. We will see that the perturbations of these models are stable up to present time, and that they predict interesting features that can be constrained with actually data. The confrontation of these models to observations is reviewed in the next chapter.

4.1 Localised Models

In order to compute the cosmological background evolution for the two models presented hereabove, we start by localising the models in using auxiliary fields. Indeed, it is more convenient to solve local differential equations rather than more complicate integro-differential ones.

Localisation of the RT Model

The localised version of the RT model we consider is given by (Maggiore, 2014),

$$G_{\mu\nu} + \frac{1}{3}m^2(Xg_{\mu\nu})^T = 8\pi G T_{\mu\nu}\,, \tag{4.4}$$

$$-\Box X = R\,, \tag{4.5}$$

where, from the second equation, one can write $X = -\Box^{-1}R$, and plugging it into the first gives back the original nonlocal theory. The transverse part in Eq. (4.4) is given by,

$$(Xg_{\mu\nu})^T = Xg_{\mu\nu} + \frac{1}{2}\big(\nabla_\mu W_\nu + \nabla_\nu W_\mu\big)\,. \tag{4.6}$$

The behavior of W_μ is obtained by applying ∇^μ to this expression and solving,

$$2\nabla^\mu(-Xg_{\mu\nu}) = -2\partial_\nu X = \nabla^\mu\big(\nabla_\mu W_\nu + \nabla_\nu W_\mu\big)\,, \tag{4.7}$$

and therefore the total system of localized differential equations reads,

$$G^\nu_\mu + \frac{1}{3}m^2\left[X\delta^\nu_\mu + \frac{1}{2}\big(\nabla_\mu W^\nu + \nabla^\nu W_\mu\big)\right] = 8\pi G\, T^\nu_\mu\,, \tag{4.8}$$

$$-\Box X = R\,, \tag{4.9}$$

$$\partial_\mu X = -\frac{1}{2}\nabla_\nu\big(\nabla_\mu W^\nu + \nabla^\nu W_\mu\big)\,, \tag{4.10}$$

$$\nabla_\mu T^\mu_\nu = 0\,. \tag{4.11}$$

Observe that if the additional term in Eq. (4.8) is seen as an additional matter part, Eq. (4.10) simply enforces its covariant conservation. Furthermore, it is the first derivative structure $\sim \nabla W$ into Eq. (4.8) that makes its implementation into an action difficult [1].

According to the discussion in Sec. 3.1.2, for some coordinate system x^μ where ∂_0 is timelike, the auxiliary fields X, W_μ have homogeneous solutions constrained to vanish on the initial hypersurface at $x^0_{\rm in} = t_{\rm in}$. Moreover, we consider the "minimal" case where their initial conditions are vanishing as well,

$$X(t_{\rm in}) = \partial_0 X(t_{\rm in}) = 0\,, \qquad W_\mu(t_{\rm in}) = \partial_0 W_\mu(t_{\rm in}) = 0\,, \quad \text{for all } \mu\,, \tag{4.12}$$

which is phenomenologically motivated by the fact that the Ricci scalar is negligible on an FLRW background during the epoch of radiation domination. Evolving the system forward in time then amounts to solve the equations with a retarded Green's function.

1. Indeed, if one tried to integrate straightforwardly these terms into an action one solution would be $g^{\mu\nu}\nabla_\mu W_\nu$, but this is a total derivative and vanishes under the integral. Nevertheless, one could imagine these terms as seen as friction terms coming from a higher dimensional spacetime, much as FLRW background lead to the appearance of single time derivatives $\partial_t\phi$.

Localisation of the RR Model

Here, we expose the localised version of the RR model,

$$S = \frac{1}{16\pi G}\int \mathrm{d}^4x\sqrt{-g}\ \left[R - \frac{1}{6}m^2 R\frac{1}{\Box^2}R\right]. \tag{4.13}$$

which takes a different form than the one discussed in Sec. 3.2. It reads (Maggiore and Mancarella, 2014),

$$S = \frac{1}{16\pi G}\int \mathrm{d}^4x\sqrt{-g}\ \left[R\left(1-\frac{m^2}{6}S\right) - \xi_1\big(\Box U + R\big) - \xi_2\big(\Box S + U\big)\right], \tag{4.14}$$

where $\xi_{1,2}$ are Lagrange multiplier, whose constraints applications leads back to the nonlocal form (4.13). The equations of motion derived from Eq. (4.14) read,

$$G^\mu_\nu - \frac{1}{6}m^2 K^\mu_\nu = 8\pi G\, T^\mu_\nu\,, \tag{4.15}$$

$$\Box U = -R \quad , \quad \Box S = -U\,, \tag{4.16}$$

where,

$$K^\mu_\nu \equiv 2SG^\mu_\nu - 2\nabla^\mu\partial_\nu S + 2\delta^\mu_\nu\Box S + \delta^\mu_\nu\partial_\rho S\partial^\rho U - (1/2)\delta^\mu_\nu U^2 - \left(\partial^\mu S\partial_\nu U + \partial_\nu S\partial^\mu U\right), \tag{4.17}$$

which is separately conserved $\nabla_\mu K^\mu_\nu = 0$, as can been checked using Eqs. (4.16).

Fluid Energy-Momentum Tensor

At cosmological scales, we interpret the matter distribution as being a continuum, i.e. a fluid. The energy momentum tensor of a fluid in the rest frame of a freely falling observer u^μ comoving with it decomposes as,

$$T^{\mu\nu} = (\rho + p)u^\mu u^\nu + g^{\mu\nu}p + \pi^{\mu\nu}\,, \qquad u^\mu \equiv \frac{\mathrm{d}x^\mu}{\mathrm{d}\tau}\,, \tag{4.18}$$

where $\mathrm{d}\tau \equiv \sqrt{-\mathrm{d}s^2}$, is the observers proper time, u^μ is therefore a unit timelike four-vector $u^\mu u_\mu = -1$, ρ the energy density, p the pressure and $\pi_{\mu\nu}$ the anisotropic stress in the fluid's rest frame. The latter are defined as,

$$\rho = u_\mu u_\nu T^{\mu\nu}\,, \qquad p = \frac{1}{3}h_{\mu\nu}T^{\mu\nu}\,, \qquad \pi^{\mu\nu} = \left(h^\mu_\rho h^\nu_\sigma - \frac{1}{3}h^{\mu\nu}h_{\rho\sigma}\right)T^{\rho\sigma}\,, \tag{4.19}$$

where $h^{\mu\nu} \equiv g^{\mu\nu} + u^\mu u^\nu$, is the induced metric, so that $u^\mu\pi_{\mu\nu} = 0$, $g^{\mu\nu}\pi_{\mu\nu} = 0$.

4.2 Cosmological Background Solutions

We now specialise the metric to a flat FLRW background in cosmic time t and comoving cartesian spatial coordinates. The line element reads,

$$\mathrm{d}s^2 = \bar{g}_{\mu\nu}\mathrm{d}x^\mu\mathrm{d}x^\nu = -\mathrm{d}t^2 + a^2(t)\mathrm{d}\vec{x}^2\,, \qquad H \equiv \frac{\dot{a}}{a}\,, \tag{4.20}$$

where the scale factor $a(t)$ is related to the redshift z by $1+z = 1/a$, H is the Hubble expansion rate parameter and the dot $\dot{}$ denotes the derivative with respect to t. In this coordinate system,

the observes' proper time is the cosmic time so that one has $u^\mu = \dot{x}^\mu = \big(1, \vec{0}\big)$, and the energy momentum tensor is given by,

$$\bar{T}_{00} = \bar{\rho}\,, \qquad \bar{T}_{ij} = \bar{p}\,\delta_{ij}\,, \qquad \bar{\pi}_{\mu\nu} = 0\,, \tag{4.21}$$

where we use overbars to denote background quantities $\bar{\rho}$, $\bar{X}$, $\bar{W}_\mu$, etc. Let us also define the equation of state parameter $\bar{p}(t) = w(t)\bar{\rho}(t)$. The conservation of energy momentum $\nabla_\nu T^{\mu\nu} = 0$ then implies,

$$\partial_t \bar{\rho}(t) = -3H[1 + w(t)]\bar{\rho}(t)\,. \tag{4.22}$$

We also define the dimensionless Hubble parameter $h(t) = H(t)/H_0 \equiv 100\,h_0\,\mathrm{kms}^{-1}\mathrm{Mpc}^{-1}$, where $H_0 \equiv H(t_0)$ is the Hubble parameter at present cosmic time t_0, i.e. the Hubble constant. As it will sometimes be convenient to use, we define the number of e-folds $x \equiv \log a$ as alternative time coordinate and we denote the derivatives with respect to it by a prime, e.g. $\partial\bar{U}/\partial x \equiv \bar{U}'$. We also introduce the critical density of the Universe,

$$\bar{\rho}_c(t) \equiv \frac{3H(t)^2}{8\pi G}\,, \tag{4.23}$$

to which the energy densities other than spatial curvature sum up, and we will denote $\bar{\rho}_0 \equiv \bar{\rho}_c(t_0)$ its present value. The density fractions read $\Omega_i(t) \equiv \bar{\rho}_i(t)/\bar{\rho}_0$, where $\bar{\rho}_i(t)$ is the energy density of a given species e.g. radiation ($i = R$), matter ($i = M$), neutrinos ($i = \nu$), dark energy ($i = \mathrm{de}$), etc, and sums up to one today, in the case of a flat Universe $\Omega_K = 0$. We will write the total density fraction of matter as $\Omega(t)$, i.e. when dark energy and curvature density fractions are not included. It is also useful to introduce the quantity $\gamma \equiv m^2/(9H_0^2)$, related to the mass appearing in the nonlocal models.

Recall that in such a geometry, the Einstein equations with a cosmological constant Λ lead to the Friedmann equations,

$$H^2 = \frac{8\pi G}{3}\bar{\rho} + \frac{\Lambda}{3}\,, \tag{4.24}$$

$$\frac{\ddot{a}}{a} = -\frac{4\pi G}{3}\big(\bar{\rho} + 3\bar{p}\big) - \frac{\Lambda}{3}\,, \tag{4.25}$$

which can be solved once the relation $\bar{p}(\bar{\rho})$ is specified.

4.2.1 Background Solution for RT

Background Equations

On a FLRW background there is no preferred direction, so that all the spatial derivative vanish and also $\bar{W}_i = 0$. From Eqs. (4.9) and (4.10) one gets,

$$\ddot{X} + 3H\dot{X} = 6(\dot{H} + 2H^2)\,, \tag{4.26}$$

$$\ddot{W}_0 + 3H\dot{W}_0 - 3H^2\bar{W}_0 = \dot{X}\,, \tag{4.27}$$

respectively, while the modified first Friedmann equation is obtained form the (00) component of Eq. (4.8) which yields,

$$H^2 - \frac{m^2}{9}\big(X - \dot{W}_0\big) = \frac{8\pi G}{3}\bar{\rho}\,, \tag{4.28}$$

dividing by H_0^2, going to coordinate time x and choosing for convenience the new variable $\bar{S} = H_0 \bar{W}_0$, the system reads,

$$h^2 = \Omega(x) + \gamma \bar{Y}(x)\,, \tag{4.29}$$

$$\bar{X}'' + (3+\zeta)\bar{X}' = 6(2+\zeta)\,, \tag{4.30}$$

$$\bar{X}' = h\big[\bar{S}'' + (3+\zeta)\bar{S}' - 3\bar{S}\big]\,, \tag{4.31}$$

$$\bar{Y}(x) \equiv \big(\bar{X} - h\bar{S}'\big)\,. \tag{4.32}$$

Late Time Phantom Dark Energy

The above system is solved from the specification of the matter content $\Omega(x)$, whereas the initial conditions for the auxiliary fields are taken as vanishing, as we have already discussed in Sec. 3.1.2 and will develop in more details below. From Eq. (4.29) one can identify the *effective dark energy* density fraction,

$$\Omega_{\rm de}(x) \equiv \gamma \bar{Y}(x)\,. \tag{4.33}$$

which replaces the one of the cosmological constant Ω_Λ. Here, we consider for simplicity a dust component $w_M = 0$ with $\Omega_M = 0.3175$ and a radiation one $w_R = 1/3$ with $\Omega_R = 4.15 \times 10^{-5}/h_0$ (Ade et al., 2014a) so that $\Omega = \Omega_M e^{-3x} + \Omega_R e^{-4x}$, and choose the reduced Hubble constant to be $h_0 = 0.7$. We integrate numerically the system forward in time using the *Mathematica* software (Wolfram, 2010), and setting the initial conditions deep in RD, at $x_{\rm in} = -15$. The parameter γ is tuned so as to close the Universe at present time [2], similarly to the way the value of Λ is set in ΛCDM. In this case, this leads to the value $\gamma \simeq 0.0504$, corresponding to $m \simeq 0.67 H_0$. Thus, as expected, the scale where the modification to GR sets in is in the far infrared $\sim H_0$. This is also realised because of the fact that the auxiliary fields start with vanishing initial conditions. Indeed, given that the background Ricci scalar $\bar{R}$ is negligible compared to the total energy scale during RD, $\bar{R}/H^2 = 6(2+\zeta) \sim 0$, the auxiliary field are therefore not sourced, as can be directly seen from Eq. (4.30). However, once the scalar curvature becomes relevant, i.e. at the time of radiation-matter equality $x_{\rm eq} \sim -8$, the background auxiliary fields get excited, and give raise to an effective dark energy component (4.33). We display the evolution of the auxiliary fields $\bar{X}$ and $\bar{S}$ in the right panel of Fig. 4.1 together with the Hubble parameter predicted by the model (upper left panel) and its relative difference with the one in ΛCDM (lower left panel) for the same fiducial cosmology. One can indeed see that the amplitude of the background auxiliary fields monotonically grow from $\sim x_{\rm eq}$ until today. Moreover, one also notices that the amplitude of the expansion rate is lowered at percent level at low redshift, once dark energy domination sets in $z \lesssim 2$. To understand this fact, we define $\zeta \equiv h'/h = \bar{\rho}'/(2\bar{\rho})$ and use Eq. (4.24) together with the energy density conservation Eq. (4.22), to generically write,

$$w(t) = -1 - \frac{2}{3}\zeta(t)\,. \tag{4.34}$$

In the present case, during the period of dark energy domination, one obtains the effective dark energy equation of state,

$$w_{\rm de}(x) = -1 - \frac{\bar{Y}'(x)}{3\bar{Y}(x)}\,, \tag{4.35}$$

2. This practically means that we tune γ, so as to set $h(x=0) \simeq 1$, to a precision of several digits in the simulation.

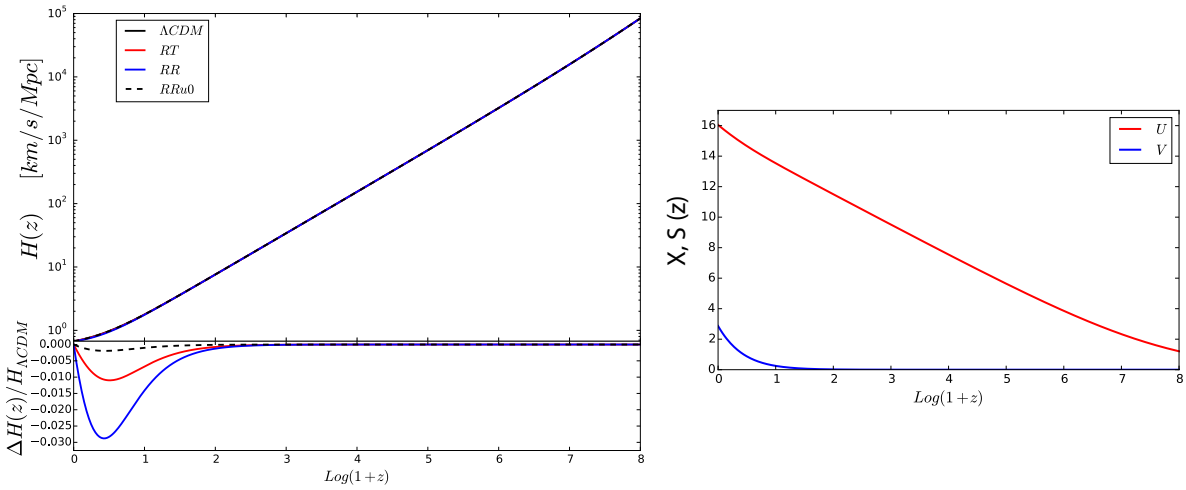

Figure 4.1 – Upper left: Hubble parameter H as a function of $\log(1+z) = -x$ in the ΛCDM model (black), RT model (solid red), RR (solid blue), RRu0 (dashed black). Lower left: Relative error between the Hubble parameters in RT (solid red), RR (solid blue) and RRu0 (dashed black) with respect to ΛCDM. Right: Auxiliary fields $\bar{X}$ (red) and $\bar{S}$ (blue) as functions of $\log(1+z) = -x$ in the RT model.

which generically deviates from minus one, that is, the dark energy is *dynamical*. In Fig. 4.2, we plot the corresponding energy density (left panel) and equation of state (right panel). Observe from,

$$\bar{\rho}'_{\rm de}(x) = -3[1 + w_{\rm de}(x)]\bar{\rho}_{\rm de}(t)\,. \tag{4.36}$$

that, since $\bar{\rho}'_{\rm de}$ is positive, as the auxiliary fields start to grow from zero until today, and $\bar{\rho}_{\rm de}$ is positive as well, the equation of state must be smaller than minus one, $w_{\rm de}(x) < -1$, in order to compensate for the minus sign in front of the second term. This is the case throughout the whole evolution in this model and shows that the effective dark energy described by the RT model is on the *phantom* side, and violates the null energy condition $w \geq -1$. Furthermore, solving for the evolution of the dark energy density fraction from the conservation equation (4.36), one obtains,

$$\Omega_{\rm de}(z) = \Omega_{\rm de}\, \exp\left(3\int_0^z {\rm d}z'\, \frac{1 + w_{\rm de}(z')}{(1+z')}\right). \tag{4.37}$$

At low redshift, when the dark energy is dominant, this can be approximated by,

$$\Omega_{\rm de}(z \approx 0) \simeq \Omega_{\rm de}\, \left(1 + 3z\, \delta w_0\right), \tag{4.38}$$

where we wrote $w_{\rm de}(z \approx 0) \simeq -1 + \delta w_0$, with $|\delta w_0| \ll 1$ and constant, which is a sensible approximation for the present discussion. One can see that for the case of a phantom dark energy $\delta w_0 < 0$, the predicted density fraction $\Omega_{\rm de}(z)$ is generically smaller than Ω_Λ at $z \gtrsim 0$ as shown in the left panel of Fig. 4.3, and this explains why the Hubble parameter that can be written as,

$$H(z) = H_0\big[\Omega(z) + \Omega_{\rm de}(z)\big]^{1/2}, \tag{4.39}$$

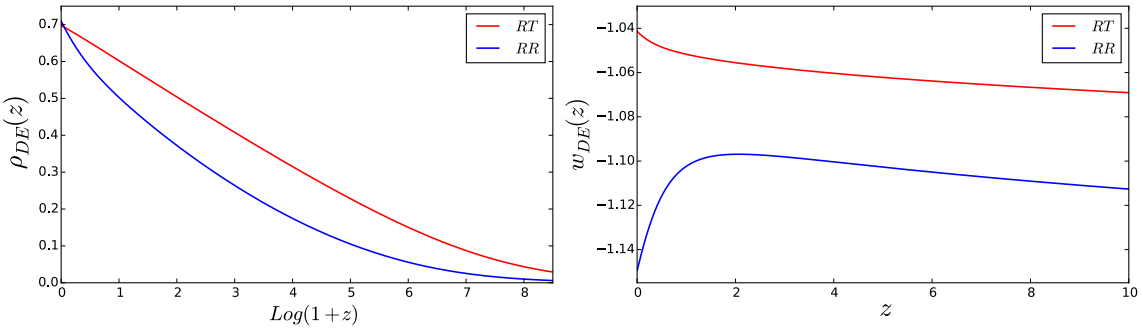

Figure 4.2 – Left panel: Dark energy densities $\bar{\rho}_{\rm de}$ as functions of $\log(1+z) = -x$ in the RT model (red) and in RR (blue). Right panel: Dark energy equations of state $w_{\rm de}$ as functions of z for the RT model (red) and for RR (blue).

is smaller as well. In turn, the dark matter density fraction $\Omega_M(z \lesssim 2)$ is generically larger, and we will see below how this influences the growth of large scale structures. Moreover, geometry-dependent quantities are also affected, as for instance the luminosity distance that we show in the right panel of Fig. 4.3, and is defined as,

$$D_L(z) \equiv (1+z)\int_0^z \frac{\mathrm{d}z'}{H(z')} = \sqrt{\frac{L}{4\pi F}}\,, \tag{4.40}$$

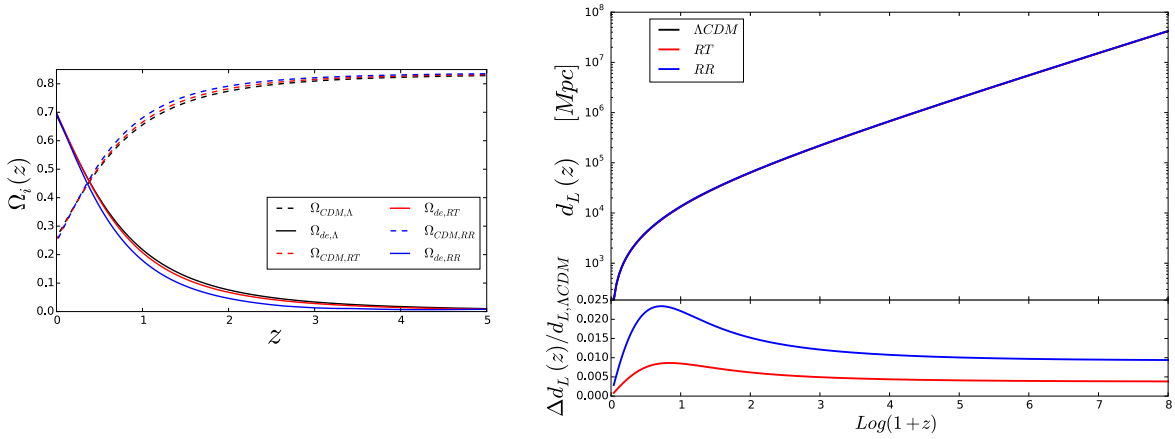

Figure 4.3 – Left panel: The dark energy density franctions $\Omega_{\rm de}$ as a function of z for ΛCDM (solid black), RT (solid red) and RR (solid blue) together with their respective cold dark matter quantities (dashed).Upper right panel: Luminosity distance D_L as a function of $\log(1+z) = -x$ in the ΛCDM model (black), RT model (red) and RR (blue). Lower right panel: Relative error between the luminosity distances in RT (red) and RR (blue) with respect to ΛCDM.

where L is the intrinsic luminosity of an object in the sky and F its energy flux, or also the angular diameter distance $D_A(z) = D_L(z)/(1+z)^2 \equiv x/\delta\theta$, where x is the physical distance between two objects and $\delta\theta$ the observed angle between them. This means that into phantom

dark energy models, at fixed redshift, luminous objects are pushed further away in the sky and subtend a smaller angle compared to the ones in a ΛCDM cosmology. One can also fit the dark energy equation of state in using the standard Chevallier-Polarski-Linder (CPL) parametrisation (Chevallier and Polarski, 2001; Linder, 2003),

$$w(a) = w_0 + w_a(1-a)\,, \tag{4.41}$$

and, in the case of the fiducial cosmology we are considering one obtains,

$$w_0 \simeq -1.04\,, \qquad w_a \simeq -0.02\,. \tag{4.42}$$

Interestingly, the behavior of this dark energy is therefore very close to the one of ΛCDM, but still leads to percent-level deviations in the background geometry.

4.2.2 Background Solution for RR

We now discuss the FLRW background evolution equations for the RR model (4.15) (Maggiore and Mancarella, 2014). Introducing the variable $\bar{V}(x) = H_0^2\bar{S}(x)$, the equations for the auxiliary fields (4.16) read,

$$\bar{U}'' + (3+\zeta)\bar{U}' = 6(2+\zeta)\,, \tag{4.43}$$

$$\bar{V}'' + (3+\zeta)\bar{V}' = h^{-2}\bar{U}\,, \tag{4.44}$$

where,

$$h^2 = \frac{\Omega(x) + (\gamma/4)\bar{U}^2}{1 - 3\gamma(\bar{V}' + \bar{V} - \bar{U}'\bar{V}'/6)}\,, \tag{4.45}$$

and,

$$\Omega \equiv \Omega_R e^{-4x} + \Omega_M e^{-3x}\,, \tag{4.46}$$

$$\zeta \equiv \frac{h'}{h} = \frac{1}{2(1-3\gamma V)}\left[h^{-2}\Omega' + 3\gamma\left(h^{-2}\bar{U} + \bar{U}'\bar{V}' - 4\bar{V}'\right)\right]. \tag{4.47}$$

Late Time (more) Phantom Dark Energy

In particular, one can identify the dark energy density fraction in that case,

$$\Omega_{\rm de}(x) = \frac{\gamma}{4}\bar{U}^2 + 3\gamma h^2\left(\bar{V}' + \bar{V} + \frac{1}{6}\bar{U}'\bar{V}'\right), \tag{4.48}$$

and find the equation of state $w_{\rm de}(x)$ in using Eqs. (4.34) and (4.47). For the same fiducial cosmology as the one specified in Sec. 4.2.1, one finds $\gamma \simeq 0.0089247$ corresponding a mass $m \simeq 0.283H_0$. Under the identification, $\bar{U} \leftrightarrow \bar{X}$ and $\bar{V} \leftrightarrow \bar{S}$, the behavior of the auxiliary fields are very similar to the ones in the RT model, and we refer the reader to the right panel of Fig. 4.1, for a qualitative description. As we can see from the right panel of Fig. (4.2), for the RR model, the dark energy equation of state is generically smaller than the one in RT. Using the CPL parametrisation (4.41), one finds,

$$w_0 \simeq -1.144\,, \qquad w_a \simeq -0.084\,, \tag{4.49}$$

given the fiducial cosmology assumed here. As a consequence, through the same reasoning as the one outlined above, the dark energy density fraction in the RR model is lowered compared to the one in RT, and therefore also ΛCDM, and this induces a larger deviation in the Hubble parameter at late time. This fact also reverberates on geometrical quantities such as the luminosity and angular diameter distance, as can be seen in the right panel of Fig. 4.3.

4.2.3 RD Initial Conditions From Earlier Stages: RRu0

From this analysis, we see that the RT and RR nonlocal modified gravity models exhibit self-accelerating solutions at late time. In both models, this is caused by a phantom effective dark energy component, i.e. with an equation of state $w_{\rm de} < -1$, whose energy density departs from zero as soon as the Universe enters in MD. Indeed, in RD the background Ricci scalar $\bar{R}$ is negligible compared to the overall energy scale of the Universe, therefore the modifications to gravity are negligible too, as can be seen directly from Eqs. (4.30) and (4.43). For this reason, we adopted the point of view were the initial conditions for these background auxiliary fields are set to zero deep in RD. Notice however that for this choice of initial conditions being legitimate in RD, one needs to assume that the secular growth of the background auxiliary fields $\bar{X}$, $\bar{W}_0$, $\bar{U}$, etc, induced in earlier stages of the Universe is negligible at that time. For the case of inflationary scenarios, it can been argued that the modification to gravity does not show up, as it is only IR relevant and therefore suppressed by the inflationary energy scale. In any case, this question deserves further attention, and needs a detailed numerical study for been correctly addressed [see (Maggiore, 2015; Cusin et al., 2016c; Belgacem et al., 2018a), where such scenarios were considered along these lines]. Of course, the configuration reached by the auxiliary field in RD is likely to depend on the particular inflationary scenario one considers, but also on other processes affecting the scalar curvature into the early Universe. Examples are provided by electroweak or QCD phase transitions, conformal anomalies, or during RD itself through the presence of thermalised SM particles [see e.g. (Caldwell and Gubser, 2013)]. This issue was recently anticipated in Ref. (Nersisyan et al., 2016) for the RR model, where the authors studied the effect of varying the auxiliary fields' initial conditions deep into RD over a broad range of values. Interestingly, they unveiled the existence of a bifurcation into the associated dynamical system, leading to another phenomenologically viable cosmology of the nonlocal model. This other branch is reached in fixing the initial conditions for the field $\bar{U}$ below a given threshold (roughly ≈ -15, see the reference for details) leading to an evolution that is radically different from the one presented hereabove. In this second branch, the effective dark energy remains non-phantom during the whole evolution, approaching a plateau at $w = -1$ at the present epoch, leading to a de Sitter phase of expansion, while evolving toward a radiation-like fluid $w = -1/3$ in the far future.

Here, we briefly review the results of previous works (Maggiore, 2014; Foffa et al., 2014b; Maggiore, 2017), where the dependence on the initial conditions for background auxiliary fields set in RD is considered to originate from an earlier inflationary phase, idealised by a de Sitter geometry. This considerably simplifies the problem as one assumes a phase dominated by a cosmological constant-like perfect fluid with equation of state $w = -1$, for which the function ζ defined in Eq. (4.34) is therefore vanishing, $\zeta = 0$. In the case of constant ζ, the background equations for the auxiliary fields [Eqs. (4.30),(4.31) for RT and Eqs. (4.43),(4.44) for RR] can be solved analytically and we refer the reader to the above references for detailed expressions. For the present discussion, the most relevant conclusions are found into the evolution of $\bar{X} \leftrightarrow \bar{U}$, since it is this field that dominates the dark energy density in both nonlocal models, a posteriori. This fact can be seen for instance at late time from Eqs. (4.33), (4.48) and the right panel of Fig. 4.1 [the derivative of $\bar{S} \leftrightarrow \bar{V}$ is $\mathcal{O}(\bar{S})$ at that time]. Thus, we focus on solutions to the equation of the form,

$$\bar{f}'' + (3 + \zeta)\bar{f}' = 6(2 + \zeta)\,, \tag{4.50}$$

where $\bar{f} \equiv \bar{X}$ in RT and $\bar{f} \equiv \bar{U}$ in RR [see Eqs. (4.30),(4.43), respectively]. As discussed above, the nonlocal structure of the theory constrains the homogeneous solutions to vanish, so that

one must fix $\bar{f}(x_i) = \bar{f}'(x_i) = 0$, where x_i is the initial time when the de Sitter phase starts. The solution for constant $\zeta = -3(1+w)/2$ can be written as,

$$\bar{f}(x) = \frac{2(1-3w)}{(1-w)}(x - x_i) + \frac{4}{3}\frac{(1-3w)}{(1-w)^2}\left(e^{-\frac{3}{2}(1-w)(x-x_i)} - 1\right). \tag{4.51}$$

which vanishes in RD $w = 1/3$, as expected. Otherwise, for fluids with $w < 1/3$, this solution has a constant mode which, together with an exponentially suppressed one, provide its homogeneous solutions, while the source induces a linearly growing one. In particular, this implies that during an early accelerated phase $w < -1/3$, the linearly growing mode will lead to a non-vanishing initial condition at the exit of this phase, and will therefore provide non-zero initial conditions deep in RD [3]. In de Sitter phase $w = -1$, the solution reads,

$$\bar{f}(x) = 4(x - x_i) + \frac{4}{3}\left(e^{-3(x-x_i)} - 1\right), \tag{4.52}$$

which, at the end of the de Sitter phase, can be therefore be rewritten as,

$$\bar{f}(x_f) \simeq 4\Delta N\,, \tag{4.53}$$

where $\Delta N \gg 1$, is the number of e-folds of the idealised inflationary scenario. For typical inflationary theories consistent with data, $\Delta N \simeq 60$ is a good approximation, (Ade et al., 2015b), so that $\bar{f}(x_f) \simeq 240$. It can be shown that the contributions of the other fields besides the equivalent of $\bar{f}$ in the RT and RR models are negligible at the end of such a phase (Maggiore, 2017). Assuming now that this solution smoothly connects with standard RD, i.e. taking this value as initial conditions in RD, neglecting the "reheating phase" and eventual non-trivial time derivative value for $\bar{U}(x_f)$ induced by this process, the model describes an expansion rate having qualitatively the same behavior as ΛCDM at late time. This can be seen from the black dashed line on the lower left panel of Fig. 4.1. In the following, we will denote this model by RRu0 (where u_0 is the initial value of $\bar{U}$ deep in RD). These conclusions are similar for the RT model, which is even closer from ΛCDM at late time.

It is the lack of a fundamental understanding of the emergence of these nonlocal models that makes the interpretation of these results difficult. Indeed, if the nonlocal corrections are emerging at the low-energy effective level, their use in a highly energetic early Universe context is not legitimated, and the above results cannot be trusted. However, if these terms emerge from a mechanism valid on all scales, they should be legitimately considered for early physical processes. As such, two phenomenological strategies are in order. Either one adopts the first point of view and starts the evolution in both models deep in RD, assuming that the initial conditions for the auxiliary fields provided by early processes are negligible, and therefore uses the "minimal" version of the RT and RR models. Or one supposes that the nonlocal corrections are valid at high energies as well, which makes it possible to supplement the nonlocal models with a sector describing the physics of the early Universe, e.g. by a primordial inflationary phase. In the latter case, observe that the RR model finds a sort of canonical embedding into Starobinsky inflation when complemented with a term R^2. This theory then describes an inflationary phase at early times and a phase of cosmic acceleration at late time. In that case, the action reads (Maggiore, 2015),

$$S = \frac{1}{16\pi G}\int \mathrm{d}^4x\sqrt{-g}\,\left[R + \frac{1}{6M_{\rm S}^2}R\left(1 - \frac{\Lambda_{\rm S}^4}{\Box^2}\right)R\right], \tag{4.54}$$

3. Notice that processes taking place in between the inflationary and radiation era, such as a reheating phase, could affect this conclusion. However, the fact that the field is sourced by the Ricci curvature scalar, and contains at least a constant homogeneous mode, would generically imply that the cannot be driven to zero in any way and give raise to a non-vanishing value for it at the entrance of RD.

where $M_S^2 \simeq 10^{13}$GeV is the characteristic Starobinsky mass scale and $\Lambda_S \equiv M_S^2 m^2$.

4.3 Linear Cosmological Perturbations in Nonlocal Gravity

In this section, we present how linear cosmological perturbation theory applies to the RT (4.1) and RR (4.2) nonlocal models, following the work of (Dirian et al., 2014). Subsequently, we introduce the framework and expose the corresponding equations of motion governing the linear cosmological dynamics in the models. We then solve numerically these equations in a simplified context, where perturbations of an early dominating radiation and a late time dominating dust components are considered. We then present how various quantities deviate from the ones predicted by a ΛCDM cosmology. Furthermore, as the effective dark energy described by both nonlocal models is dynamical, it also gives raise to effective dark energy perturbations to which we review the phenomenology.

4.3.1 Linear Perturbation Theory

Metric and Auxiliary Fields in the Newtonian Conformal Gauge

We set up the linear perturbative treatment over FLRW spacetime in the localised formulation of both nonlocal model, whose corresponding equations are found in Secs. 4.1 and 4.1, for the RT and RR model respectively. We write all the field variables present in these equations as a FLRW background quantity (denoted with an overbar) plus an associated perturbation, e.g. $U = \bar{U} + \delta U$, where one imposes $|\delta U/\bar{U}| \ll 1$. The metric field is weakly perturbed as, $g_{\mu\nu} = \bar{g}_{\mu\nu} + h_{\mu\nu}$, where $h_{\mu\nu}$ is the linear perturbation field. Focusing only on the scalar sector for the moment, the perturbed line element is generically written as (Bardeen, 1980; Kodama and Sasaki, 1984; Ma and Bertschinger, 1995),

$$ds^2 = a(\eta)^2\big[-(1+2\psi)\mathrm{d}\eta^2 + 2\partial_i B\, d\eta\, \mathrm{d}x^i + \big((1+2\phi)\delta_{ij} + \partial_i\partial_j E\big)\mathrm{d}x^i\mathrm{d}x^j\big]\,, \tag{4.55}$$

where η is the conformal time, whose derivative are denoted by a prime here, $\partial_\eta\psi \equiv \psi'$, and we have adopted the sign convention used in (Bardeen, 1980; Kodama and Sasaki, 1984), which relates to the one used in (Ma and Bertschinger, 1995) in performing the replacement,

$$\psi \to \psi_{\mathrm{MB}}\,, \qquad \phi \to -\phi_{\mathrm{MB}}\,. \tag{4.56}$$

In this framework, invariance under (passive) diffeomorphisms $x^\mu \to x'^\mu(x)$, is realised at the linearly perturbated level too, so $x'^\mu(x) = x^\mu + \xi^\mu$, with ξ^μ infinitesimal. The background geometry is kept fixed under infinitesimal coordinate transformation, so as its variation is reverberated on the fields perturbations. As such, the metric perturbation field transforms as,

$$h_{\mu\nu} \longrightarrow h_{\mu\nu} - \mathcal{L}_\xi\big(\bar{g}_{\mu\nu} + h_{\mu\nu}\big) = h_{\mu\nu} - \mathcal{L}_\xi\bar{g}_{\mu\nu} + \mathcal{O}\big(h_{\mu\nu}^2\big)\,. \tag{4.57}$$

as the associated Lie derivative $\mathcal{L}_\xi$ along the vector field ξ^μ reads,

$$\mathcal{L}_\xi h_{\mu\nu} = \xi^\rho\partial_\rho h_{\mu\nu} + 2\partial_{(\mu}\xi^\rho h_{\rho\nu)}\,, \tag{4.58}$$

Focusing on the scalar sector of the vector field $\xi^\mu \equiv \big(A, \partial_i C\big)$, one can deduce the transformation properties of ψ, ϕ, B and E,

$$\psi \to \Psi \equiv \psi - \frac{1}{a}\big(aA\big)' \quad , \quad B \to B - C' + A\,, \tag{4.59}$$

$$\phi \to \Phi \equiv \phi - \mathcal{H}A \qquad , \quad E \to E - C\,. \tag{4.60}$$

Choosing $C = E$ and $A = E' - B$, we fix the so-called *conformal Newtonian* or *longitudinal* gauge (Mukhanov et al., 1992), where the transformed field $E_{\rm new} = B_{\rm new} = 0$. The line element then reduces to,

$$ds^2 = a^2(\eta)\big[-(1+2\Psi)d\eta^2 + (1+2\Phi)\delta_{ij}dx^i dx^j\big]\,, \tag{4.61}$$

and we define the potentials of (Ma and Bertschinger, 1995), as,

$$\psi \equiv \Psi\,, \qquad \phi \equiv -\Phi\,, \tag{4.62}$$

In this gauge, one has redefined the new fields,

$$\Psi = \psi + \frac{1}{a}\big(aE' - B\big)' \quad , \quad \Phi = \phi - \mathcal{H}(E' - B)\,, \tag{4.63}$$

which can easily be checked to be gauge invariant combinations. These are typically referred to as the Bardeen potentials (Bardeen, 1980) and, being gauge invariant, are observable. This transformation also applies to the additional auxiliary fields perturbations introduced in the localisation of the RT and RR models. For instance, in the case of the RT model, one redefines,

$$\delta X \to \delta X_{\rm new} = \delta X - (E' - B)\bar{X}'\,, \tag{4.64}$$

$$\delta W_0 \to \delta W_0^{\rm new} = \delta W_0 - \big((E' - B)\bar{W}_0\big)' \quad , \quad \delta W_i \to \delta W_i^{\rm new} = \delta W_i - \partial_i(E' - B)\bar{W}_0\,. \tag{4.65}$$

Stress Energy Tensor and Conservation Equations

We also linearly perturb the energy momentum tensor for matter fluids defined in Sec. 4.1. The definition of the observes' velocity field u^μ implies,

$$u^\mu(\eta) = \frac{1}{a}\big((1-\Psi), v^i\big)\,, \tag{4.66}$$

and to first order in perturbation the energy momentum tensor then reads,

$$T^0_{\ 0} = -(\bar{\rho} + \delta\rho)\,, \tag{4.67}$$

$$T^0_{\ i} = \delta_{ij}v^j(\bar{\rho} + \bar{p})\,, \tag{4.68}$$

$$T^i_{\ j} = (\bar{p} + \delta p)\delta^i_j + \pi^i_{\ j}\,. \tag{4.69}$$

Defining the longitudinal part of the velocity three-vector $\theta \equiv \bar{g}^{ij}\partial_i v_j = \bar{\nabla}_i v^i$, one can work out the scalar transformation properties of each components,

$$\delta\rho \to \delta\rho - A\bar{\rho}'\,, \quad \theta \to \theta + \Delta A\,, \quad \delta p \to \delta p - 3A\bar{p}'\,, \tag{4.70}$$

where $\Delta \equiv \delta^{ij}\partial_i\partial_j$, is the flat Laplace operator. The traceless-transverse $\pi^i_{\ j}$ (helicity-2) is gauge invariant in itself. Defining also the density contrast $\delta \equiv \delta\rho/\bar{\rho}$, we can write the corresponding gauge invariant quantity,

$$\delta^\star \equiv \delta - 3\mathcal{H}\Delta^{-1}\theta(1+w)\,, \tag{4.71}$$

where Δ^{-1} is the Green's function of the Laplacian. In conformal time, the energy-momentum conservation condition $\nabla_\mu T^\mu_{\ \nu} = 0$ for the background is given by,

$$\bar{\rho}' = -3\mathcal{H}(1+w)\bar{\rho}\,, \tag{4.72}$$

while for the linear perturbations, it is convenient to express the pressure perturbation as (Sapone and Kunz, 2009; Albarran et al., 2017),

$$\frac{\delta p}{\bar{\rho}} \equiv c_{\rm s}^2\delta - 3\mathcal{H}(1+w)\big(c_{\rm s}^2 - c_{\rm s,a}^2\big)\Delta^{-1}\theta\,, \tag{4.73}$$

$$= c_{\rm s}^2\delta^\star + 3\mathcal{H}(1+w)c_{\rm s,a}^2\Delta^{-1}\theta\,, \tag{4.74}$$

where $c_{\rm s}^2$ is the rest frame sound speed of the fluid and the adiabatic sound speed is defined as,

$$c_{\rm s,a}^2 \equiv \frac{\bar{p}'}{\bar{\rho}'} = w - \frac{w'}{3\mathcal{H}(1+w)}\,, \tag{4.75}$$

in particular, for fluids with constant equation of state one has $c_{\rm s}^2 = c_{\rm s,a}^2 = w$, and thus $c_{\rm s}^2 = \delta p/\delta\rho$. In that case, the time component of the conservation equation at linear order leads to,

$$\delta' = -\big(3\Phi' + \theta\big)(1+w)\,, \tag{4.76}$$

while the divergence of the spatial component reads,

$$\theta' = -(1-3w)\mathcal{H}\theta - \Delta\Psi - \Delta\sigma - \frac{c_s^2}{1+w}\Delta\delta\,, \tag{4.77}$$

where one has defined,

$$(\bar{\rho}+\bar{p})\sigma \equiv \frac{1}{a^2}\left(\frac{\partial^i\partial^j}{\Delta} - \frac{1}{3}\delta^{ij}\right)\pi_{ij}\,. \tag{4.78}$$

We lower and raise the indices with the spatial background metric $\bar{g}_{ij}$.

4.3.2 Linear Cosmological Perturbations in RT

In this section, for later convenience, we start by expressing the cosmological background equations in conformal time and then present the corresponding linearised equations for the cosmological perturbations.

Background Equations in Conformal Time

Applying the background metric Eq. (4.61) to the localised equations of motion for the RT model written in Sec. 4.1 yields,

$$\mathcal{H}^2 - \frac{m^2}{9}\left[a^2\bar{X} - \bar{W}_0' + \mathcal{H}\bar{W}_0\right] = \frac{8\pi G}{3}a^2\bar{\rho}\,, \tag{4.79}$$

$$\mathcal{H}' + \frac{\mathcal{H}^2}{2} + \frac{m^2}{6}\left(\mathcal{H}\bar{W}_0 - a^2\bar{X}\right) = -4\pi G a^2\bar{p}\,, \tag{4.80}$$

for the modified Friedmann equation, whereas the evolution equations for the auxiliary fields are given by,

$$\bar{X}'' + 2\mathcal{H}\bar{X}' = 6(\mathcal{H}' + \mathcal{H}^2)\,, \tag{4.81}$$

$$\bar{W}_0'' - \big(\mathcal{H}' + 4\mathcal{H}^2\big)\bar{W}_0 = a^2\bar{X}'\,, \tag{4.82}$$

Linear Perturbations Equations

We will now expose the equations of motion at first order in perturbation. As vector components generically decay and are negligible in the late Universe, we are only interested in the scalar sector. We decompose the vector perturbations along their transverse and longitudinal parts with respect to ∂_i as $\delta W_i = \delta W_i^T + \partial_i \delta W$. Moreover, we work in Fourier space as the modes of field perturbations decouple at linear level and therefore generically write $\delta W_k \equiv \delta W$, $\Psi_k \equiv \Psi$, etc. The modified Einstein equations lead to,

$$k^2\Phi + 3\mathcal{H}(\Phi' - \mathcal{H}\Psi) - \frac{m^2}{6}\left[a^2\delta X - \delta W_0' + \mathcal{H}\delta W_0 + 2\Psi\bar{W}_0' + \big(\Psi' - 2\mathcal{H}\Psi\big)\bar{W}_0\right] = 4\pi G a^2\bar{\rho}\delta\,, \tag{4.83}$$

$$k^2(\Phi' - \mathcal{H}\Psi) + \frac{m^2}{6}\left[k^2\mathcal{H}\delta W - \frac{1}{2}k^2\delta W' + k^2\Psi\bar{W}_0 - \frac{1}{2}k^2\delta W_0\right] = -4\pi G(1+w)a^2\bar{\rho}\theta\,, \tag{4.84}$$

$$k^2(\Psi + \Phi) - \frac{m^2}{3}k^2\delta W = 12\pi G(1+w)a^4\bar{\rho}\sigma\,, \tag{4.85}$$

$$\Phi'' - \Psi(\mathcal{H}^2 + 2\mathcal{H}') - \mathcal{H}(\Psi - 2\Phi)' + \frac{k^2}{3}(\Psi + \Phi) \tag{4.86}$$

$$- \frac{m^2}{6}\left[a^2\delta X - \big(\Phi' - 2\mathcal{H}\Psi\big)\bar{W}_0 - \mathcal{H}\delta W_0 - \frac{k^2}{3}\delta W\right] = -4\pi G c_s^2 a^2\bar{\rho}\delta\,, \tag{4.87}$$

which correspond to the (00), $(0i)$, traceless and trace part of the (ij) components of the modified Einstein equations. We will keep this order throughout. The equations governing the dynamics of the auxiliary fields perturbations read,

$$\delta X'' + k^2\delta X + 2\mathcal{H}\delta X' = 2k^2(\Psi + 2\Phi) + 6\Phi'' - (6\mathcal{H} - \bar{X}')(\Psi - 3\Phi)'\,, \tag{4.88}$$

$$\delta W_0'' - \big(\mathcal{H}' + 4\mathcal{H}^2 - k^2/2\big)\delta W_0 = \big[k^2\Psi + \Psi'' - (8\mathcal{H}^2 + 2\mathcal{H}')\Psi - \mathcal{H}(\Psi - 9\Phi)'\big]\bar{W}_0 - k^2/2\delta W' + 2\mathcal{H}k^2\delta W + 3(\Psi - \Phi)'\bar{W}_0' + 2\Psi\bar{W}_0'' + a^2\delta X'\,, \tag{4.89}$$

$$\delta W'' - 2(\mathcal{H}' + 2\mathcal{H}^2 - k^2)\delta W = - 4\mathcal{H}\delta W_0 - \delta W_0' + 4\bar{W}_0'\Psi + 2\big(\Psi' - \Phi' + 2\mathcal{H}\Psi\big)\bar{W}_0 + 2a^2\delta X\,. \tag{4.90}$$

where we used the auxiliary background equations to discard terms. We then use the conservation equations Eqs. (4.76) and (4.77) in Fourier space to close the system. It is also convenient to express them in terms of e-folding time $x = \log a$ and, in that case, define the new variables,

$$\bar{V}_0 = e^{-x}H_0\bar{W}_0\,, \quad \delta V_0 = e^{-x}H_0\delta W_0\,, \quad \delta Z = H_0^2\delta W\,, \tag{4.91}$$

Using $\gamma \equiv m^2/(9H_0^2)$ and $\rho_0 \equiv 3H_0^2/(8\pi G)$, Eqs. (4.83)-(4.87) then become,

$$\hat{k}^2\Phi + 3(\partial_x\Phi - \Psi) = \frac{3}{2h^2\rho_0}\left[\bar{\rho}\delta + \gamma\rho_0\big(\delta X - h\partial_x\delta V_0 + 2h\Psi\partial_x\bar{V}_0 + h\partial_x\Psi\bar{V}_0\big)\right], \tag{4.92}$$

$$\hat{k}^2\big(\partial_x\Phi - \Psi\big) = -\frac{3}{2h^2\rho_0}\left[\bar{\rho}(1+w)\hat{\theta} + \hat{k}^2\gamma\rho_0\left(h^2\delta Z - \frac{h^2}{2}\partial_x\delta Z + h\Psi\bar{V}_0 - \frac{h}{2}\delta V_0\right)\right], \tag{4.93}$$

$$\hat{k}^2(\Psi + \Phi) = \frac{9}{2h^2\rho_0}e^{2x}\bar{\rho}(1+w)\sigma + 3\hat{k}^2\gamma\delta Z\,, \tag{4.94}$$

$$\partial_x^2\Phi + (3+\zeta)\partial_x\Phi - \partial_x\Psi - (3+2\zeta)\Psi + \frac{\hat{k}^2}{3}(\Phi + \Psi) = -\frac{3}{2h^2\rho_0}\left[c_{\rm s}^2\delta\bar{\rho} - \gamma\rho_0\left(\delta X - h(\partial_x\Phi - 2\Psi)\bar{V}_0 - h\delta V_0 - \frac{\hat{k}^2}{3}h^2\delta Z\right)\right], \tag{4.95}$$

where we have also introduced $\hat{k} \equiv k/(e^x H)$ and $\hat{\theta} \equiv \theta/(e^x H)$. The equations for the auxiliary fields now read,

$$\partial_x^2\delta X + (3+\zeta)\partial_x\delta X + \hat{k}^2\delta X + \big[2\Psi(3+\zeta) - (\partial_x\Psi - 3\partial_x\Phi)\big]\partial_x\bar{X} = 2\hat{k}^2(\Psi+2\Phi) + 6\big[\partial_x^2\Phi + (4+\zeta)\partial_x\Phi\big] - 6\partial_x\Psi\,, \quad (4.96)$$

$$\partial_x^2\delta V_0 + (3+\zeta)\partial_x\delta V_0 + (\hat{k}^2/2)h(\partial_x\delta Z - 4\delta Z) = \big[2(3+\zeta)\Psi + 3(\partial_x\Psi - \partial_x\Phi)\big]\partial_x\bar{V}_0 + \big[\partial_x^2\Psi + (3+\zeta)\partial_x\Psi + 6\partial_x\Phi\big]\bar{V}_0 - \big[(1/2)\hat{k}^2 - 3\big](\delta V_0 - 2\Psi\bar{V}_0) + 2\Psi\partial_x\bar{V}_0 + h^{-1}\partial_x\delta X\,, \quad (4.97)$$

$$\partial_x^2 Z + (1+\zeta)\partial_x\delta Z + 2\big(\hat{k}^2 - (3+\zeta)\big)\delta Z = 2h^{-2}\delta X - h^{-1}\big[\partial_x\delta V_0 + 5\delta V_0 - 4\Psi\partial_x\bar{V}_0 - 2(\partial_x\Psi - \partial_x\Phi + 4\Psi)\big]\,, \quad (4.98)$$

and the matter perturbation conservation equations are given by,

$$\partial_x\delta = -(3\partial_x\Phi + \tilde{\theta})(1+w)\,, \quad (4.99)$$

$$\partial_x\tilde{\theta} = -\big(2 - 3w + \zeta\big)\hat{\theta} + \hat{k}^2\left[\Psi + \sigma + \frac{c_s^2}{1+w}\delta\right], \quad (4.100)$$

Tensor Perturbations

Next, we compute the evolution equations for linear tensor perturbations in the RT model (Dirian et al., 2016). In that case, the line element in conformal time reads,

$$\mathrm{d}s^2 = a^2(\eta)[-\mathrm{d}\eta^2 + \big(\delta_{ij} + h_{ij}^{TT}\big)\mathrm{d}x^i\mathrm{d}x^j]\,, \quad (4.101)$$

where $h_{ij,TT}$ is the traceless-transverse tensor perturbation, $\delta^{ij}h_{ij}^{TT} = 0$, $\partial^i h_{ij}^{TT} = 0$. For the RT model, one finds,

$$\partial_\eta^2 h_{ij}^{TT} + \left(2\mathcal{H} - \frac{m^2}{3}\bar{W}_0\right)\partial_\eta h_{ij}^{TT} - \Delta h_{ij}^{TT} = 16\pi G a^2\ \pi_{ij}\,. \quad (4.102)$$

Observe this equation is modified in its friction term, it is not exclusively driven by the Hubble flow as in GR, but also by a contribution from the background auxiliary field $\bar{W}_0$. The source here is the anisotropic stress tensor π_{ij}, which is non-vanishing when relativistic particles are present during the evolution (Weinberg, 2004; Durrer and Kahniashvili, 1998). The fact that this term vanishes in the present situation is due to the fact that we address a simplified treatment to the description of the radiation component, effectively treating photon as non-relativistic particles. A correct description is provided by writing the energy-momentum stress tensor in terms of the phase-space thermal distribution function which evolve according to the Boltzmann equation [see e.g. (Ma and Bertschinger, 1995)].
As the field $\bar{W}_0$ is positive at late time (see the $\bar{S}$ background field in the right panel of Fig. 4.1), its effect is to effectively decrease the background friction in Eq. (4.103). This implies the prediction of a larger amplitude for the large scale GWs at present time, as one can see from Fig. 4.4. A similar modification was also observed in (Deffayet and Menou, 2007), within the framework of the DGP model (Dvali et al., 2000), that we describe in Sec. 2.4. As we will discuss in Chapter 6, such a modified friction for GWs leads to the introduction of a modified notion of luminosity distance, the *GW luminosity distance*, which is not equal to its electromagnetic counterpart as in standard GR. Therefore, appreciating the difference between the distance-redshift relation from luminous objects, e.g. distant SNIa or quasars, and the distance-redshift relation provided by binary mergers, in particular binary neutrons stars coalescence, can provide

a stringent test for GR and modified gravity theories. Furthermore, an aspect that became recently very relevant for the viability of modified gravity theories is the propagation speed of the gravitational waves that they describe. Indeed, the recent observations by the *LIGO* and *Virgo* interferometers of the GWs from the binary neutron star (BNS) coalescence GW170817 (Abbott et al., 2017h), together with the observation of its γ-ray burst counterpart GRB170817A by *Fermi–GBM* (Goldstein et al., 2017) and *INTEGRAL* (Savchenko et al., 2017), provide a strong constraint on the present speed of GWs, $|c_{\rm gw}/c-1| = \mathcal{O}\big(10^{-15}\big)$ (Abbott et al., 2017i). Therefore, models modifying the dispersion relation of GWs are typically ruled out. In our case, decomposing the field perturbations on the tensor eigenfunctions of the Laplacian, e.g. $h_{ij}^{TT} = H^{(T)}Q_{ij}^{(T)}$ (Durrer, 2008), one can write,

$$\partial_\eta^2 H^{(T)} + \left(2\mathcal{H} - \frac{m^2}{3}\bar{W}_0\right)\partial_\eta H^{(T)} + k^2 H^{(T)} = 16\pi G a^2\,\pi^{(T)}\,, \tag{4.103}$$

trading the metric and matter fields for,

$$H^{(T)}\big(\eta,\vec{x}\big) = \frac{1}{\tilde{a}(\eta)}\chi\big(\eta,\vec{k}\big)\,, \quad \pi^{(T)}\big(\eta,\vec{x}\big) = \frac{1}{\tilde{a}(\eta)}\tilde{\pi}\big(\eta,\vec{k}\big)\,, \tag{4.104}$$

and defining,

$$\frac{\tilde{a}'}{\tilde{a}} \equiv \mathcal{H}\left[1 - \frac{m^2}{6\mathcal{H}}\bar{W}_0\right], \tag{4.105}$$

we obtain,

$$\tilde{\chi}'' + \left(k^2 - \frac{\tilde{a}''}{\tilde{a}}\right)\tilde{\chi} = 16\pi G a^2\,\tilde{\pi}\,. \tag{4.106}$$

At solar system scales, $k \gg 1$, and the k^2 term dominates the dispersion relation, showing that the GWs propagate at the speed of light in the RT model. This model is therefore compatible with the aforementioned observations.

4.3.3 Linear Perturbation Equations in RR

Scalar Perturbations

We now discuss in details the cosmological perturbations of the RR model, in the localised version of its equations of motion (4.8), (Dirian et al., 2014). The modified Friedmann equations in conformal time read,

$$\left(1 - \frac{m^2}{3}\bar{S}\right)\mathcal{H}^2 - \frac{m^2}{18}\left(\frac{1}{2}a^2\bar{U}^2 + 6\mathcal{H}\bar{S}' - \bar{S}'\bar{U}'\right) = \frac{8\pi G}{3}a^2\bar{\rho}\,, \tag{4.107}$$

$$\left(1 - \frac{m^2}{3}\bar{S}\right)\left(\mathcal{H}' + \frac{\mathcal{H}^2}{2}\right) - \frac{m^2}{12}\left(\frac{1}{2}a^2\bar{U}^2 + 2\mathcal{H}\bar{S}' + \bar{S}'\bar{U}' + 2\bar{S}''\right) = -4\pi G a^2\bar{p}\,, \tag{4.108}$$

while for the auxiliary equations one has,

$$\bar{U}'' + 2\mathcal{H}\bar{U}' = 6\left(\mathcal{H}' + \mathcal{H}^2\right), \qquad \bar{S}'' + 2\mathcal{H}\bar{S}' = a^2\bar{U}\,. \tag{4.109}$$

To first order in linear perturbations one obtains the modified Einstein equations,

$$\begin{aligned}\left(1 - \frac{m^2}{3}\bar{S}\right)\left(k^2\Phi + 3\mathcal{H}\left(\Phi' - \mathcal{H}\Psi\right)\right) &= 4\pi G a^2\bar{\rho}\delta - \frac{m^2}{6}\Big[-\frac{1}{2}a^2\bar{U}\delta U \\ &+ \big(6\mathcal{H}\Psi - 3\Phi' - \Psi\bar{U}'\big)\bar{S}' + \frac{1}{2}\big(\bar{U}'\delta S' + \bar{S}'\delta U'\big) - 3\mathcal{H}^2\delta S - 3\mathcal{H}\delta S' - k^2\delta S\Big]\,,\end{aligned} \tag{4.110}$$

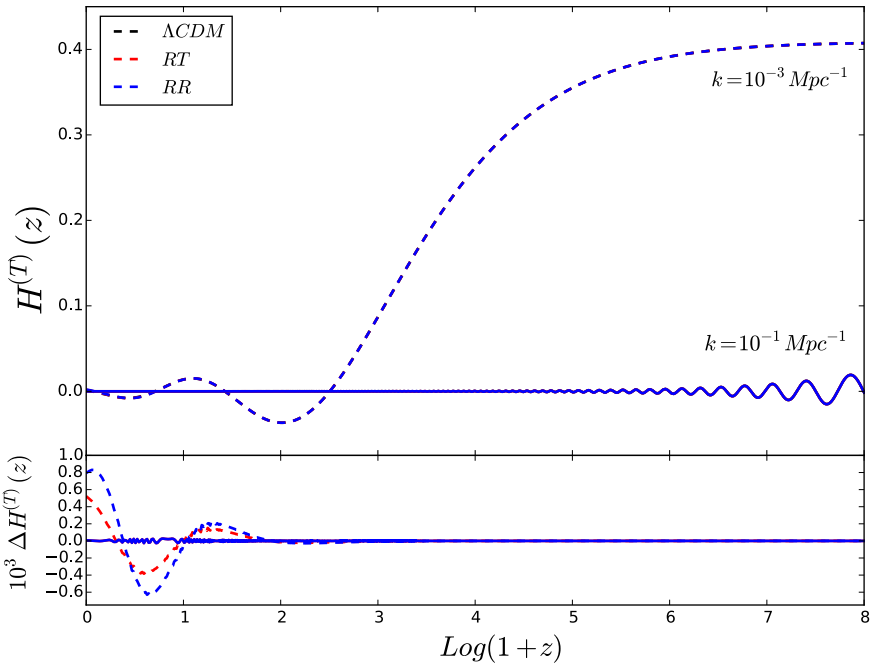

Figure 4.4 – Upper panel: Gravitational waves amplitude $H^{(T)}$ as a function of $\log(1+z) = -x$ in the RT model (red) and in RR (blue) for wavenumber $k = 10^{-3}\,\mathrm{Mpc}^{-1}$ (dashed) and $k = 10^{-1}\,\mathrm{Mpc}^{-1}$ (solid) for the same fiducial cosmology. Lower panel: The absolute difference with respect to ΛCDM in RT (red) and RR (blue).

$$\left(1-\frac{m^2}{3}\bar{S}\right)k^2(\Phi'-\mathcal{H}\Psi)-\frac{m^2k^2}{6}\Big[\delta S'-\bar{S}'\Psi-\mathcal{H}\delta S + \frac{1}{2}\left(\bar{U}'\delta S+\bar{S}'\delta U\right)\Big] = -4\pi G a^2\hat{\theta}\bar{\rho}(1+w)\,, \quad (4.111)$$

$$\left(1-\frac{m^2}{3}\bar{S}\right)k^2(\Psi+\Phi)-\frac{m^2k^2}{3}\delta S = 12\pi G a^4\bar{\rho}(1+w)\sigma\,, \quad (4.112)$$

$$\left(1-\frac{m^2}{3}\bar{S}\right)\left(\Phi''-\Psi(\mathcal{H}^2+2\mathcal{H}')-\mathcal{H}(\Psi'-2\Phi')+\frac{k^2}{3}(\Psi+\Phi)\right) - \frac{m^2}{6}\Big[\frac{1}{2}a^2\bar{U}\delta U-2\Psi\bar{S}''+\left(2\Phi'-2\mathcal{H}\Psi-\Psi'-\Psi\bar{U}'\right)\bar{S}'+\delta S''+\mathcal{H}\delta S'+\left(\mathcal{H}^2+2\mathcal{H}'\right)\delta S + \frac{2k^2}{3}\delta S+\frac{1}{2}\left(\bar{U}'\delta S'+\bar{S}'\delta U'\right)\Big] = -4\pi G a^2 c_{\rm s}^2\bar{\rho}\delta\,, \quad (4.113)$$

and the evolution of the auxiliary fields read,

$$\delta U''+2\mathcal{H}\delta U'+k^2\delta U-\left(\Psi'-3\Phi'\right)\bar{U}' = 6\Phi''-6\mathcal{H}\left(\Psi'-3\Phi'\right)+2k^2\left(\Psi+2\Phi\right)\Big), \quad (4.114)$$

$$\delta S''+2\mathcal{H}\delta S'+k^2\delta S-\left(\Psi'-3\Phi'\right)\bar{S}'-2\Psi\left(\bar{S}''+2\mathcal{H}\bar{S}'\right) = a^2\delta U\,. \quad (4.115)$$

The conservation equations used for closing the system are provided in Eqs. (4.76),(4.77) in real space. Going to time $x = \log a$ and defining the new variables, $\bar{V} \equiv H_0^2\bar{S}$, $\delta V \equiv H_0^2\delta S$ these

become,

$$\big(1-3\gamma\bar{V}\big)\Big(\hat{k}^2\Phi+3\left(\partial_x\Phi-\Psi\right)\Big)= \\ \frac{3}{2\rho_0 h^2}\bar{\rho}\delta-\frac{3\gamma}{2}\Big[-\frac{1}{2h^2}\bar{U}\delta U+\big(6\Psi-3\partial_x\Phi-\Psi\partial_x\bar{U}\big)\partial_x\bar{V}+\frac{1}{2}\big(\partial_x\bar{U}\partial_x\delta V+\partial_x\bar{V}\partial_x\delta U\big) \\ -3\delta V-3\partial_x\delta V-\hat{k}^2\delta V\Big], \quad (4.116)$$

$$\big(1-3\gamma\bar{V}\big)\hat{k}^2(\partial_x\Phi-\Psi)= \\ -\frac{3}{2\rho_0 h^2}\hat{\theta}\bar{\rho}(1+w)+\frac{3\gamma\hat{k}^2}{2}\Big[\partial_x\delta V-\partial_x\bar{V}\Psi-\delta V+\frac{1}{2}\left(\partial_x\bar{U}\delta V+\partial_x\bar{V}\delta U\right)\Big], \quad (4.117)$$

$$\hat{k}^2(\Psi+\Phi)\big(1-3\gamma\bar{V}\big)-3\gamma\hat{k}^2\delta V=\frac{9}{2\rho_0 h^2}e^{2x}\bar{\rho}(1+w)\sigma\,, \quad (4.118)$$

$$\Big(1-3\gamma\bar{V}\Big)\Big(\partial_x^2\Phi+(3+\zeta)\partial_x\Phi-\partial_x\Psi-(3+2\zeta)\Psi+\frac{\hat{k}^2}{3}(\Phi+\Psi)\Big) \\ =-\frac{3}{2\rho_0 h^2}c_s^2\bar{\rho}\delta-\frac{3\gamma}{2}\Big(\frac{1}{2h^2}\bar{U}\delta U-2\Psi\partial_x^2\bar{V}+\big[2\partial_x\Phi-2(2+\zeta)\Psi-\partial_x\Psi-\Psi\partial_x\bar{U}\big]\partial_x\bar{V} \\ +\partial_x^2\delta V+(2+\zeta)\partial_x\delta V+\frac{2\hat{k}^2}{3}\delta V+(3+2\zeta)\delta V+\frac{1}{2}\big(\partial_x\bar{U}\partial_x\delta V+\partial_x\bar{V}\partial_x\delta U\big)\Big), \quad (4.119)$$

while the evolution equations for the auxiliary field perturbations are given by,

$$\partial_x^2\delta U+(3+\zeta)\partial_x\delta U+\hat{k}^2\delta U-2\Psi\partial_x^2\bar{U}-\big[2(3+\zeta)\Psi+\partial_x\Psi-3\partial_x\Phi\big]\partial_x\bar{U} \\ =2\hat{k}^2(\Psi+2\Phi)+6\big[\partial_x^2\Phi+(4+\zeta)\partial_x\Phi\big]-6\big[\partial_x\Psi+2(2+\zeta)\Psi\big], \quad (4.120)$$

$$\partial_x^2\delta V+(3+\zeta)\partial_x\delta V+\hat{k}^2\delta V-2\Psi\partial_x^2\bar{V}-\big[2(3+\zeta)\Psi+\partial_x\Psi-3\partial_x\Phi\big]\partial_x\bar{V}=\frac{\delta U}{h^2}\,. \quad (4.121)$$

Tensor Perturbations

The evolution equations for the tensor perturbations are also modified in the RR model. They read,

$$\Big(1-\frac{m^2}{3}\bar{S}\Big)\Big[\partial_\eta^2 H^{(T)}+2\mathcal{H}\partial_\eta H^{(T)}+k^2H^{(T)}\Big]-\frac{m^2}{3}\partial_\eta\bar{S}\partial_\eta H^{(T)}=16\pi G a^2\;\pi^{(T)}\,. \quad (4.122)$$

and are characterised by a modification of the background friction, as for the case of the RT model (4.103). This boosts the amplitude of the large scales modes GWs at late time, as can be seen from Fig. 4.4. Additionally, they also feature an effective coupling to the source,

$$G_{\rm eff,gw}(\eta)/G\equiv\Big(1-\frac{m^2}{3}\bar{S}\Big)^{-1}. \quad (4.123)$$

In the far future as $x\to+\infty$, we have $(m^2/3)\bar{S}(x)\to1^-$ (Dirian and Mitsou, 2014), so that $G_{\rm eff,gw}(x)\to+\infty$, and the tensor modes become strongly coupled to matter. However, as we will see below (see Fig. 4.5), in the early past until today $G_{\rm eff,gw}(x)/G-1\lesssim6\%$, so that the coupling to the source can only mildly affect observable predictions. Observe that such a modified coupling also appears in the scalar perturbation sector for the RR model, Eqs. (4.110)-(A.22). Concerning the speed of the GWs in the RR model, performing the same manipulations

as in Sec. (4.3.2), we find a similar expression as in Eq. (4.106), with,

$$\frac{\tilde{a}'}{\tilde{a}} = \mathcal{H}\left[1 - \left(1 - \frac{m^2}{3}\bar{S}\right)^{-1}\frac{m^2}{6\mathcal{H}}\partial_\eta \bar{S}\right] = \mathcal{H}\left[1 - \frac{1}{2\mathcal{H}}\partial_\eta \log\left(G_{\rm eff,gw}(x)/G\right)\right], \tag{4.124}$$

which, in the subhorizon limit, shows that the RR model also describes GWs propagating at the speed of light. More details will be provided in Chapter 6.

4.3.4 Perturbation of Initial Conditions

Initial Conditions for Radiation and Dust

Regarding the matter content, as for the background evolution presented above, we assume a simplified scenario where the evolution start into RD and evolves into a phase a matter (dust, CDM) domination. Radiation has a sounds speed $c^2_{{\rm s},R} = 1/3$ while non-relativistic matter has $c^2_{{\rm s},M} = 0$. In that case, the conservation equations reduce to,

$$\partial_x \delta_M = -(3\partial_x\Phi + \hat{\theta}_M)\,, \qquad \partial_x \delta_R = -\frac{4}{3}(3\partial_x\Phi + \hat{\theta}_R)\,, \tag{4.125}$$

$$\partial_x \hat{\theta}_M = -(2+\zeta)\hat{\theta}_M + \hat{k}^2\Psi\,, \quad \partial_x \hat{\theta}_R = -(1+\zeta)\hat{\theta}_R + \hat{k}^2\left[\Psi + \frac{\delta_R}{4}\right]. \tag{4.126}$$

where $\{\delta_R, \theta_R\}$, $\{\delta_M, \theta_M\}$ are the radiation and matter density contrast and velocity divergence, respectively. Such a matter configuration implies that the anisotropic stress generically vanishes $\sigma_{M,R} = 0$, however in this case, this does not imply that the gravitational potentials are proportional to each other $\Psi \neq -\Phi$, since there an anisotropic stress component characterising the effective dark energy perturbations in both nonlocal models [see Eqs. (4.94),(4.118)]. Taking the derivative of the first equation of (4.125) and using the second one, one can compute the growth equation,

$$\delta''_M + (2+\zeta)\delta_M = -\left(\Phi'' + (2+\zeta)\Phi'\right) - \hat{k}^2\Psi\,. \tag{4.127}$$

Concerning the initial conditions for the gravitational potential Ψ and the matter perturbations δ_i and θ_i ($i = R,M$), we choose adiabatic initial conditions provided by early physics processes such as inflation, integrating the system from RD at $x_{\rm in} = -15$. We are interested in the perturbations whose wavelengths lie well outside the size of the Hubble horizon, i.e. $\hat{k}(x_0) \ll 1$, since at subhorizon scales the radiation, CDM perturbations do not grow. Moreover, the primoridial spectrum is taken as been slightly tilted so that (Amendola and Tsujikawa, 2010),

$$A^2(k) = \frac{50\pi^2}{9}\left(\frac{k}{H_0}\right)^{n_s - 1}\delta_H^2\,, \tag{4.128}$$

where $n_s \simeq 0.96$ is the spectral index and $\delta_H^2 \simeq 3.2 \times 10^{-10}$, the amplitude of the gravitational potential. To second order in k^2 the initial conditions for the Bardeen potentials and matter

quantity read (Durrer, 2008),

$$\Phi(x_{in}) = -\Psi(x_{in}) = A(k)\frac{3\sqrt{3}}{\hat{k}_{in}} j_1\big(\hat{k}_{in}/\sqrt{3}\big)\,, \tag{4.129}$$

$$\approx A(k)\bigg(1 - \frac{\hat{k}_{in}^2}{30} + \frac{\hat{k}_{in}^4}{2520} + \mathcal{O}(k^6)\bigg)\,, \tag{4.130}$$

$$\delta_R(x_{in}) = \frac{4}{3}\delta_M(x_{in}) = \frac{6A(k)}{\hat{k}_{in}^3}\bigg(\hat{k}_{in}(6-\hat{k}_{in}^2)\cos\big(\hat{k}_{in}/\sqrt{3}\big) + 2\sqrt{3}\big(\hat{k}_{in}^2 - 3\big)\sin\big(\hat{k}_{in}/\sqrt{3}\big)\bigg)\,,$$

$$\approx A(k)\bigg(2 + \frac{7\hat{k}_{in}^2}{15} - \frac{23\hat{k}_{in}^4}{1260} + \mathcal{O}(k^6)\bigg)\,, \tag{4.131}$$

$$\theta_M(x_{in}) = \theta_R(x_{in}) = -\frac{3A(k)}{2\hat{k}_{in}}\bigg(6\hat{k}_{in}\cos\big(\hat{k}_{in}/\sqrt{3}\big) + \sqrt{3}(\hat{k}_{in}^2 - 6)\sin\big(\hat{k}_{in}/\sqrt{3}\big)\bigg)\,, \tag{4.132}$$

$$\approx A(k)\bigg(-\frac{\hat{k}_{in}^2}{2} + \frac{\hat{k}_{in}^4}{20} + \mathcal{O}(k^6)\bigg)\,, \tag{4.133}$$

where $\hat{k}_{in} \equiv \hat{k}(x_{in})$. We also define $\kappa \equiv \hat{k}_{\rm eq} = k/k_{\rm eq}$, where $k_{\rm eq} = a_{\rm eq}H_{\rm eq}$ is the size of the horizon at matter-radiation equality. Choosing two different representative values $\kappa = 0.1,\, 5$, allows us to follow the behavior of modes that were inside and outside the horizon at equality. Indeed, as $k_{\rm eq} \simeq 0.014 h_0/{\rm Mpc} \simeq 42 H_0$, a value of $\kappa = 0.1$ corresponds to $k/H_0 = 4$, i.e. a mode that enters the horizon at late time $z \simeq 1.5$, whereas $\kappa = 5$ give $k/H_0 = 210$, which entered so horizon already in RD.

Initial Conditions for Auxiliary Field Perturbations

Concerning the auxiliary sector in both models, as discussed into Sec. 3.1.2, the corresponding initial data are constrained at full nonlinear level, due to the nonlocal structure of the underlying theory. At background level, we have seen in Sec. 4.2.3, that the lack of understanding of the mechanism generating such nonlocal corrections, and therefore of their domain of validity, the initial conditions of the auxiliary fields can be taken to vanish in RD, or be fixed to a finite value provide by the evolution of the system during earlier stages of the Universe, to which the nonlocal models are considered to make explicitly part. At linear perturbation level, the situation is similar. Splitting the auxiliary fields into a background and linear perturbation part, one imposes,

$$X(t_{\rm in}) \approx \bar{X}(t_{\rm in}) + \delta X_k(t_{\rm in}) = \text{constant}\,, \tag{4.134}$$

on the initial spacelike hypersurface $\Sigma_{t_{\rm in}}$. The linear perturbations should remain small,

$$\delta X(t_{\rm in})/\bar{X}(t_{\rm in}) \ll 1\,, \tag{4.135}$$

so that perturbation theory remains valid. The issue is now to know whether or not one is allowed to incorporate the nonlocal corrections into a model describing early Universe physics. Indeed, in the case where these corrections originate from some low energy limit of a more fundamental theory, these terms are not legitimate to be used for describing a highly energetic phase such as during the early Universe. Without the knowledge of such an eventual, more fundamental theory, this question therefore cannot be answered. In a bottom-up approach to this question, two strategies can be adopted. The first is to consider that such corrections are only relevant for infrared physics, and therefore do not contribute to the description of

early Universe physics. In that case, one can safely set vanishing initial conditions for the auxiliary field in RD, as their effects only become relevant once matter domination sets in. The second strategy consists in assuming that such corrections make genuinely part of the model describing early physics, and in that case one should concretely embed these corrections into the corresponding theory, such as one describing an inflationary period. Then, the initial conditions in RD for the auxiliary sector at background and linear perturbation level are directly provided by inflationary physics, and for linear perturbations in the very same way than the primordial curvature perturbation spectrum seeds the underlying dark matter distribution, and therefore the gravitational potentials Φ and Ψ at that time. An approximate evaluation of the values of the auxiliary fields at the exit of such an inflationary phase can be performed at the background level, as reviewed in Sec. 4.2.3. At the level of linear perturbations, as is illustrated in Sec. 3.1.2 and discussed further in (Maggiore, 2017) [see also Sec. 3.2.1 of Ref. (Belgacem et al., 2018b)], that the initial conditions for the auxiliary field perturbations in the RR model are related to the ones of the gravitational potentials,

$$\delta U_k(t_{\rm in}) \sim \Phi_k(t_{\rm in})\,, \qquad \delta U_k'(t_{\rm in}) \sim \Phi_k'(t_{\rm in})\,. \tag{4.136}$$

In the following, we review results of linear perturbation theory applied to both nonlocal modified gravity models. We will only consider the "minimal" version of the above nonlocal models, i.e. when the initial data of the auxiliary sector is constrained to vanish. We then provide details on the dark energy phenomenology that both models describe.

4.4 Results of Linear Perturbation Theory

We integrate the linear perturbation equations for the scalar sector in the "minimal" version of the RT and RR model, i.e. where the initial conditions of the auxiliary variables are overall vanishing. The matter content is specified to be a simplified scenario involving an early radiation phase (from $x_{\rm in} = -15$) and a late dust (CDM) dominated era, realised by perfect fluid fields. As hereabove, the cosmological constant is set to zero in the case of the nonlocal models, $\Lambda = 0$ and fudged so as to close the Universe today in ΛCDM. We use the time-time component of the Einstein equations for closing the system. Initial conditions for the other fields and fixed fiducial cosmology are provided in the previous sections.

4.4.1 Indicators of Deviations from GR

We define a set of commonly used functions for appreciating the deviations to GR induced by the nonlocal models at linear perturbation level [see e.g. (Kunz, 2012)].

RT Model

We first introduce the modified Poisson equations for the gravitational potential. This equation is generically used in composing the time-time and time-space component of the modified Einstein equations. The case of the RT model yields,

$$\begin{aligned}\hat{k}^2\Phi = \frac{3}{2h^2}\Bigg[&\Omega_R e^{-4x}\left(\delta_R + \frac{4}{\hat{k}^2}\hat{\theta}_R\right) + \Omega_M e^{-3x}\left(\delta_M + \frac{3}{\hat{k}^2}\hat{\theta}_M\right)\\ &+ \gamma\left(\delta X - h\partial_x\delta V_0 - \frac{3h}{2}\delta V_0 + 2h\Psi\partial_x\bar{V}_0 + h\partial_x\Psi\bar{V}_0 + 3h\Psi\bar{V}_0 + 3h^2\delta Z - \frac{3h^2}{2}\partial_x\delta Z\right)\Bigg]\,,\end{aligned} \tag{4.137}$$

from which one can read,

$$\frac{G_{\rm eff}}{G}(x) = 1 + \frac{A(x)}{B(x)}\,, \tag{4.138}$$

with,

$$\begin{aligned} A(x) &\equiv \gamma\left(\delta U - h\partial_x\delta V - \frac{3h}{2}\delta V + 2h\Psi\partial_x\bar{V} + h\partial_x\Psi\bar{V} + 3h\Psi\bar{V} + 3h^2\delta Z - \frac{3h^2}{2}\partial_x\delta Z\right), \\ B(x) &\equiv \Omega_R e^{-4x}\left(\delta_R + \frac{4}{\hat{k}^2}\hat{\theta}_R\right) + \Omega_M e^{-3x}\left(\delta_M + \frac{3}{\hat{k}^2}\hat{\theta}_M\right). \end{aligned} \tag{4.139}$$

Then the modified Poisson equation (4.147) can be rewritten as

$$k^2\Phi = 4\pi G_{\rm eff}(x;k)a^2\rho_0\left[\Omega_R e^{-4x}\left(\delta_R + \frac{4}{\hat{k}^2}\hat{\theta}_R\right) + \Omega_M e^{-3x}\left(\delta_M + \frac{3}{\hat{k}^2}\hat{\theta}_M\right)\right]. \tag{4.140}$$

This shows that $G_{\rm eff}(x;k)$ plays the role of an effective time-dependent gravitational "constant", which also depends on the mode k. We show the plot of the effective Newton constant on the left panel of Fig. 4.5. Not surprisingly, the effective Newton constant converges to G at small scales (red dashed line), while it is enhanced at larger scales (blue solid line). One could have expected this behavior as the nonlocal correction is generically modifying the theory in its infrared regime, as seen directly from the corresponding covariant equations of motion. The effective Newton constant can be interpreted as describing the effect of a fifth force induced by new degrees of freedom beside the gravitational ones, and can be effectively interpreted as the auxiliary fields in the present case. This affects the gravitational attraction of (dust) matter and is therefore relevant for structure formation. Its features depend on the specific structure of modified gravity model at hand and is one of its fingerprint. However, in the case of the RT model, we see that this quantity is $\sim 1\%$ and therefore this model will be harder to discriminate compared to the ΛCDM one.

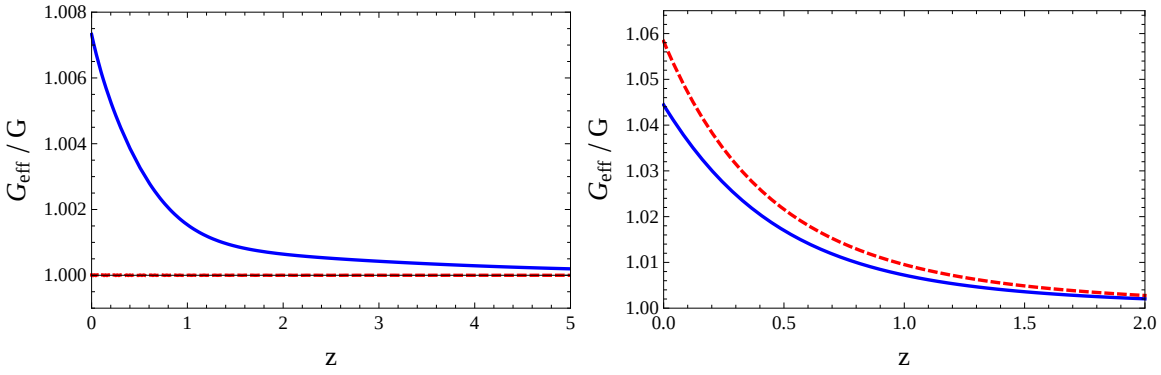

Figure 4.5 – Effective Newton constant $G_{\rm eff}/G(z,k)$ in the RT model (left panel) and in RR (right panel). The blue solid lines correspond to $\kappa = 0.1$ while the red dashed lines are for $\kappa = 5$. From (Dirian et al., 2014).

Together with $G_{\rm eff}$, a second indicator is the gravitational slip (Zhang et al., 2007; Amendola et al., 2008b),

$$\eta(x,k) = \frac{\Phi + \Psi}{\Phi}\,. \tag{4.141}$$

which characterises the presence of anisotropic stress, and in particular the one induced by an effective dark energy component as in both nonlocal models. Fig. 4.6 shows the gravitational slip η (left panel) and the anisotropic stress $\pi(z,k) \equiv \Psi + \Phi$ (right panel). We see that both quantities are very small on small scale (red dashed lines) and become larger on large scales (solid blue lines), the RT model induces an anisotropic stress affecting the difference between both gravitational potential are the level of 2% at present time.

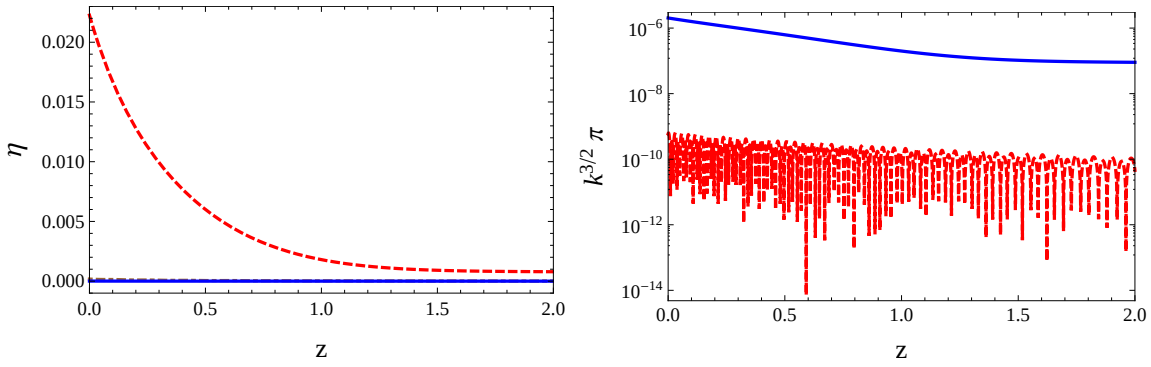

Figure 4.6 – Gravitational slip η (left panel) and the dimensionless anisotropic stress $k^{3/2}\pi$ (right panel) in the RT model. The blue solid lines correspond to $\kappa = 0.1$ while the red dashed lines are for $\kappa = 5$. From (Dirian et al., 2014).

Alternatively, two useful quantities are the functions $\mu(x,k)$ (Daniel et al., 2010) and $\Sigma(x,k)$ (Amendola et al., 2008b), which we define as,

$$\Psi = [1+\mu(x;k)]\Psi_{\rm GR}\,, \tag{4.142}$$

$$\Psi - \Phi = [1+\Sigma(x;k)](\Psi-\Phi)_{\rm GR}\,, \tag{4.143}$$

where the subscript denotes the same quantities computed in ΛCDM on the same fiducial cosmology. The quantity characterises the deviation to the gravitational potential in GR (modulo dark energy anisotropic stress) and Σ provides access to the deviation in the lensing potential. The advantage of this parametrisation is that it neatly separates the modifications to the motion of non-relativistic particles, which is described by μ, from the modification to light propagation, which is encoded in Σ. For modes well inside the horizon, the growth equation Eq. (4.127) becomes,

$$\delta_M'' + (2+\zeta)\delta_M' = -\hat{k}^2(1+\mu)\Psi_{\rm GR}\,. \tag{4.144}$$

If one neglects the anisotropic stress induced by relativistic matter $\Psi_{\rm GR} = -\Phi_{\rm GR}$ and using $k^2\Phi_{\rm GR} = 4\pi G a^2 \rho_M (\delta_M)_{\rm GR}$, where $(\delta_M)_{\rm GR}$ are the matter density perturbation in ΛCDM, one can write,

$$\delta_M'' + (2+\zeta)\delta_M' - \frac{3}{2}(1+\mu)\,\frac{\Omega_M(\delta_M)_{\rm GR}}{a^3 h^2(x)} = 0\,, \tag{4.145}$$

which shows how the growth of structures is affected by μ. The quantities $(G_{\rm eff}/G, \eta)$ and (μ, Σ) are not independent and can be related to each other, the detailed relations are found in (Dirian et al., 2014). We show how the growth function defined by,

$$g(z,k) \equiv \frac{\delta \log \delta_M}{\delta \log a}\,, \tag{4.146}$$

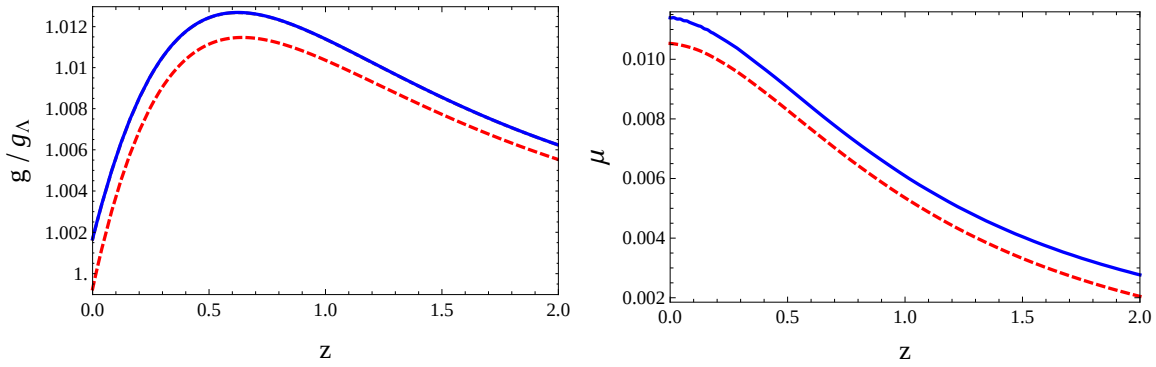

Figure 4.7 – Ratio of the growth function $g(z,k)$ with respect to the one in ΛCDM (left panel) and the deviation parameter μ (right panel) in the RT model. The blue solid lines correspond to $\kappa = 0.1$ while the red dashed lines are for $\kappa = 5$. From (Dirian et al., 2014).

is affected into the RT model in the left panel of Fig. 4.7, while we show the plot of the deviation parameter $\mu(z,k)$ in the right panel. We can see that the corresponding corrections to GR are also at percent level in that model. For the RT model, the function $\Sigma(z,k)$ is shown in the left panel of Fig. 4.8. Overall, we see that, for fixed fiducial cosmology, the linear perturbations

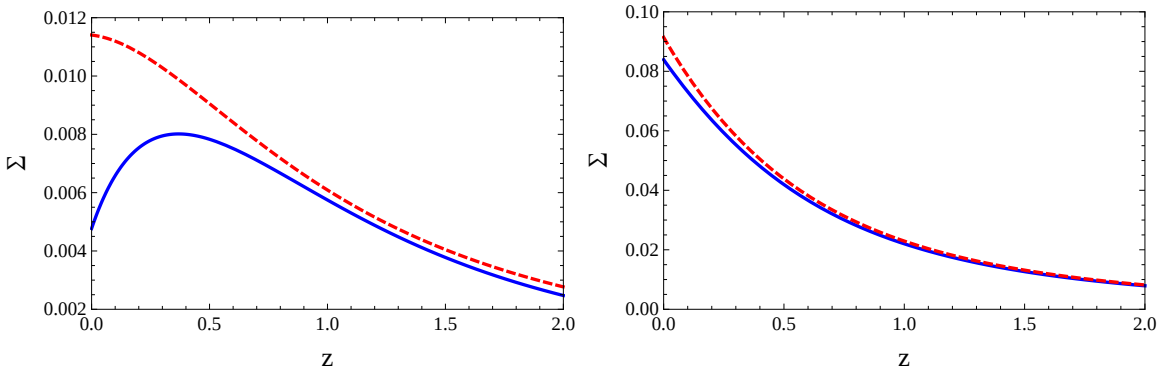

Figure 4.8 – Deviation parameter $\Sigma(z,k)$ fo the RT model (left panel) and for the RR model (right panel). The blue solid lines correspond to $\kappa = 0.1$ while the red dashed lines are for $\kappa = 5$. From (Dirian et al., 2014).

of the RT model deviate from the ones in ΛCDM at $\sim$ 1–2% level. Supplemented by a quasi-similar background evolution as well, it is quite surprising to find this model so close to ΛCDM, while its theoretical structure is completely different. The tendency of the nonlocal model is to induces a higher growth of structures at late time compared to ΛCDM, as witnessed by an enhanced effective Newton constant, a higher growth function and a positive μ. This is also partially because the Hubble parameter is lowered at late time (see the left panel of Fig. 4.1), so that the CDM density fraction $\Omega_M(z)$ is higher at late time, and structures are less smeared out by the expansion and can more easily grow. Heavier structures also deepen the gravitational potential well that increase in turn the lensing potential whose deviation to ΛCDM is provided by Σ. Such trend will induces shift in the cosmological parameters inferred from the nonlocal model, given the data, as we will discuss in details in the next chapter.

RR Model

We now perform the same analysis in the framework of the RR model. In that case, one can compute the modified Poisson equation,

$$(1-3\gamma\bar{V})\hat{k}^2\Phi = \frac{3}{2h^2}\left[\Omega_R e^{-4x}\left(\delta_R + \frac{4}{\hat{k}^2}\hat{\theta}_R\right) + \Omega_M e^{-3x}\left(\delta_M + \frac{3}{\hat{k}^2}\hat{\theta}_M\right)\right] - \frac{3\gamma}{2}\Bigg[-(\hat{k}^2+6)\delta V - \frac{1}{2h^2}\bar{U}\delta U + \left(3\Psi - 3\Phi' - \Psi\bar{U}'\right)\bar{V}' + \frac{1}{2}\bar{U}'(\delta V' + 3\delta V) + \frac{1}{2}\bar{V}'(\delta U' + 3\delta U)\Bigg], \tag{4.147}$$

and one can read the effective Newton constant,

$$\frac{G_{\rm eff}(x,k)}{G} \equiv \frac{1}{1-3\gamma\bar{V}(x)}\left[1 - \frac{P(x,k)}{R(x,k)}\right], \tag{4.148}$$

where,

$$P(x,k) \equiv \frac{3\gamma}{2}\Bigg[-(\hat{k}^2+6)\delta V - \frac{1}{2h^2}\bar{U}\delta U + \left(3\Psi - 3\Phi' - \Psi\bar{U}'\right)\bar{V}' + \frac{1}{2}\bar{U}'(\delta V' + 3\delta V) + \frac{1}{2}\bar{V}'(\delta U' + 3\delta U)\Bigg], \tag{4.149}$$

$$R(x,k) \equiv \frac{3}{2h^2}\left[\Omega_R e^{-4x}\left(\delta_R + \frac{4}{\hat{k}^2}\hat{\theta}_R\right) + \Omega_M e^{-3x}\left(\delta_M + \frac{3}{\hat{k}^2}\hat{\theta}_M\right)\right]. \tag{4.150}$$

We show $G_{\rm eff}/G(z,k)$ into the right panel of Fig. 4.5 [4]. We see that the deviation with respect to ΛCDM is higher into this model, of the order of $\sim 6\%$. Moreover, in that case, the amplitude of $G_{\rm eff}$ *increases* with increasing values of k. This goes against the usually intuition that the model provides stronger deviations in the infrared. We find that $G_{\rm eff}$ saturates at the k values considered in Fig. 4.5, i.e. when k is increased (decreased) , the red (blue) curve remains the same. In particular, for increasing values of k, $G_{\rm eff}$ does not smoothly converge to G, as in the RT model (see left panel of the same figure). The reason for this is that, in the small scale limit $k \gg 1$, the effective Newton constant keeps a residual background dependence. This fact can be seen in considering the leading contribution in $\hat{k} = k/(aH)$, into Eqs. (4.120),(4.121), which lead to,

$$\delta U = 2(\Psi + 2\Phi)\,, \qquad \delta V = \mathcal{O}\left(\frac{1}{\hat{k}^2}\right)\Psi\,, \tag{4.151}$$

which yields,

$$\frac{G_{\rm eff}}{G}(x, k \gg 1) = \frac{1}{1-3\gamma\bar{V}(x)}\left[1 + \mathcal{O}\left(\frac{1}{\hat{k}^2}\right)\right]. \tag{4.152}$$

Lunar Laser Ranging Constraints. As mentioned in (Barreira et al., 2014b), when taken at face value, such a residual time-dependence is in conflict with Lunar Laser Ranging experiments (LLR), putting bounds on the time variation of the Newton constant, $\dot{G}_{\rm eff}/G = (4 \pm 9) \times 10^{-13}{\rm yr}^{-1}$ (Williams et al., 2004). The RR model with $u_0 = 0$ (see Sec. 4.2.3) in the present

4. This connects to the discussion about gravitational wave-source coupling addressed in Sec. 4.3.3

scenario predicts, $\dot{G}_{\rm eff}/G = 92 \times 10^{-13}{\rm yr}^{-1}$, and therefore would be ruled out by such a test. Nevertheless, LLR are performed on the Earth-Moon scale and it is not at all obvious that one can extrapolate the solution on the largest cosmological scales, down to galactic and solar system ones [5]. Note however that the RR model with $u_0 = 250$, potentially escapes this discrepancy as it is very close from a ΛCDM cosmology.

In Fig. 4.9, we show the gravitational slip η (left panel) and the anisotropic stress π in the RR model. Observe than η has the opposite sign as compared to the same quantity in the RT model. It also describes a larger anisotropic stress generated by the effective dark energy component (recall that for the matter content we are considering, the anisotropic stress vanishes). The behaviors of the deviation parameter $\Sigma(z,k)$, is shown in Fig. 4.8, while the

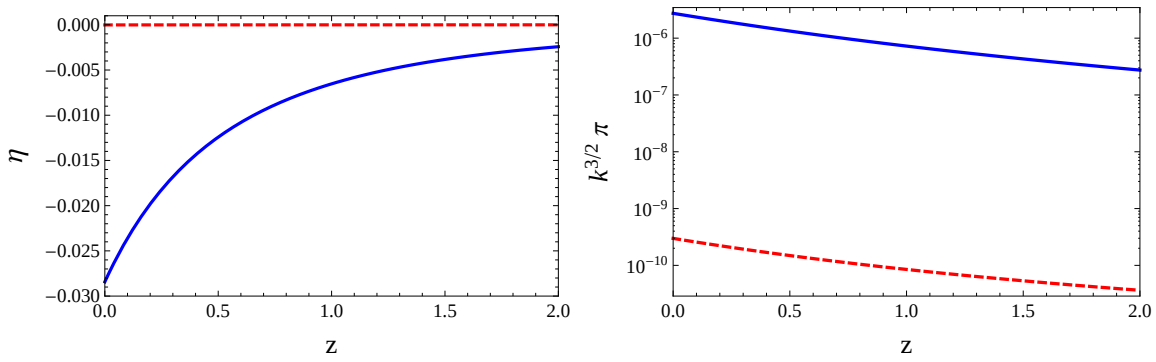

Figure 4.9 – Gravitational slip η (left panel) and the dimensionless anisotropic stress $k^{3/2}\pi$ (right panel) in the RT model. The blue solid lines correspond to $\kappa = 0.1$, the brown dot-dashed line to $\kappa = 1$, while the red dashed lines are for $\kappa = 5$. From (Dirian et al., 2014).

growth function $g(z,k)$ relative to that in ΛCDM and the deviation parameter μ are shown into the left and right panel of Fig. 4.10, respectively. We see that for these functions as well, the deviations with respect to GR are higher than in the RT model, of the order of $5-10\%$ level. All deviations induced by the RR model with respect to ΛCDM saturate as $k \gg 1$, except for the gravitational slip shown in the left panel of Fig. 4.9. This can be seen from the expression of the dark energy anisotropic stress that can be identified into Eq. (4.118).

In this section, we have introduced various useful functions for characterising deviations of modified gravity models with respect to ΛCDM. These show that the nonlocal models describe stable perturbations, and are therefore suitable for cosmological applications. In particular, we have seen that the RT model is close to ΛCDM at background and linear perturbation level, in that it presents overall deviations of percent level. As we will discuss in the next chapter, discriminating such a model from ΛCDM by using current data is difficult. However, future large scale structure surveys such as *Euclid* (Laureijs et al., 2011; Amendola et al., 2013), *SKA* (Dewdney et al., 2009; Yahya et al., 2015), *DESI* (Levi et al., 2013; DESI Collaboration et al., 2016a,b), are likely to be able to measure the aforementioned quantities (or slight variations of them) at percent level precision. Together with complementary data from SNIa and CMB observations, they prove to be able to put tight constraints of such small amplitude deviations

5. Work on this is in progress. It is interesting to observe that, in the case of scalar-tensor theories in which the scalar degree-of-freedom has a shift symmetry, it can happen that such a residual time-dependence does not decouple. In that case, the equations of motion for the scalar admit a separation of variable $\varphi(r,t) = \varphi(r) + \varphi(t)$, with $\dot{\varphi} \sim H(t)$, and the cosmological residual time dependence remains at small scales (Babichev et al., 2011). In the RR nonlocal model, however there is no such a shift symmetry and this argument therefore does not apply.

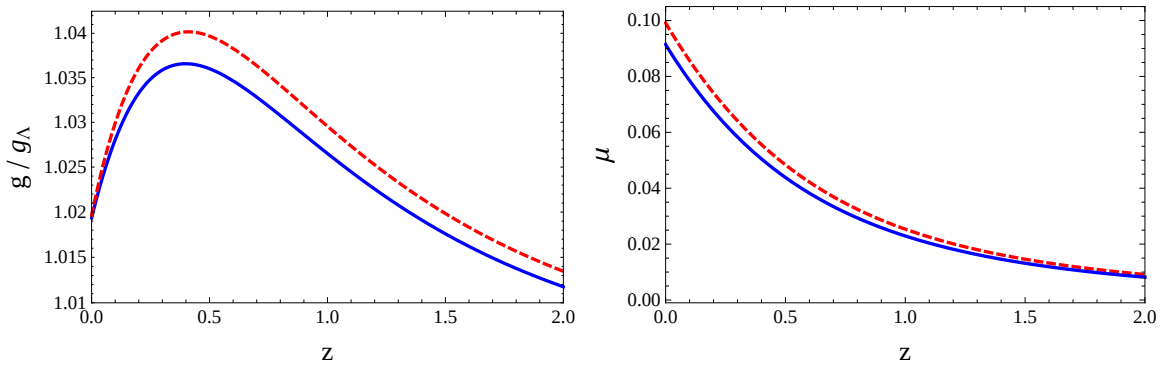

Figure 4.10 – Ratio of the growth function $g(z,k)$ with respect to the one in ΛCDM (left panel) and the deviation parameter μ (right panel) in the RR model. The blue solid lines correspond to $\kappa = 0.1$ while the red dashed lines are for $\kappa = 5$. From (Dirian et al., 2014).

from the ΛCDM scenario. In the case of the minimal RR model, i.e. where the initial data of the auxiliary fields are taken to be vanishing in RD, we have seen that such deviations were much larger, of the order of 5–10%, and could therefore be quite well constrained be presently available data. The RR model therefore also provides a good candidate for playing the role of a target model, used to develop the theoretical and methodological tools the aforementioned galaxy surveys are based on. In particular, it can be used for forecasting future constraints obtained from such surveys, and therefore for predicting to what extent the model can be distinguished from ΛCDM, given future data (Casas et al., 2018). Nevertheless, as we have seen, the RR model possesses a residual background dependence that generically makes its deviations with respect to ΛCDM finite and scale independent at small scales. In particular, it features a time dependence in the effective Newton constant $G_{\text{eff}}(x,k)$ at the present time which, interpreted at face value, is ruled out by constraint from LLR. However, such a residual background dependence originates from the choice of the FLRW expanding solution, supposedly not valid at solar system scales, where the latter experiments are realised. The question asking whether or not such background dependence decouples as one enters into virialised structures deserves further attention.

Before we turn to a more quantitative analysis aiming to constrain the RT and RR model with current, high-precision data in the next chapter, we provide some more details on the dark energy phenomenology described by the RT and RR models in a subsequent section.

4.4.2 Effective Dark Energy Perturbations

In Sect. 4.2, we have seen that, at the cosmological background level, the nonlocal corrections of the RT and RR models can be interpreted as an effective dark energy energy with density ρ_{de} and a equation of state $w_{\text{de}} = p_{\text{de}}/\rho_{\text{de}}$.

RT Model

The same effective fluid description can be applied to the linear perturbations induced by the nonlocal terms. Observing that the linearised Einstein equations Eqs. (4.92)-(4.95) can be recast

as,

$$\hat{k}^2\Phi + 3(\Phi' - \Psi) = \frac{4\pi G}{H^2}\sum_i \delta\rho_i, \tag{4.153}$$

$$\hat{k}^2\big(\Phi' - \Psi\big) = -\frac{4\pi G}{H^2}\sum_i \bar{\rho}_i(1+w_i)\hat{\theta}_i, \tag{4.154}$$

$$\hat{k}^2(\Psi + \Phi) = \frac{12\pi G e^{2x}}{H^2}\bar{\rho}_{\rm DE}(1+w_{\rm DE})\sigma_{\rm DE}, \tag{4.155}$$

$$\Phi'' + (3+\zeta)\Phi' - \Psi' - (3+2\zeta)\Psi + \frac{\hat{k}^2}{3}(\Phi+\Psi) = -\frac{4\pi G}{H^2}\sum_i \delta p_i\,, \tag{4.156}$$

where the sums over i run over radiation, matter and dark energy, one can extract,

$$\delta\rho_{\rm de} \equiv \gamma\rho_0\big(\delta X - h\delta V_0' + 2h\Psi\bar{V}_0' + h\bar{V}_0\Psi'\big)\,, \tag{4.157}$$

$$\Omega_{\rm de}(1+w_{\rm de})\hat{\theta}_{\rm de} \equiv \hat{k}^2\gamma\left(h^2\delta Z - \frac{h^2}{2}\delta Z' + h\Psi\bar{V}_0 - \frac{h}{2}\delta V_0\right), \tag{4.158}$$

$$\Omega_{\rm de}(1+w_{\rm de})\sigma_{\rm de} \equiv \frac{2}{3}\hat{k}^2\gamma e^{-2x}h^2\delta Z\,, \tag{4.159}$$

$$\delta p_{\rm de} \equiv -\gamma\rho_0\left(\delta X - h(\Phi' - 2\Psi)\bar{V}_0 - h\delta V_0 - \frac{\hat{k}^2}{3}h^2\delta Z\right), \tag{4.160}$$

which are respectively the density perturbation, peculiar velocity divergence, anisotropic stress and pressure perturbation of the effective dark energy fluid. The equation of state $w_{\rm de}$ is defined into Eq. (4.35). We can also define the dark energy density contrast and the effective sound speed for the dark energy perturbations [6],

$$\delta_{\rm de} \equiv \frac{\delta\rho_{\rm de}}{\bar{\rho}_{\rm de}}\,, \qquad \hat{c}^2_{s,{\rm de}}(x) \equiv \frac{\delta p_{\rm de}(x)}{\delta\rho_{\rm de}(x)}\,. \tag{4.161}$$

In the left panel of Fig 4.11, we show the dark energy density constrast $\delta_{\rm de}$ (red dashed line) as compared to that of matter δ_M at large scales ($\kappa = 0.1$), while the right panel shows the same quantities at small scales ($\kappa = 5$). We see from these plots that the RT model (similarly to the RR model, see below) describes a *clustering* effective dark energy, which is generically the case when $w_{\rm de}(z) \neq -1$. We see that the dark energy density perturbation is negligible compared to the one of dust matter. In Fig. 4.12, we show the velocity divergence for the effective dark energy (left panel) as compared to the one of matter (right panel). Here also, the perturbation associated to the nonlocal models are negligible compared to those of CDM.
In Fig. 4.13, we show its anisotropic stress (left panel) and its speed of sound (right panel). Observe that the sound speed is very high at large scales, and could therefore share common features with theories describing a dark energy with infinite sound speed (Afshordi et al., 2007a,b). as discussed into the latter references., an infinite speed of sound does not always imply a loss of causality. This can also be understood for the structure of the RT model, where causality is imposed at the level of the equations of motion by taking the nonlocal operators (Green's functions) to be of the retarded kind.

6. We use a hat here to stress that this is not the usual rest-frame speed of sound. In any way, for large $\hat{k}$ the difference between the two definitions vanishes as can be seen form Eq. (4.74).

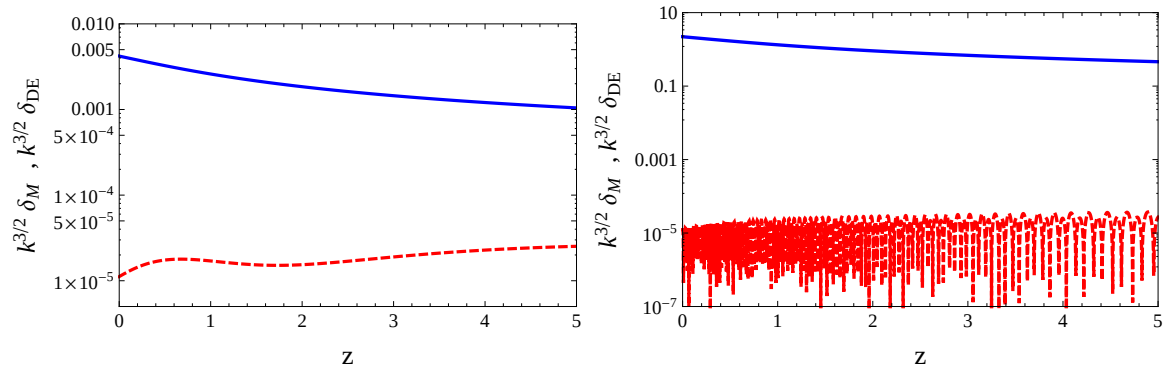

Figure 4.11 – Left panel: Dimensionless density contrast of dark energy $k^{3/2}\delta_{\rm de}(z)$ (red dashed line) compared to the one of matter $k^{3/2}\delta_M$ (blue solid line) in the RT model for $\kappa = 0.1$. Right panel: The same as for the left panel but for $\kappa = 5$. Inspired from (Dirian et al., 2014).

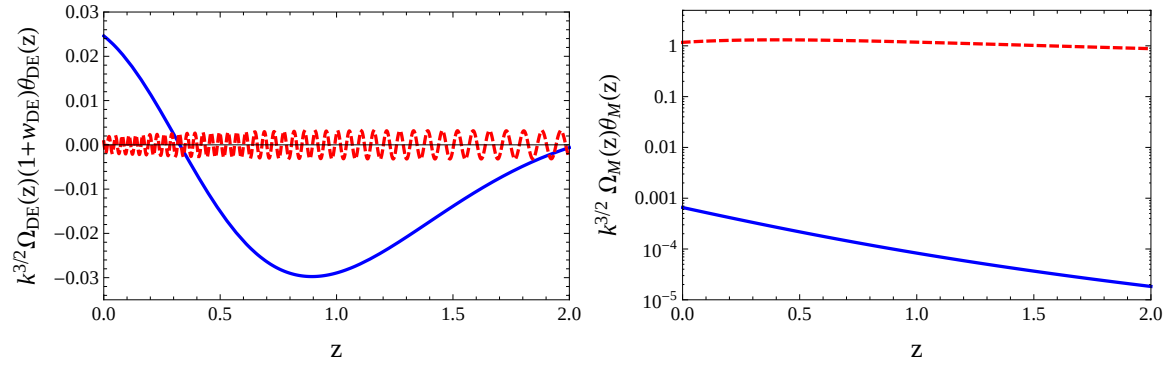

Figure 4.12 – Left panel: Dimensionless dark energy velocity divergence $k^{3/2}\Omega_{\rm de}(1+w_{\rm de})\hat{\theta}_{\rm de}(z)$ for $\kappa = 0.1$ (blue solid line) and $\kappa = 5$ (red dashed line). Right panel: Dimensionless velocity divergence of dust matter $k^{3/2}\Omega_M\hat{\theta}_M(z)$ for $\kappa = 0.1$ (blue solid line) and $\kappa = 5$ (red dashed line). Inspired from (Dirian et al., 2014).

RR Model

In repeating the same steps as outlined above, one can find the effective dark energy perturbation quantities for the RR model,

$$\delta\rho_{\rm de} \equiv \rho_0\gamma h^2\Big[2\bar{V}\left(\hat{k}^2\Phi + 3\left(\Phi' - \Psi\right)\right) + \frac{1}{2h^2}\bar{U}\delta U - \left(6\Psi - 3\Phi' - \Psi\bar{U}'\right)\bar{V}' - \frac{1}{2}\left(\bar{U}'\delta V' + \bar{V}'\delta U'\right) + 3\delta V + 3\delta V' + \hat{k}^2\delta V\Big], \quad (4.162)$$

$$\Omega_{\rm de}\left(1+w_{\rm de}\right)\hat{\theta}_{\rm de} \equiv -\gamma h^2\hat{k}^2\left[2\bar{V}(\Phi' - \Psi) + \delta V' - \bar{V}'\Psi - \delta V + \frac{1}{2}\left(\bar{U}'\delta V + \bar{V}'\delta U\right)\right], \quad (4.163)$$

$$\Omega_{\rm de}(1+w_{\rm de})\sigma_{\rm de} \equiv \frac{2}{3}h^2\hat{k}^2\gamma e^{-2x}\left[\bar{V}\left(\Phi + \Psi\right) + \delta V\right], \quad (4.164)$$

$$\delta p_{\rm de} \equiv -\rho_0\gamma h^2\Big[2\bar{V}\left(\Phi'' + (3+\zeta)\Phi' - \Psi' - (3+2\zeta)\Psi + \frac{\hat{k}^2}{3}(\Phi + \Psi)\right) + \frac{1}{2h^2}\bar{U}\delta U - 2\Psi\bar{V}'' + \left(2\Phi' - 2(2+\zeta)\Psi - \Psi' - \Psi\bar{U}'\right)\bar{V}' + \delta V'' + (2+\zeta)\delta V' + \frac{2\hat{k}^2}{3}\delta V + (3+2\zeta)\delta V + \frac{1}{2}\left(\bar{U}'\delta V' + \bar{V}'\delta U'\right)\Big]. \quad (4.165)$$

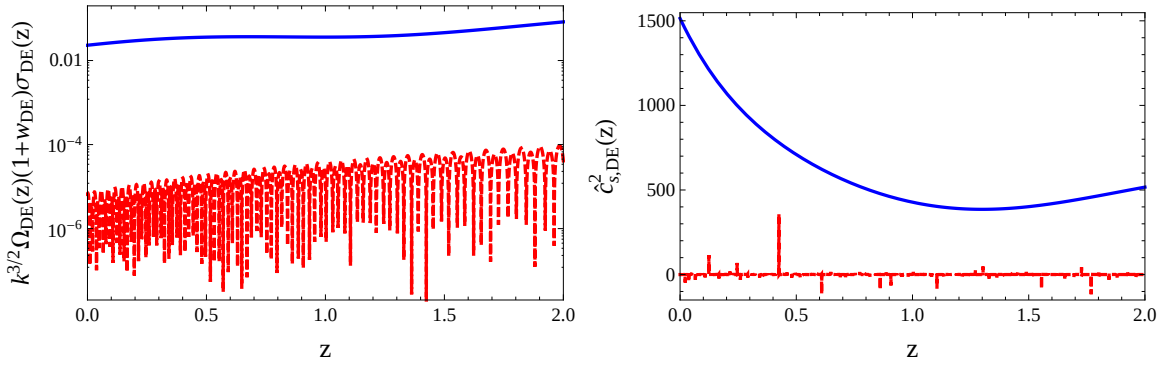

Figure 4.13 – Left panel: Dimensionless anisotropic stress of dark energy $k^{3/2}\Omega_{\rm de}(1+w_{\rm de})\sigma_{\rm de}(z)$ for $\kappa = 0.1$ (blue solid line) and $\kappa = 5$ (red dashed line), in the RT model for $\kappa = 5$. Right panel: The speed of sound $\hat{c}^2_{\rm s,de}(z)$ for $\kappa = 0.1$ (blue solid line) and $\kappa = 5$ (red dashed line). Inspired from (Dirian et al., 2014).

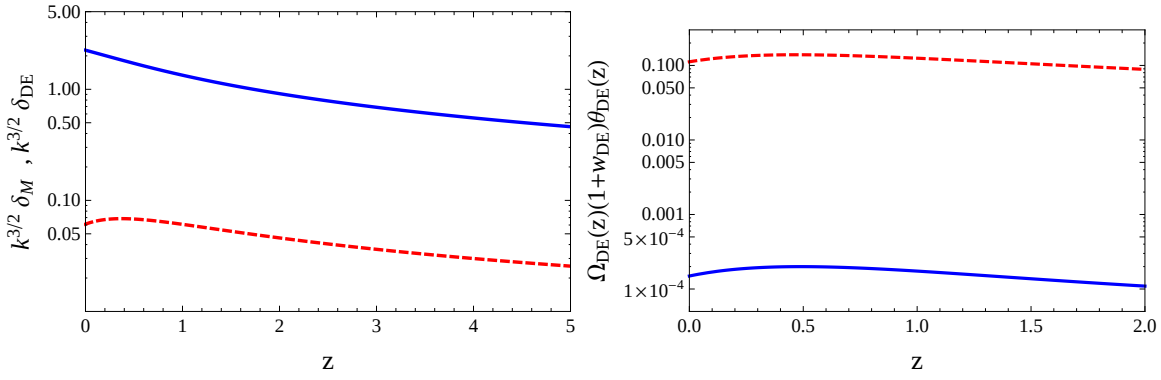

Figure 4.14 – Left panel: Dimensionless density contrast of dark energy $k^{3/2}\delta_{\rm de}(z)$ (red dashed line) compared to the one of matter $k^{3/2}\delta_M(z)$ (blue solid line) in the RR model for $\kappa = 5$. Right panel: The dimensionless velocity divergence $k^{3/2}\Omega_{\rm de}(1+w_{\rm de})\hat{\theta}_{\rm de}(z)$ for $\kappa = 0.1$ (blue solid line) and $\kappa = 5$ (red dashed line). Inspired from (Dirian et al., 2014).

We show the effective dark energy dimensionless density contrast (left panel) and velocity divergence (right panel) in Fig. 4.14. We see that, compared to the same quantities in the RT model (see Figs. 4.11,4.12), the dark energy density contrast is higher in RR, but still remains negligible compared to that of matter. Observe that the velocity divergence acquires higher values as one decreases the scale, and is however negligible compared to that of matter [7]. This is not the case for the anisotropic stress shown into the left panel of Fig. 4.15, which tends to smaller values as the scale is lowered. Observe also from the right panel of the same figure that the effective dark energy for the RR model has a negative sound speed at large scales.
As the dark energy is clustering, is also interesting to plot the power spectrum of dark energy

7. This can be seen in comparing the latter with the matter velocity divergence in the RT model shown the right panel of Fig. 4.12, which is of the same order as the one found in RR.

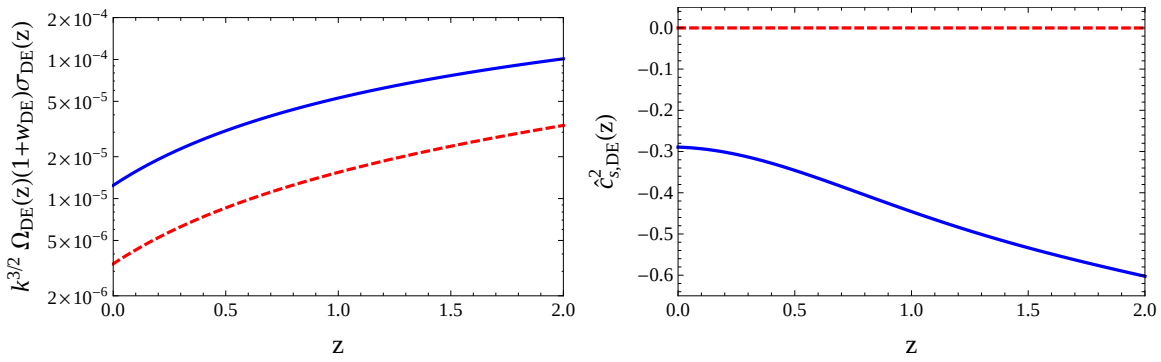

Figure 4.15 – Left panel: Dimensionless anisotropic stress of dark energy $k^{3/2}\Omega_{\rm de}(1+w_{\rm de})\sigma_{\rm de}(z)$ for $\kappa = 0.1$ (blue solid line) and $\kappa = 5$ (red dashed line), in the RR model for $\kappa = 5$. Right panel: The speed of sound $\hat{c}^2_{\rm s,de}(z)$ for $\kappa = 0.1$ (blue solid line) and $\kappa = 5$ (red dashed line). Inspired from (Dirian et al., 2014).

density perturbations at $z = 0$,

$$P_{\rm de}(k) = (2\pi)^3\langle|\delta^\star_{\rm de}(k)|^2\rangle\,, \tag{4.166}$$

where the * denotes the gauge invariant quantity (4.71). The power spectrum in the RR model is shown is shown in Fig. 4.16 where it can be compared with the one of matter. In particular, we see that the dark energy density perturbations exhibit the same scale dependence as the matter perturbations.

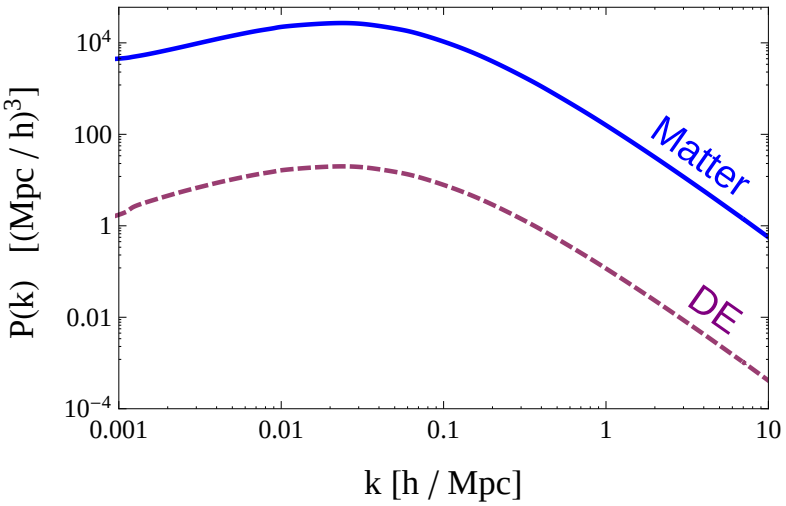

Figure 4.16 – The dimensionless power spectrum for dark energy (purple dashed line) compared to the one of dust matter (blue solid line) at present time $z = 0$. From (Dirian et al., 2014).

This section reviews the dynamical dark energy phenomenology induced by the RT and RR nonlocal modified gravity models. In particular, we have seen that the density and velocity divergence perturbations associated to the dark energy are negligible as compared to the ones

of matter, and that both feature a small anisotropic stress. In that sense, we can conclude that the effective dark energies described by both models is quite *smooth*, i.e. that its most relevant modifications to GR are found at the background level.

Summary

In this chapter, we have presented the phenomenology of the nonlocal RT and RR models in the cosmological context.

In Sec. 4.2, we have seen that the RT (4.1) and RR (4.2), nonlocal modified gravity models provide a phase of accelerated expansion at late time, without the need of a cosmological constant Λ. In particular, we have shown that such an acceleration is caused by an effective *dynamical* dark energy component, i.e. with time-dependent density $\bar{\rho}_{\rm de} \equiv \bar{\rho}_{\rm de}(z)$ and equation of state $w_{\rm de}(z) \neq -1$, whose density fraction is fixed in tuning the mass parameter m appearing in both models, so as to close the Universe at the present time. A dynamical dark energy component generically implies that it is also *clustering*, that is, it features non-trivial linear cosmological perturbations. Furthermore, we have seen that the effective dark energy component described by both models is on the *phantom* side, i.e. $w_{\rm de}(z) < -1$ (Maggiore, 2014; Maggiore and Mancarella, 2014). As also discussed, this generically leads to a lower dark energy density fraction $\Omega_{\rm de}(z)$ at late time, and therefore to a lower expansion rate $H(z)$, as compared to the one in the standard ΛCDM model, for the same fiducial cosmology. For the equation of state today, as the RR model predicts $w^0_{\rm de} \simeq -1.15$, while the RT model gives $w^0_{\rm de} \simeq -1.04$, the late time expansion rate in the former is therefore pushed to lower values than in the latter (see Fig. 4.1). These overall deviations are of the order of a few percents, so their background phenomenology is quite close from the one of ΛCDM.

In Sec. 4.3, following (Dirian et al., 2014), we have studied the linear cosmological perturbations in the scalar and tensor sectors for both nonlocal models and shown that the perturbations in both models are stable into their respective scalar and tensor sectors. In particular, we saw that their linear tensor perturbations propagate at the speed of light, which implies that both models are compatible with the recent observation of GWs from a BNS merger, together with its optical counterpart. In addition, both models feature a modification of the Hubble friction term in their linear tensor evolution equation, that involves a lower damping of the GWs amplitude they describe at late time. As we will discuss in Sec. 6, this can have profound implications for observational constraints purposes. We then turned to the analysis of the linear scalar perturbations described by both nonlocal models, in particular by using useful indicators such as the μ, η, Σ parameters (see Sec. 4.4.1), at fixed cosmological parameter values. We have seen that both models display percents-level deviations with respect to ΛCDM, in particular showing that they describe an enhanced growth and lensing power, together with the presence of an additional anisotropic stress component (slip) associated to their respective effective dark energies. We have also seen that the linear perturbations associated with these effective dark energies are small with respect to that of non-relativistic matter, which means that the effective dark energy components in both models is quite smooth.

This shows that the nonlocal models provide good candidates for been constrained with present and future cosmological data. Consequently, we now turn to the review of such observational constraints, where the models were implemented into a modification of the linear Einstein-Boltzmann CLASS for being able to provide more realistic cosmological predictions. Moreover, the models will also be compared to the ΛCDM one, as well as an extension of it, within a Bayesian framework.

Chapter 5

Observational Contraints and Bayesian Model Comparison

In this chapter, we review the results of works of (Dirian et al., 2015, 2016; Dirian, 2017) [1], where observational constraints and Bayesian model comparison between nonlocal and ΛCDM cosmologies were carried out. For doing so, both model have been implemented in a modified version of the linear Einstein-Boltzmann solver CLASS (Blas et al., 2011), and cosmological parameter inference was performed with the Markov Chain Monte Carlo (MCMC) code Montepython (Audren et al., 2013), interfaced with CLASS. An explanatory of the implementation is provided in App. A together with the corresponding equations. The code itself is publicly available on GitHuB (URL) and, in the case of the RR model, has been compared against a modified version [2] of CAMB (Lewis), in the modified Einstein-Boltzmann code comparison program of (Bellini et al., 2018). In the latter work, both codes were shown to agree at subpercent level in CMB and matter power spectra.

In Sec. 5, we first present the data that we use into the subsequent analysis. We then specify the cosmological framework considered for embedding the nonlocal gravity models into cosmological statistical ones, and show the results drawn from observational constraints, that is, their cosmological parameters inference and their performance when compared to the standard ΛCDM model. We provide a comprehensive analysis of the deviations observed in parameter inference when going from ΛCDM to the nonlocal models, and present the relevant structural features for understanding these deviations. We will then perform Bayesian model selection by using the Savage-Dickey density ratio method in Sec. 5.2, before we confront the models to growth rate data in Sec. 5.3. We will see that an eventual tension into the RR nonlocal model appears when constrained with CMB+BAO+SNIa data, and we subsequently find a way for it to be resolved in Sec. 5.5. We will see that extending the initial baseline by allowing the absolute neutrino mass to vary into the fit resolves this discrepancy and makes the nonlocal model statistically equivalent to ΛCDM. In particular, we show that such an extension leads to an interesting constraint on the absolute neutrino mass given the RR model, which is preferred by growth rate data as well, as compared to the case where the mass is fixed to its initial baseline value.

1. See also the earlier analysis of (Nesseris and Tsujikawa, 2014), where the RT model was constrained and compared to ΛCDM given CMB, SNIa, BAO and growth rate data, different from those described below. However, into this reference, the observational constraints were carried out by using the so-called CMB shift parameters [see e.g. (Shafer and Huterer, 2014)], which are less robust under cosmology change compared to the ones inferred from the CMB spectra themselves.

2. This version is not publicly available, but can been obtained on request (Barreira).

5.1 Observational Constraints

We consider three cosmological models made of the nonlocal RT and RR modified gravity, and standard ΛCDM. We perform cosmological parameter estimation through Bayesian parameter inference given current, high precision complementary cosmological data. We start by presenting the data and provide details about the parametrisation used into the models. We then present our results and corresponding goodness-of-fit, before comparing them within a Bayesian framework.

5.1.1 Datasets

The main datasets considered throughout the analysis are the same as the ones used in the *Planck* 2015 analysis, in particular in (Ade et al., 2015d) for constraining the base ΛCDM model, and in (Ade et al., 2015e) for constraining various effective dark energy parametrisations. This choice has been made so as to consider the most conservative data up to date at the time, where the systematic uncertainties are mostly under control. For completeness, we review them briefly in this section, referring the reader to the original papers for more detailed explanations.

CMB. We consider the likelihoods given in the recent *Planck* 2015 analysis (Adam et al., 2015) from measurements of the angular (cross-)power spectra of the CMB [3]. In particular, we take the (full-mission) lowTEB data for low multipoles ($\ell \leq 29$) and the high-ℓ Plik TT,TE,EE (cross-half-mission) ones for the high multipoles ($\ell > 29$) of the temperature and polarization auto- and cross- power spectra (Ade et al., 2015e; Planck Wiki, 2015).

Furthermore, since the nonlocal models describe dynamical and clustering dark energies that emerge at late time (see Secs 4.2, 4.3), we also include the temperature +polarization (T+P) lensing data (where only the conservative multipole range $\ell = 40 - 400$ is used), that provide CMB constraints on late time cosmology, and more generically allow one to break degeneracies in the primary CMB anisotropies (Aghanim et al., 2016c; Ade et al., 2015f).

In addition to CMB data, following the *Planck* analysis (Ade et al., 2015d,e), we also include datasets from astrophysical measurements in a complementary perspective, i.e. so as to break further CMB degeneracies and reach tighter constraints on the parameter space. In particular, we consider the following datasets.

Type Ia Supernovae. Observations of distant SNIa provide powerful constraints on the cosmological parameters, in particular independent from the ones inferred from CMB and BAO data. They provide an estimate of the distance-redshift relation that can be represented by the Hubble diagram Fig. 1.3. Essentially, it is the measurement of the SNIa's redshift, obtained by spectroscopic analysis of the light of the SNIa itself or of its host galaxy, and of its apparent rest frame B-band peak magnitude $m_B^\star$, that allows one to access this relation via e.g.,

$$m_B^\star = 5\log_{10}\left(\frac{d_L}{10\text{Mpc}}\right) + \left(M_B - \alpha \times X_1 + \beta \times C\right), \tag{5.1}$$

where $d_L \equiv H_0 D_L$ is the Hubble free luminosity distance, M_B, α, β are nuisance parameters fitted simultaneously with the data and X_1, C are the stretch and colour measures respectively which, together with $m_B^\star$, are estimated from fitting SNIa spectral sequence models to specific

3. CMB data from the *Planck* 2013 nominal mission temperature data (Ade et al., 2014c) were used instead in (Dirian et al., 2015).

photometric data [see e.g. (Amanullah et al., 2010; Betoule et al., 2014) and references therein]. The parameter M_B depends on the absolute magnitude of the SNIa and on the Hubble constant H_0, so distant SNIa do not provide any constraints on the latter. We consider the data of the *SDSS-II/SNLS3* Joint Light-curve Analysis (JLA) (Betoule et al., 2014), using the complete (non-compressed) corresponding likelihoods. Combining these with the ones obtained from the *Planck* data allows to put an independent constraint on the matter density fraction Ω_M, and breaks the geometric CMB degeneracy in the H_0–Ω_M plane. This proves to be particularly useful in constraining the nonlocal models, as we will see in more details below.

Baryon Acoustic Oscillations. As discussed in detail in Sec. 4.2, the RR and RT nonlocal models have a phantom dark energy equation of state, $w_{\rm de}(z) < -1$ for $z \geq 0$. Thus, the history of the growth of structures in the late universe is modified compared to a ΛCDM scenario. To further test this feature, it is useful to build a distance ladder by using different BAO scale measurements. As datasets, we consider the isotropic constraints provided by *6dFGS* at $z_{\rm eff} = 0.106$ (Beutler et al., 2011), *SDSS-MGS DR7* at $z_{\rm eff} = 0.15$ (Ross et al., 2015) and *BOSS LOWZ* at $z_{\rm eff} = 0.32$ (Anderson et al., 2014). These data provide measurements of the low redshift acoustic-scale distance ratio $D_{\rm V}(z_{\rm eff})/r_{\rm d}$, where,

$$D_V(z) \equiv \left[z(1+z)^2 \frac{D_A(z)^2}{H(z)} \right]^{1/3}, \tag{5.2}$$

is the spatially-averaged dilation factor with $D_A(z)$, the angular diameter distance defined into Sec. 4.2.1 and $r_{\rm d}$ is the sound horizon at the drag epoch which can be obtained from Eq. (5.7), evaluated at the drag redshift $z_{\rm d}$ instead of the recombination one z_*. We also include the anisotropic constraints from *CMASS* at $z_{\rm eff} = 0.57$ (Anderson et al., 2014). Anisotropic constraints separate the clustering effects into their longitudinal and transverse component relative to the line-of-sight. This allows one to put separate constraints on the ratios $H(z_{\rm eff})/r_{\rm d}$ and $D_{\rm A}(z_{\rm eff})/r_{\rm d}$, and breaks the degeneracy in the $D_{\rm A}$-H plane which arises in isotropic constraints.

We will perform several analyses including different combinations of these datasets. First we will constrain the models given the *Planck* 2015 likelihoods only, second we will join to them the ones of *JLA* and BAO, and finally we will further add two different priors on H_0 provided by different local observations.

H_0 prior. The values of H_0 we will consider are $H_0 = 70.6 \pm 3.3$ km s^{-1}Mpc^{-1} (Efstathiou, 2014) and $H_0 = 73.8 \pm 2.4$ km s^{-1}Mpc^{-1} (Riess et al., 2011). In particular, we will use the value $H_0 = 73.8 \pm 2.4$ km s^{-1}Mpc^{-1}, as an example of the impact of a high value of H_0. More recent analysis of local measurements have been done since then, and give $H_0 = 73.02 \pm 1.79$ km s^{-1}Mpc^{-1} (Riess et al., 2016) and 73.48 ± 1.66 km s^{-1}Mpc^{-1} (Riess et al., 2018). The latter measurement features a tension with the *Planck* ΛCDM value of H_0 found in (Aghanim et al., 2016b), at 3.7σ, while the data used in the former have been re-analysed by using Bayesian hyper-parameters, leading to $H_0 = 73.75 \pm 2.11$ km s^{-1}Mpc^{-1}, and exhibiting a tension with *Planck* ΛCDM at 3.1σ (Cardona et al., 2017) [see also Sec. 1.3.8 for more details].

Redshift-Space Distortions. Finally, we will also dedicate a section where we compare the three models using $f\sigma_8$ growth rate data obtained from Redshift-Space Distortions (RSD) measurements. The measurements used are those collected from *6dF GRS* (Beutler et al., 2012) at $f\sigma_8(0.067) = 0.423 \pm 0.055$, *SDSS LRG* (Oka et al., 2014) at $f\sigma_8(0.3) = 0.49 \pm 0.08$

, *SDSS MGS* (Howlett et al., 2014) at $f\sigma_8(0.15) = 0.63^{+0.027}_{-0.24}$, *BOSS LOWZ* (Chuang et al., 2016) at $f\sigma_8(0.32) = 0.371 \pm 0.091$, *BOSS CMASS* (Samushia et al., 2014) at $f\sigma_8(0.57) = 0.441 \pm 0.0434$ [4], *WiggleZ* (Blake et al., 2012) at $f\sigma_8(0.44) = 0.413 \pm 0.08$, $f\sigma_8(0.6) = 0.39 \pm 0.063$, $f\sigma_8(0.73) = 0.437 \pm 0.072$) and *VIPERS* (de la Torre et al., 2013) at $f\sigma_8(0.8) = 0.47 \pm 0.08$. Such a constraint will be done *a posteriori*, that is, $f\sigma_8$ data are fitted within each model, once the normalisation of the power spectrum is fixed to its respective CMB+SNIa+BAO bestfit obtained a priori.

5.1.2 Parameter Space and MCMC

The datasets outlined above will be used for constraining the three statistical models that for definiteness we denote by $\mathcal{M}_\Lambda$, $\mathcal{M}_{\rm RT}$ and $\mathcal{M}_{\rm RR}$ and are associated to their respective cosmological models. For the consistency of our analysis, the initial conditions (inflationary scenario), ionization history and matter content of the universe will be chosen following the *Planck* baseline (Ade et al., 2014d, 2015d). In each of the nonlocal models we have a parameter, m^2, that replaces the cosmological constant in ΛCDM, so the nonlocal models have the same number of parameters as ΛCDM. Furthermore, in the spatially flat case that we are considering, in ΛCDM the dark energy density fraction Ω_Λ can be taken as a derived parameter, fixed in terms of the other parameters by the flatness condition. Similarly, in the nonlocal models m^2 can be taken as a derived parameter, fixed again by the flatness condition. Thus, not only the nonlocal models have the same number of parameters as ΛCDM, but in fact these can be chosen so that the independent parameters are exactly the same in the nonlocal models and in ΛCDM, which facilitates the comparison.

For the neutrino content will use the same values used in the *Planck* 2015 baseline analysis (Ade et al., 2015d), i.e. a massless component and a massive one with mass M_ν. The prior on the latter is set to,

$$P(M_\nu|\Lambda\text{CDM}) = \delta(M_\nu/\text{eV} - 0.06)\,, \tag{5.3}$$

which corresponds to the lower bound set by oscillations experiments under the assumption of a normal mass hierarchy (see Sec. 5.5.6 for more details), and its temperature is tuned for reproducing predictions from neutrino decoupling computations (Mangano et al., 2005). We then fixe the effective number of massless neutrino species so as to reproduce a total effective number of relativistic components of $N_{\rm eff} = 3.046$ in the early Universe [see e.g. (Lesgourgues and Pastor, 2006)].

As independent cosmological parameters, we take the Hubble parameter today H_0, the physical baryon and cold dark matter density fractions today $\omega_b = \Omega_b h^2$ and $\omega_c = \Omega_c h^2$, respectively, the amplitude A_s of primordial scalar perturbations, the spectral tilt n_s and the reionization optical depth $\tau_{\rm re}$, so we have a continuous 6-dimensional parameter space. We choose improper flat priors on all these parameters, except for $\tau_{\rm re}$ which is taken to be bounded from below at the value of 0.01, in accordance with Gunn-Peterson trough observations [see e.g. (Becker et al., 2001)]. The corresponding vector in the base model parameter space is therefore given by,

$$\theta_{\rm base} = \big(H_0,\, \omega_b,\, \omega_c,\, \ln(10^{10}A_s),\, n_s,\, \tau_{\rm re}\big)\,. \tag{5.4}$$

This parameter space will be explored via a Metropolis-Hasting sampling algorithm. Our construction of the MCMC proceeds in two steps. The first consists in constructing a chain using

4. Replacing the latter *BOSS* data by the more recent results of (Alam et al., 2016) does not significantly affect the statistical conclusions drawn in our analyses.

wide Gaussian proposal distributions, which for all three models is taken to be centered initially on the *Planck* best fit values obtained for ΛCDM. The posterior distribution obtained then provides a new proposal distribution (covariance matrix) for a second run, where we restart from the best-fit points of the latter posterior such that the burn-in is avoided. In order to get reliable results and well shaped final distributions, we constructed several (in general 3–7) chains of 2×10^5 trials each and adjusted the jumping factor so as to get an acceptance rate $0.2 < r < 0.4$. The convergence of the set of chains is checked through a Gelman-Rubin convergence diagnostic. The best-fit points for each distribution are then refined by starting from the best-fit values of the (final) global run, and constructing a "cold" chain, i.e. a chain controlled by a constant temperature parameter T introduced into the MCMC acceptance probability as,

$$\alpha(\theta_n, \theta_{n+1}) = \min\left\{1, \left(\frac{P(\theta_{n+1})}{P(\theta_n)}\right)^{1/T}\right\}, \tag{5.5}$$

where θ_n is the n-th point sampled in parameter space and $P(\theta_n)$ its likelihood. Therefore the lower T is, the stronger the chain will converge towards the nearest maximum of the likelihood distribution [5]. In our analysis we choose $T = 0.02$, [6].

5.1.3 Results

	Planck			BAO+*Planck*+*JLA*		
Param	ΛCDM	RT	RR	ΛCDM	RT	RR
$100\ \omega_b$	$2.225^{+0.016}_{-0.016}$	$2.224^{+0.016}_{-0.016}$	$2.227^{+0.016}_{-0.016}$	$2.228^{+0.014}_{-0.015}$	$2.223^{+0.014}_{-0.014}$	$2.213^{+0.014}_{-0.014}$
ω_c	$0.1194^{+0.0014}_{-0.0015}$	$0.1195^{+0.0014}_{-0.0015}$	$0.1191^{+0.0014}_{-0.0015}$	$0.119^{+0.0011}_{-0.0011}$	$0.1197^{+0.0011}_{-0.00096}$	$0.121^{+0.001}_{-0.001}$
H_0	$67.5^{+0.65}_{-0.66}$	$68.86^{+0.69}_{-0.7}$	$71.51^{+0.81}_{-0.84}$	$67.67^{+0.47}_{-0.5}$	$68.76^{+0.46}_{-0.51}$	$70.44^{+0.56}_{-0.56}$
$\ln(10^{10}A_s)$	$3.064^{+0.025}_{-0.025}$	$3.057^{+0.026}_{-0.026}$	$3.047^{+0.026}_{-0.025}$	$3.066^{+0.019}_{-0.026}$	$3.056^{+0.021}_{-0.023}$	$3.027^{+0.027}_{-0.023}$
n_s	$0.9647^{+0.0048}_{-0.0049}$	$0.9643^{+0.0049}_{-0.005}$	$0.9649^{+0.0049}_{-0.0049}$	$0.9656^{+0.0041}_{-0.0043}$	$0.9637^{+0.0039}_{-0.0041}$	$0.9601^{+0.004}_{-0.0039}$
$\tau_{\rm re}$	$0.0653^{+0.014}_{-0.014}$	$0.06221^{+0.014}_{-0.014}$	$0.05733^{+0.014}_{-0.014}$	$0.06678^{+0.011}_{-0.013}$	$0.0611^{+0.011}_{-0.013}$	$0.04516^{+0.014}_{-0.012}$
$z_{\rm re}$	$8.752^{+1.4}_{-1.2}$	$8.442^{+1.5}_{-1.2}$	$7.932^{+1.5}_{-1.2}$	$8.893^{+1.1}_{-1.2}$	$8.359^{+1.2}_{-1.2}$	$6.707^{+1.7}_{-1.2}$
σ_8	$0.8171^{+0.0089}_{-0.0089}$	$0.8283^{+0.0092}_{-0.0096}$	$0.8487^{+0.0097}_{-0.0096}$	$0.817^{+0.0076}_{-0.0095}$	$0.8283^{+0.0085}_{-0.0093}$	$0.8443^{+0.01}_{-0.0099}$
$\chi^2_{\rm min}$	12943.3	12943.1	12941.7	13631.0	13631.6	13637.0
$\Delta\chi^2_{\rm min}$	1.6	1.4	0	0	0.6	6.0

	BAO+*Planck*+*JLA*+($H_0 = 70.6$)			BAO+*Planck*+*JLA*+($H_0 = 73.8$)		
Param	ΛCDM	RT	RR	ΛCDM	RT	RR
$100\ \omega_b$	$2.229^{+0.014}_{-0.015}$	$2.223^{+0.014}_{-0.014}$	$2.215^{+0.014}_{-0.014}$	$2.233^{+0.014}_{-0.014}$	$2.226^{+0.014}_{-0.014}$	$2.217^{+0.014}_{-0.014}$
ω_c	$0.1188^{+0.001}_{-0.0011}$	$0.1197^{+0.001}_{-0.0011}$	$0.1208^{+0.00099}_{-0.001}$	$0.1185^{+0.00097}_{-0.0011}$	$0.1194^{+0.001}_{-0.001}$	$0.1207^{+0.00096}_{-0.00097}$
H_0	$67.75^{+0.48}_{-0.47}$	$68.75^{+0.49}_{-0.48}$	$70.57^{+0.54}_{-0.56}$	$67.93^{+0.48}_{-0.43}$	$68.91^{+0.49}_{-0.5}$	$70.65^{+0.52}_{-0.54}$
$\log(10^{10}A_s)$	$3.069^{+0.024}_{-0.024}$	$3.056^{+0.026}_{-0.022}$	$3.03^{+0.021}_{-0.021}$	$3.077^{+0.026}_{-0.019}$	$3.061^{+0.026}_{-0.022}$	$3.031^{+0.018}_{-0.022}$
n_s	$0.9662^{+0.0042}_{-0.0042}$	$0.9637^{+0.0041}_{-0.0042}$	$0.9607^{+0.0039}_{-0.0041}$	$0.9671^{+0.0041}_{-0.0041}$	$0.9645^{+0.004}_{-0.0041}$	$0.9611^{+0.0038}_{-0.004}$
$\tau_{\rm re}$	$0.06883^{+0.012}_{-0.013}$	$0.06099^{+0.014}_{-0.011}$	$0.04701^{+0.011}_{-0.011}$	$0.07275^{+0.014}_{-0.01}$	$0.0641^{+0.013}_{-0.012}$	$0.04791^{+0.01}_{-0.011}$
$z_{\rm re}$	$9.081^{+1.2}_{-1.1}$	$8.341^{+1.4}_{-1}$	$6.922^{+1.3}_{-1.1}$	$9.435^{+1.3}_{-0.85}$	$8.636^{+1.3}_{-1.1}$	$7.02^{+1.1}_{-1.2}$
σ_8	$0.8179^{+0.0089}_{-0.0089}$	$0.8283^{+0.0095}_{-0.0089}$	$0.8452^{+0.0085}_{-0.0086}$	$0.8197^{+0.0096}_{-0.0075}$	$0.8298^{+0.0095}_{-0.0086}$	$0.8456^{+0.0081}_{-0.0088}$
$\chi^2_{\rm min}$	13631.9	13631.9	13637.0	13637.5	13636.1	13638.9
$\Delta\chi^2_{\rm min}$	0	0	5.1	1.4	0	2.8

Table 5.1 – Parameter tables of the means, standard deviations and (effective) χ^2 goodness-of-fit for the ΛCDM, RT and RR the models. The $\Delta\chi^2$ values are taken with respect to the lowest value within each dataset, where $\chi^2 \equiv -2\ln\mathcal{L}$, with $\mathcal{L}$ being the likelihood function.

5. Observe that nothing guarantees that the corresponding maximum reached is *the* global one, but starting the evaluation from the best-fit point obtained from the global run provides already representative best-fit values, sufficient for the purpose of our study.

6. Notice that there is a typo here in (Dirian et al., 2016), where we wrote $T = 50$ instead of $T = 1/50$.

Interpretation	$\Delta\chi^2$	$\ln B_{01}$
"inconclusive"	$0-2$	$0-1$
"weak"	$2-6$	$1-2.5$
"moderate-to-strong"	$6-10$	$2.5-5$
"strong"	>10	>5

Table 5.2 – Scale used for comparing model $\mathcal{M}_1$ against model $\mathcal{M}_0$ in this work, i.e. for interpetating their BIC difference $\Delta\chi^2_{01} \equiv \chi^2_1 - \chi^2_0$ and their log-Bayes factors $\ln B_{01}$. Positivity of the latter tends to favor $\mathcal{M}_0$. These scales are taken as a rule of thumb inspired by Secs. 2.6-2.10 of Ref. (Burnham and Anderson, 2002) in accordance with the (more conservative) Jeffreys' scale of Ref. (Trotta, 2008) [see also Ref. (Efstathiou, 2008) for a comparison of the latter with the original scale proposed by Jeffrey].

In Table 5.1, we show the mean values together with their corresponding 1σ uncertainties (68% confidence interval) and the χ^2 goodness-of-fit for ΛCDM, the RT model and the RR model, for different combinations of datasets. In the upper left table, we only use the *Planck* CMB data presented in the previous subsection, while in the upper right table, we combine them with BAO and *JLA* SNIa. In the two lower tables we further add a prior on H_0, namely $H_0 = 70.6 \pm 3.3$ for the lower left table and a high value $H_0 = 73.8 \pm 2.4$, for the lower right table. Beside giving the mean values of our six cosmological parameters, we also give the derived parameter values of σ_8 and of the effective redshift to reionization $z_{\rm re}$. For illustration, the triangle plot displaying the inferred distribution of the six cosmological parameters given *Planck* 2015 CMB data is shown in Fig. 5.1.
Before we present the results from Bayesian model selection, we will make use of an approximation of it which is sensible enough for the statistical case we consider in this section. We use the so-called Bayesian Information Criterion (BIC) that is given by [see e.g. (Trotta, 2008) for more details],

$$\mathrm{BIC} \equiv \chi^2 + k \ln N \,, \tag{5.6}$$

where χ^2 is the goodness-of-fit, k is the number of parameters and N the number of data points. The lower the BIC the better the model. Since k and N are equal within the models that we compare throughout this work, we can therefore only use the difference $\Delta\chi^2_{ij}$ between models $\mathcal{M}_i$ and $\mathcal{M}_j$, as a BIC diagnostic. This criterion originates from an approximation of the Bayesian evidence assuming gaussianity of the posterior, a likelihood dominated regime and weak correlations between parameters. In the present case, we will see that the conclusions drawn from this approximate version and from genuine Bayesian model selection are similar. However, into the next section, we will see a case where the BIC diagnostic fails in giving the right conclusions as compared to the Bayesian case. The interpretation of Bayes factor values and their associated (approximate) $\Delta\chi^2_{ij}$ values we adopt in this work are found into Table 5.2.

We now turn to the interpretation of the data shown into Table 5.1, in particular commenting on the various parameter shifts that one can observe in going from one model to the other. This relies on the underlying structural features of the model that we discuss now.

Understanding the Parameter Shifts

The parameter shifts between the models can be understood by looking at their relevant deviations when compared to each other. Focusing on the constraints for *Planck*-only, a first

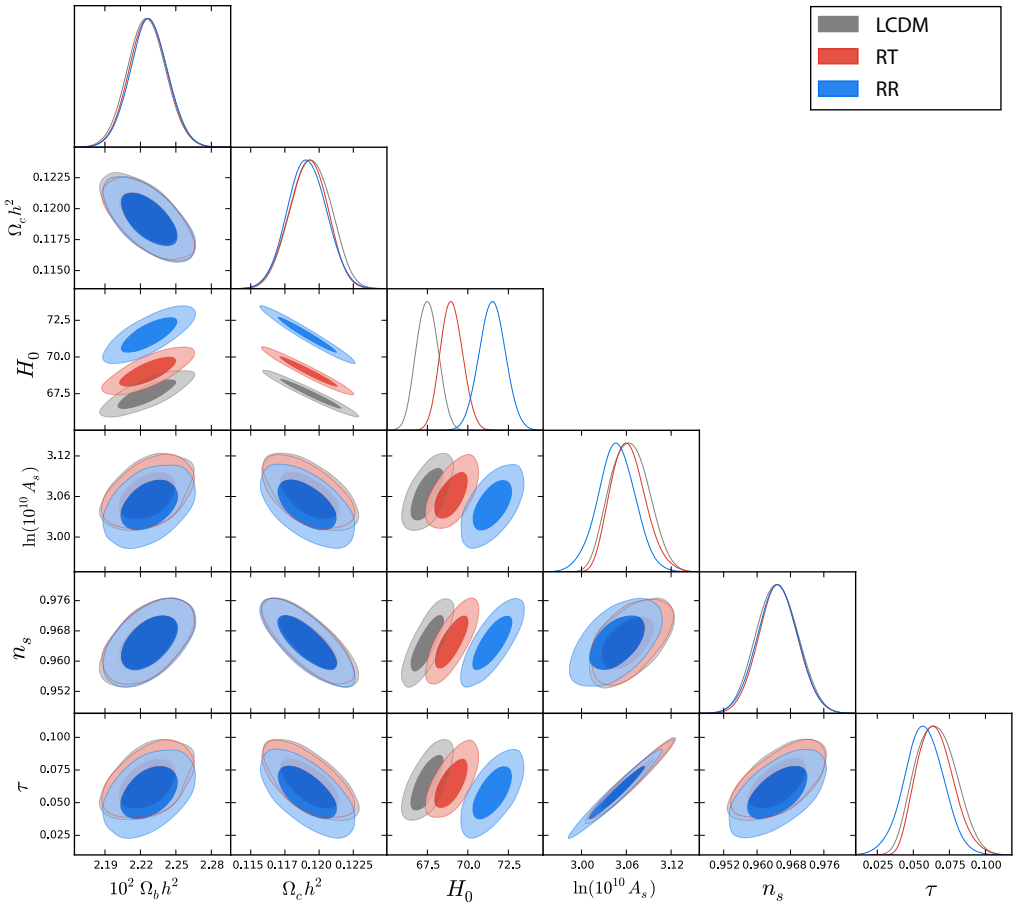

Figure 5.1 – Triangle plot for *Planck* 2015. The dark shaded contours correspond to 1σ (68% confidence interval) and the light shaded to 2σ (95% confidence interval) .

noteworthy point is that the differences between the results in the three cosmologies are statistically non-significant ($\lesssim 1\sigma$) for all parameters in $\theta_{\rm base}$, with the exception of the background-related parameter H_0 which undergoes the most significant shift ($\sim 2\sigma$ in RT and $\sim 5\sigma$ in RR). Notice also that σ_8, derived at the linear level, undergoes a significant change in RR ($\sim 3\sigma$), while it shifts to a milder level in RT ($\sim 1\sigma$). As noticed from nonlinear structure formation studies in the case of the RR model (Barreira et al., 2014b), the σ_8-enhancement results from the stronger clustering in the RR nonlocal model, mostly induced by a lower expansion rate (see the red curve in the upper left panel of Fig. 5.14), that reduces the Hubble friction to matter perturbations. This effect is supplemented by, although to a smaller extent, a higher late time gravitational strength modelled by a time-dependent effective Newton constant $G_{\rm eff}(z,k)$ (see the right panel of Fig. 4.5). More clustering also increases the lensing power, as shown into the lower left panel of Fig. 5.14, and in turn smooths out temperature fluctuations more efficiently. Moreover, this requires a smaller primordial amplitude A_s that comes together with a delayed reionization epoch, given that the CMB damping tail constrains well the combination $A_s\, e^{-2\tau_{\rm re}}$ at high-ℓ, [7]. We illustrate the higher growth of the nonlocal models

7. Observe that the preference for a lower optical depth to reionization $\tau_{\rm re}$ within the nonlocal models compared to ΛCDM is consistent with the results found from the recent analysis of the *Planck* HFI data (Aghanim et al., 2016b).

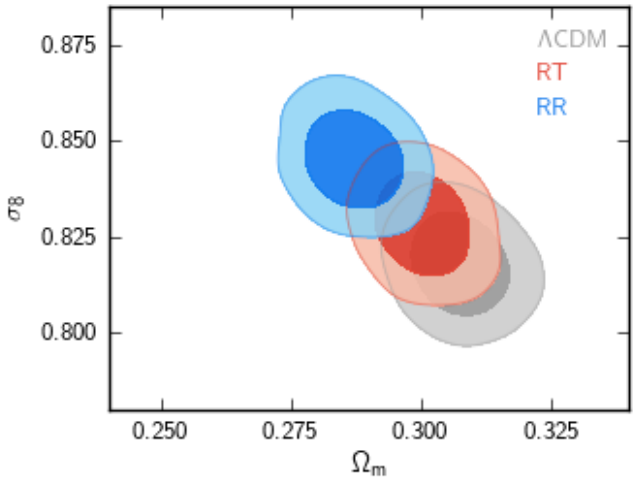

Figure 5.2 – $\sigma_8 - \Omega_m$ 2-dimensional marginalised likelihood for ΛCDM (grey), RT (red), RR (blue) *Planck*+BAO+*JLA*+($H_0 = 70.6$). Dark and light shaded contours corresponding to 1σ and 2σ respectively.

in Fig. 5.2, where we plot the 2-dimensional marginalised likelihood in the $\sigma_8 - \Omega_m$ plane, given *Planck*+BAO+*JLA*+($H_0 = 70.6$) data.
Regarding the *Planck* constrains on H_0, its mean values are inferred to be larger as the equation of state today $w^0_{\rm de}$ becomes lower. In RT, we find $H_0 \approx 68.86 \pm 0.7$ km s^{-1} Mpc^{-1} for $w^0_{\rm de} \simeq -1.04$, while in RR we have $H_0 \approx 71.51 \pm 0.84$ km s^{-1} Mpc^{-1} for $w^0_{\rm de} \simeq -1.15$, and this is to be compared to ΛCDM whose value reads $H_0 \approx 67.50 \pm 0.66$ km/s/Mpc with $w^0_{\rm de} = -1$. This preference for higher H_0 a fortiori originates from the late time emerging, quite smooth and phantom nature of the nonlocal models' effective dark energy, compared to that modelled by a cosmological constant Λ. In the following, we attempt to provide a comprehensive explanation of this fact.

As discussed in Sec. 4.2, at fixed cosmological parameters, a smaller equation of state at late time implies a smaller dark energy fraction $\Omega_{\rm de}(z)$ and in turn a smaller expansion rate $H(z)$. From the point of view of *Planck* data, modifications to $H(z)$ at low redshift alter the predicted acoustic-distance scale ratio θ_*, which determines the position of the acoustic peaks of the CMB temperature power spectrum. The scale θ_* is measured to a very good precision by *Planck* ($\lesssim 0.1\%$ at 1σ in the case of base ΛCDM) and is robust under cosmology change. It is expressed as $\theta_* \equiv r_*/D_A(z_*)$, where r_* is the sound horizon at the redshift of recombination z_* and $D_A(z_*)$ the comoving angular diameter distance to recombination defined as,

$$r_* \equiv \int_{z_*}^{\infty} \frac{c_s}{H(z)}\,{\rm d}z\,, \tag{5.7}$$

$$D_A(z_*) \equiv \int_0^{z_*} \frac{{\rm d}z}{H(z)}\,, \tag{5.8}$$

where c_s is the sound speed of the primordial plasma,

$$c_s = 1/\sqrt{3\,[1 + 3\Omega_b/(4\Omega_\gamma)]}\,, \tag{5.9}$$

with Ω_γ the photon density fraction today. For definiteness, we recall here the expression of the

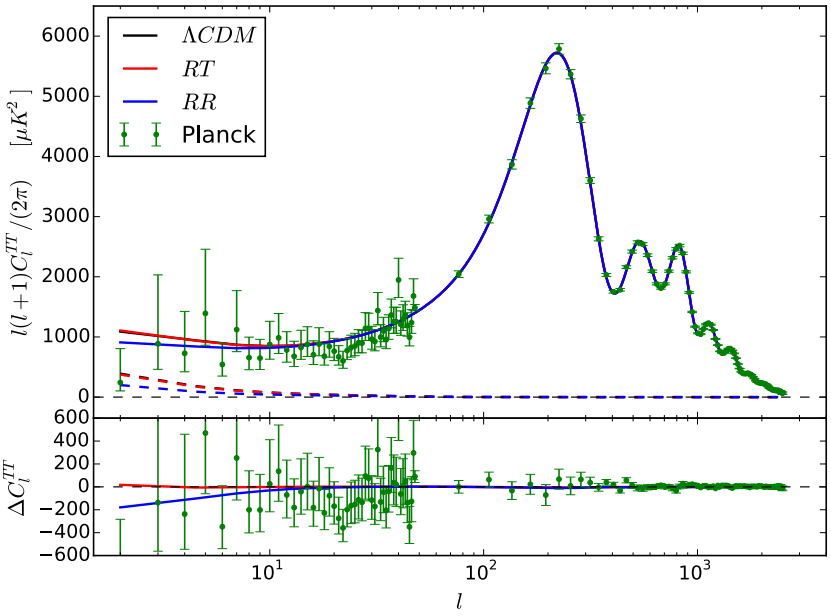

Figure 5.3 – Upper plot: temperature power spectrum (thick), and the separate contribution from the late ISW contributions (dashed), for ΛCDM (black), RT (red) and RR (blue), using the best fit values of the parameters determined from BAO+*JLA*+*Planck*. The black and red lines are indistinguishable on this scale. The lower plot shows the residuals for ΛCDM and difference of RT (red) and RR (blue) with respect to ΛCDM. Data points are from *Planck* 2015 (Ade et al., 2015d) (green bars). Error bars correspond to $\pm 1\sigma$ uncertainty.

Hubble parameter defined by [see Eq. (4.39)],

$$H(z) = \left[100\,\omega(z) + H_0^2\Omega_{\rm de}(z)\right]^{1/2}, \tag{5.10}$$

where we have used $H_0 \equiv 100\,h\ \mathrm{km\,s^{-1}\,Mpc^{-1}}$, denoted the dark energy density fraction present in the Universe at redshift z by $\Omega_{\rm de}(z)$ and by $\omega(z) \equiv \Omega(z)h^2$, the one including all the other components, that is, the physical density fraction of CDM $\omega_{cdm}(z)$, and of baryons $\omega_b(z)$, in the case of the baseline, but also other ingredients available in extensions of it, such as the density fraction of massive neutrinos ω_ν. For fixed cosmological parameter values, r_* does not change significantly from ΛCDM to RT or RR, because it is a function of early time background configurations and does not depend on the particular (late time) dark energy modelling. At late time however, such a modelling becomes important and the lower expansion rate in the nonlocal models lead to a larger $D_A(z_*)$, which in turn lowers θ_*. The lower acoustic scale shifts the CMB temperature power spectrum towards higher multipoles ℓ, yielding the poor fit to the data, as seen in the case of the RR model in the upper right panel of Fig. 5.14.

In the case of the *Planck* baseline, this discrepancy can be resolved in shifting either the background quantities H_0, ω_b or ω_{cdm} (or equivalently Ω_b or Ω_{cdm}) present into the $H(z)$ expression Eq. (5.10). However, the shape information of the first CMB peaks such as their position and their relative height provide strong, model-independent constraints on both ω_b and ω_{cdm} [see e.g. (Ade et al., 2014a; Aghanim et al., 2016a) for more details] and there is therefore only significant room for H_0 to vary. Consequently, since the dark energy featured by both nonlocal models is phantom, implying that $\Omega_{\rm de}$ is decreased compared to Ω_Λ for fixed parameter values, H_0 is doomed to increase. For the case of the RR model, the blue curves in Fig. 5.14 show the same as the green ones, but with H_0 adjusted to $H_0 = 71.31\ \mathrm{km\,s^{-1}\,Mpc^{-1}}$ so

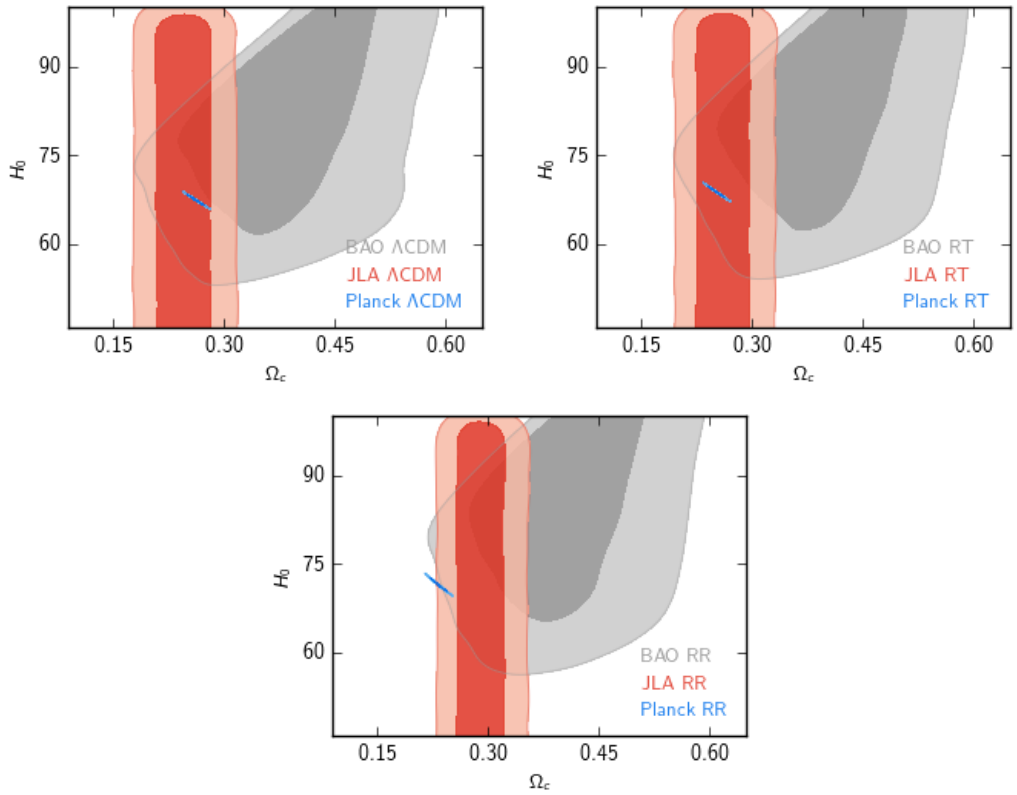

Figure 5.4 – The separate 1σ and 2σ contours for *Planck* CMB (blue), BAO (grey) and *JLA* SNIa (red) in the (H_0, Ω_c) plane for the ΛCDM (upper left), RT (upper right) and RR (lower).

as to yield the same θ_* as in the best-fitting ΛCDM model to *Planck*. This yields a cosmological scenario that is very similar to the best-fitting RR model to *Planck* (red curves in Fig. 5.14). The goodness-of-fit of the RR model given *Planck* is better than the base ΛCDM with $\Delta\chi^2 = 1.6$, as one can see from Table 5.1. As shown in Fig. 5.3, this is mostly because of the lower power in the low-ℓ part of the CMB temperature power spectrum, induced by a smaller ISW effect dominating at large-scales. Such a preference being "inconclusive" according to the classification reported in our Table 5.2, both models are therefore statistically equivalent given *Planck* 2015 CMB data. The same conclusion applies to the RT model which is favored over ΛCDM with $\Delta\chi^2 = 0.2$ *Planck* 2015 CMB data.

Appearance of a Tension in RR

However, once we join BAO and SNIe to CMB data, the ΛCDM and RT models remain statistically indistinguishable, with $\Delta\chi^2_{\Lambda\mathrm{CDM},RT} = 0.6$ in favor of ΛCDM, while the BIC diagnostic lies on the weak/moderate-to-strong boundary for evidence against the RR model with $\chi^2_{\Lambda\mathrm{CDM},RR} \simeq 6.0$ ($\sim 2.5\sigma$), as compared to ΛCDM. As the most significant deviations in the nonlocal models with respect to ΛCDM lies into their H_0 values, the origin of this result can be understood by looking at the two-dimensional marginalised likelihoods in the $H_0 - \Omega_c$ plane, shown in Fig. 5.4. We see that for the RT and ΛCDM models, the separate contours obtained from CMB, BAO and SNIa are in agreement, while for the RR model, a tension appears between CMB and SNIa and, although to a milder level, between CMB and BAO.

Below, we will perform an analysis of this issue and provide solutions for it to be resolved. For

Data	RT	RR
Planck	$5.17(4) \times 10^{-2}$	$9.35(7) \times 10^{-3}$
Planck+BAO+*JLA*	$5.15(4) \times 10^{-2}$	$9.21(7) \times 10^{-3}$
Planck+BAO+*JLA*+($H_0 = 70.6$)	$5.15(4) \times 10^{-2}$	$9.22(7) \times 10^{-3}$
Planck+BAO+*JLA*+($H_0 = 73.8$)	$5.17(4) \times 10^{-2}$	$9.24(7) \times 10^{-3}$

Table 5.3 – Mean values for $\gamma = m^2/(9H_0^2)$.

the moment, observe that the preference of the nonlocal models for higher H_0 values is consistent with those obtained from local measurements, unlike in the case of ΛCDM which is in tension when the latter are joined with *Planck*. As such, including a higher prior for H_0 into the global fit to CMB+BAO+SNIa data, ameliorates the goodness-of-fit of the nonlocal models. For the smaller value $H_0 = 70.6 \pm 3.3$ kms^{-1}Mpc^{-1} given in (Efstathiou, 2014) the situation changes little. The ΛCDM and RT model are still statistically equivalent, and the RR model is still disfavored, although to a smaller extent since now it only shows weak evidence for being ruled out (see Table 5.2). In the case of a higher value such as $H_0 = 73.8 \pm 2.4$ kms^{-1}Mpc^{-1} provided by (Riess et al., 2011), the RT model displays weak evidence against ΛCDM, whereas the RR model is brought to values of $\Delta\chi^2$ approaching the lower bound of the weakly disfavored interval. In all cases, ΛCDM and the RT model are statistically indistinguishable, with differences in favor of one or the other depending on the datasets and priors used.

From the above results, we can also obtain the mean value for the derived parameter m^2 of the nonlocal models through,

$$\gamma = \frac{m^2}{9H_0^2}\,, \tag{5.11}$$

that enters in the study of the cosmological evolution (see Sec. 4.2 for details). Based on the values of the parameters given in Table 5.1, we find the values of γ given in Table 5.3.

Finally, by having also determined the best fit values of the cosmological parameters, it is interesting to display explicitly how the CMB data are fitted by the three models. We use for definiteness their respective bestfits determined from *Planck*+BAO+*JLA*. In Figs. 5.5, 5.6, we show, for the three models, the fit to the EE spectrum, the BB spectrum and the lensing potential, respectively.

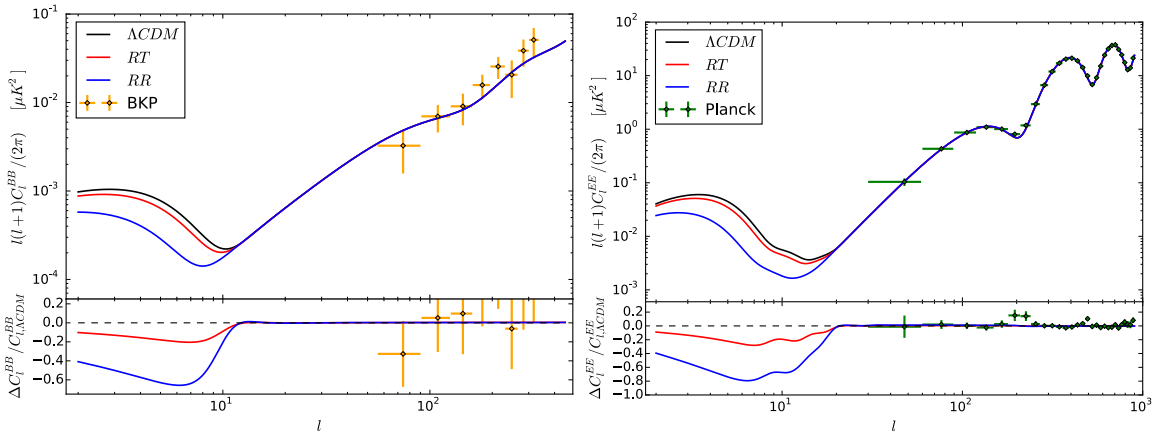

Figure 5.5 – Left panel: As in Fig. 5.3 for the lensed BB spectra, instead of *Planck* 2015 the data points are from the joint *BICEP2*+*Keck*+*Planck* (Ade et al., 2015c) (orange crosses). Right panel: As in Fig. 5.3 for the lensed EE spectra.

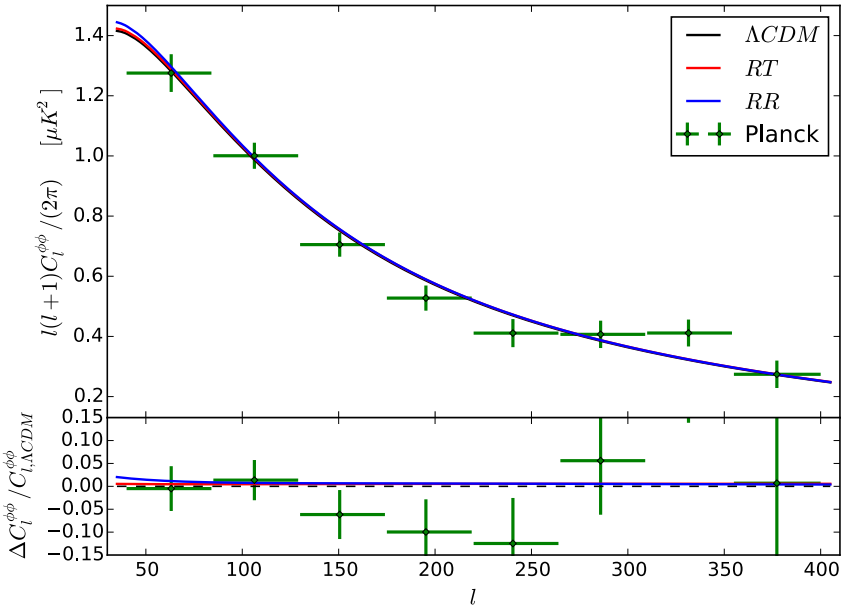

Figure 5.6 – The lensed $\phi\phi$ spectra (lensing potential).

5.2 Bayesian Model Comparison

5.2.1 The Bayes Factor

In the previous section, in order to compare the performance of the RT, RR and ΛCDM models, we have used the BIC diagnostic (5.6) by computing the differences $\Delta\chi^2_{ij}$. This method is not genuinely Bayesian, and only leads to sensible results if the assumptions outlined above are satisfied by the posterior distributions under interest, so it is possible that the results drawn from it are biased. The method for performing Bayesian model selection consists in the computation of Bayes factors (Trotta, 2007). In this section, we use Bayes factors to compare the three models of interest among each other, given the *Planck*+BAO+*JLA* data. Starting from Bayes theorem,

$$P(\theta|d,\mathcal{M}) = \frac{P(d|\theta,\mathcal{M})P(\theta|\mathcal{M})}{P(d|\mathcal{M})}\,, \tag{5.12}$$

which says that the posterior distribution, i.e. the probability of the parameters θ given the data d and the model $\mathcal{M}$, $P(\theta|d,\mathcal{M})$, equals the product of the likelihood function $P(d|\theta,\mathcal{M})$ by the prior $P(\theta|\mathcal{M})$, divided by the evidence $P(d|\mathcal{M})$ (marginal likelihood). General Bayesian model comparison is based on the model probability $P(\mathcal{M}|d)$. This number is however difficult to interpret in absolute terms, and instead one considers relative model probabilities. Using again Bayes theorem we can express the relative model probability for two models $\mathcal{M}_i$ and $\mathcal{M}_j$ as,

$$\frac{P(\mathcal{M}_i|d)}{P(\mathcal{M}_j|d)} = \frac{P(d|\mathcal{M}_i)}{P(d|\mathcal{M}_j)}\frac{P(\mathcal{M}_i)}{P(\mathcal{M}_j)} \equiv B_{ij}\frac{P(\mathcal{M}_i)}{P(\mathcal{M}_j)}\,, \tag{5.13}$$

i.e. up to the prior model probabilities $P(\mathcal{M})$ the relative model probabilities are just given by the Bayes factors B_{ij} which are defined as the ratio of the evidences computed within the two models $\mathcal{M}_i$ and $\mathcal{M}_j$. The Bayes factors correspond to betting odds, their numerical value is

conventionally translated into statements about the evidence of model i with respect to model j using the Jeffreys' scale. A way to interpret that scale is provided in Table 5.2 [8].

For multi-parameter models, the computation of the respective evidences is in general numerically expensive. However when the models to compare with each other can be nested together, i.e. can be embedded in a larger model that reduces to one model in a limit, and to the other model in another limit, this task is made easier by the Savage-Dickey density ratio (SDDR) method. In our context this nesting is possible and the SDDR can be applied.

5.2.2 Model Nesting and Savage-Dickey Density Ratio

Our task is to calculate the Bayes factors $B_{\Lambda i}$ constructed out of the evidence computed assuming the ΛCDM model, our null hypothesis, and one of the two nonlocal models of interest ($i = \mathrm{RT}, \mathrm{RR}$), the alternative hypothesis, for a given set of data. Computing the evidence for a model is generally quite hard as it requires a high-dimensional integration. Marginalising Eq. (5.12) over θ we find immediately that,

$$P(d|\mathcal{M}) = \int \mathrm{d}\theta \; P(d|\theta, \mathcal{M}) P(\theta|\mathcal{M}) \,. \tag{5.14}$$

If however two models are nested, it becomes possible to use the SDDR instead to find directly the Bayes factor between the models. In order to be able to exploit the SDDR, we consider the extended model constructed from each of the nonlocal models by adding a cosmological constant. For the RT model, the equation of motion (4.1) is then modified into,

$$G_{\mu\nu} - \frac{m^2}{3}\left(g_{\mu\nu}\Box^{-1}R\right)^{\mathrm{T}} + g_{\mu\nu}\Lambda = 8\pi G\, T_{\mu\nu} \,, \tag{5.15}$$

while for the model RR the action (4.2) becomes,

$$S = \frac{1}{16\pi G}\int \mathrm{d}^4x\sqrt{-g}\,\left[R - 2\Lambda - \frac{1}{6}m^2 R\frac{1}{\Box^2}R\right] . \tag{5.16}$$

Because of the absence of a vDVZ discontinuity, the model (5.15) reduces to ΛCDM in the limit $m^2 \to 0$, and to the RT model in the limit $\Lambda \to 0$, and similarly the model (5.16) reduces in these limits to ΛCDM and to the RR model, respectively. Of course, the models (5.15) and (5.16) could be interesting in their own right. However, we will only use them as a tool for comparing the RT and RR models to ΛCDM.

These two models for gravity allow us to construct two associated statistical models, denoted $\mathcal{M}_{\Lambda+\mathrm{RT}}$ and $\mathcal{M}_{\Lambda+\mathrm{RR}}$ respectively, which can be constrained by the data with the same method described in the previous section. The only difference with respect to the analysis performed previously is that now the total dark energy component is a mixture of the one induced by the cosmological constant, Ω_Λ, and the one induced by the nonlocal modification of gravity Ω_{X_i}, which depends on the the mass parameter m. These models therefore have an extended parameter space that we take to be spanned by

$$\tilde{\theta} = (H_0, \omega_b, A_s, n_s, \tau_{\mathrm{re}}, \Omega_\Lambda, \Omega_{X_i}) \,. \tag{5.17}$$

Observe that now the physical dark matter density fraction ω_c is taken as a derived parameter, and instead we vary the density fractions of the two types of dark energy. We choose to proceed

8. Some subtleties may appear in the use of the Jeffreys' scale when comparing models with a different number of parameters (Nesseris and Garcia-Bellido, 2013), which however is not our case.

in this way in order to keep maximal control on the choice of prior for the latter, since this condition can be very important when using the SDDR method (Wagenmakers et al., 2010) that we discuss now.

Consider the nested model $\mathcal{M}_{\Lambda+i}$ (where i = RT or RR). Since this model is a nesting of $\mathcal{M}_\Lambda$ and $\mathcal{M}_i$, we assume (by continuity) that its likelihood function taken at $\Omega_\Lambda = 0$ reproduces the one of $\mathcal{M}_i$, and equivalently putting $\Omega_{X_i} = 0$ reproduces the one of $\mathcal{M}_\Lambda$,

$$P\big(d|\bar{\theta}_\Lambda, \Omega_\Lambda = 0, \mathcal{M}_{\Lambda+i}\big) = P\big(d|\bar{\theta}_\Lambda, \mathcal{M}_i\big)\,, \tag{5.18}$$

$$P\big(d|\bar{\theta}_{X_i}, \Omega_{X_i} = 0, \mathcal{M}_{\Lambda+i}\big) = P\big(d|\bar{\theta}_{X_i}, \mathcal{M}_\Lambda\big)\,, \tag{5.19}$$

where $\bar{\theta}_j \equiv \tilde{\theta} \setminus \{\Omega_j\}$, and that the same conditions hold on the prior. We can therefore write,

$$\begin{aligned} P(d|\mathcal{M}_\Lambda) &= \int \mathrm{d}\bar{\theta}\, P\big(d|\bar{\theta}, \mathcal{M}_\Lambda\big) P\big(\bar{\theta}|\mathcal{M}_\Lambda\big) \\ &= \int \mathrm{d}\bar{\theta}\, P\big(d|\bar{\theta}_{X_i}, \Omega_{X_i} = 0, \mathcal{M}_{\Lambda+i}\big) P\big(\bar{\theta}_{X_i}, \Omega_{X_i} = 0|\mathcal{M}_{\Lambda+i}\big) \\ &= P\big(d|\Omega_{X_i} = 0, \mathcal{M}_{\Lambda+i}\big)\,. \end{aligned} \tag{5.20}$$

Applying now Bayes theorem to the third equality,

$$P\big(d|\Omega_{X_i} = 0, \mathcal{M}_{\Lambda+i}\big) = \frac{P\big(\Omega_{X_i} = 0|d, \mathcal{M}_{\Lambda+i}\big) P\big(d|\mathcal{M}_{\Lambda+i}\big)}{P\big(\Omega_{X_i} = 0|\mathcal{M}_{\Lambda+i}\big)}\,, \tag{5.21}$$

leads to the SDDR,

$$B_{\Lambda(\Lambda+i)} \equiv \frac{P(d|\mathcal{M}_\Lambda)}{P\big(d|\mathcal{M}_{\Lambda+i}\big)} = \frac{P\big(\Omega_{X_i} = 0|d, \mathcal{M}_{\Lambda+i}\big)}{P\big(\Omega_{X_i} = 0|\mathcal{M}_{\Lambda+i}\big)}\,, \tag{5.22}$$

which tells us that the Bayes factor of the comparison between the nested model $\mathcal{M}_{\Lambda+i}$ and its sub-model $\mathcal{M}_\Lambda$ is equal to the ratio of the marginalised one-dimensional posterior distribution and marginalised one-dimensional prior of Ω_{X_i} obtained from the extended model, evaluated at the point where the simpler model is nested inside the extended model (i.e. at $\Omega_{X_i} = 0$). Intuitively, this can be understood as a measure of the amount by which the prior evolved into the posterior through knowledge update given by new data. If the posterior grows at $\Omega_{X_i} = 0$, this means that this value tends to be preferred by the data, i.e. $\mathcal{M}_\Lambda$ is preferred, and the Bayes factor increases. Conversely, if the posterior decreases, a non-zero value of Ω_{X_i} is preferred.

The procedure outlined above allows us to compare $\mathcal{M}_\Lambda$ (or equivalently $\mathcal{M}_i$) with the nested model $\mathcal{M}_{\Lambda+i}$. However, we eventually want to compare directly $\mathcal{M}_\Lambda$ with $\mathcal{M}_i$. This can be done by comparing both to the extended model,

$$\begin{aligned} B_{\Lambda i} &\equiv \frac{P(d|\mathcal{M}_\Lambda)}{P(d|\mathcal{M}_i)} = \frac{P(d|\mathcal{M}_\Lambda)}{P(d|\mathcal{M}_{\Lambda+i})} \frac{P(d|\mathcal{M}_{\Lambda+i})}{P(d|\mathcal{M}_i)} \\ &= \frac{B_{\Lambda(\Lambda+i)}}{B_{i(\Lambda+i)}} = \frac{P(\Omega_{X_i} = 0|d, \mathcal{M}_{\Lambda+i})}{P(\Omega_\Lambda = 0|d, \mathcal{M}_{\Lambda+i})}\,. \end{aligned} \tag{5.23}$$

The expression involving the ratio of the Bayes factors holds by statistical coherence, but in the last identity we have assumed the similarity of the marginalised one-dimensional prior, $P\big(\Omega_{X_i} = 0|\mathcal{M}_{\Lambda+i}\big) = P\big(\Omega_\Lambda = 0|\mathcal{M}_{\Lambda+i}\big)$. This shows how the SDDR method greatly simplifies the computation of the Bayes factor for the comparison of two models that can be nested together. Indeed, one only needs to know the final posterior distribution of the nested model, for

some set of data, which can be obtained by standard MCMC methods as the one we use [although occasionally multiple chains at different temperatures may be needed, see e.g. appendix A of (Mukherjee et al., 2011) for an example in a different context]. Then, one has just to take the ratio of two numbers, the marginalised 1d posterior of Ω_Λ evaluated at $\Omega_\Lambda = 0$, and the same for Ω_{X_i}, within the extended model. If the priors do not cancel then one just computes the actual Bayes factors between the extended and the two nested models and uses their ratio.

The last point that we need to discuss is the choice that we made for the parameters to vary for constructing the posterior distribution of the nested model, and their respective prior distribution. In Bayesian inference the choice of a (subjective) prior is part of the approach and should be chosen with care. In order to have sensible results, one needs to provide the least informative prior given by the current knowledge, before seeing the data. Since in the nested model we have two types of dark energies, Ω_{X_i} and Ω_Λ, the flatness condition reads $\Omega_{X_i} + \Omega_\Lambda + \Omega_c = 1 - \Omega_R$. In order to treat both type of dark energies on the same footing, we choose to vary both Ω_Λ and Ω_{X_i} and to take ω_c as derived. For the same reason, we prefer to impose a flat prior on Ω_Λ and Ω_{X_i} rather than on, say, Λ and m^2. It is natural to assume that the density fractions vary in the interval $[0, 1]$. To avoid boundary effects that could affect the determination of the SDDR, we actually extend the allowed range of values to,

$$\Omega_\Lambda \in [-0.2, 1.2], \qquad \Omega_{X_i} \in [-0.2, 1.2]\,, \tag{5.24}$$

with a uniform prior and we then remove values that lie outside $[0, 1]$ from the chain. The prior for both parameter being the same, the last equality in (5.23) therefore make sense, and this formula can be applied in our case.

We can now compute the likelihoods of the nested model, perform the corresponding parameter estimation, and compute the Bayes factors using the SDDR. The results are shown in Table 5.4 and illustrated into Fig. 5.7, where we show the one dimensional marginalised posteriors on the dark energy density fractions $\Omega_{\rm de}$ and Ω_Λ in the nested models in the case of the two datasets considered, i.e. given *Planck*+BAO+*JLA* (left panel) and *Planck*+BAO+*JLA*+($H_0 = 73.8 \pm 2.4$) (right panel).

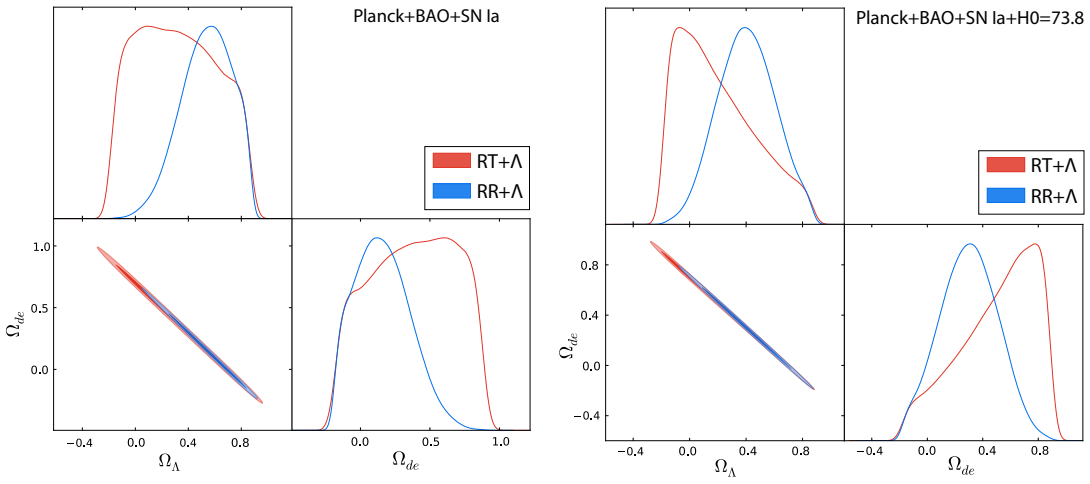

Figure 5.7 – One and two dimensional marginalised porteriors for the dark energy fraction $\Omega_{\rm de}$ and Ω_Λ in the nested models RT+Λ (red) and in RR+Λ (blue), given the *Planck*+BAO+*JLA* (left panel) and the *Planck*+BAO+*JLA*+$H_0 = 73.8$ (right panel) datasets.

	Planck+BAO+*JLA*	
Param	RT + Λ	RR + Λ
$100\ \omega_b$	$2.225^{+0.014}_{-0.014}$	$2.225^{+0.015}_{-0.015}$
H_0	$68.18^{+0.65}_{-0.68}$	$68.28^{+0.79}_{-1}$
$\log(10^{10}A_s)$	$3.059^{+0.017}_{-0.02}$	$3.061^{+0.026}_{-0.025}$
n_s	$0.9646^{+0.004}_{-0.0041}$	$0.9646^{+0.0044}_{-0.0044}$
$\tau_{\rm re}$	$0.06323^{+0.0096}_{-0.011}$	$0.06379^{+0.014}_{-0.013}$
Ω_Λ	$0.357^{+0.35}_{-0.33}$	$0.538^{+0.24}_{-0.17}$
Ω_X	$0.3368^{+0.34}_{-0.35}$	$0.1566^{+0.17}_{-0.24}$
Ω_{cdm}	$0.2569^{+0.0025}_{-0.023}$	$0.2561^{+0.0076}_{-0.0072}$
$z_{\rm re}$	8.568^{+1}_{-1}	$8.604^{+1.4}_{-1.2}$
σ_8	$0.8217^{+0.033}_{-0.0012}$	$0.8238^{+0.011}_{-0.012}$
$\chi^2_{\rm min}$	13631.0	13630.8
$B_{\Lambda i}$	1.02	22.67

	Planck+BAO+*JLA*+($H_0 = 73.8 \pm 2.4$)	
Param	RT + Λ	RR + Λ
$100\ \omega_b$	$2.23^{+0.013}_{-0.014}$	$2.227^{+0.015}_{-0.015}$
H_0	$68.62^{+0.64}_{-0.58}$	$69.08^{+0.92}_{-1}$
$\log(10^{10}A_s)$	$3.066^{+0.017}_{-0.017}$	$3.059^{+0.028}_{-0.026}$
n_s	$0.9656^{+0.0039}_{-0.0039}$	$0.9649^{+0.0045}_{-0.0045}$
$\tau_{\rm re}$	$0.06716^{+0.0092}_{-0.0092}$	$0.06328^{+0.015}_{-0.014}$
Ω_Λ	$0.2445^{+0.13}_{-0.44}$	$0.3993^{+0.21}_{-0.22}$
Ω_X	$0.454^{+0.42}_{-0.17}$	$0.3025^{+0.22}_{-0.21}$
Ω_{cdm}	$0.2527^{+0.0035}_{-0.022}$	$0.2501^{-0.00052}_{-0.03}$
$z_{\rm re}$	$8.935^{+0.93}_{-0.86}$	$8.537^{+1.5}_{-1.3}$
σ_8	$0.8257^{+0.036}_{-0.0017}$	$0.8306^{+0.018}_{-0.035}$
$\chi^2_{\rm min}$	13636.1	13635.4
$B_{\Lambda i}$	0.39	2.38

Table 5.4 – Best fit values and Bayes factors for the nested models. Left: using *Planck*+BAO+*JLA* data. Right: adding also $H_0 = 73.8 \pm 2.4\ \mathrm{km\,s^{-1}\,Mpc^{-1}}$ of (Riess et al., 2011).

As could have been expected, the mean values for the nested model $\mathcal{M}_{\Lambda+\rm RT}$ are always intermediate between the values obtained for $\mathcal{M}_\Lambda$ and those for $\mathcal{M}_{\rm RT}$, compare with Table 5.1, and the same for the nested model $\mathcal{M}_{\Lambda+\rm RR}$. The conclusions drawn from the values of the Bayes factors are fully consistent with that obtained in Section 5.1.3 simply using $\Delta\chi^2_{ij}$. Namely, without a prior on H_0, the RT model and ΛCDM are statistically indistinguishable while, on the scale of Table 5.2, the evidence of ΛCDM against the RR model is on "moderate-to-strong". Adding a high prior on H_0 is preferred by the nonlocal models, so the log-Bayes factor for the RT model becomes negative, but still the model shows inconclusive/weak evidence against ΛCDM, with $B_{\rm RT,\Lambda} \simeq 1/0.39 \simeq 2.6$ ($\ln B_{\rm RT,\Lambda} = 0.9$), and the RR model is now only slightly disfavored with respect to ΛCDM, by a similar amount, $B_{\Lambda,\rm RR} \simeq 2.4$. Also the evidence of the RT model with respect to the RR model can be computed easily, with $B_{\rm RT,RR} = B_{\rm RT,\Lambda}/B_{\rm RR,\Lambda} = B_{\Lambda,\rm RR}/B_{\Lambda,\rm RT}$ ranging from a value $22.67/1.02 \simeq 22.22$ using *Planck*+BAO+*JLA* data, to a value $2.38/0.39 \simeq 6.10$, when adding the high prior on the Hubble constant, $H_0 = 73.8 \pm 2.4\ \mathrm{km\,s^{-1}\,Mpc^{-1}}$.

We have seen that, because the nonlocal models exhibit a phantom behavior, they lead to a lower Hubble expansion rate at late time. As such, given *Planck* 2015 CMB data, it implies that these models generically prefer a higher values of H_0, because of the presence a geometric degeneracy in the acoustic-distance scale ratio. Breaking this degeneracy by using SNIa and BAO data allows to put stronger constraint on the underlying cosmological models and, in particular, we have seen that this led to an internal tension into the RR model between CMB and SNIa data. Such a tension reverberates into a "moderate-to-strong" evidence against the model when compared to ΛCDM in a Bayesian way. This tension is mostly present into the RR model rather than into the RT one, because the former features a stronger phantom dark energy than the latter, and compared to ΛCDM. The RT model is statistically equivalent to ΛCDM in all studied cases. In Sec. 5.1.3, we have seen that the nonlocal models also generically preferred a higher values of σ_8 as well. In order to test further such deviation, we constrain the RT, RR and ΛCDM models using growth rate $f\sigma_8$ data.

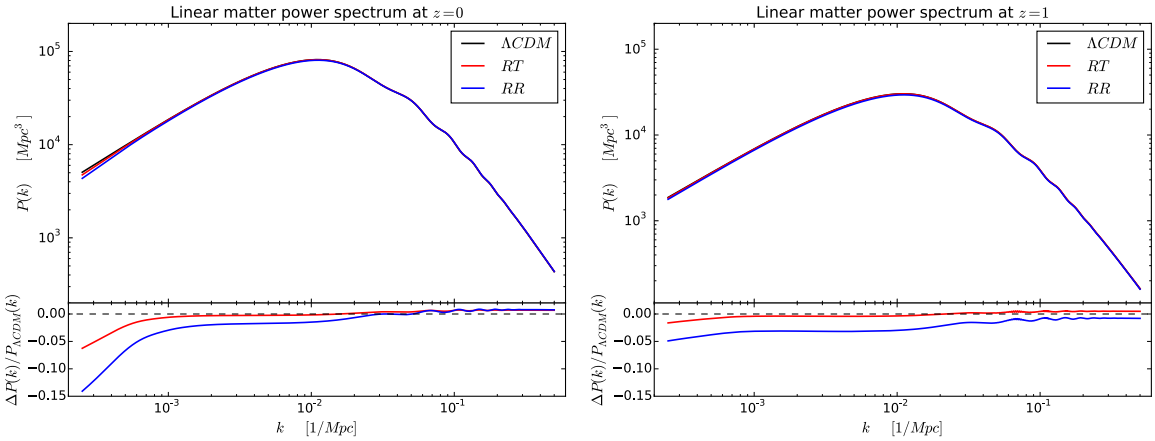

Figure 5.8 – Upper left: linear matter power spectrum at $z = 0$ for ΛCDM (black), RT (red) and RR (blue). Lower left: relative difference of RT (red) and RR (blue), with respect to ΛCDM. Right: the same for $z = 1$

5.3 Growth Rate Data and Structure Formation

RSD probe the velocity field, and are usually expressed as a constraint on the combination $f\sigma_8$, where $f \equiv \mathrm{d}\ln\sigma_8/\mathrm{d}\ln a$, is the growth function (Ade et al., 2015e), and σ_8 is the variance of the linear matter power spectrum in a radius of 8 Mpc today. The translation to $f\sigma_8$ requires a fiducial model, which is taken to be ΛCDM. This could lead to problems when using the data for constraining modified gravity models, especially if they exhibit a significant scale-dependence. However, the linear matter power spectrum of the RT and RR models look very much like that of ΛCDM on the relevant scales, as can be seen from Fig. 5.8, which show the linear matter power spectra at redshifts $z = 0$ (left panel) and $z = 1$ (right panel), respectively. For this reason we expect that we can use the RSD data to provide at least a rough test of our nonlocal models. Furthermore, since RSD are mostly degenerated with the Alcock-Paczynski (AP) effect, measurements of $f\sigma_8$ are often combined with measurements of the angular diameter distance D_A and the Hubble parameter H at the corresponding effective redshift, or some combination of the latter. Whenever this is the case, we marginalise over these measurements and consider only the ones associated to $f\sigma_8$. From this point of view, the treatment which follows is only illustrative of the constraints partially imposed by RSD on the models under consideration. Of course, a more thorough study would consist in including the RSD datasets into a fit performed with MCMC techniques, similarly to what we performed in the previous section for CMB, SNIa and BAO data. For the purpose of our study, we fix the best-fit values of the models from the *Planck*+BAO+*JLA* data and check if the predicted growth of perturbations agrees with the marginalised $f\sigma_8$ data. The results and the corresponding data used are shown in Fig. 5.9[9]. We find that the corresponding χ^2 obtained from the data in Fig. 5.9 for ΛCDM, the RT and RR models are,

$$\chi^2_{\mathrm{min},\Lambda\mathrm{CDM}} = 3.9\,, \qquad \chi^2_{\mathrm{min,RT}} = 4.7\,, \qquad \chi^2_{\mathrm{min,RR}} = 6.5\,. \tag{5.25}$$

9. Notice that the data point of SDSS LRG analysed by (Oka et al., 2014) is taken to be the resulting data from their "full fit" since other fits are explicitly based on ΛCDM-dependent priors such as the ones imposed on $\sigma_{8,\mathrm{nl}}$ (which is not applicable in our case, see Ω_M–σ_8 contours in fig. 5.2) or neglecting the AP effect which is motivated by the fit using the fiducial cosmology.

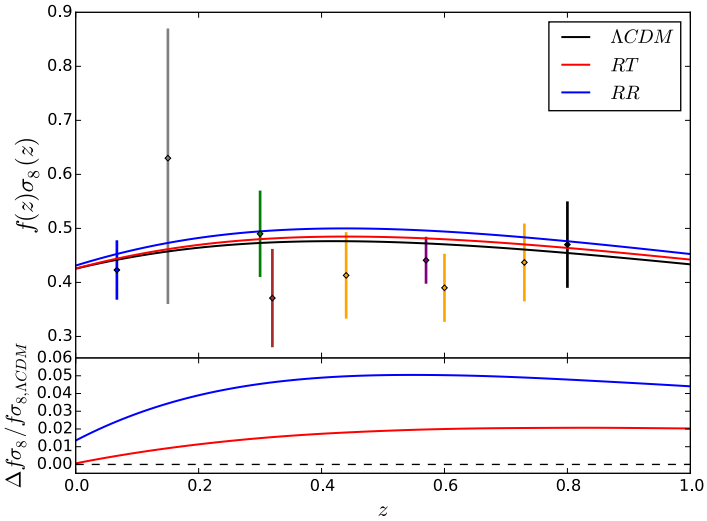

Figure 5.9 – Upper panel: Growth rate computed in ΛCDM (black), RT (red) and RR (blue) constrained with various data points given in Sec. 5.1.1. Lower panel: Relative difference of the growth rate computed in RT (red) and in RR (blue) with respect to ΛCDM.

We see that the nonlocal models generically predict a larger growth rate, although for the RT model the difference with ΛCDM is again not statistically significant, even when combined with the results found into Table 5.1. Joining these constraints to the *Planck*+BAO+*JLA*, the goodness-of-fit become,

$$\Delta\chi^2_{\Lambda\mathrm{CDM,RT}} = 0.6 + 0.8(\mathrm{post}) = 1.4\,, \qquad \Delta\chi^2_{\Lambda\mathrm{CDM,RR}} = 6.0 + 2.6\,(\mathrm{post}) = 8.6\,, \tag{5.26}$$

and in particular show that ΛCDM provides "moderate-to-strong" evidence against the RR model, while is still statistically equivalent to the RT one.

We also compute several other quantities which are relevant for the comparison with structure formation (in particular for assessing the possibility of discriminating the models with future observations), using for each model its own fiducial cosmology, e.g. the respective mean values of the parameters obtained from *Planck*+BAO+*JLA* data. As we have seen in Sec. 4.4.1, when studying structure formation and lensing, several indicators are used in the literature for parametrising deviations from ΛCDM, in particular the functions μ (4.142) and Σ (4.143) [10]. In order to make contact with results in the literature (Ade et al., 2015e), it is convenient to define them as,

$$\Psi = \mu(k,z)\Psi_{\mathrm{GR}}\,, \tag{5.27}$$

$$\Psi - \Phi = \Sigma(k,z)(\Psi-\Phi)_{\mathrm{GR}}\,, \tag{5.28}$$

where, again, the subscript denotes the quantities computed in GR, assuming a ΛCDM model, or as,

$$-k^2\Psi = 4\pi G a^2 \mu_P(k,z)\rho\Delta\,, \tag{5.29}$$

$$-k^2(\Psi-\Phi) = 8\pi G a^2 \Sigma_P(k,z)\rho\Delta\,, \tag{5.30}$$

10. The following results differ in particular from those presented in Sec.4.4.1, where instead a ΛCDM fiducial cosmology for evolving the RT and RR models was used.

[The subscript P in μ_P and Σ_P indicates that these definitions agree with those of the *Planck* analysis (Ade et al., 2015e)]. In these definitions, we compare the actual value of the gravitational potentials Φ and Ψ to the value expected in GR due to the matter and radiation perturbations $\rho\Delta = \rho_m\Delta_m + \rho_r\Delta_r$, where Δ is the gauge invariant density perturbation defined as $\delta^\star$ in Eq. (4.71). In Fig. 5.10, we plot $\mu_P(k,z)$ (left panel) and $\Sigma_P(k,z)$ (right panel) for two

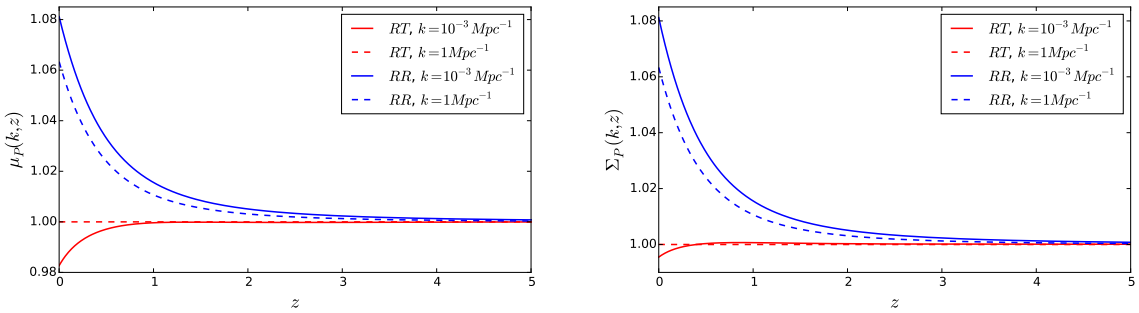

Figure 5.10 – Deviations of the nonlocal models from ΛCDM for the gravitational potential parametrised by μ_P (left panel) and Σ_P (right panel).

representative momenta, as a function of z, for the three models. We see that, for the RT model, the deviations from ΛCDM are tiny, below one percent, while for the RR model they reach a maximum value up to 3–4% at the typical redshifts, say, $z \gtrsim 0.5$ relevant for observation of structure formation. A discussed, a second useful pair of indicators is provided by gravitational slip η and the effective Newton constant $G_{\rm eff}/G$. The slip function is given by,

$$\eta_P(k,z) = -\frac{\Phi}{\Psi}\,, \tag{5.31}$$

This quantity is equal to one in ΛCDM when the anisotropic stress is negligible. The effective Newton constant $G_{\rm eff}$ is defined in Sec. 4.4.1. Observe that $G_{\rm eff}(k,z)/G$ is the same as the function $Q(k,z)$ of (Ade et al., 2015e). We plot these quantities in Fig. 5.11, together with the combination $2[\mu_P(k,z)-1]+[\eta_P(k,z)-1]$, which is the one used in the *Planck* 2015 dark energy paper (Ade et al., 2015e). Finally, we show the difference $\Psi-\Phi$ both at large and small scales in Fig. 5.12.

What we learn from these figures is that, at the typical redshifts of interest for the comparison with observations of structure formation, say $z \gtrsim 0.5$, as far as structure formation is concerned the RT model differs from ΛCDM at a level of at most 1%, which is quite small compared to existing experimental uncertainties, but could be observable with future missions such as the *Euclid* (Amendola et al., 2013), *SKA* (Dewdney et al., 2009; Yahya et al., 2015) or *DESI* (Levi et al., 2013; DESI Collaboration et al., 2016a,b) large scale structure surveys (see Sec. 5.5.4 for more on this). In contrast, the RR model shows differences which, at $z \simeq 0.5$, can be as large as 6%, as for instance for the combination shown in the lower panel of Fig. 5.11. As we see from the upper left panel of Fig. 5.11, these deviations go in the direction of producing a stronger effective Newton constant, and therefore more structures. This contributes to explaining with the growth displayed in Fig. 5.9, is stronger for the nonlocal models than for ΛCDM. A further, and main reason, is that, for the same values of the cosmological parameters, the expansion rate in the RT and RR model is generically lower than in ΛCDM as can be seen in the left panel of Fig. 4.1, and this contributes also to the enhancement of clustering [11].

11. This fact was also noticed in (Barreira et al., 2014b), in the case of the RR model, where N-body simulations

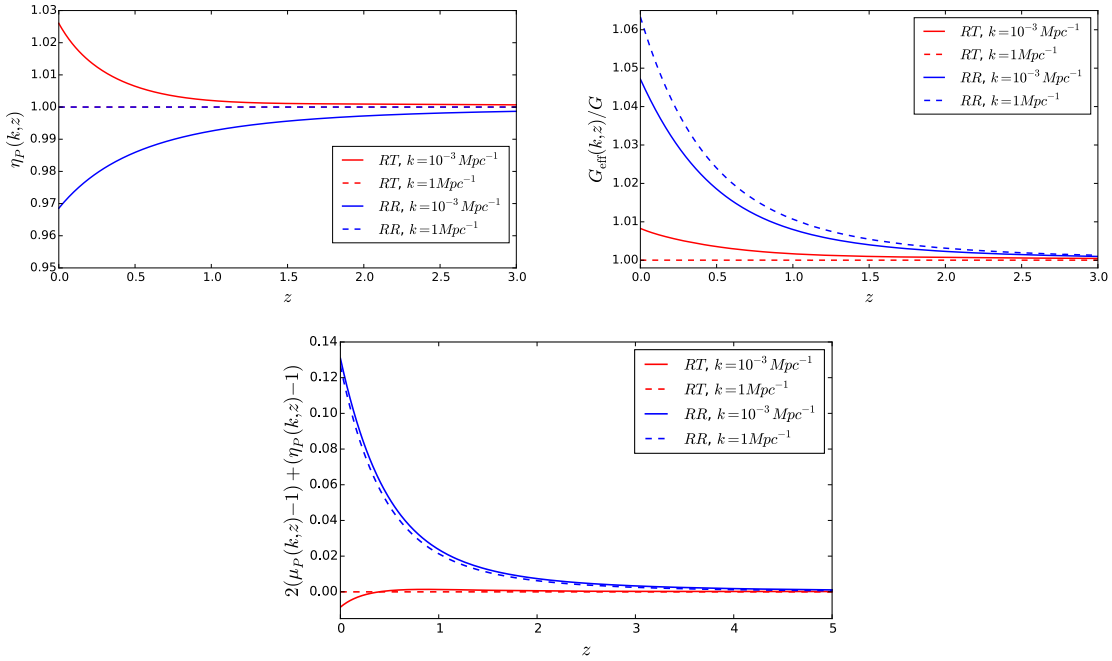

Figure 5.11 – The gravitational slip η_P (upper left), the effective Newton constant $G_{\rm eff}(k,z)/G$ (upper right) and the combination used in the *Planck* 2015 dark energy paper (Ade et al., 2015e), for the nonlocal models. Solid lines correspond to large scales: $k = 10^{-3}\,\mathrm{Mpc}^{-1}$ and dashed lines to small scales: $k = 1\,\mathrm{Mpc}^{-1}$

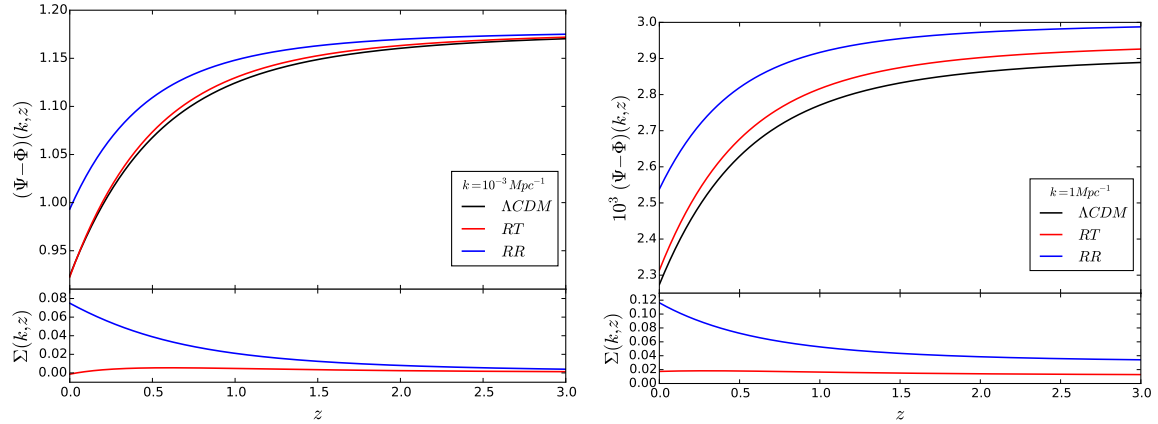

Figure 5.12 – The difference of the potentials $\Psi - \Phi$ at large scales: $k = 10^{-3}\,\mathrm{Mpc}^{-1}$ (left) and at small scales: $k = 1\,\mathrm{Mpc}^{-1}$ (right), and their relative ratio to ΛCDM.

5.4 Interlude: Inflationary Instabilities of the RT Model

After the above analysis was accomplished, a study of the cosmological evolution of the RT model, when initial conditions were fixed during a phase of primordial inflation, was performed into (Belgacem et al., 2018a). In that reference, the authors found that, although the RT

revealed deeper gravitational potential wells and massive haloes slightly more abundant and concentrated. See also (Barreira et al., 2015a,b), where lensing features of the RR model were analysed though N-body simulations.

model has viable solutions at the background level, its linear cosmological perturbations develop instabilities that makes it non-viable from such a phenomenological point of view.

In particular, they find that the auxiliary fields have runaway solutions that source the metric potential so as $\Psi \sim \Phi \sim \gamma e^{2\Delta N}$, where $\gamma = m^2/(9H_0^2) \sim \mathcal{O}(10^{-4})$, and ΔN, is the number of inflationary e-folds. A typically number of e-folds of $\Delta N \simeq 60$, implies a value for the gravitational potential at the end of inflation of the order of 10^{52}, which, despite the fact that it is larger than one and therefore cannot be trust at linear perturbation level, clearly signals the appearance of a non-negligible growing mode, spoiling the condition $\Psi \sim \Phi \sim 10^{-4}$, at the end of inflation.

In conclusion, because of this instability, the RT model cannot be considered as a valid theory deriving for instance from a quantum effective action valid at all energy scales. This is why we will therefore not consider the RT model further in the analyses presented below. For the RR model, no instabilities are generated during an inflationary period, it therefore be used for generating a viable power spectrum of primordial matter fluctuations (Belgacem et al., 2018a).

5.5 Neutrino Mass Constraints in the RR Model

In this section, we analyse in more details the origin of the tension into the RR model and find a solution for resolving it. In particular, we will see that changing the neutrino sector of the aforeused baseline (see Sec. 5.1.2) from one dominant active mass-eigenstate to three degenerated ones, whose absolute mass is taken as a free parameter, restores the concordance of the nonlocal model to a non-negligible extent. Effectively, such a resolution exploits degeneracies between modified gravity effects of the nonlocal model and those caused by a more massive neutrino component. Similar degeneracies have already been noticed in local modified gravity theories, for instance at linear level in TeVeS (Skordis et al., 2006), covariant galileons (Barreira et al., 2014a), K-mouflage (Barreira et al., 2015) and recently in Horndeski models (Bellomo et al., 2017), but also at the nonlinear one through N-body simulations of $f(R)$ scenarios in (Baldi et al., 2014).

5.5.1 Understanding the Tension

From the above discussion of Sec. 5.1.3, we have deduced that the late time phantom nature of the RT and RR effective dark energies induces an increase in H_0 given *Planck* data, as this helps to resolve the mismatch with the CMB peaks position constraining the acoustic-distance scale ratio θ_* (c.f. Fig. 5.14 for case of RR). As such, the nonlocal models fit the *Planck* CMB data as well as ΛCDM, and the RR model even finds slightly more consistency with the data because of a lower a contribution from the late time ISW effect to the temperature anisotropies auto-correlation spectrum (see Fig. 5.3), in a region that is however dominated by cosmic variance.

The agreement with observations of the RR model however degrades when one joins the BAO+*JLA* datasets to *Planck*. The observational tensions that arise in the analyses are better illustrated in Fig. 5.13. The figure shows the 2d marginalised constraints in the $H_0 - \Omega_m$ plane for ΛCDM (left panel) and RR (right panel), obtained individually using the *Planck* dataset (red), SNIa data (grey) and BAO data (green). Contrary to ΛCDM, for the RR model, the marginalised posterior suggests a $\sim 3-4\sigma$ level tension between *Planck* and SNIa data. According to the discussion in Sec. 5.1.3, this can be understood in looking at the luminosity distance

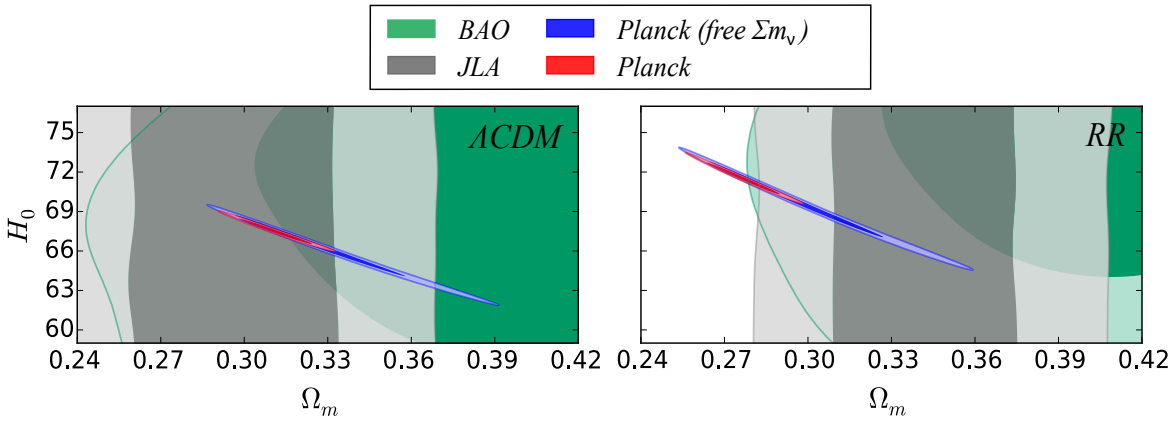

Figure 5.13 – Two dimensional marginalised constraints on the $H_0 - \Omega_m$ plane in the ΛCDM (top) and *RR* (bottom) models obtained with the *Planck* (red), BAO (green) and *JLA* (grey) datasets. The blue contours are the same as the red ones, but for constraints in which $\sum m_\nu$ is a free parameter. For fixed colour, the two contour shades indicate 1σ and 2σ confidence level. The BAO and *JLA*contours do not change appreciably when $\sum m_\nu$ varies so we do not display them explicitly.

relevant for SNIa lightcurves,

$$D_L(z) \equiv (1+z)\int_0^z \frac{\mathrm{d}z'}{H(z')}\,, \tag{5.32}$$

where the expression for $H(z)$ is found in Eq. (5.10). SNIa measurements only constrain the total matter density Ω_m, whereas H_0 has been integrated out via marginalisation on the absolute magnitude. Here the fact that the dark energy in the RR model is on the phantom side has the net effect of raising Ω_M towards higher values in RR than in ΛCDM, for fixed luminosity distance, so as to compensate for a lower dark energy density fraction $\Omega_{\rm de}(z)$ compared to Ω_Λ at late time. This shift has already been seen in the previous section in Fig. 5.4 and is again illustrated here by the grey contours in Fig. 5.13. We find $\Omega_M|_{\Lambda\rm CDM} = 0.298 \pm 0.035$ and $\Omega_M|_{\rm RR} = 0.343 \pm 0.033$, exhibiting a $\sim 1\sigma$ shift between the two models, given SNIa *JLA* data. However, this trend is inconsistent with *Planck*'s preference, since the latter provides tight constraints on $\sim \Omega_m h^2$ from the CMB spectra shape information, which, together with an increase in H_0, forces Ω_M to go down [12]. This results in an overall dominant CMB-SNIa tension in the RR model, that makes it non-concordant and disfavors it with respect to ΛCDM by $\Delta\chi^2 = 6.0$, given *Planck*+BAO+*JLA* data. Furthermore, a posteriori constraints from RSD data have also been studied in Sec. 5.3, and they increase the overall tension even more, up to $\Delta\chi^2\big|_{\rm PBJ} + \Delta\chi^2\big|^{\rm post}_{\rm rsd} = 8.6$ ($\sim 3\sigma$) compared to ΛCDM, providing strong evidence against the nonlocal model when compared to ΛCDM, given *Planck*+BAO+*JLA*+(post) RSD data.

5.5.2 Solving the Tension in RR with Massive Neutrinos

The aforementioned tension can be solved by considering extensions of the initial model, that is, allowing other physically relevant parameters, otherwise fixed, to vary. Adding such new components will open new possibilities in the global parameter space and possibly provide an

12. This behavior is a generic one for reasonably smooth phantom dark energy, as indicated by the degenerate directions in the $\Omega_m - w_0$ plane while constraining w_0CDM models given equivalent CMB and SNIa data as those used in this work [see e.g. Fig. 16 of (Betoule et al., 2014)].

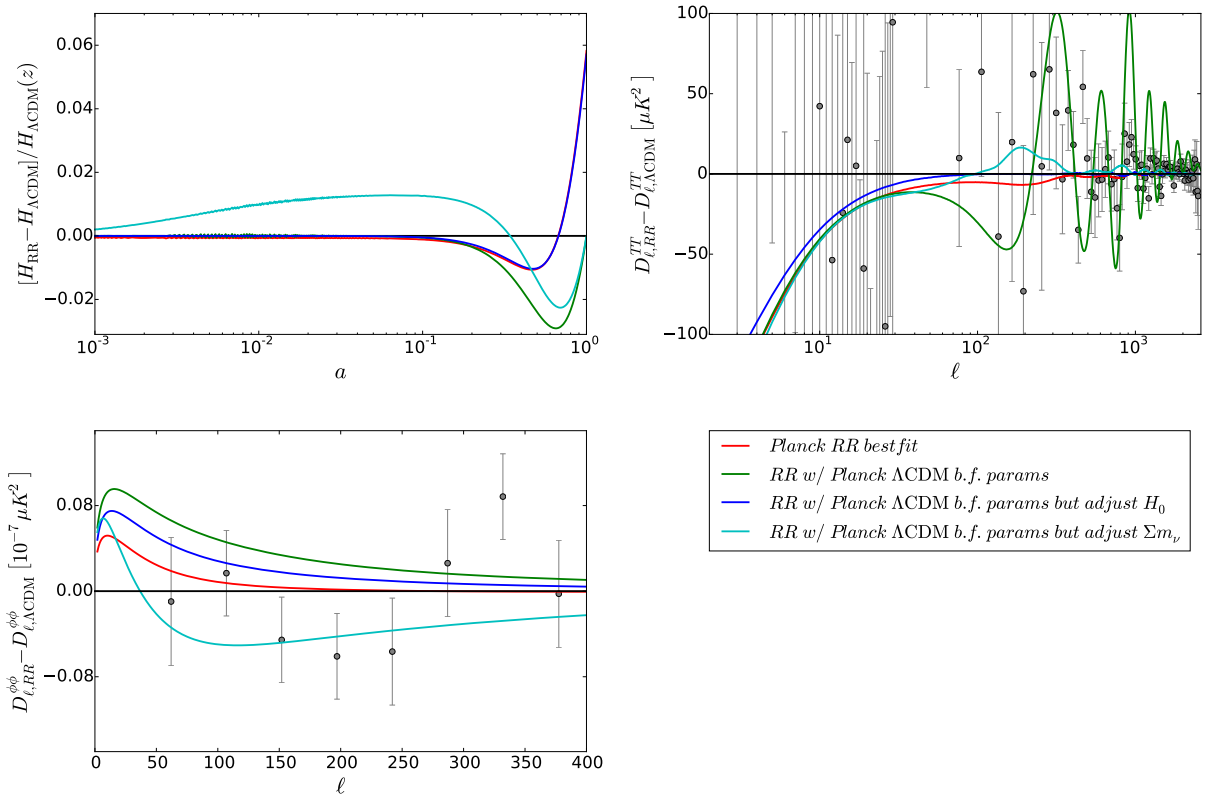

Figure 5.14 – Hubble expansion rate (upper left), CMB temperature power spectrum (upper right) and CMB lensing power spectrum (lower left) for a few illustrative RR cosmologies, plotted as the relative difference to the best-fitting ΛCDM cosmology to the *Planck* dataset. The red curve displays the prediction of the best-fitting RR model to the *Planck* dataset. The green curves show the prediction of the RR gravity model with the same parameters as the best-fitting ΛCDM model to *Planck* data. The remainder curves show the same as the green ones, but with $H_0 = 71.31$ km/s/Mpc (blue) or $\sum m_\nu = 0.423$ eV (cyan), which have been adjusted to yield the same angular acoustic scale $\theta_* = 0.010414$ as ΛCDM. In the upper right and lower left panels, the grey symbols with errorbars show the power spectra as measured by *Planck* (Ade et al., 2015b).

access to a new global maximum of the posterior probability distribution. The consequence of such a procedure is however the introduction of new degeneracies in the extended cosmological model coming together with a loss of constraining power for fixed data combination.

The extension we consider in this work assumes three active massive species with degenerated mass-eigenstates, i.e. the sum of their masses respects $\sum m_\nu \equiv 3m_0$, where the absolute neutrino mass m_0 is taken to be a free parameter. Their temperature and the additional massless neutrino component are fixed respecting the same conditions as those of the initial baseline (see Sec. 5.1.2). We therefore adopt the following parametrisation,

$$\theta_\nu = \left(H_0, 100\,\omega_b, \omega_{cdm}, \ln(10^{10}A_s), n_s, \tau, \Sigma\, m_\nu\right), \tag{5.33}$$

and the prior interval on the additional parameter is taken to be uniform and compact $\sum m_\nu \in [0, 5]$ eV, consistent with existing data (see subsection 5.5.6 for more details and references on the latter choice). The cosmological models denoted by ΛCDM and RR are parametrised by $\theta_{\rm base}$, while their extended versions build out of θ_ν will be called νΛCDM and νRR respectively.

The consideration of this extension is justified for three reasons. First, constraints on $\sum m_\nu$ coming from terrestrial experiments are very weak, therefore there no obvious reason to fix $\sum m_\nu = 0.06\,\text{eV}$ on empirical grounds. Indeed, this value only corresponds to the smallest mass-splitting measured by oscillations experiments (see subsection 5.5.6 for more details and references). Second, an increase in neutrino masses would not alter the expansion rate at early times if the neutrinos are still relativistic at photon decoupling, so that CMB anisotropies remain unaffected, and raise the energy density of pressureless matter (after they turn non-relativistic), which therefore increases the expansion rate during the matter dominated era. Third, the free-streaming behavior exhibited by a more massive neutrino component helps to tame the growth rate of structures and therefore potentially lowers the additional discrepancy caused by the inclusion of RSD data [see e.g. (Archidiacono et al., 2017; Vagnozzi et al., 2017, 2018) for analyses of the effects induced by massive neutrinos on cosmological observables]. Thus, we can expect that the RR model would prefer a higher value of $\sum m_\nu$ than 0.06 eV, with a corresponding decrease of the CMB-SNIa tension. This is what is discussed in more details in the following.

	Planck			
Param	ΛCDM	νΛCDM	RR	νRR
$100\omega_b$	$2.225^{+0.016}_{-0.016}$	$2.220^{+0.017}_{-0.017}$	$2.227^{+0.016}_{-0.016}$	$2.222^{+0.017}_{-0.017}$
ω_{cdm}	$0.1194^{+0.0014}_{-0.0015}$	$0.1198^{+0.0015}_{-0.0016}$	$0.1191^{+0.0014}_{-0.0015}$	$0.1196^{+0.0015}_{-0.0016}$
H_0	$67.50^{+0.65}_{-0.66}$	$66.12^{+2.1}_{-1.2}$	$71.51^{+0.81}_{-0.84}$	$69.57^{+2.5}_{-1.6}$
$\ln\left(10^{10}A_s\right)$	$3.064^{+0.025}_{-0.025}$	$3.080^{+0.030}_{-0.034}$	$3.047^{+0.026}_{-0.025}$	$3.071^{+0.032}_{-0.035}$
n_s	$0.9647^{+0.0048}_{-0.0049}$	$0.9637^{+0.0050}_{-0.0050}$	$0.9649^{+0.0049}_{-0.0049}$	$0.9639^{+0.0051}_{-0.0052}$
τ	$0.06530^{+0.014}_{-0.014}$	$0.07312^{+0.016}_{-0.018}$	$0.05733^{+0.014}_{-0.014}$	$0.06905^{+0.017}_{-0.018}$
$\sum m_\nu$ [eV]	0.06 (fixed)	< 0.50 (2σ)	0.06 (fixed)	< 0.51 (2σ)
σ_8	$0.8171^{+0.0089}_{-0.0089}$	$0.7949^{+0.033}_{-0.016}$	$0.8487^{+0.0097}_{-0.0096}$	$0.8212^{+0.038}_{-0.020}$
$\Delta\chi^2_{Planck}$	0 ($\chi^2 = 12943.30$)	-0.04	-1.6	-1.6

Table 5.5 – Summary of the means, standard deviations and (effective) χ^2 goodness-of-fit values for the one-dimensional marginalised likelihood distributions of the ΛCDM, νΛCDM, RR and νRR models obtained with the *Planck* dataset. The $\Delta\chi^2$ values are taken with respect to the ΛCDM χ^2 values for each dataset, where $\chi^2 \equiv -2\ln\mathcal{L}$, with $\mathcal{L}$ being the likelihood function. All bounds shown correspond to 1σ unless explicitly stated otherwise.

Table 5.5 summarises the constraints on the νΛCDM and νRR models obtained with the *Planck* dataset (third and fifth columns), that can be compared with the results found in Sec. 5.1.3 for ΛCDM and RR that we report here for convenience (second and fourth columns). We see that the goodness-of-fit in the RR case does not change under the variation of $\sum m_\nu$, however, H_0 and σ_8 are now shifted to a smaller extend as compared to the shift between the RR and ΛCDM models. The cyan curves in Fig. 5.14 illustrate such facts in showing the same as the blue curves, but instead of adjusting H_0 to give the same θ_* as in ΛCDM, one adjusts the neutrino masses to $\sum m_\nu = 0.42$ eV. The upper left panel of Fig. 5.14 also confirms that this drastically helps to improve the goodness-of-fit to *Planck* data compared to the RR model when using the ΛCDM best-fitting parameters. This is a clear sign that the degenerate effects of H_0, $\sum m_\nu$ and a late time phantom dark energy on θ_* can therefore be exploited to try to reconcile the *Planck* and *JLA* constraints given the RR nonlocal gravity.

Figure 5.13 illustrates better the beneficial impact of varying $\sum m_\nu$ in the constraints given the RR model compared to the ΛCDM one. The blue contours show the *Planck* constraints on the H_0–Ω_m plane when $\sum m_\nu$ is a free parameter [quoted "*Planck* (free Σm_ν)" for definiteness].

	Planck+BAO+*JLA*			
Param	ΛCDM	$\nu\Lambda$CDM	RR	νRR
$100\omega_b$	$2.228^{+0.014}_{-0.015}$	$2.229^{+0.014}_{-0.015}$	$2.213^{+0.014}_{-0.015}$	$2.221^{+0.014}_{-0.015}$
ω_{cdm}	$0.1190^{+0.0011}_{-0.0011}$	$0.1189^{+0.0011}_{-0.0011}$	$0.1210^{+0.0010}_{-0.0010}$	$0.1197^{+0.0012}_{-0.0012}$
H_0	$67.67^{+0.47}_{-0.50}$	$67.60^{+0.66}_{-0.55}$	$70.44^{+0.56}_{-0.56}$	$69.49^{+0.79}_{-0.80}$
$\ln\left(10^{10}A_s\right)$	$3.066^{+0.019}_{-0.026}$	$3.071^{+0.026}_{-0.029}$	$3.027^{+0.027}_{-0.023}$	$3.071^{+0.032}_{-0.032}$
n_s	$0.9656^{+0.0041}_{-0.0043}$	$0.9661^{+0.0043}_{-0.0043}$	$0.9601^{+0.0040}_{-0.0039}$	$0.9635^{+0.0043}_{-0.0045}$
τ	$0.06678^{+0.011}_{-0.013}$	$0.06965^{+0.014}_{-0.015}$	$0.04516^{+0.014}_{-0.012}$	$0.06880^{+0.017}_{-0.017}$
$\sum m_\nu$ [eV]	0.06 (fixed)	< 0.21 (2σ)	0.06 (fixed)	$0.219^{+0.083}_{-0.084}$
σ_8	$0.8170^{+0.0076}_{-0.0095}$	$0.8157^{+0.013}_{-0.011}$	$0.8443^{+0.010}_{-0.0099}$	$0.8215^{+0.017}_{-0.017}$
$\Delta\chi^2_{Planck}$	0 ($\chi^2 = 12943.42$)	-0.14	-0.14	-1.52
$\Delta\chi^2_{BAO}$	0 ($\chi^2 = 4.42$)	0	2.48	2.38
$\Delta\chi^2_{JLA}$	0 ($\chi^2 = 683.2$)	-0.12	3.56	2.5
$\Delta\chi^2_{total}$	0 ($\chi^2 = 13631.04$)	-0.26	5.9	3.36

Table 5.6 – As for Table 5.5, but obtained with the *Planck*+BAO+*JLA* dataset.

For the nonlocal gravity model, the *Planck* contour is now overlapping the SNIa one. This illustrates the fact that allowing $\sum m_\nu$ to vary weakens the CMB-SNIa tension, as quantified by the corresponding individual $\Delta\chi^2$ values reported in Table 5.6.

A remarkable aspect of the combination of the *Planck*, BAO and *JLA* data in the constraints given RR nonlocal gravity is the evidence for non-vanishing neutrino masses. Figure 5.15 shows that $\sum m_\nu > 0$ at $\sim 2\sigma$ level, with the best-fit value $\sum m_\nu \approx 0.21$ eV (see Table 5.6 for the corresponding means value). As depicted above, such a shift is primarily caused by the relatively smooth, late time and phantom nature featured by the effective dark energy described by the *RR* nonlocal model. These constraints are very different than in $\nu\Lambda$CDM for which the data only sets an upper bound on $\sum m_\nu$. In the following, we will see that such a preference of the $\nu\Lambda$CDM model for lower values of $\sum m_\nu$ reflects one of its weakness in a Bayesian model comparison context, and therefore opens room for alternative dark energy models including similarly a varying $\sum m_\nu$ to compete with it.

5.5.3 Bayesian Model Comparison in ν-extended Models

In the following, we compare the $\nu\Lambda$CDM and νRR models given *Planck*+BAO+*JLA* data computing the associated Bayes factor $B_{\nu\Lambda,\nu\mathrm{RR}}$ and set it side by side with the BIC diagnostic (5.6) that is reported in Table 5.6. We recall that degrees of significance used in this work are reported in Table 5.2 for definiteness of the discussion. A Bayes factor B_{01} comparing model $\mathcal{M}_0$ against model $\mathcal{M}_1$ can be though of as telling betting odds of $B_{01}:1$ in favor of the former given the data.

For computing $B_{\nu\Lambda,\nu\mathrm{RR}}$ we use a combination of statistical coherence and the Savage-Dickey density ratio (SDDR) (see Sec. 5.2 for details) that exploits the nested structure of the overall

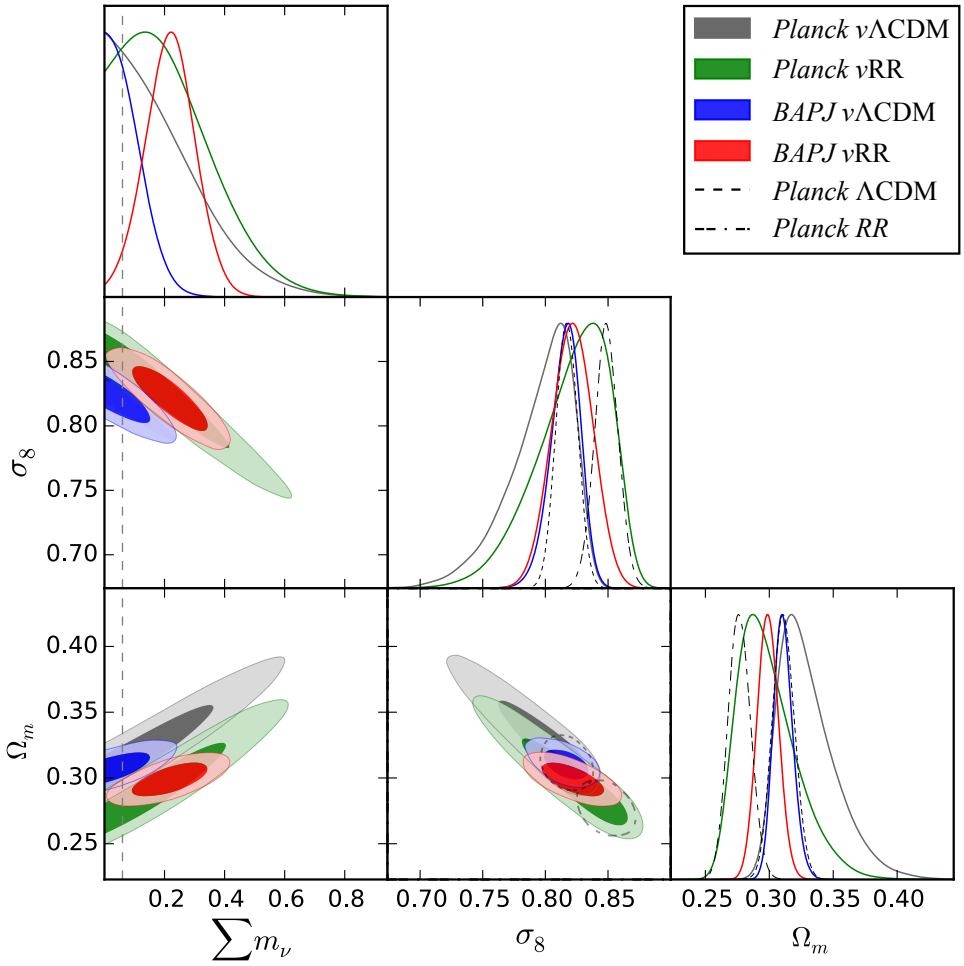

Figure 5.15 – One and two dimensional marginalised constraints on the parameters $\sum m_\nu$, σ_8 and Ω_M in the νRR and $\nu\Lambda$CDM models, obtained with the *Planck* and *Planck*+BAO+*JLA* datasets. For fixed colour, the two contour shades indicate 1σ and 2σ limits. The dashed and dot-dashed curved lines indicate the 1σ results obtained when $\sum m_\nu$ is fixed to 0.06 eV in ΛCDM and RR, respectively, given *Planck* CMB data. The vertical dashed line represents $\sum m_\nu = 0.06$ eV.

models discussed here. This allows one to get $B_{\nu\Lambda,\nu\mathrm{RR}}$ in a rather economic way in writing,

$$B_{\nu\Lambda,\nu\mathrm{RR}} \equiv \frac{P(d|\mathcal{M}_{\nu\Lambda})}{P(d|\mathcal{M}_{\nu\mathrm{RR}})} \tag{5.34}$$

$$= \frac{P(d|\mathcal{M}_{\nu\Lambda})}{P(d|\mathcal{M}_{\Lambda})}\frac{P(d|\mathcal{M}_{\Lambda})}{P(d|\mathcal{M}_{\mathrm{RR}})}\frac{P(d|\mathcal{M}_{\mathrm{RR}})}{P(d|\mathcal{M}_{\nu\mathrm{RR}})} \tag{5.35}$$

$$= \frac{B_{\mathrm{RR},\nu\mathrm{RR}}}{B_{\Lambda,\nu\Lambda}} B_{\Lambda,\mathrm{RR}}\,, \tag{5.36}$$

where $P(d|\mathcal{M}_i)$ is the marginal likelihood (evidence) of the data d given the model $\mathcal{M}_i$. The factor $B_{\Lambda,\mathrm{RR}}$ appearing above is one of the main results of Sec. 5.2 and has been computed to be $B_{\Lambda,\mathrm{RR}} = 22.7$. The remaining factors are computed for the model $i = \Lambda, \mathrm{RR}$ through the

SDDR,

$$B_{i,\nu i} = \frac{P\big(\sum m_\nu = 0.06 \,\big|\, d, \mathcal{M}_{\nu i}\big)}{P\big(\sum m_\nu = 0.06 \,\big|\, \mathcal{M}_{\nu i}\big)}\,, \tag{5.37}$$

which is the ratio of the marginalised one-dimensional posterior distribution to the marginalised one-dimensional prior of $\sum m_\nu$ obtained from the extended model, evaluated at the point where the simpler model is nested inside the extended model (i.e. at $\sum m_\nu = 0.06$). Since we chose the same prior for both $\nu\Lambda$CDM and νRR parameter spaces (in particular on $\sum m_\nu$) their contribution simplifies. Eq. (5.36) then yields,

$$B_{\nu\Lambda,\nu\mathrm{RR}} = \frac{P\big(\sum m_\nu = 0.06 \,\big|\, d, \mathcal{M}_{\nu\mathrm{RR}}\big)}{P\big(\sum m_\nu = 0.06 \,\big|\, d, \mathcal{M}_{\nu\Lambda}\big)}\, B_{\Lambda,\mathrm{RR}}\,, \tag{5.38}$$

and we find, given *Planck*+BAO+*JLA* data,

$$B_{\nu\Lambda,\nu\mathrm{RR}} = \frac{1}{12.5} \times 22.7 = 1.8 = e^{0.6}\,, \tag{5.39}$$

which is one of the main results of (Dirian, 2017). It tells that νRR is statistically equivalent to $\nu\Lambda$CDM with odds of $1.8:1$ in favor of the latter, instead of being "moderately-to-strongly" disfavored with odds $22.7:1$, when the neutrino mass is fixed. The result is invariant under prior changes on $\sum m_\nu$ (as long as they are assumed to be equal) and leads to several implications. This result shows that allowing $\sum m_\nu$ to vary within $[0, 5]$ eV helps to reconcile RR-gravity with the data as already noticed above, but it also has the effect of penalising the ΛCDM cosmology. This can be seen through the fact that applying the BIC method to compare $\nu\Lambda$CDM against νRR given *Planck*+BAO+*JLA* leads to biased results. Indeed, comparing the shifts endured by the results of both methods in varying $\sum m_\nu$ we obtain,

$$\mathrm{BIC} : \Delta\chi^2\big|_{\Lambda,\mathrm{RR}} \;=\; 5.9 \;\to \Delta\chi^2\big|_{\nu\Lambda,\nu\mathrm{RR}} \;=\; 3.4\,, \tag{5.40}$$

$$\mathrm{Bayes} : \ln B_{\Lambda,\mathrm{RR}} \;=\; 3.1 \;\to \ln B_{\nu\Lambda,\nu\mathrm{RR}} \;=\; 0.6\,, \tag{5.41}$$

all in favor of ΛCDM given *Planck*+BAO+*JLA* data. Referring to Table 5.2, one can see a significant discrepancy between the results from the BIC differences and Bayes factors. While the former announces a reduction from "weak"/"moderate-to-strong" only to "weak" evidence in favor of $\nu\Lambda$CDM, Bayesian model comparison tells that the latter "moderate-to-strong" evidence is in fact comfortably reduced to an "inconclusive" one. These two results are discrepant because of the loss of validity of the assumptions made in computing the BIC, which is only an approximation of the Bayes evidence (see Sec. 5.1.3). In particular as, beside of the net maximum likelihood shift encapsulated in $\Delta\chi^2$ favoring the RR model, Occam's razor further penalises the $\nu\Lambda$CDM one. Obviously one should therefore trust the result of Eq. (5.41).

In what follows, we address a rough analysis for trying to understand to which extent allowing the absolute neutrino mass to vary is beneficial for the RR model, given *Planck*+BAO+*JLA* data. Coming back to Eq. (5.37), in our present context we can write,

$$B_{i,\nu i} = \frac{P\big(\sum m_\nu = 0.06 \,\big|\, d, \mathcal{M}_{\nu i}\big)}{P\big(\sum m_\nu = 0.06 \,\big|\, \mathcal{M}_{\nu i}\big)} = \frac{L_i}{V_i} P_i\,, \tag{5.42}$$

where L_i is the value of the marginalised 1d posterior for $\sum m_\nu$ (normalised to its maximum) at the nesting point, V_i is the volume of it and P_i is the upper bound of the prior on the sum

of the neutrino masses, $\sum m_\nu \in [0, P_i]$. We find,

$$L_{\rm RR} = 0.19 \quad , \qquad V_{\rm RR} = 0.2\,, \tag{5.43}$$

$$L_\Lambda = \ 1.0 \quad , \qquad V_\Lambda \ = 0.08\,, \tag{5.44}$$

where we have set $P_i = 5$ in either cases. One can then compute,

$$B_{\Lambda,\nu\Lambda} = 12.5 \times 5 = 62.5 \quad , B_{\rm RR,\nu RR} = 1 \times 5\,, \tag{5.45}$$

which in particular shows that the Λ-based model provides "moderate-to-strong" evidence with odds of $62.5:1$ for fixing $\sum m_\nu = 0.06$ eV. Although the latter has a non-negligible contribution coming from the prior, it also has a non-negligible one from the likelihood (essentially originating from boundary effects), which is a handicap when compared against models preferring higher neutrino masses such as the RR one. As can be seen from Fig. 5.15, this is because the $\nu\Lambda$CDM marginalised posterior on $\sum m_\nu$ hits the lower bound of the prior at 0.06 eV, which involves a loss of posterior volume and a waste of prior one. This means that allowing the absolute neutrino mass to vary in ΛCDM, does not extract relevant information from the data. In the RR case the situation is different since non-vanishing neutrino masses are preferred at 2σ level, exploiting therefore better the *Planck*+BAO+*JLA* data. This contributes to Occam's razor effect intrinsically taken into account in Bayesian model comparison and partially explains why the RR nonlocal model undergoes a favorable and significant change when compared against ΛCDM after allowing $\sum m_\nu$ to vary [see Eq. (5.41)]. Moreover, this also explains why the BIC difference effectively fails when comparing $\nu\Lambda$CDM against νRR given *Planck*+BAO+*JLA* data, because it is only sensitive to the maximum of the posteriors, not to their entire volume.

The RR nonlocal model described by the action (4.2) is therefore statistically equivalent (given *Planck*+BAO+*JLA* data) to Einstein gravity supplemented by a cosmological constant Λ when reconsidering the prior on the neutrino sector, that is, when one changes the cosmological parametrisation from (5.4) to (5.33). This has been made possible exploiting an apparent degeneracy at the background level between H_0, $\sum m_\nu$ and the phantom nature of the effective dark energy described by the nonlocal model, which was illustrated in Fig. 5.13. In what follows we provide an outlook motivating the use of additional data, in particular coming from galaxy surveys, for being able to make a distinction between the $\nu\Lambda$CDM and the νRR cosmological models.

5.5.4 Constraints a Posteriori from Redshift-Space Distortions data

Apart from secondary CMB anisotropies such as ISW or lensing effects, the constraints on $\sum m_\nu$ mostly come from background-geometrical features when considering the *Planck*+BAO +*JLA* dataset. However, massive neutrinos give rise to characteristic inhomogeneous and anisotropic signatures induced by their thermal velocity flow. In particular, they do not cluster inside regions delimited by their free-streaming scale. Below that scale, the neutrino perturbations are smoothed out and this causes a suppression of the late time matter power spectrum at mid-to-small cosmological scales, a decrease of the lensing power and of the growth of structures in a scale-dependent manner within the linear regime (Hu et al., 1998; Lesgourgues and Pastor, 2014; Giusarma et al., 2018), as well as non-linear effects (Adamek et al., 2016; Inman and Pen, 2017). Additional data putting stronger constraints on these features are therefore relevant to include into the global fit. Nevertheless, the presence of an appreciable fraction of massive neutrinos can have partial degenerate effects with a positive fifth force present in modified gravity scenarios. A fifth force should be present at late time in the RR model and it was found in

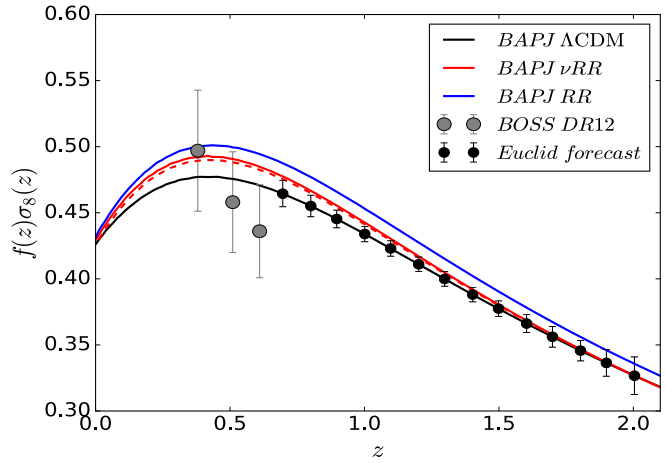

Figure 5.16 – Time evolution of the growth rate $f\sigma_8$ for the best-fitting ΛCDM, RR and νRR models to the *Planck*+BAO+*JLA* dataset. For the case of the νRR model (red), the solid and dashed lines display the result at $k = 0.01\,h\,\mathrm{Mpc}^{-1}$ and $k = 0.5\,h\,\mathrm{Mpc}^{-1}$, respectively. For the ΛCDM and RR models the growth rate is scale-independent (apart from the very small scale-dependency induced by the small neutrino fraction, $\sum m_\nu = 0.06$ eV). The grey symbols show the observational determination from the final *BOSS* DR12 release (Alam et al., 2016). The black symbols show the forecasted precision for *Euclid*, centered around the ΛCDM result.

(Barreira et al., 2014b; Dirian et al., 2016) (see our Secs. 4.4.1 and 5.3) that it enhances the growth of linear and non-linear structures compared to the one described by ΛCDM. As we have seen in Sec. 5.3, constraints on the linear growth rate of structure modelled by $f\sigma_8$ favored the ΛCDM model over the nonlocal one and this was quantified by a BIC of $\Delta\chi^2 = 2.6$. This value was computed a posteriori, that is, given that $f\sigma_8$ was derived from each model on its *Planck*+BAO+*JLA* bestfit. In this part, we study the impact of a massive neutrino component on the linear growth rate of structure using the same method.

The degenerate effects present between a massive neutrino fraction and linear growth rate are well-illustrated from the degeneracy direction observed in the $\sigma_8 - \sum m_\nu$ plane in Fig. 5.15, where one can see that they are anti-correlated: the higher the massive neutrino fraction $\Omega_\nu \sim \sum m_\nu$, the lower σ_8. Given *Planck* data, the mean value inferred on σ_8 for ΛCDM is smaller than the one provided by RR, in agreement with the higher growth within the nonlocal model, and their mean values are generically smaller in the ν-extended case. For *Planck* only, we find that the departure of the best-fit value of $\sum m_\nu$ from the lower bound of the prior in RR cosmology is caused by the addition of the *Planck* CMB lensing power spectrum which is sensitive to a weighted projection of density fluctuations along the line-of-sight. Joining BAO+SNIa data pulls the total matter density fraction Ω_M to higher values, involving a stronger increase in the absolute neutrino mass that preserves the value of σ_8 close to the one inferred in ΛCDM. Focusing on the growth, Fig. 5.16 shows the time evolution of $f\sigma_8$ for the best-fitting ΛCDM, RR and νRR models to the *Planck*+BAO+*JLA* dataset. As anticipated, the growth rate is lower in νRR compared that in the RR model. The figure also displays the most recent observational determinations of $f\sigma_8$ from the DR12 *BOSS* analysis (Alam et al., 2016) (grey symbols with errorbars). Using these data, the reduced $\chi^2_{\rm red}$ values for the ΛCDM, RR and νRR models are, respectively [13], $\chi^2_{\rm red} = 0.58$, $\chi^2_{\rm red} = 1.38$ and $\chi^2_{\rm red} = 0.97$. More pragmatically for comparison

13. These values do not consider the mid-redshift data point. This is because the associated galaxy sample completely overlaps with those of the other two points which are independent. The number of degrees of freedom

with previous results, we compute the corresponding χ^2 values using the same data points as in Sec. 5.3, that are listed in Sec. 5.1.1. The corresponding goodness-of-fit read,

$$\chi^2_{\Lambda\mathrm{CDM}} = 3.9\,, \qquad \chi^2_{\mathrm{RR}} = 6.5\,, \qquad \chi^2_{\nu\mathrm{RR}} = 5.2\,, \tag{5.46}$$

which shows that the fit is indeed improved in going from RR to νRR with BIC values changing from $\Delta\chi^2 = 2.6$ to $\Delta\chi^2 = 1.3$, but still in favor of ΛCDM. Therefore, we can conclude that allowing $\sum m_\nu$ to be a free parameter helps to decrease the discrepancy of the RR nonlocal gravity model with growth rate measurements and brings down the total discrepancy from $\Delta\chi^2\big|_{\mathrm{PBJ}} + \Delta\chi^2\big|^{\mathrm{post}}_{\mathrm{rsd}} = 8.5$ ($\sim 3\sigma$) to $\Delta\chi^2\big|_{\mathrm{PBJ}} + \Delta\chi^2\big|^{\mathrm{post}}_{\mathrm{rsd}} = 4.6$ ($\sim 2\sigma$) given *Planck*+BAO+*JLA*+(post)RSD data, which induces a significant change in the (although approximated) statistical conclusion.

In turn, this shows that the data considered in this work do not possess enough constraining power to clearly distinguish between ΛCDM and RR cosmologies. Nevertheless, the situation is expected to be different for a survey like e.g. *Euclid* (Amendola et al., 2013). This is illustrated by the black symbols in Fig. 5.16, which show an estimate of the forecast errorbars for this future mission [taken from Fig. 3 of Ref. (Majerotto et al., 2012)], centred around the ΛCDM fiducial cosmology. One notes that the difference between ΛCDM and νRR is larger than the forecast precision of *Euclid* for $z < 1$, from which we can conclude that, despite partial degeneracies between the effects of massive neutrinos and the RR-modifications to gravity, there is still room for future RSD data to be used to help distinguishing between ΛCDM and RR cosmologies.

As a final remark, a larger fraction of massive neutrinos in cosmological models contributes to an increased scale-dependence in the linear growth of structure. This may raise some concerns when confronting models like the best-fitting νRR model to *Planck*+BAO+*JLA* against $f\sigma_8$ values, because the latter are usually extracted from galaxy survey data using RSD models assuming the growth to be scale-independent [see e.g. Ref. (Johnson et al., 2014) for an exception to this fact and Ref. (Barreira et al., 2016) for a validation study of RSD modelling in DGP gravity which exhibits scale-independent linear growth]. If the scale-dependence in the νRR is non-negligible compared to the precision targeted, extra care is required in the analysis of the data before observational constraints can be performed. To test such a fact, we plot in Fig. 5.16 the evolution of $f\sigma_8$ in the νRR model for $k = 0.01\,h\,\mathrm{Mpc}^{-1}$ (red solid) and $k = 0.5\,h\,\mathrm{Mpc}^{-1}$ (red dashed). One notes that the k-dependence is small compared to the expected precision of *Euclid*, which suggests that standard methods can be used to constrain the νRR model.

Contraints from Other Surveys and Forecasts. In addition, constraints using other probes of the large scale structure such as the currently available galaxy clustering and cosmic shear data of *DES Y1* (Abbott et al., 2017j), or from future surveys such as *SKA* (Dewdney et al., 2009; Yahya et al., 2015) or *DESI* (Levi et al., 2013; DESI Collaboration et al., 2016a,b), together with weak gravitational lensing data such as those of *CFHTLenS* (Heymans et al., 2012) or *KiDS-450* (Kuijken et al., 2015), also prove to be of particular interest for constraining the ν-extended models. Indeed, measuring the cosmic shear induced by the large-scale structure allows to put constraints on the nature of the dark energy as well as on the absolute neutrino mass (Joudaki et al., 2016), although, given current data, to a smaller extent than the *Planck*+BAO+*JLA* dataset considered in this work. Moreover, weak lensing measurements reported in (Heymans et al., 2012; Kuijken et al., 2015) display a tension with *Planck* CMB observations, given the ΛCDM model, and systematic issues first need to be correctly addressed before these data can be used in combination with *Planck* for constraining modified gravity

is therefore two.

models. However, such systematic issues have recently been pointed out into (Troxel et al., 2018), where it was shown that taking into account survey boundary and masks effects into the shape noise term of the cosmic shear analytic covariance matrix, improves agreement between the *KiDS-450* cosmic shear constraints and the results of *Planck* as well as *DES Y1*. A study of forecast constraints from the future *Euclid* and *SKA* galaxy clustering and weak lensing surveys and the galaxy clustering *DESI* survey is currently under way (Casas et al., 2018).

5.5.5 A Word on H_0

As already noticed previously, another interesting outcome of the constraints on the RR model relates to the preferred values of H_0. For the best-fitting ΛCDM model to the *Planck*+BAO +*JLA* dataset, one finds $H_0 = 67.67^{+0.47}_{-0.50}\,\mathrm{km\,s^{-1}\,Mpc^{-1}}$ (c.f. Table 5.5), which lies $\sim 1\sigma$ below the determination from local measurements discussed in Ref. (Efstathiou, 2014), which sets $H_0 = 70.6 \pm 3.3\,\mathrm{km\,s^{-1}\,Mpc^{-1}}$ (note that this value becomes $H_0 = 72.5 \pm 2.5\,\mathrm{km\,s^{-1}\,Mpc^{-1}}$ if other assumptions are made into the analysis). More recently, the work of (Riess et al., 2018) sets a higher value of $73.48 \pm 1.66\,\mathrm{km\,s^{-1}\,Mpc^{-1}}$ [see also Refs. (Riess et al., 2011; Humphreys et al., 2013; Riess et al., 2016)]. Furthermore, recent determinations of H_0 using hyperparameters, $H_0 = 73.75 \pm 2.11\,\mathrm{km\,s^{-1}\,Mpc^{-1}}$ (Cardona et al., 2017), or from gravitational lensing time delay methods, $H_0 = 71.9^{+2.4}_{-3.0}\,\mathrm{km\,s^{-1}\,Mpc^{-1}}$ (Bonvin et al., 2017), are also significantly away from the ΛCDM bestfit.

The seriousness of the above-mentioned H_0 tensions is still subject to current debates and one still needs to understand better the role of systematics before claiming the need of new physics [see e.g. Refs. (Di Valentino et al., 2016; Luković et al., 2016; Bernal et al., 2016)]. Nevertheless, taking the current measurements at face value, one notes that for the best-fitting νRR model to the *Planck*+BAO+*JLA* dataset one has $H_0 = 69.49^{+0.79}_{-0.80}\,\mathrm{km\,s^{-1}\,Mpc^{-1}}$, which significantly ameliorates the agreement with the local determinations and would therefore improve further the global fit.

5.5.6 The Importance of Terrestrial Determinations of $\sum m_\nu$

The current constraints on neutrino masses that are independent of cosmology arise from terrestrial experiments. The lower bounds on $\sum m_\nu$ come from neutrino oscillations experiments which, assuming a massless eigenstate, set $\sum m_\nu \gtrsim 0.05$ eV and $\sum m_\nu \gtrsim 0.1$ eV for normal and inverted mass hierarchies respectively. The current best upper bounds are obtained by analysing the high-energy part of the spectrum of Tritium β-decay in experiments such as *MAINZ* and *TROITSK* and set the electron neutrino mass to $m_{\nu_e} \lesssim 2.2$ eV (2σ) which corresponds to $\sum m_\nu \lesssim 6.6$ eV in our context. Future Tritium β-decay experiments such as *KATRIN* will be sensitive to mass scales $\sum m_\nu \lesssim 0.6$ eV at 90% confidence level. The sensitivity can be even better if neutrinos turn out to be Majorana particles, in which case neutrinoless double β decay experiments should be able to probe the region corresponding to $\sum m_\nu \gtrsim 0.3$ eV with high precision [14] [see e.g. (Drexlin et al., 2013; Dell'Oro et al., 2016; Vergados et al., 2016; Engel and Menéndez, 2017) for reviews]. These forecast sensitivities can therefore be proven useful for confirming cosmological observations. As it has been shown throughout our study, the determination of the absolute neutrino mass scale from cosmological probes depends on the assumed cosmological model. As such, if terrestrial neutrino experiments will detect non-minimal neutrino masses, we will need to modify the standard ΛCDM cosmological model.

14. Note that the quoted upper bounds assume specific models of nuclear matrix elements.

5.6 Conclusions

In this chapter, we have perform observational constraints on the RT (4.1) and RR (4.2) nonlocal models, and compared them to standard ΛCDM by using Bayesian model selection techniques. For being able to do so, the nonlocal models have been implemented in a modified version of the CLASS linear Einstein-Boltzmann solver (see App. A for details), that allowed us to constrain these models with the MCMC cosmological parameter extraction code Montepython interfaced with CLASS. For putting tight constraints on the models, we considered current, high precision complementary data including *Planck* 2015 observations of temperature, polarisation and lensing of the CMB, isotropic and anisotropic BAO data, distant SNIa from *JLA*, local measurements of H_0, as well as structure formation RSD data (see Sec. 5.1.1 for details).

In a first approach in Sec. 5.1.2, following (Dirian et al., 2015, 2016), we have considered to embed the modified gravity models into statistical cosmological ones in following the *Planck* 2015 baseline, where, in particular, the cosmological parameter space is six dimensional. Bayesian parameter inference then revealed that the nonlocal models where statistically equivalent to ΛCDM given *Planck* 2015 data, and that only a small number of parameters were significantly shifted when going form ΛCDM to the nonlocal models. Indeed, in Sec. 5.1.3, we have seen that both models exhibit significantly higher values for H_0 and σ_8 (see Table 5.1) and argued that such a fact was mostly due to the quite smooth, phantom nature of the late time emerging effective dark energy present in the nonlocal models. Furthermore, in joining SNIa and BAO data to those of *Planck*, we observed the appearance of a dominating CMB-SNIa tension in the Ω_M–H_0 plane, provided the RR model. This tension disfavors RR with respect to ΛCDM, while under the same circumstances the RT model was shown to remain equivalent to the standard one, given CMB+BAO+SNIa data. We then performed Bayesian model selection in Sec. 5.2, by using the Savage-Dickey density ratio method for nested models presented in Sec. 5.2.2. We found that the conclusions drawn for such an analysis where equivalent to the ones obtained from a rough comparison of the χ^2 goodness-of-fit inferred from the models, given the data. That is, the ΛCDM model shows "moderate-to-strong" evidence, with odds of $22:1$, against the RR nonlocal model, given *Planck*+BAO+*JLA* data, while provides "inconclusive" conclusions compared to the RT model given the same data. In particular, we have seen that, as the nonlocal model prefer a higher value of H_0, adding a higher prior on H_0 into the global fit leads to the statistical equivalence of all the models among each other.

As such, and given that the nonlocal models also provide of different structure formation history compared to ΛCDM, we have performed observational constraints considering growth rate data from RSD measurements in Sec. 5.3. These constraints were done *a posteriori*, that is, once the normalisation of the matter power spectrum has been set on the respective *Planck*+BAO+*JLA* bestfit within each models. We found that the nonlocal models feature a higher growth of structures modelled by $f\sigma_8$, and that their fit to the data is less preferred than the one of ΛCDM. Joining these results to the CMB+BAO+SNIa ones, we have concluded that the RT model is statistically equivalent to ΛCDM, whereas the latter (and therefore both) shows "moderate-to-strong" evidence against the RR model. Again, in either case, the addition of a higher prior on H_0 favors the nonlocal models, and tames the discrepancy displayed by the RR one. Nevertheless, in (Belgacem et al., 2018a), the RT model has been shown to feature instabilities at the level of linear perturbations during a primordial inflationary phase and, as a consequence, we excluded it from our further analyses.

In Sec. 5.5, following (Dirian, 2017), we revisited the observational constraints of the RR model discussed in the previous section. We have shown that the CMB-SNIa tension, which degrades its performance in the framework of the initial baseline considered, mostly results from

the quite smooth, late time and phantom nature of the effective dark energy described by the nonlocal model. In fact, for fixed parameter values, the latter induces a decrease on the late time Hubble expansion rate $H(z \approx 0)$ compared to that described by ΛCDM. Such a fact generically implies a smaller acoustic scale θ_* for the CMB, that is corrected by the inference of a higher value of H_0 given *Planck* data, as well as a larger luminosity distance that is compensated by a larger Ω_M given SNIa data. Since the shape information from CMB temperature power spectrum constrains well ω_M, which is a multiplicative combination of H_0 and Ω_M, the trends inferred from the nonlocal model are contradictory and a tension appears, as illustrated in Fig. 5.13. In Sec. 5.5.2, we have then shown that allowing the absolute neutrino mass to be a free parameter, a fact that is allowed by current experimental bounds, resolved the tension in the nonlocal gravity model. The ν-extended nonlocal model, denoted νRR, ends up to be statistically equivalent to $\nu\Lambda$CDM given CMB+BAO+SNIa data, with odds of $1.8:1$ in favor of $\nu\Lambda$CDM. In Sec. 5.5.3, we have shown that the compatibility between νRR and $\nu\Lambda$CDM was caused by a better fit of the nonlocal model to the data, but also by the Occam's razor effect penalising the $\nu\Lambda$CDM model, because of its preference for small absolute neutrino masses. As a result, the absolute neutrino mass is inferred to be non-zero $\sum m_\nu > 0$ at $\sim 2\sigma$ level given the nonlocal model, with the best-fitting value $\sum m_\nu \approx 0.21$ eV. In the same perspective as in the case of the initial baseline, we have then placed constraints from RSD data a posteriori on both models in Sec. 5.5.4. These constraints have been shown to be improved as well by the presence of a higher neutrino fraction Ω_ν into the nonlocal cosmology. Further determinations from local measurements of H_0 were discussed, as these are in better agreement with the nonlocal gravity model inferring a value of $H_0 = 69.49^{+0.79}_{-0.80}\,\mathrm{km\,s^{-1}\,Mpc^{-1}}$, which is $\sim 2\sigma$ above $H_0 = 67.67^{+0.47}_{-0.50}\,\mathrm{km\,s^{-1}\,Mpc^{-1}}$, inferred from ΛCDM given CMB+BAO+SNIa. This provides one more example showing that the cosmological constraints on the absolute neutrino mass depends on the assumed cosmological model, because of degenerate effects between modifications to gravity and massive neutrinos. Still, our study also suggests that the use of additional data coming from future galaxy redshift surveys could reduce such a degeneracy in the studied case and potentially discriminate between the $\nu\Lambda$CDM and νRR models. We have provided an illustration to this fact in considering forecast constraints from *Euclid* RSD data. A more quantitative analysis is left for future work [see e.g. (Casas et al., 2018)].

The studies performed in this chapter focused on constraining modifications to GR at the background and linear *scalar* perturbation level. In the next chapter, we will see that complementary information to these constraints can be obtained from observations of GWs produced by inspiralling binaries. As we will show, these potentially allow to constrain modifications to GR at the background and linear *tensor* perturbation level, in particular through a modified notion of GW luminosity distance present in modified gravity theories, originating from a modified propagation of GWs in the modified gravity model.

Chapter 6

Modified Gravitational Wave Propagation and Standard Sirens

In this chapter, we present our recent works (Belgacem et al., 2017, 2018b,c), and, in particular, closely follow that of (Belgacem et al., 2018c), where forecast constraints from next generation GW interferometers such as *LISA* or the *Einstein Telescope* (*ET*) (Sathyaprakash et al., 2012) , were put on the RR model. Despite the fact that in this model the GWs propagate at the speed of light, their propagation equations feature a modified friction term. We show that modified gravity models having this characteristic give raise to a modified notion of luminosity distance to the GWs source. Taking the RR model as a prototypical example, we show that the deviation of the optical to GW distance-redshift relation can be parametrised by a fitting function including two parameters (Ξ_0, n), with $n = 5/2$ in the nonlocal model. We evaluate the forecast sensitivity of *ET* to Ξ_0 and find that it can be measured more accurately than the dark energy equation of state parameter w_0, in particular when the redshift-distance relation is calibrated to other distance indicators such as CMB+BAO+SNIa. This enhances the prospects for testing dark energy with standard sirens, and to discriminate gravity models from ΛCDM. We illustrate this fact in forecasting the number of multi-messenger sources needed to be detected by *ET* for being able to distinguish between the RR and the ΛCDM model.

6.1 Standard Sirens as a Probe of Dark Energy

In the last few years, the spectacular observations of the GWs from binary black-hole coalescences by the *LIGO/Virgo* collaboration (Abbott et al., 2016a,b, 2017a,b,c), as well as the observations of the GWs from the binary neutron star merger GW170817 (Abbott et al., 2017i), of the associated γ-ray burst (Goldstein et al., 2017; Savchenko et al., 2017; Abbott et al., 2017g), and the follow-up studies of the electromagnetic counterpart (Abbott et al., 2017f), have opened the way for (multi-messenger) gravitational-wave astrophysics and cosmology.

It has long been recognised [see e.g. (Schutz, 1986, 2001)], that the detection of GWs from coalescing compact binaries allows to access a measurement of their luminosity distance, making them "standard sirens" (Holz and Hughes, 2005), which are the GW analogue of standard candles. Recalling the expression of the luminosity distance as a function of redshift (see Sec. 4.2 for more details),

$$D_L(z) = (1+z)\int_0^z \frac{\mathrm{d}z'}{H(z')}\,, \tag{6.1}$$

with,

$$H(z) = H_0 \left[\Omega_M (1+z)^3 + \Omega_{\rm de}(z)\right]^{1/2}, \tag{6.2}$$

where we have neglected the contribution of radiation, which is negligible at the redshifts relevant for standard sirens. In the limit $z \ll 1$, one recovers the Hubble law $D_L(z) \simeq H_0^{-1} z$, so from a measurement at such redshifts one can only get information on H_0. This is the case of GW170817, which is at $z \simeq 0.01$. Indeed, from the observation of GW170817 has been extracted a value $H_0 = 70.0^{+12.0}_{-8.0}\ \mathrm{km\,s^{-1}\,Mpc^{-1}}$ (Abbott et al., 2017d), that rises to $H_0 = 75.5^{+11.6}_{-9.6}\ \mathrm{km\,s^{-1}\,Mpc^{-1}}$, if one includes in the analysis a modelling of the broadband X–ray to radio emission to constrain the inclination of the source, as well as a different estimate of the peculiar velocity of the host galaxy (Guidorzi et al., 2017). The cosmological significance of this measurement can be traced to the discrepancy between the local H_0 measurement (Riess et al., 2016) [see also (Riess et al., 2018) for a more recent estimate] and the value obtained from the *Planck* CMB data (Ade et al., 2015d), which are in tension at 3σ level, corresponding to odds of $10:1$ for ΛCDM being the true model in a Bayesian framework (Feeney et al., 2017). The current accuracy on H_0 from the measurement with the single standard siren GW170817 is not accurate enough to arbitrate this tension. However, each standard siren provides an independent measurement of H_0, so with N standard sirens with comparable signal-to-noise ratio, the error scales approximately as $1/\sqrt{N}$. The analysis of (Chen et al., 2017; Feeney et al., 2018) indicates that with about 50–100 standard sirens one could discriminate between the local measurement and the *Planck* ΛCDM value.

The next generation of GW interferometers, such as the space interferometer *LISA* (Audley et al., 2017), which is expected to fly by 2034, as well as third-generation ground-based interferometer currently under study, such as *ET* (Sathyaprakash et al., 2012) in Europe and *Cosmic Explorer* (Abbott et al., 2017e) in the US, will have the ability to detect standard sirens at much higher redshifts. The information that one could get is then potentially much richer, since the result is now in principle sensitive to the dark energy density fraction $\Omega_{\rm de}(z)$ or, equivalently, to the dark energy equation of state $w_{\rm de}(z)$ at those redshifts. Building up a distance ladder from standard sirens then proves to provide an efficient way from probing the nature of the dark energy. Several studies have been performed to investigate the accuracy that one could obtain in this way on $w_{\rm de}(z)$, for instance by provid ing forecasts on the w_0, or on the (w_0, w_a) parameters of the CPL parametrisation (4.41) parametrisation (Dalal et al., 2006; MacLeod and Hogan, 2008; Cutler and Holz, 2009; Nissanke et al., 2010; Sathyaprakash et al., 2010; Zhao et al., 2011; Del Pozzo, 2012; Nishizawa et al., 2012; Taylor and Gair, 2012; Camera and Nishizawa, 2013; Caprini and Tamanini, 2016; Tamanini et al., 2016), or also by trying to reconstruct the whole function $w_{\rm de}(z)$, (Cai and Yang, 2017).

Below, following the recent works of (Belgacem et al., 2017, 2018b,c), we perform a more complete analysis of the predictions of generic modified gravity models for standard sirens. As the latter references illustrate, when the dark energy sector of a theory differs from a simple cosmological constant, this can affect both the background evolution and the cosmological perturbations. The change in the background evolution is expressed by a non-trivial dark energy equation of state $w_{\rm de}(z)$, while linear cosmological perturbations are affected in the scalar, vector and in the tensor sector [1]. In particular, modifications in the tensor sector can be very important for standard sirens and, as we will see, their effect on the luminosity distance can be more easily observed than that due to a non-trivial dark energy equation of state.

1. On cosmological solutions, vector perturbations usually only have decaying modes and are irrelevant, in GR as well as in typical modified gravity models.

In Sec. 6.2, we discuss the structure of cosmological perturbations in modified gravity theories, studying in particular the tensor sector. As an explicit example, we will use the RR model described in Sec. 3.2. This will also allow us to propose a simple parametrisation of the effect of modified propagation on the luminosity distance, in terms of a single parameter Ξ_0 [or at most a pair of parameters (Ξ_0, n)], that extends the pair (w_0, w_a) that parametrises the modification of the background evolution. We will see that, among these four parameters, Ξ_0 can be the most important for observational purposes with standard sirens. In Section 6.3, using parameter estimation through MCMC techniques, we study the accuracy with which we can measure w_0, w_a and Ξ_0, in different combinations, using the forecast sensitivity of *ET*, and combining it with *Planck* 2015 CMB, BAO and *JLA* SNIa to reduce the degeneracies between these parameters and H_0 and Ω_M. In Sec. 6.4, we turn to concrete forecast constraints on RR nonlocal model and study the extent to which one will be able to discriminate it from ΛCDM, as a function of the number of standard sirens observed by *ET*. Finally in Sec. 6.5, we will study further observable effects related to modified GW propagation, due to the modification of the transfer function that connects a primordial GW spectrum to that observed at later epochs.

6.2 GW Propagation in Modified Gravity

As we have illustrated in Sec. 4.2, at the cosmological background level, a convenient parametrisation of the dark energy density evolution is provided by the CPL (w_0, w_a) parametrisation (4.41). At the level of linear scalar perturbations, deviations from a cosmological constant can be encoded into various indicators such as μ, Σ, η (see Sec. 4.4.1 for more details), that can also be parametrised in the same spirit, but possibly exhibiting a dependence on the wavenumber, so as to be able to forecast constraints on the associated parameter space [see e.g. (Ade et al., 2015e; Casas et al., 2017)].

When studying standard sirens, one is rather interested in the modification of the linear perturbation equations in the tensor sector, i.e. in the modification of the propagation equation of GWs over the cosmological background, such as Eq. (4.103) for the RT model and Eq. (4.122) for RR. For definiteness, let us recall that in GR, tensor perturbations over a FLRW background in conformal time satisfy,

$$\tilde{h}_A'' + 2\mathcal{H}\tilde{h}_A' + \vec{k}^2\tilde{h}_A = 16\pi G a^2\,\tilde{\sigma}_A\,, \tag{6.3}$$

where $\tilde{h}_A(\eta, \vec{k})$ are the Fourier modes of the GW amplitude, $A = +, \times$ labels the two polarisations and the source term $\tilde{\sigma}_A(\eta, \vec{k})$ is related to the helicity-2 part of the anisotropic stress tensor [see e.g. (Maggiore, 2018)]. In a generic modified gravity model, each term in this equation could a priori be modified by a function of redshift and wavenumber. A modification to the source term would induce a change in the production mechanism and therefore in the phase of an inspiralling binary. To understand the effect of changes in the terms $2\mathcal{H}\tilde{h}_A'$ or $\vec{k}^2\tilde{h}_A$, let us first consider the free propagation in GR. We then set $\tilde{\sigma}_A = 0$, and introduce a field $\tilde{\chi}_A$ as,

$$\tilde{h}_A(\eta, \vec{k}) = \frac{1}{a(\eta)}\tilde{\chi}_A(\eta, \vec{k})\,. \tag{6.4}$$

Then Eq. (6.3) becomes,

$$\tilde{\chi}_A'' + \left(\vec{k}^2 - \frac{a''}{a}\right)\tilde{\chi}_A = 0\,. \tag{6.5}$$

For modes well inside the horizon, such as the GWs targeted by ground-based and space-borne

detectors, the term a''/a is totally negligible with respect to $\vec{k}^2$,[2] and one gets a standard wave equation showing that GWs propagate at the speed of light.

In contrast, the factor $1/a$ in Eq. (6.4), that was inserted to get rid of the Hubble friction term proportional to $\tilde{h}'_A$ in Eq. (6.3), describes how the GW amplitude decreases in the propagation across cosmological distances, from the source to the observer. In particular, for inspiraling binaries, this factor combines with other factors coming from the transformation of masses and frequency from the source frame to the detector frame, to produce a dependence of the GW amplitude on the luminosity distance [see e.g. Section 4.1.4 of (Maggiore, 2007)],

$$\tilde{h}_A(\eta, \vec{k}) \sim \frac{1}{D_L(z)}\,. \tag{6.6}$$

From this discussion, one see that tampering with the coefficient of the $\vec{k}^2\tilde{h}_A$ term in Eq. (6.3) is very dangerous, since this would modify the speed of propagation of GWs. This is by now excluded, at the level of $|c_{\rm gw} - c|/c = \mathcal{O}(10^{-15})$ at $z = 0$, by the observation of GW170817 /GRB 170817A (Abbott et al., 2017g), and has ruled out a large class of scalar-tensor and vector-tensor modifications of GR (Baker et al., 2017; Creminelli and Vernizzi, 2017; Ezquiaga and Zumalacárregui, 2017; Sakstein and Jain, 2017). We next study the effect of modifying the coefficient of the friction term, $2\mathcal{H}\tilde{h}'_A$. To do so, consider the propagation equation,

$$\tilde{h}''_A + 2\mathcal{H}[1 - \delta(\eta)]\tilde{h}'_A + \vec{k}^2\tilde{h}_A = 0\,, \tag{6.7}$$

where $\delta(\eta)$ is a function that parametrises the deviation from GR, and that we have taken to be independent of the wavenumber. In this case, to eliminate the friction term, we must introduce $\tilde{\chi}_A(\eta, \vec{k})$ from,

$$\tilde{h}_A(\eta, \vec{k}) = \frac{1}{\tilde{a}(\eta)}\tilde{\chi}_A(\eta, \vec{k})\,, \tag{6.8}$$

where,

$$\frac{\tilde{a}'}{\tilde{a}} = \mathcal{H}[1 - \delta(\eta)]\,. \tag{6.9}$$

Then we obtain,

$$\tilde{\chi}''_A + \left(\vec{k}^2 - \frac{\tilde{a}''}{\tilde{a}}\right)\tilde{\chi}_A = 0\,. \tag{6.10}$$

Once again, inside the horizon, the term $\tilde{a}''/\tilde{a}$ is totally negligible, so GWs propagate at the speed of light. However, now the amplitude of $\tilde{h}_A$ is proportional to $1/\tilde{a}$ rather than $1/a$. As a result, rather than being just proportional to $1/D_L(z)$, the GW amplitude observed today, after the propagation from the source to the observer, will have decreased by a factor,

$$\frac{\tilde{a}_{\rm em}}{\tilde{a}_{\rm obs}} \equiv \frac{\tilde{a}(z)}{\tilde{a}(0)}\,, \tag{6.11}$$

instead of a factor $a_{\rm em}/a_{\rm obs} = a(z)/a(0)$, where the labels refer to the emission time (at redshift z) and the observation time at redshift zero, respectively. Therefore,

$$\tilde{h}_A \sim \frac{\tilde{a}(z)}{\tilde{a}(0)}\,\frac{a(0)}{a(z)}\,\frac{1}{D_L(z)} = \frac{\tilde{a}(z)}{a(z)}\,\frac{1}{D_L(z)}\,, \tag{6.12}$$

2. More precisely, for GWs from astrophysical sources with frequencies in the range of ground-based interferometer, $(a''/a)\vec{k}^{-2}$ corresponds to an effective change of the propagation speed $\Delta c/c = \mathcal{O}(10^{-41})$ (with a weak time dependence: since, in MD, $a''/a \propto \eta^{-2} \propto 1/a = 1+z$, $\Delta c/c$ changes by a factor $1+z = \mathcal{O}(1)$ in the propagation from the source at redshift z to us). Even if this gives rise to an integrated effect over the propagation time, still this is totally negligible compared to the bound $|c_{\rm gw} - c|/c < \mathcal{O}(10^{-15})$ from GW170817, which of course also comes from an effect integrated over the propagation time. For wavelengths comparable to the horizon size, for which the term $(a''/a)\vec{k}^{-2}$ is not so small, one can use a WKB approximation, as in (Nishizawa, 2017).

where $D_L(z) \equiv D_L^{\rm em}(z)$, is the usual notion of luminosity distance appropriate for electromagnetic signals and, since only the ratios $\tilde{a}(z)/\tilde{a}(0)$ and $a(z)/a(0)$ enter, without loss of generality we can choose the normalisations $\tilde{a}(0) = a(0) = 1$. Then, we see that in such a modified gravity model we must in general distinguish between the usual luminosity distance appropriate for electromagnetic signal, $D_L^{\rm em}(z)$, which is given by Eq. (6.1), and a GW luminosity distance $D_L^{\rm gw}(z)$, with,

$$D_L^{\rm gw}(z) = \frac{a(z)}{\tilde{a}(z)}\, D_L^{\rm em}(z)\,. \tag{6.13}$$

Standard sirens measure $D_L^{\rm gw}(z)$, rather than $D_L^{\rm em}(z)$. Eq. (6.9) can be rewritten as,

$$(\log a/\tilde{a})' = \delta(\eta)\mathcal{H}(\eta)\,, \tag{6.14}$$

whose integration gives (Belgacem et al., 2017, 2018b),

$$D_L^{\rm gw}(z) = D_L^{\rm em}(z)\, \exp\left\{-\int_0^z \frac{{\rm d}z'}{1+z'}\,\delta(z')\right\}\,. \tag{6.15}$$

To sum up, in modified gravity, all terms in Eq. (6.3) can in principle be different from GR. A modification of the source term affects the phase of the binary waveforms; the recent BH–BH observations, in particular of GW150914 and GW151226, have set some limit on such modifications, although for the moment not very stringent (Abbott et al., 2016d). A late time modification of the $\vec{k}^2\tilde{h}_A$ term changes the current speed of gravity, and is now basically excluded. A modification of the $2\mathcal{H}\tilde{h}'_A$ term changes the amplitude of the GW signal received from a source at cosmological distance. This is particularly interesting because it implies that the luminosity distance measured with standard sirens is in principle different from that measured with standard candles or other electromagnetic probes such as CMB or BAO. This could therefore provide a "smoking gun" signature of modified gravity.

In Sec. 4.3.3, we have seen that the modified propagation equation for tensors reads,

$$\tilde{h}''_A + 2\mathcal{H}\left(1 - \frac{1}{2\mathcal{H}}\partial_\eta \log\left(G_{\rm eff,gw}(\eta)/G\right)\right)\tilde{h}'_A + \vec{k}^2\tilde{h}_A = 16\pi G_{\rm eff,gw}(\eta)\, a^2\, \tilde{\sigma}_A\,. \tag{6.16}$$

where,

$$G_{\rm eff,gw}(\eta)/G \equiv \left(1 - \frac{m^2}{3}\bar{S}(\eta)\right)^{-1}\,. \tag{6.17}$$

First, we see that the coupling of gravitational waves to the source is modified by an effective Newton's constant $G_{\rm eff,gw}(\eta)$. In Sec. 4.4.1, we have found that this was the small scale limit of the effective Newton's constant computed in the scalar sector, from the Poisson equation Eq. (4.4.1). As such, the issue drawn into Sec. 4.4.1, about the residual time dependence of the Newton's constant in the small scale limit applies here as well, that is, does this dependence get screened once one considers the system into cluster-scale virialised objects? If this is true, the production mechanism of GWs will not be altered by the modification of GR provided by RR, otherwise, this would induce a change in the phase of inspiralling binaries, as this function differs from G at a few percent level at low redshifts (see the right panel of Fig. 4.5). Such a question still deserves further attention.
Second, observe that the speed of gravity is unchanged and,

$$\delta(\eta) = \frac{1}{2\mathcal{H}}\partial_\eta \log\left(G_{\rm eff,gw}(\eta)/G\right) \quad \Leftrightarrow \quad \delta(z) = -(1+z)\mathcal{H}\,\partial_z \log\left(\sqrt{G_{\rm eff,gw}(z)/G}\right)\,, \tag{6.18}$$

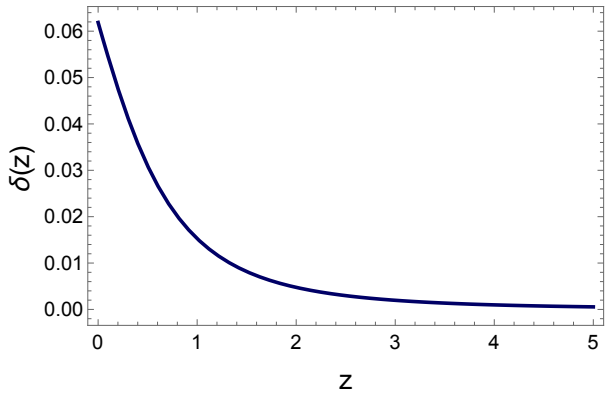

Figure 6.1 – The function $\delta(z)$ in the RR nonlocal model.

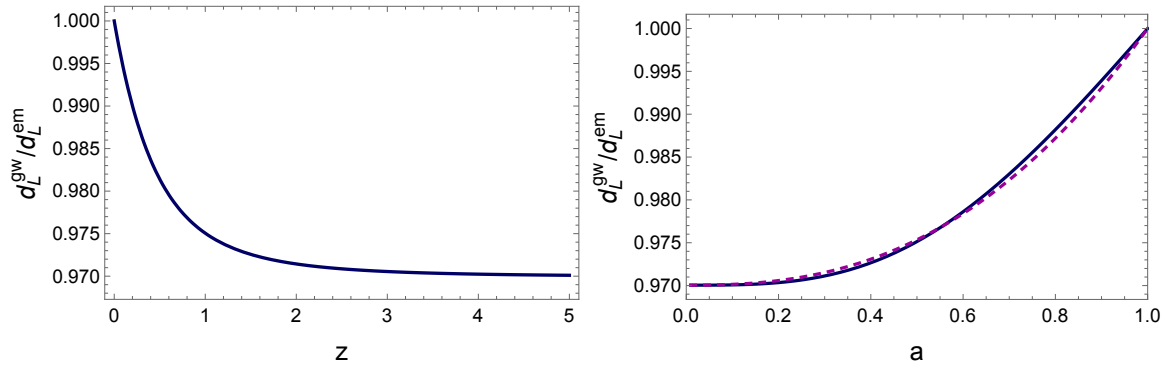

Figure 6.2 – The ratio $D_L^{\rm gw}(z)/D_L^{\rm em}(z)$ in the RR nonlocal model, as a function of redshift (left panel) and as a function of the scale factor a (solid line), compared to the fitting function (6.20) with $n = 5/2$ (dashed) (right panel).

which is shown in the left panel of Fig. 6.1 as a function of redshift. At large redshifts, this function goes to zero because the modifications to GR only appear close to the recent cosmological epoch. The corresponding ratio of the gravitational and electromagnetic luminosity distances is given by (Belgacem et al., 2017),

$$D_L^{\rm gw}(z) = D_L^{\rm em}(z)\sqrt{\frac{G_{\rm eff}(z)}{G_{\rm eff}(0)}}\,. \tag{6.19}$$

where we have replaced $G_{\rm eff,gw}$ by $G_{\rm eff}$, in taking the subhorizon limit, valid for the processes involved here. It is interesting to observe that this characteritic structure involving $G_{\rm eff}$, which parametrises the modification of the growth of structures, is also recovered in a subclass of Horndeski theories called "no slip gravity" (Linder, 2018). The ratio of the luminosity distance from GWs to the one from optical sources is shown in Fig. 6.2. The fact that $\delta(z)$ goes to zero at large z implies that $D_L^{\rm gw}(z)/D_L^{\rm em}(z)$ saturates to a constant value, while $[D_L^{\rm gw}/D_L^{\rm em}](z=0) = 1$, because all notions of distance in cosmology become equivalent as $z \to 0$. In the right panel of Fig. 6.2, we show the same ratio as a function of the scale factor a, and we compare it with the simple fitting function,

$$\frac{D_L^{\rm gw}(a)}{D_L^{\rm em}(a)} = \Xi_0 + a^n(1-\Xi_0)\,, \tag{6.20}$$

with $n = 5/2$ and $\Xi_0 = 0.970$. Observe that the parametrisation (6.20) is such that, for small a, i.e. at large redshift, $D_L^{\rm gw}(z)/D_L^{\rm em}(z)$ goes to the constant value Ξ_0, while at $a = 1$,

$D_L^{\rm gw}(z)/D_L^{\rm em}(z) = 1$. Note that this simple parametrisation reproduces the exact function quite well in that case.

Modified propagation equation of the form of Eq. (6.7) have also been previously found in other modified gravity models. To the best of our knowledge this was first observed in (Deffayet and Menou, 2007) within the DGP model (Dvali et al., 2000) described in Sec. 2.4. In this case, the effect is due to the fact that gravity leaks into extra dimensions at scales larger than the DGP scale, and this affects the $1/a$ behavior of the amplitude of a gravitational signal. A more recent discussion of the modification to the GW luminosity distance induced by the leakage of gravity into extra dimension is given in (Pardo et al., 2018), where this effect is used to put constraints on the number of extra dimensions or on the associated screening scale. Modification of the propagation equation has also been found in Einstein-Aether models and in scalar-tensor theories of the Horndeski class in (Saltas et al., 2014; Lombriser and Taylor, 2016; Amendola et al., 2017b; Arai and Nishizawa, 2017; Linder, 2018). This indicates that a modified propagation equation for the tensor modes of the form of Eq. (6.7) is quite generic in alternatives to ΛCDM; see also (Gleyzes et al., 2015b) for a discussion within the effective field theory approach to dark energy, and (Nishizawa, 2017) for a general formalism for testing gravity with GW propagation.

Observe also that, when $\delta(z) > 0$ at all redshifts, as in the RR model, (or more generally, when $\int_0^z {\rm d}z'/(1+z')\delta(z') > 0$), we have $D_L^{\rm gw}(z) < D_L^{\rm em}(z)$. Since the GW amplitude is proportional to $1/D_L^{\rm gw}(z)$, this means that a GW source is magnified with respect to the GR prediction, and can therefore be seen to larger distances.

6.3 Measuring w_0, w_a, Ξ_0 with Standard Sirens

We next discuss the prospects for measuring the dark energy equation of state and modified GW propagation from experiments like *LISA* or *ET*.

6.3.1 Understanding the Role of Degeneracies

Before presenting the results of the MCMC analysis on the accuracy of w_0, w_a and Ξ_0, given forecasts of standard sirens together with data from other probes, it is useful to understand in physical terms why the parameter Ξ_0 [or, more generally, the function $\delta(z)$], that describes modified GW propagation, can be more relevant than the dark energy equation of state $w_{\rm de}(z)$, for studies of dark energy with standard sirens. To this purpose, let us first start from a simple wCDM model, with a fixed value of w_0, and let us ask how a set of measurements of the luminosity distances with standard sirens could help in discriminating it from ΛCDM. For wCDM, $w_{\rm de}(z) = w_0$ is constant and the dark energy conservation equation implies [see Eq. (4.37)],

$$\Omega_{\rm de} = \Omega_{\rm de}(1+z)^{3(1+w_0)}\,, \tag{6.21}$$

where $\Omega_{\rm de}$ is fixed in terms of Ω_M by the flatness condition, $\Omega_M + \Omega_{\rm de} = 1$. Thus,

$$D_L(z; H_0, \Omega_M, w_0) \;=\; \frac{1+z}{H_0}\int_0^z \frac{{\rm d}z'}{\sqrt{\Omega_M(1+z')^3 + (1-\Omega_M)(1+z')^{3(1+w_0)}}}\,,$$

where we have written explicitly the dependence on the cosmological parameters. We first consider,

$$\frac{\Delta D_L}{D_L} \equiv \frac{D_L(z; H_0, \Omega_M, w_0) - D_L^{\Lambda{\rm CDM}}(z; H_0, \Omega_M)}{D_L^{\Lambda{\rm CDM}}(z; H_0, \Omega_M)}\,. \tag{6.22}$$

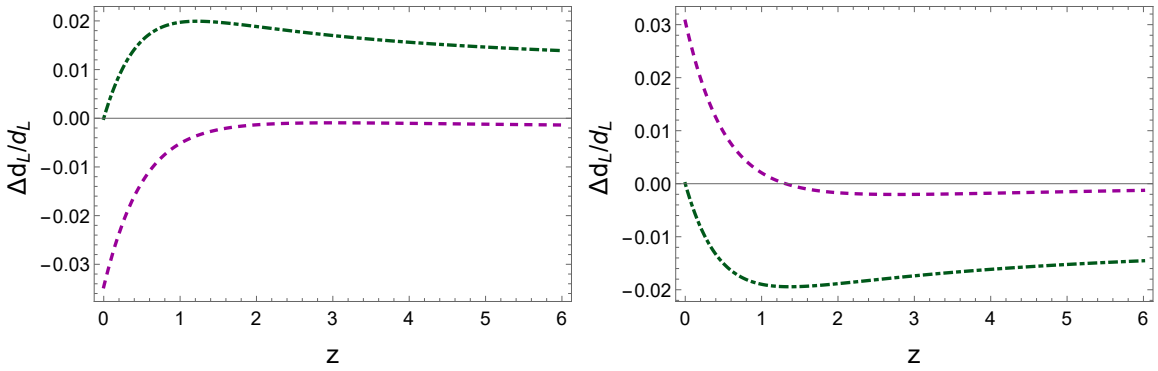

Figure 6.3 – The relative difference $\Delta D_L/D_L$ between wCDM with $w = -1.1$ and ΛCDM (left panel) and wCDM with $w = -0.9$ and ΛCDM (right panel). Green, dot-dashed curve: using the same values of Ω_M, H_0 for the two models. Magenta, dashed curve: using in each model its own best-fit values of Ω_M, H_0.

This is the relative difference between the luminosity distance in wCDM with a given value of w_0, and the luminosity distance in ΛCDM (where $w_0 = -1$), at fixed Ω_M, H_0. For $w_0 = -1.1$ ($w_0 = -0.9$), this quantity is shown as the green, dot-dashed curve in the left panel (right panel) of Fig. 6.3.

However, as the nature of the dark energy affects the Hubble parameter through a different dark energy density (6.21), constraints from model independent distance scales, such as the acoustic-distance scale ratio at recombination [see Eq. (5.7)], or the BAO/SNIa distance ladders, will generically shift H_0 and Ω_M to compensate for the change in w. Therefore, the above quantity is not the one relevant to observations and one musts not only use the chosen value of w_0 in Eq. (6.22), but also the predictions of wCDM for Ω_M and H_0, that are obtained by constraining wCDM given distance indicators provided by CMB+BAO+SNIa data. Moreover, this must be compared with the prediction of ΛCDM obtained in the same way. Thus the relevant quantity, when comparing the predictions of wCDM with w_0 fixed to the predictions of ΛCDM is rather,

$$\overline{\left(\frac{\Delta D_L}{D_L}\right)} \equiv \frac{D_L(z; H_0^{w_0}, \Omega_M^{w_0}, w_0) - D_L^{\Lambda\mathrm{CDM}}(z; H_0, \Omega_M)}{D_L^{\Lambda\mathrm{CDM}}(z; H_0, \Omega_M)}\,, \tag{6.23}$$

where we have denoted by $H_0^{w_0}, \Omega_M^{w_0}$ the values obtained from parameter estimation in wCDM with the given w_0, and by H_0, Ω_M the values obtained in ΛCDM (more precisely, one should use the relative derived priors in the two models; in this discussion we will use the best-fit values for making the presentation simpler). We quantify this statement by a series of MCMC constructed for constraining both ΛCDM and wCDM (with $w = -1.1$ and with $w_0 = -0.9$) given the same dataset of cosmological observations. In particular, we use the CMB+BAO+SNIa dataset described in detail in Sec. 5.1.1. Given these data, Bayesian parameter estimation for ΛCDM gives the best-fit parameters [3],

$$H_0 = 67.64\ \mathrm{km\,s^{-1}\,Mpc^{-1}}\,, \qquad \Omega_M = 0.3087\,, \tag{6.24}$$

In contrast, for wCDM with $w_0 = -1.1$, we get,

$$H_0 = 70.10\ \mathrm{km\,s^{-1}\,Mpc^{-1}}\,, \qquad \Omega_M = 0.2908\,, \tag{6.25}$$

3. These correspond to the best-fit values obtained from the distributions given in Sec. 5.1.3, given the CMB+BAO+SNIa data (see the upper right panel of Table 5.1).

while, for wCDM with $w_0 = -0.9$, we find,

$$H_0 = 65.66 \text{ km s}^{-1} \text{ Mpc}^{-1}\,, \qquad \Omega_M = 0.3241\,. \tag{6.26}$$

The magenta dashed curves in Figs. 6.3 show the relative difference in luminosity distance (6.23), obtained using for each model its own best-fit values of H_0 and Ω_M. We see two important effects.

1. At redshifts $z \gtrsim (1\text{–}2)$, the relative difference of luminosity distances becomes much smaller (in absolute value) than that obtained by keeping Ω_M and H_0 fixed (and given by the green dot-dashed curves), and this suppression is of about one order of magnitude. For instance, for $w_0 = -1.1$, keeping fixed Ω_M and H_0, the relative difference of luminosity distances at $z = 2$ is 1.77%, while, once parameter estimation in the respective models is taken into account, this becomes -0.16%.
2. As $z \to 0$, the green curves in the two panels of Fig. 6.3 go to zero. This is of course a consequence of the fact that, for $z \ll 1$, (6.1).(6.2) reduces to $D_L(z) \simeq H_0^{-1} z$, and to compute the green curves we have used the same value of H_0 in the two models. In contrast, the magenta curves do not go to zero, since for each model we are using its own bestfit value of H_0 given CMB+BAO+SNIa data. Observe that the fact that the relative difference in Eq. (6.23) does not go to zero at $z = 0$ is precisely the reason that allows the *LIGO/Virgo* measurement of H_0 to have potentially interesting cosmological consequences. Bayesian parameter estimation to the CMB data in different cosmological models predict different values of H_0, and therefore a local measurement of H_0, whether with standard candles or with standard sirens, can discriminate among different cosmological models.

If GW propagation is the same as in GR, the feature that one needs to detect with standard sirens, to distinguish the modified gravity model from ΛCDM, is then given by the magenta lines in both panel of Fig. 6.3, which is much smaller (in absolute value) than the one that would be obtained if H_0 and Ω_M were externally fixed quantities, determined independently of the cosmological model (green dot-dashed lines).

Let us now assume that, in the modified gravity theory of interest, on top of a modified dark energy equation of state, there is also a modified GW propagation. Then, for standard sirens, the relevant quantity is the GW luminosity distance $D_L^{\rm gw}(z)$ given in Eq. (6.15). In particular, for models (such as the RR model), where the parametrisation (6.20) is valid at redshifts $z \gtrsim 0.5\text{–}1$ relevant for *LISA* and *ET*, $D_L^{\rm gw}(z)$ basically differs from $D_L^{\rm em}(z)$ by the factor Ξ_0. In contrast, in ΛCDM the luminosity distance for standard sirens is the same as the standard electromagnetic luminosity distance. Thus, the relevant quantity for discriminating a modified gravity model from ΛCDM is now,

$$\overline{\left(\frac{\Delta D_L}{D_L}\right)}^{\rm gw} \equiv \frac{D_L^{m,{\rm gw}}(z; H_0^m, \Omega_M^m) - D_L^{\Lambda{\rm CDM}}(z; H_0, \Omega_M)}{D_L^{\Lambda{\rm CDM}}(z; H_0, \Omega_M)}\,, \tag{6.27}$$

where the superscript "m" denotes the quantities relative to the modified gravity model, given the data. Writing, $D_L^{m,{\rm gw}} \simeq \Xi_0 D_L^{m,{\rm em}}$, we get,

$$\begin{aligned}\overline{\left(\frac{\Delta D_L}{D_L}\right)}^{\rm gw} &\simeq (\Xi_0 - 1)\frac{D_L^{m,{\rm em}}(z; H_0^m, \Omega_M^m)}{D_L^{\Lambda{\rm CDM}}(z; H_0, \Omega_M)} + \frac{D_L^{m,{\rm em}}(z; H_0^m, \Omega_M^m) - D_L^{\Lambda{\rm CDM}}(z; H_0, \Omega_M)}{D_L^{\Lambda{\rm CDM}}(z; H_0, \Omega_M)} \\ &\simeq (\Xi_0 - 1) + \overline{\left(\frac{\Delta D_L}{D_L}\right)}\,. \end{aligned} \tag{6.28}$$

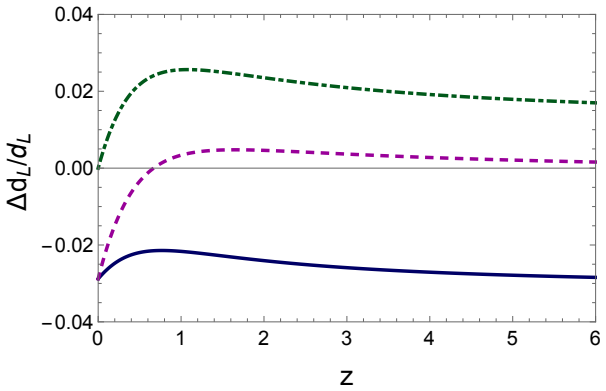

Figure 6.4 – The relative difference $\Delta D_L/D_L$ between the nonlocal RR model and ΛCDM. Green, dot-dashed curve: using the same values of Ω_M, H_0 for the two models. Magenta, dashed curve: using in each model its own best-fit values of Ω_M, H_0. Blue solid curve: the relative difference using, for the RR model, the GW luminosity distance (and the respective best-fit values of Ω_M, H_0 for the two models).

The last term is the relative difference in the electromagnetic luminosity distances introduced in Eq. (6.23). We have seen in the example of wCDM with $w_0 = -0.9$ or -1.1 that, even if w_0 differ from -1 by 10%, eventually, because of the compensating effect of H_0 and Ω_M, this term in absolute value is only of order (0.1–0.2)%. Thus, if Ξ_0 differs from one by more than this, it will dominate the signal. This is indeed what happens in the RR model, where $w_{\rm de}(z)$ differs from -1 by about 15%, quite similarly to the wCDM model with $w_0 = -1.1$, and $|\Xi_0 - 1| \simeq 3\%$, as we see from Fig. 6.2. The situation for the relative difference of luminosity distances in the RR model is illustrated in Fig. 6.4, where the green and magenta curves are obtained as in Fig. 6.3, while the blue solid curve is the relative difference of luminosity distances (6.27) where, for the RR model, we use the GW luminosity distance which is different than from its optical counterpart, unlike in ΛCDM. We see that the features that allows us to distinguish the RR model from ΛCDM, represented by the blue curve, is much larger in absolute value than that obtained neglecting modified GW propagation, represented by the dashed magenta curve. These results illustrates that, in modified gravity theories where GW propagation differs from GR, the measurement of luminosity distances of standard sirens can be more sensitive to modified propagation than to the dark energy equation of state. It implies that the prospects for detecting deviations from ΛCDM, in particular for next generation intereferometers, are better than previously expected.

6.3.2 Standard Sirens and Modified Gravity with ET

We now wish to determine more quantitatively the prospects for studying dark energy and modified gravity with future GW experiments, performing parameter estimation forecasts for standard sirens combined with CMB+BAO+SNIa real (prior) data. For definiteness, we will focus on *ET*. At its projected sensitivity, *ET* could have access to binary neutrons star (BNS) mergers up to redshifts $z \sim 8$, corresponding to 10^5–10^6 events per year (Sathyaprakash et al., 2010). However, only a fraction of the GW events will have an observed associated γ-ray burst. Estimates of the probability of observing the γ-ray burst are quite uncertain, depending on the opening angle of the jet (typically estimated between 5° and 20°) and of the efficiency of the network of existing and future γ-ray telescopes (Regimbau et al., 2015). A typical working hypothesis is that *ET* might observe $\mathcal{O}(10^3)$ BNS with electromagnetic counterpart over a

three-year period (Sathyaprakash et al., 2010; Zhao et al., 2011) [4].

We then proceed as follows. We generate a catalog of BNS detections for *ET*, with $N_s = 10^3$ sources, all taken to have an electromagnetic counterpart. We choose a fiducial model, that we take to be ΛCDM with $H_0 = 67.64$ and $\Omega_M = 0.3087$, and we generate our simulated data assuming that, for a source at redshift z_i, the actual luminosity distance will be $D_L^{\Lambda\mathrm{CDM}}(z_i; H_0, \Omega_M)$. The measured value of the luminosity distance is then randomly extracted from a Gaussian distribution centered on $D_L^{\Lambda\mathrm{CDM}}(z_i; H_0, \Omega_M)$ and width $\sigma_i \equiv \Delta D_L(z_i)$ obtained from an estimate of the error on the luminosity distance at *ET*. For this error, we assume the expression given in (Zhao et al., 2011),

$$\frac{\Delta D_L(z)}{D_L(z)} = 0.1449z - 0.0118z^2 + 0.0012z^3 \,. \tag{6.29}$$

To generate our catalog of events, we use the standard expression of the number density of the observed events between redshift z and $z + \mathrm{d}z$, which is given by $f(z)\mathrm{d}z$, where,

$$f(z) = \frac{4\pi \mathcal{N} r(z) D_L^2(z)}{H(z)(1+z)^3} \,, \tag{6.30}$$

and $r(z)$ is the coalescence rate at redshift z [see e.g. (Zhao et al., 2011)] [5]. The normalisation constant $\mathcal{N}$ is determined by requiring that the total number of sources N_s be given by,

$$N_s = \int_{z_{\min}}^{z_{\max}} \mathrm{d}z \, f(z) \,. \tag{6.31}$$

We take $z_{\max} = 2$, as in (Zhao et al., 2011), to have a typical signal-to-noise ratio above 8, and we also use a lower cutoff $z_{\min} = 0.03$, to exclude sources for which a modelisation of the local Hubble flow is necessary, before including them in the analysis. For $r(z)$, we follow (Cutler and Holz, 2009; Zhao et al., 2011; Cai and Yang, 2017) and we use the form $r(z) = (1 + 2z)$, for $z \leq 1$, $r(z) = (15 - 3z)/4$ for $1 < z < 5$, and $r(z) = 0$ for $z \geq 5$, that is based on a fit to the observationally determined star formation history discussed in (Schneider et al., 2001). A sample of the luminosity distance of 1000 sources generated according to these distributions is shown in the left panel of Fig. 6.5, while in the right panel, we show their number distribution, as a function of redshift.

We then perform parameter estimation in using MCMC methods for constraining H_0, Ω_M, and different combinations of w_0, w_a and Ξ_0, as specified below, assuming for the GW luminosity distance the form Eq. (6.20) with $n = 5/2$, [6] and we study to what forecast accuracy we are able to recover the values $w_0 = -1$, $w_a = 0$ and $\Xi_0 = 1$ of our fiducial ΛCDM model.

4. Information of the redshift could also be obtained statistically, by exploiting the narrowness of the neutron star mass function [see (Taylor and Gair, 2012) and references therein] or by using tidal effects in neutron stars (Messenger and Read, 2012).

5. Equation (6.30) is derived by observing that the comoving volume between comoving distances $D_c(z)$ and $D_c(z) + \mathrm{d}(D_c)$ is $4\pi D_c^2(z)\mathrm{d}(D_c)$. One then uses $\mathrm{d}(D_c) = [\mathrm{d}(D_c)/\mathrm{d}z]\mathrm{d}z = \mathrm{d}z/H(z)$, and $D_c(z) = D_L(z)/(1+z)$. Thus the observed event distribution is proportional to $4\pi(\mathrm{d}n/\mathrm{d}t_{\mathrm{obs}})D_L^2(z)/[H(z)(1+z)^2]$, where $\mathrm{d}n/\mathrm{d}t_{\mathrm{obs}}$ is the number of events per unit time in the observer frame. Time in the observer frame, t_{obs}, is related to time in the source frame, t_s, by $\mathrm{d}t_{\mathrm{obs}} = (1+z)\mathrm{d}t_s$, which provides the extra factor of $(1+z)$ at the denominator. Thus $r(z)$ is the number of event per unit time, with respect to the unit of time relevant at redshift z.

6. We expect that the precise choice of the value of n will be of limited relevance. Indeed, the parametrisation (6.20) is meaningful for a class of theories where the modifications to GR start to become important only in the recent epoch, so that $\delta(z)$ vanishes at large z. Then, $D_L^{\mathrm{gw}}(z)/D_L^{\mathrm{em}}(z)$ goes to a constant at large z, as in Fig. 6.2. Since most of the sources for *ET* or *LISA* are at $z \gtrsim 0.5$, in a first approximation one could even replace $D_L^{\mathrm{gw}}(z)/D_L^{\mathrm{em}}(z)$ just by its asymptotic constant value Ξ_0. The value of n only determines the precise way in which $D_L^{\mathrm{gw}}(z)/D_L^{\mathrm{em}}(z)$ approaches unity as $z \to 0$.

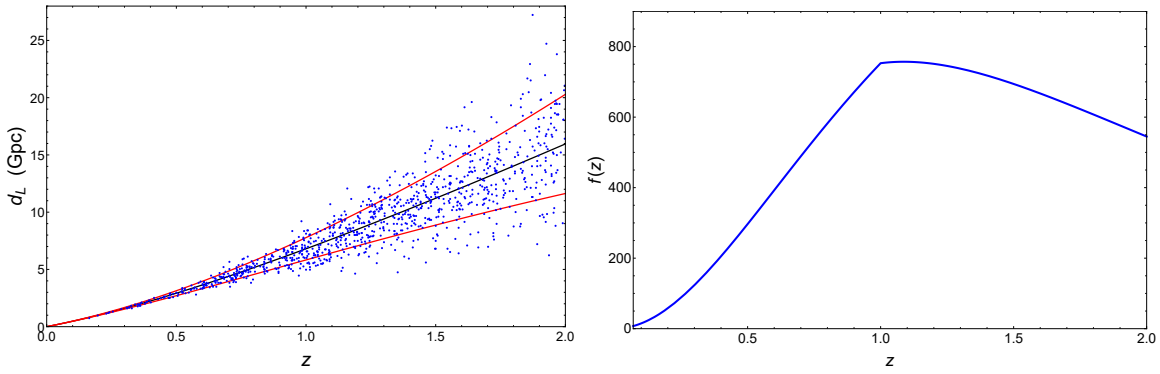

Figure 6.5 – Left panel: a sample of 1000 sources distributed in redshift according to eq. (6.30), and scattered in $D_L(z)$ according to the ET error estimate (6.29). The black and red curves show the theoretical prediction for $D_L(z)$ and the 1σ ET error, respectively. The cosmological model assumed is ΛCDM with $\Omega_M = 0.3087$ and $H_0 = 67.64$. Right panel: the number distribution of the sources as a function of the redshift.

As already discussed in (Zhao et al., 2011; Cai and Yang, 2017), because of the degeneracies with H_0 and Ω_M, limited information can be obtained on w_0 and w_a by using only standard sirens. Moreover, as can be seen for instance from the parameter dependence of $D_L^{\rm gw}(z)$ in Eq. (6.28), this also extends to Ξ_0. Indeed, by using 10^3 standard sirens and no other datasets, using (w_0, Ξ_0) as extra parameters with respect to ΛCDM, and computing the corresponding one-dimensional marginalised likelihoods for w_0 or for Ξ_0, we obtain that w_0 and Ξ_0 can be measured with an error $\Delta w_0 = 0.41$ and $\Delta\Xi_0 = 0.17$, respectively, given ET forecast sensitivity. As expected, this level of accuracy is not very interesting, particularly for w_0, and we need other cosmological datasets to break the degeneracies, so as to tighten these constraints. In particular, we use the same CMB, BAO and SNIa datasets that we used here-above and in Sec. 5. We examine separately the cases where we include only w_0, the pair (w_0, w_a), or the two parameters (Ξ_0, w_0), as extensions of the standard ΛCDM model.

(1) We first consider the wCDM model, where w_0 is the only extra parameter. The left panel of Fig. 6.6 shows the two-dimensional marginalised likelihood in (w_0, Ω_M) plane, with the separate contributions from standard sirens, *Planck* 2015 CMB data, BAO and *JLA* SNIa. From the corresponding one-dimensional marginalised likelihood, we obtain $\Delta w_0 = 0.049$ given CMB+BAO+SNIa, and

$$\Delta w_0 = 0.032\,, \tag{6.32}$$

when joining also 10^3 standard sirens.

(2) We next consider the (w_0, w_a) CPL parametrisation [see Eq. (4.41)]. The right panel of Fig. 6.6, shows the two-dimensional marginalised likelihood in (w_0, w_a) plane, again with the separate contributions from standard sirens, CMB, BAO and SNIa. From the corresponding one-dimensional marginalised likelihoods, we find that w_0 and w_a can be reconstructed with the accuracy,

$$\Delta w_0 = 0.099\,,\,, \qquad \Delta w_a = 0.313\,. \tag{6.33}$$

Following (Huterer and Turner, 2001; Hu and Jain, 2004; Albrecht et al., 2006; Zhao et al., 2011), it is convenient to express the results in terms of the constraint on $w(z)$ at the best pivot redshift z_p, defined as the value of redshift for which $w(z)$ is best constrained. For the (w_0, w_a) parametrisation, the pivot scale factor a_p is obtained by minimising $\langle(\delta w_0 + (1-a)\delta w_a)^2\rangle$, where

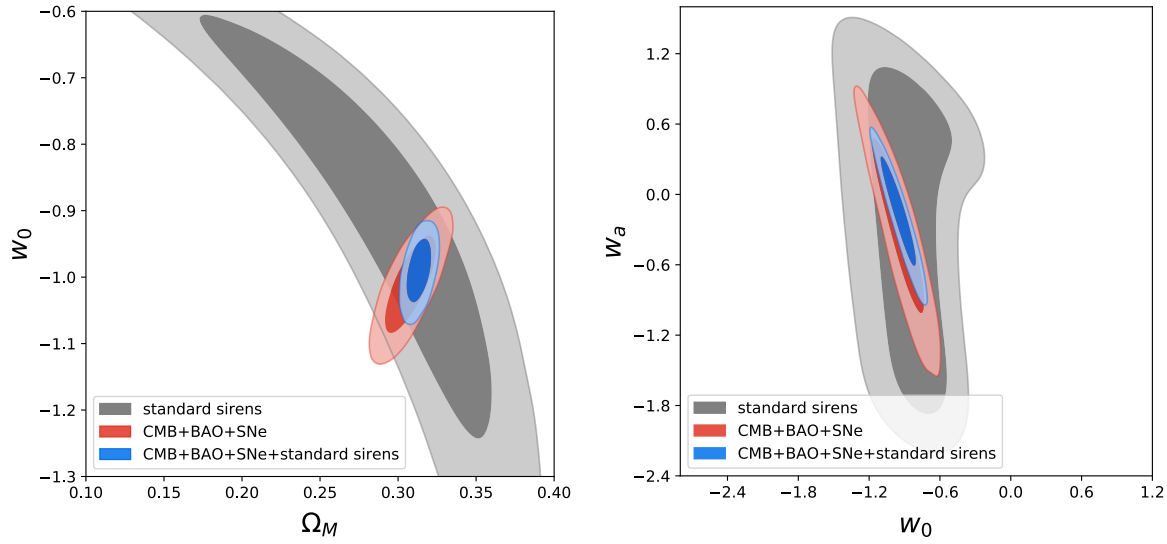

Figure 6.6 – Two-dimensional marginalised likelihood in the (Ω_M, w_0) plane in wCDM (left panel) and in the (w_0, w_a) plane in $w_0 w_a$CDM (right panel), with the contribution from CMB+BAO+SNIa (red), the contribution from 10^3 standard sirens at ET (grey) and the overall combined contours (blue). Dark and light shaded regions represent 1 and 2σ uncertainties respectively.

$(\Delta w_0)^2 = \langle(\delta w_0)^2\rangle$ and $(\Delta w_a)^2 = \langle(\delta w_a)^2\rangle$. This gives,

$$1 - a_p = -\frac{\langle \delta w_0 \delta w_a \rangle}{(\Delta w_a)^2}\,, \tag{6.34}$$

and is in the cosmological past if the correlation $\langle \delta w_0 \delta w_a \rangle$ is negative. One can then show (Albrecht et al., 2006), that at the Fisher matrix level, i.e. assuming that the likelihood is Gaussian in all parameters, the error on $w_p \equiv w(z_p)$ is the same as the error on w_0 in the wCDM model, in which the dark energy equation of state is taken to be constant in time. For the pivot redshift, given by $1 + z_p = 1/a_p$, Eq. (6.34) gives,

$$z_p = -\left(1 + \frac{\Delta w_a}{\rho \Delta w_0}\right)^{-1}\,, \tag{6.35}$$

where,

$$\rho \equiv \frac{\langle \delta w_0 \delta w_a \rangle}{\Delta w_0 \Delta w_a}\,, \tag{6.36}$$

is the correlation coefficient of w_0 and w_a. The corresponding error on w_p is then given by,

$$\Delta w_p = \Delta w_0 \sqrt{1 - \rho^2}\,. \tag{6.37}$$

Using the values for Δw_0 and Δw_a found in Eq. (6.33), the corresponding value $\rho = -0.909$ from parameter estimation, and inserting them into Eqs. (6.35),(6.37), one obtains,

$$z_p = 0.402\,, \qquad \Delta w_p = 0.041\,. \tag{6.38}$$

Observe that this value is larger but consistent with the one given in eq. (6.32). These results can be directly compared with that of (Zhao et al., 2011), as we have followed their strategy

for generating the catalogue of sources, through Eqs. (6.29), (6.30), and we are using the same number of standard sirens, $N_s = 10^3$. With respect to (Zhao et al., 2011), we are performing a Bayesian analysis, rather than a Fisher matrix analysis, and we are using the real *Planck* 2015 data rather than the forecasts [only available at the time when (Zhao et al., 2011) was written], as well as more recent data for SNIa and BAO, so our inference results for the (w_0, w_a) parametrisation can be considered as an updated of the results of (Zhao et al., 2011), that found $\Delta w_0 = 0.045$, $\Delta w_a = 0.174$ at a pivot redshift $z_p = 0.313$.

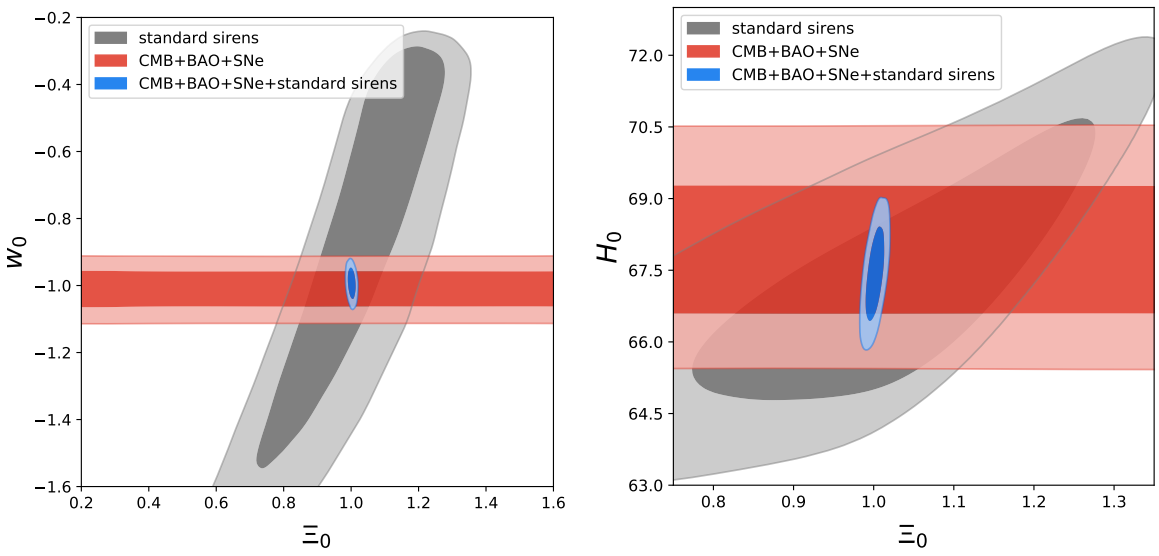

Figure 6.7 – The two-dimensional marginalised likelihood in the (Ξ_0, w_0) plane (left panel) and in the (Ξ_0, H_0) plane (right panel), with the combined contribution from CMB+BAO+SNIa (red), the contribution from 10^3 standard sirens at ET (grey), and the total combined result (blue). Dark and light shaded regions represent 1 and 2σ uncertainties respectively.

(3) We finally introduce also the parameter Ξ_0 in our extension of ΛCDM, writing the GW luminosity distance as in Eq. (6.20) (with $n = 5/2$), and taking (Ξ_0, w_0) as the parameters that describe the dark energy sector of the theory. The left panel of Fig. 6.7 shows the marginalised two-dimensional likelihood in the Ξ_0–w_0 plane, displaying the limit from CMB+BAO+SNIa (which is insensitive to Ξ_0), the separate contribution from standard sirens, and the combined limit from CMB+BAO+SNIa+standard sirens. The right panel of Fig. 6.7 and Fig. 6.8 show the analogous marginalised two-dimensional likelihoods in the Ξ_0–H_0 and in the Ξ_0–Ω_M plane, respectively. From the corresponding marginalised one-dimensional likelihoods we find,

$$\Delta\Xi_0 = 0.008\,, \quad \Delta w_0 = 0.032\,. \tag{6.39}$$

We see that Ξ_0 can be measured to a precision four times better than w_0, consistently with the discussion in Sec. 6.3.1. For the relative error on H_0 we find $\Delta H_0/H_0 = 1.8 \times 10^{-2}$ given the combined CMB+BAO+SNIa data, whereas joining also 10^3 standard sirens at *ET* it reduces to,

$$\frac{\Delta H_0}{H_0} = 1.0 \times 10^{-2}\,. \tag{6.40}$$

Note that by using only standard sirens, we get $\Delta H_0/H_0 = 2.8 \times 10^{-2}$, which is of course larger but still quite interesting.

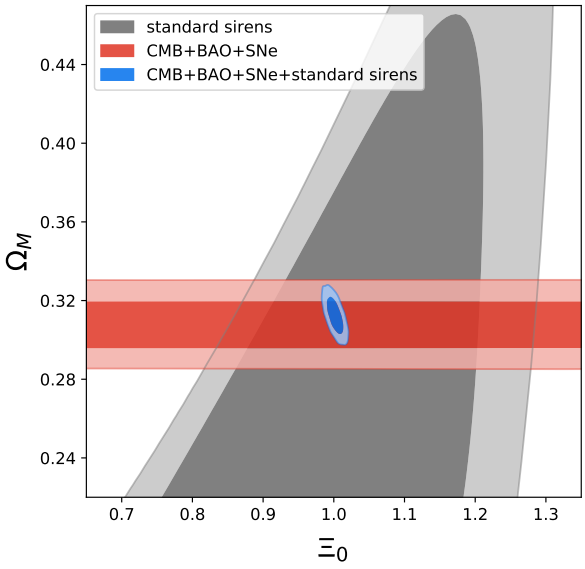

Figure 6.8 – The two-dimensional marginalised likelihood in the (Ξ_0, Ω_M) plane, with the combined contribution from CMB + BAO + SNIa (red), the contribution from 10^3 standard sirens (grey), and the total combined result (blue).

6.4 Testing the RR model with *ET*

In the previous section, we considered generic parametrisation made of Ξ_0, w_0, w_a, being phenomenological parametrisations that are expected to describe a large class of models, although in a less predictive manner. In that case, a natural way to proceed is to fix the number of standard sirens to a plausible value, and compute the corresponding accuracy that can be obtained on the parameters, as in Eq. (6.39). In this section, we consider a specific model, namely the RR nonlocal model presented in Sec. 3.2, and we rather ask what is the minimum number of standard sirens required to distinguish it from ΛCDM.

6.4.1 Testing the "Minimal" RR model

When, rather than a phenomenological parametrisation, we consider a concrete model, such as the RR model, that gives a specific prediction for $w_{\rm de}(z)$ and $\delta(z)$, the interesting question is what is the minimum number of standard sirens required to distinguish it from ΛCDM. To this purpose, we start by taking ΛCDM given CMB+BAO+SNIa data as fiducial cosmology, where $H_0 = 67.64$ and $\Omega_M = 0.3087$ [see Eq. (6.24)]. We then generate 10^4 samples each containing 10^3 BNS, distributed in redshift according to Eq. (6.30), and scattered in $D_L(z)$ according to the estimate (6.29) of the *ET* error, with sources from $z_{\rm min} = 0.03$ up to $z_{\rm max} = 2$, where the upper limit is chosen so as to obtain an average signal-to-noise ratio exceeding 8. Given a set of simulated data $D_i \equiv D_L(z_i)$, with their error $\sigma_i \equiv \Delta D_L(z_i)$, we can write the χ^2 goodness-of-fit for ΛCDM,

$$\chi^2_{\Lambda\rm CDM} = \sum_{i=1}^{N_s} \frac{[D_L^{\Lambda\rm CDM}(z_i; H_0, \Omega_M) - D_i]^2}{\sigma_i^2}\,, \tag{6.41}$$

Since the data D_i have been extracted from a distribution that assumes that ΛCDM is the true model, by construction for large N_s the reduced chi-square $\chi^2_{\Lambda\rm CDM}/N_s$ will be of order one.

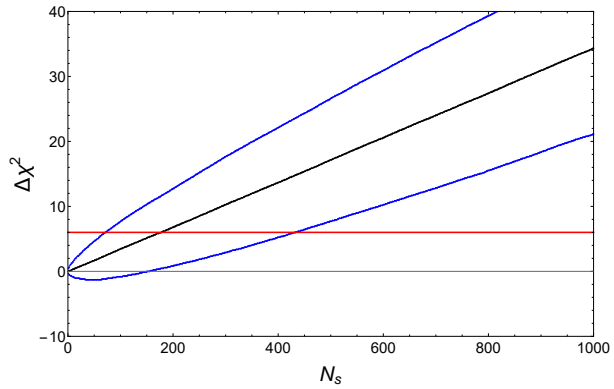

Figure 6.9 – Average and standard deviation of $\Delta\chi^2 = \chi^2_{\rm RR} - \chi^2_{\Lambda{\rm CDM}}$. The horizontal line corresponds to the threshold value $\Delta\chi^2 = 6$.

Similarly, we can write down the χ^2 for the prediction of the RR model,

$$\chi^2_{\rm RR} = \sum_{i=1}^{N_s} \frac{[D_L^{\rm gw,RR}(z_i; H_0^{\rm RR}, \Omega_M^{\rm RR}) - D_i]^2}{\sigma_i^2}\,, \tag{6.42}$$

where $D_L^{\rm gw,RR}$ is the GW luminosity distance of the RR model and $H_0^{\rm RR}$ and $\Omega_M^{\rm RR}$, are the best-fit values for the RR model obtained from CMB+BAO+SNIa, $\Omega_M = 0.2993$ and $H_0 = 69.44$ [7]. Since the data have been generated according to ΛCDM, for sufficiently large N_s the difference,

$$\Delta\chi^2 = \chi^2_{\rm RR} - \chi^2_{\Lambda{\rm CDM}}\,, \tag{6.43}$$

will become sufficiently large to rule out the RR model. We want to compute the minimum value of N_s for which $\Delta\chi^2$ goes above a threshold for which one can attest that ΛCDM fits the data significantly better than RR. We take this threshold value to be equal to 6. One can of course also reverse the process, generating the data according to the GW luminosity distance of the RR model, and ask what is the minimum value of N_s that is required to rule out ΛCDM, to the same significance. We have found that the procedure is completely symmetric, within our statistical uncertainty, and for definiteness, we show the results obtained by using ΛCDM as the fiducial model.

The result is shown in Fig. 6.9. First of all, one can observe that $\Delta\chi^2$ has a significant variability among the 10^4 realisations of the data that we have generated. We therefore show in Fig. 6.9 the average and the standard deviation of $\Delta\chi^2$ over these realisations, along with the reference line $\Delta\chi^2 = 6$. One can see that, on average, we need about 200 standard sirens to tell the two models apart. However, because of the large variability of $\Delta\chi^2$, to exclude that the result is due to statistical fluctuations, one would rather need about 400 sources in the pessimistic case. On the other hand, from the variability of $\Delta\chi^2$ over the different realisations, it also follows that in the more optimistic case, $\mathcal{O}(50)$ standard sirens could already give a highly significant value of $\Delta\chi^2$.

In order to understand which sources contribute most to this result, we have repeated the analysis limiting ourselves to sources with redshift $0.03 < z < 0.7$, and to sources with $0.7 < z < 2$. The results for $\Delta\chi^2$ obtained with sources with $0.03 < z < 0.7$ ($0.7 < z < 2$) is shown in the left (right) panel of Fig. 6.10. One see that, on average, it is enough to a have

7. Of course, more accurately, one should compute a likelihood with the corresponding priors, both for ΛCDM and for the RR model. However, this would not affect significantly the conclusions.

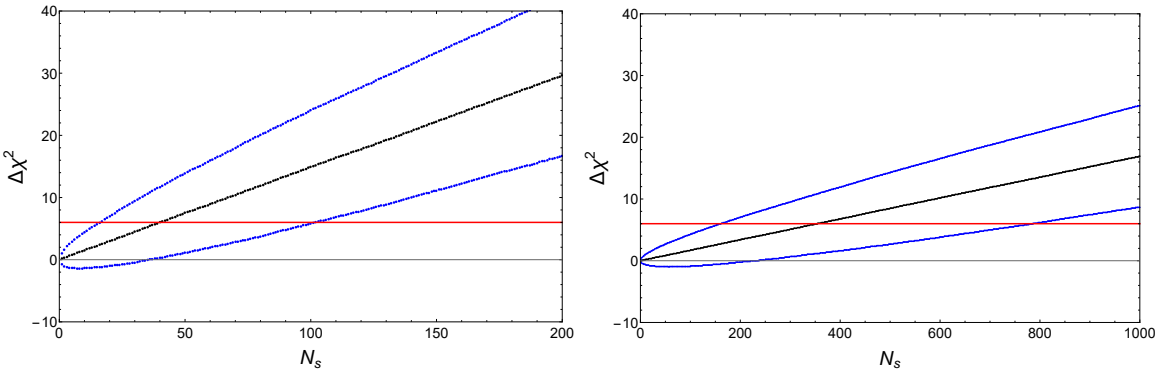

Figure 6.10 – As in Fig. 6.9, restricting to sources with redshift $0.03 < z < 0.7$ (left panel) and $0.7 < z < 2$ (right panel).

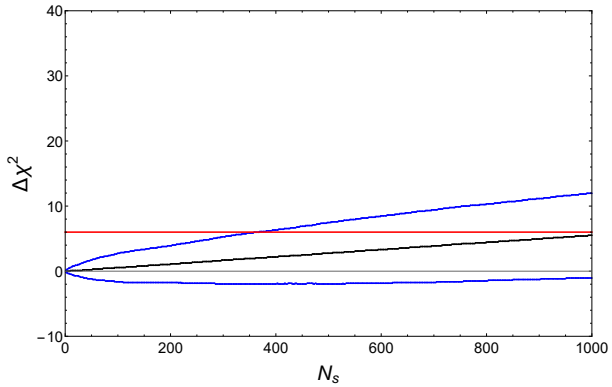

Figure 6.11 – As in Fig. 6.9, using the electromagnetic luminosity distance of the RR model.

about 40 standard sirens at $0.03 < z < 0.7$, or about 350 at $0.7 < z < 2$, to tell the two models apart. Depending on the specific realisation, in the most optimistic case it is sufficient to have about 15 standard sirens at $0.03 < z < 0.7$, or about 150 at $0.7 < z < 2$, while in the most pessimistic case we need about 100 standard sirens at $0.03 < z < 0.7$, or about 800 at $0.7 < z < 2$. These results fully confirm the conclusions of the simpler analysis performed in (Belgacem et al., 2017).

Furthermore, it is interesting to quantify how this result is affected by contributions from the dark energy equation of state of the RR model and from the modified GW propagation. To understand this point, we can artificially switch off the effect of modified GW propagation by using $D_L^{\rm em,RR}$ instead of $D_L^{\rm gw,RR}$ in eq. (6.42). The corresponding result is shown in Fig. 6.11. We see that in this case, the required number of sources is significantly higher. Indeed, the average $\Delta\chi^2$ goes above the threshold only with about 10^3 sources, while we found in Fig. 6.9 that, including also modified GW propagation, 200 sources are enough. Note also that, without the effect of modified GW propagation, the 1σ lower bound does not even have a positive $\Delta\chi^2$ with 10^3 sources. This clearly shows the importance of the effect of modified GW propagation.

6.4.2 The Model for Large Values of u_0

In this subsection, we repeat the analysis for large values of the parameter u_0. In the left panel of Fig. 6.12, we show $w_{\rm de}(z)$ for $u_0 = 250$. We see that it is now much closer to the ΛCDM value -1. Similarly, the right panel of the same figure shows the ratio $D_L^{\rm gw}(a)/D_L^{\rm em}(a)$,

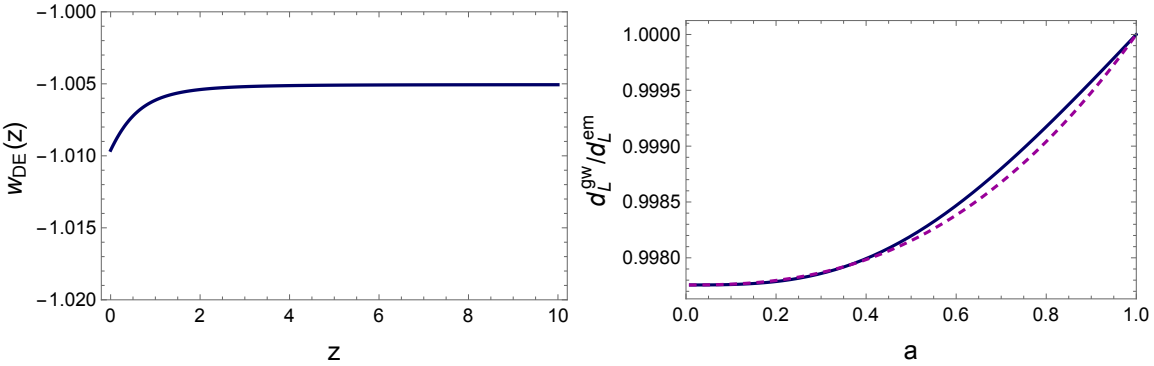

Figure 6.12 – Left panel: the dark energy equation of state in the RR nonlocal model with $u_0 = 250$. Right panel: the ratio $D_L^{\rm gw}(a)/D_L^{\rm em}(a)$ in the RR nonlocal model with $u_0 = 250$, as a function of the scale factor (solid line) compared to the fitting function (6.20) with $n = 5/2$ (dashed).

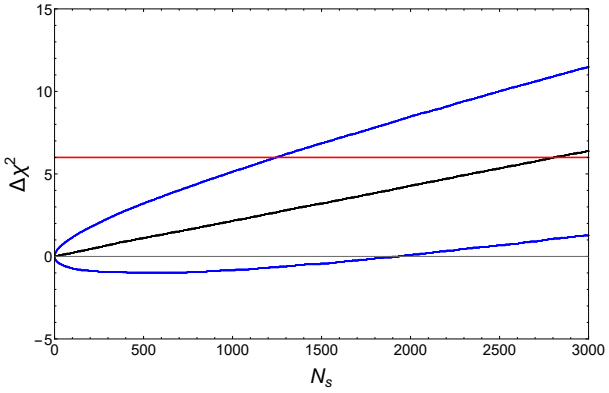

Figure 6.13 – As in Fig. 6.9, for $u_0 = 250$.

as well as the fitting function (6.20) with $\Xi_0 = 0.9978$ and $n = 5/2$ (a slightly better fit could be obtained with $n \simeq 2.3$). Determine the minimum number of standard sirens required to tell the RR model with $u_0 = 250$ apart from ΛCDM, Fig. 6.13 shows the result. In that case, on average, almost 3×10^3 sources are needed (raising to about 6×10^3 in the most pessimistic case). This is a large number of sources, but still within the number of standard sirens with electromagnetic counterpart that could be observed with *ET*, depending on the precise sensitivity (as well as on the capabilities of the γ-ray network). Furthermore, this study has been limited to standard sirens with an electromagnetic counterpart, but further information can be obtained using statistical methods, even in the absence of counterparts, see footnote 4.

6.5 Primordial GWs and Modified Transfer Function

A further consequence of modified GW propagation is that the GW transfer function that connects a primordial GW spectrum to the one observed at the present epoch is modified. Recall that the transfer function is defined by,

$$\tilde{h}_A(\eta_0, k) = T_{\rm GW}(k)\tilde{h}_A(\eta_{\rm in}, k)\,, \tag{6.44}$$

where η_0 is the present value of conformal time and $\eta_{\rm in}$ the initial value at which a primordial GW spectrum is generated. Basically, in GR the transfer function is determined by the fact

that, as long as a tensor mode is outside the horizon, it stays constant, while when it enters inside the horizon it scales as $1/a(\eta)$ times oscillating factors [see e.g. Section 19.5 of (Maggiore, 2018)]. Therefore,

$$\tilde{h}^2(\eta_0, k) \simeq \frac{1}{2}\tilde{h}^2(\eta_{\rm in}, k)\left(\frac{a_*(k)}{a_0}\right)^2 , \tag{6.45}$$

where $a_*(k)$ is the value of the scale factor when the mode with wavenumber k re-enters the horizon, a_0 is the present value of the scale factor, and the factor of $1/2$ comes from the average over the oscillating factors. A more accurate expression can be obtained following numerically the evolution across the super-horizon and sub-horizon regimes.

If the GW propagation is modified as in Eq. (6.8), inside the horizon the GW amplitude scales as $1/\tilde{a}$ rather than $1/a$. As a result, the transfer function in modified gravity is related to the GR transfer function by,

$$T^{\rm mod\,grav}(k) = \frac{\tilde{a}_*(k)}{\tilde{a}_0}\,\frac{a_0}{a_*(k)}\,T^{\rm GR}(k) = \frac{\tilde{a}_*(k)}{a_*(k)}T^{\rm GR}(k)\,, \tag{6.46}$$

where, as in Eq. (6.12), we can set $\tilde{a}(0) = a(0) = 1$, without loss of generality. Similarly to Eq. (6.15), we can rewrite this as,

$$T^{\rm mod\,grav}(k) = T^{\rm GR}(k)\,\exp\left(\int_0^{z_*(k)}\frac{{\rm d}z'}{1+z'}\,\delta(z')\right) . \tag{6.47}$$

In a model where $\delta(z)$ goes to zero at large redshifts, as the RR model, the integral saturates to its asymptotic value already at small values of z, as shown in Fig. 6.2, so it is equal to its asymptotic value $1/\Xi_0$, and is independent of k,

$$\begin{aligned} T^{\rm mod\,grav}(k) &= T^{\rm GR}(k)\,\exp\left(\int_0^{\infty}\frac{{\rm d}z'}{1+z'}\,\delta(z')\right) , \\ &= \Xi_0^{-1}\,T^{\rm GR}(k)\,. \end{aligned} \tag{6.48}$$

In the RR model, the factor Ξ_0^{-1} is larger than one and therefore enhances all GW spectra compared to the GR predictions. In terms of the energy density fraction $\Omega_{\rm gw}$, which is quadratic in the GW amplitude, we have,

$$\Omega_{\rm gw}^{\rm mod\,grav} = \Xi_0^{-2}\,\Omega_{\rm gw}\,, \tag{6.49}$$

and, in the RR model, $\Xi_0^{-2} \simeq 1.06$. Thus, for instance, the GW stochastic background generated by single-field slow roll inflation, in GR, is given by [see e.g. eq. (21.355) of (Maggiore, 2018)],

$$\Omega_{\rm gw}(f) = \frac{\pi^2}{3H_0^2}\,f^2|T_{\rm GW}(f)|^2\,r(k_*)A_{\mathcal{R}}(k_*)\,\left(\frac{f}{f_*}\right)^{n_T} , \tag{6.50}$$

where $k_* = 2\pi f_*$ is the pivot scale, r is the tensor-to-scalar ratio and $A_{\mathcal{R}}$ is the amplitude of the scalar perturbations. In modified gravity, this could change both because of modification of the production mechanism and because of modified GW propagation. In the RR model the effect of the nonlocal term at the inflationary scale is negligible (Maggiore, 2017; Belgacem et al., 2018a) and $\delta(z) = 0$ with great accuracy at the inflationary scale, so there is no modification in the generation of primordial GWs. However, the subsequent propagation is affected, and Eq. (6.51) becomes,

$$\Omega_{\rm gw}(f) = \frac{\pi^2}{3H_0^2}\,f^2|T_{\rm GW}(f)|^2\,\Xi_0^{-2}r(k_*)A_{\mathcal{R}}(k_*)\,\left(\frac{f}{f_*}\right)^{n_T} . \tag{6.51}$$

In other words, a measurement of the primordial inflationary background will not constrain directly the tensor-to-scalar ratio r, but rather the combination $\Xi_0^{-2} r$.

A similar correction enters in the ISW effect. The tensor contribution to the temperature anisotropies in the direction $\hat{n}$ is given by,

$$\frac{\delta T}{T}(\eta_0, \hat{n}) = -\frac{1}{2} n^i n^j \int_{\eta_{\rm dec}}^{\eta_0} {\rm d}\eta \left(\frac{\partial h_{ij}^{\rm TT}(\eta, \vec{x})}{\partial \eta} \right) \Big|_{\vec{x}=(\eta_0-\eta)\hat{n}} , \tag{6.52}$$

where $h_{ij}^{\rm TT}(\eta, \vec{x})$ is the transverse-traceless metric perturbation at conformal time η and position $\vec{x}$, and $\eta_{\rm dec}$ is the conformal time at decoupling. If $h_{ij}^{\rm TT}(\eta, \vec{x})$ is computed by evolving a primordial GW background up to conformal time η, in modified gravity its value at conformal time η will differ from the value in GR by a factor,

$$\alpha(\eta) \equiv \exp\left(\int_{z(\eta)}^{z_*(k)} \frac{{\rm d}z'}{1+z'} \, \delta(z') \right) \simeq \exp\left(\int_{z(\eta)}^{\infty} \frac{{\rm d}z'}{1+z'} \, \delta(z') \right) , \tag{6.53}$$

so that Eq. (6.52) can be written as,

$$\frac{\delta T}{T}(\eta_0, \hat{n}) = -\frac{1}{2} n^i n^j \int_{\eta_{\rm dec}}^{\eta_0} {\rm d}\eta \left(\frac{\partial [\alpha(\eta) h_{ij}^{\rm TT,gr}(\eta, \mathbf{x})]}{\partial \eta} \right) \Big|_{\vec{x}=(\eta_0-\eta)\hat{n}} ,$$

where $h_{ij}^{\rm TT,gr}(\eta, \vec{x})$ is the value computed in GR, by evolving to conformal time η a given primordial perturbation.

6.6 Summary

In this chapter, we have reviewed the recent work of (Belgacem et al., 2018c), where standard sirens and GWs propagation in modified gravity were studied. In particular, we have seen in Sec. 6.2, that beside a non-trivial dark energy equation of state $w_{\rm de}$, modified gravity models also typically modify the Hubble friction term of the propagation equations of GWs, which implies that the notion of luminosity distance for GWs is modified compared to the one provided by electromagnetic sources in those theories. This fact has been illustrated with an explicit example provided by the RR nonlocal model. In such a case, the ratio of the GW to the electromagnetic luminosity distance is well fitted by the parametrisation of Eq. (6.20), involving the pair (Ξ_0, n).

In Sec. 6.3, we have then discussed to which extend the dark energy equation of state parametrised by (w_0, w_a), and the modified propagation of the GWs parametrised by Ξ_0, could be measured by next generation GW experiments such as *ET*. In a first approach, we have considered two artificial wCDM models with $w = -0.9$ and $w = -1.1$, to characterise the amplitude of the deviation to ΛCDM that one should aim to detect for being able to distinguish the models. We have seen that, at the redshifts of interest for e.g. *LISA* or *ET*, this deviation into the luminosity distance is at sub-percent level, so it is quite small and therefore hard to detect. This is principally due to the fact that one should first fix the parameters within each models to their bestfit values to existing distance rulers, such as CMB+BAO+SNIa, so as to get realistic predictions. However, in considering the RR model as a prototypical example, we have seen that the feature induced in the GW-to-electromagnetic luminosity distance ratio by the modified propagation of the GWs was much more significant, at a level of several percents, which illustrates the fact that modified gravity models, and ΛCDM, can be more efficiently tested in considering such an effect.

In Sec. 6.3.2, we have analysed this fact more quantitatively by considering forecasts on various combinations of the parameters (w_0, w_a, Ξ_0), given the projected sensitivity of *ET* on measurements of neutron star binaries. Our previous expectations were confirmed, since we have found that the constraints on Ξ_0 were better than the ones on w_0, by one part in four. This means that the constraints on modified gravity theories prove to be stronger as one considers a modification of the propagation of GWs, rather than a modification to the background FLRW solution by a non-trivial equation of state.

In Sec. 6.4, we have then considered *ET* forecast constraints to get a prediction on the number of sources needed to be detected for distinguishing the RR model from ΛCDM. We have seen that, if *ET* detects 200 sources in, say, the realistic case, or 400 in the pessimistic case, one can reach a BIC $\Delta\chi^2$ above a threshold of 6, and distinguish the RR nonlocal model from ΛCDM. This analysis of course includes the modifying propagation of the GWs in the RR model into the constraints, whereas only focus on the effect induced by a different dark energy equation of state, the realistic case indicate that *ET* should detect about 10^3 sources to tell the difference, where in the pessimistic case this number is orders of magnitude larger.

Finally, in Sec. 6.5, we have seen how a modification to the friction term in the propagation equation of the GWs also affect the propagation of the primordial GWs spectrum to present time. We have seen that, using the parametrisation Ξ_0 presented previously, the GW density fraction generated by single field slow-roll inflation is modified by a factor of Ξ_0^{-2}, and in this sense, observations of the primordial inflationary background will no longer measure the tensor-to-scalar ratio r alone, but the combination $\Xi_0^{-2}r$. Similarly, the ISW effect on, e.g. the CMB temperature anisotropies, induced by GWs whose propagation equation is modified is affected as well.

Chapter 7

Conclusions

As discussed in Chapter 1, the synergy between theoretical and observational efforts led cosmologists to shape the current standard ΛCDM cosmological model. Given its minimal version defined on a continuous six-dimensional cosmological parameter space, information from current observations allow one to determine most of them at percent-level precision. The diversity of high resolution complementary measurements developed through the years makes this determination accurate and robust. A stunning consistency is found in the ΛCDM model given different high-accuracy datasets, that suggests to consider its predictions as physically sensible. However, both theoretical and observational objections still remain.

On the one hand, eighty five percent of the probed total matter into the present Universe is dark and its nature, *viz.* its microscopic composition or a more exotic mechanism able to mimic the dark matter, still remains unknown. Moreover, out of the present total cosmic energy density, data infer that seventy percent of it is made of a dark energy component responsible for the late time accelerated expansion. In the standard cosmological model, the dark energy is described by the simplest solution deriving from general relativistic first principles, a dimensionful number, the cosmological constant Λ. The origin of Λ goes back to Einstein's epoch and since then its history has been tormented. The observation of the light curves of distant SNIa revealed the late time accelerated expansion of the Universe on firm statistical grounds, a fact confirming earlier indications obtained with other cosmological probes, and led to the introduction of a non-vanishing cosmological constant Λ into the standard cosmological model, ΛCDM. The consistency of a cosmological constant with increasingly precise complementary observations has been established more firmly through the years, in particular by cosmological observations of the CMB and large-scale structures. However, a non-vanishing cosmological constant raises fundamental theoretical questions such as its origin, naturalness and late time domination.

On the other hand, the standard ΛCDM model still exhibits potentially significant observational tensions. The most remarkable one is provided by the difference in the values of H_0 inferred from CMB observations and local Hubble flow measurements. A handful of local determinations of H_0 are larger than the ones inferred from most accurate CMB measurements by several standard deviations. This tension is currently under debate and, if it happens to be shown that all the systematics are under control, could be a hint for new physics. Other discrepancies are also present, such as between predictions of the present amplitude of mass fluctuation given primary CMB anisotropies and SZ clusters counts measurements, and also between CMB anisotropies and weak lensing surveys. The conclusions are the same as for the case of H_0.

As the cosmological constant only affects the behavior of GR at cosmological scales, the existence of infrared relevant effects intrinsic to the theory, such as quantum gravitational processes under the form of renormalisation group corrections, as well as classical kinematical effects such as the backreaction of inhomogeneities on the cosmic background, can influence the value of Λ in a non-trivial way, and therefore provide a better understanding of the nature of the dark energy.

In this thesis, we focused on a particular class of modified gravity theories that prove to be potentially useful in that context. The modifications to gravity we consider are realised through the presence of nonlocal terms, typically modifying the theory of GR in its infrared regime, while solar system scales are left unchanged. As presented in Chapter 2, such nonlocalities are typically generated into the gravitational quantum effective action, as for instance through radiative corrections induced by the presence of light or massless fields, but also by the conformal anomaly as well as quantum fluctuations of the gravitational field itself, as suggested from recent lattice quantum gravity computations. Moreover, nonlocal interactions can also arise from extra-dimensions, as for instance in the DGP braneworld, and generate the degravitation mechanism.

In chapter 3, the application of the degravitation idea to the theory of massive gravity linearised over flat space led to the bottom-up construction of a phenomenological nonlocal gravity model, the so-called RR model. This model is thought to emerge from a quantum effective processes and is defined by the quantum effective action,

$$\Gamma = \frac{1}{16\pi G}\int \mathrm{d}^4x\sqrt{-g}\,\left[R - \frac{1}{6}m^2 R\frac{1}{\Box^2}R\right] + S_M[g_{\mu\nu},\psi]\,, \tag{7.1}$$

whose linearisation over flat space is identical to the one of the RT model, whose construction is described in Sec. (3.1). In both models, m is a mass scale whose origin still needs to be determined, and whose value is fixed by observations. By analysing the kinematical structure of these models, we have seen that their flat space propagators include the one of a massless graviton, beside a massless scalar and a massive scalar pole having the opposite sign in front of its kinetic term. The nonlocal structure of the theory implies that the two scalar poles are not associated to degrees of freedom of the theory. Indeed, they correspond to two auxiliary fields whose initial data are vanishing or constrained by those of the metric. Moreover, phenomenological considerations imply that the mass of the scalar needs to be of the order of the inverse age of the Universe, i.e. $\sim H_0^{-1}$. The classical instability associated to such an auxiliary field taking place at scales larger than its "Compton" wavelength, it is not the flat solution that makes sense anymore, but the cosmological FLRW one. We have seen that linear perturbations on that background are stable in the case of the RR model, because of the domination of the Hubble friction induced by a violent background expansion, ending into a Big Rip at large cosmic time. In fact, both theories describe a phantom effective dark energy component leading to a viable accelerated phase of expansion in the late Universe.

In chapter 4, we analysed the phenomenological consequences of these models within the cosmological context. We have seen that, for fixed cosmological parameters, the phantom nature of the effective dark energies described by both models induces a lower Hubble expansion at late time as compared to the ones described by ΛCDM, modifying therefore the notion of cosmological distances. Linear cosmological perturbations were shown to be stable until present, and the lower expansion rate reduces the Hubble friction to the growth of structures at late time, which therefore enhances both the clustering and the lensing power. Both models also describe a "fifth force" associated to the auxiliary degrees of freedom, which is characterised

by an effective Newton constant in the infrared, also responsible for the enhancement of the growth although to a milder level. We used different indicators to quantify their deviations with respect to the linear perturbations described by ΛCDM, and found that they were all below ten percent. We have then shown that the perturbations associated to both effective dark energies were small with respect to those of dust matter, and therefore that the dark energies described by both models are quite smooth.

Such facts allowed us to perform thorough observational constraints by implementing the models in a modified version of the Boltzmann code CLASS. In chapter 5, we put observational constraints on the nonlocal gravity models. We performed cosmological parameter estimation and apply Bayesian model selection using the MCMC code Montepython to compare the nonlocal models with standard ΛCDM. Overall, we have seen that both models are statistically equivalent to ΛCDM given CMB, SNIa, BAO and growth rate data, and that they generically prefer a higher values of the Hubble constant H_0, in better agreement with local measurements. Moreover, the RR model was shown to predict a higher value for the absolute mass of three degenerated neutrino species. We emphasize that these are highly non-trivial results given the high degree of constraints provided by the complementary cosmological data we considered.

In more details, we have seen that, given the standard (base) cosmological parametrisation, the modified angular diameter distances described by the nonlocal cosmologies tend to infer a higher value of H_0, given *Planck* 2015 CMB data, so as to compensate for the lower dark energy density fraction induced by the phantom nature of the effective dark energies described by both nonlocal models. Given these data, the three cosmological models have been shown to be statistically equivalent on Bayesian statistical grounds, through the use of the Savage-Dickey density ratio method for nested models. When joining *JLA* SNIa data together with a distance ladder built up from BAO observations at various redshifts, the performances of the RT models still remain comparable to those of ΛCDM. However, the performances of the RR model degrade, displaying a "moderate-to-strong" evidence with odds 22:1 in favor of ΛCDM, because of a dominant CMB-SNIa tension appearing in the H_0–Ω_M plane. We have then applied constraints on the models from RSD data, showing that their preference for a higher growth rate handicapped them with respect to ΛCDM. Nevertheless, the preference of the nonlocal models for a higher value of H_0 given CMB data makes them more consistent with values inferred from local measurements, and brings the nonlocal modes on the same level as ΛCDM for explaining the data, when a higher prior on H_0 is considered. We have then shown that the aforementioned tension exhibited by the RR model can be resolved by considering an extension of the initial baseline, allowing the absolute mass of three degenerated massive neutrino species to vary into the global fit. We have demonstrated that, within this extension that is perfectly allowed by current experimental bounds, the RR models explains the data at the same level than ΛCDM, with a preference for a higher absolute neutrino mass, non-vanishing at 2σ level. Indeed, in this extended baseline, the Bayes factor reduces to odds of 1.8:1 in favor of ΛCDM, rendering the models indistinguishable given CMB+SNIa+BAO data. This fact is partially due to a better goodness-of-fit of the nonlocal model, but also to Occam's razor effect that intrinsically penalises the ΛCDM models for its preference for (too) small absolute neutrino masses, and leaves therefore some room for modified gravity models to compete with it. We have also shown that a higher neutrino mass for the nonlocal model decreases the growth of structures it describes at late time, therefore making the model more consistent with RSD data. Overall, both models were shown to provide a good fit to the data, are statistically equivalent to the standard ΛCDM (and the ν-extension of it) and prefer a higher values of H_0 given CMB data, in better agreement with the value obtained from local measurements. Nevertheless, in a complementary study, the RT model has been shown to be plagued by instabilities at linear

perturbation level in a primordial inflationary phase, so that it cannot be responsible for the primordial power spectrum seeding the presently observed structures. This selects the RR model as our theoretically preferred model.

In chapter 6, inspired by the fact that the RR model describes a modified propagation for the GWs compared to ΛCDM, we have considered the potential of next generation GWs interferometers to constrain modified gravity models. In particular, the measurement of the luminosity distance from binary inspirals, referred to as standard sirens, provides a distance-redshift relation complementary to optical surveys. This fact allowed us to put constraints on the standard cosmological parameters and on the nature of the dark energy. The distance-redshift relation from standard sirens equals the one from standard candles in ΛCDM, but can be different for modified gravity theories affecting the propagation of linear tensor modes, defining a luminosity distance for GW into the model. Taking the RR nonlocal model as a prototypical example, we have shown that the ratio of the GW to the optical luminosity distance is well parametrised by the pair (Ξ_0, n), where Ξ_0 is the value at which the ratio saturates at high redshifts, while n parametrises the power of the scale factor at which it increases at low redshifts. We have shown that, compared to the constraints that standard sirens are expected to put on the dark energy equation of state today w_0, the ones on Ξ_0 were more powerful. Indeed, we found that Ξ_0 can be measured with an accuracy better than w_0 by a factor of four, given forecast data from the *Einstein Telescope* combined with recent CMB+BAO+SNIa data. This result shows that measurements of the deviation between optical and GW luminosity distances provide better constraints on modified gravity theories compared to those probing the equation of state. We have seen that this statement is well illustrated in the case of the RR model, which only needs the detection of ∼400 sources to be discriminated from ΛCDM, compared to ∼1000 when its modified tensor propagation is artificially put to zero, given the same data as mentioned hereabove. This fact makes the prospects of next generation GW experiments better than initially expected for being able to put tight constraints on the necessity to modify GR. Finally, we have also seen that such modified propagation for tensors also affects the transfer function of primordial GW to present time and the ISW effect to CMB temperature anisotropies.

In conclusion, we have studied a modified gravity model which is well motivated from the field theoretical point of view, the RR model. Many efforts in the community have already shown that it is not an easy task to build a model that describes a phase of late time cosmic acceleration and which passes several other tests. In particular, linear cosmological perturbations need to be stable and GWs are required to propagate at the speed of light, in accordance with the recent detection of GWs from a binary neutron star inspiral together with its electromagnetic counterpart. Moreover, the predictive power of the model should be high enough for competing against the standard ΛCDM model, given high resolution complementary cosmological observations, and the model still needs to feature significant deviations from ΛCDM so as to be distinguishable in the light of future experiments. In this thesis, we have shown that the RR model is able to accomplish these requirements and leads to several original predictions. Indeed, we have shown the model prefers a higher value of the Hubble constant H_0 and infers a higher absolute mass for three degenerated neutrino species as compared to ΛCDM, given recent CMB+SNIa+BAO data. These features prove to be potentially detectable with future large scale structure surveys such as *Euclid*. Moreover, the model also describes a modified propagation of the GWs as compared to the theory of GR, potentially distinguishable with next generation GWs interferometers such as the *Einstein Telescope*, as we have explicitly demonstrated. The RR model therefore provides an interesting benchmark for forecasting the constraints from such future experiments, which could eventually lead to a detection of an infrared modification to gravity within the near future.

Appendix A

Implementation of the nonlocal models in CLASS

We expose the sets of equations of motion for the RT and RR models, at the cosmological background and scalar and tensor linear perturbations level, in the format used for modifying the CLASS code. The equations are written in conformal time and the perturbations are implemented into conformal Newtonian gauge, but not in synchronous gauge. These can be derived from the expressions presented in Secs. 4.3.2 and 4.3.3, together with the convention (4.62). We also briefly comment on the global strategy used in the code for evolving them. The code itself is publicly available (URL). Concerning the RR model, it has been tested against a modified version [1] of the CAMB code (Lewis) and shown to agree at subpercent level in CMB and matter power spectra (Bellini et al., 2018).

Since both nonlocal models have the same overall structure, that is, a set of modified Einstein equations including auxiliary fields, along with second order differential equations governing the evolution of the latter, their implementation in CLASS is similar. For both models, the mass-related parameter $\gamma \equiv m^2/(9H_0^2)$ is fixed by a trial-and-error using the bisection or the secant method if the former does not converge.

A.1 Implementation of the RT model

We start by writing down the relevant cosmological background equations corresponding to the RT model. These are implemented into the background module of CLASS, `background.c`. In *background_functions()*, the (00) component of Einstein equations is used to infer algebraically the Hubble parameter $H \equiv a'/a^2$ in terms of the energy density of the matter component that one wishes to take into account. In our case it reads [2],

$$H = \frac{\gamma \bar{V} H_0^2}{2a} + \left[\left(\frac{\gamma \bar{V} H_0^2}{2a} \right) + \gamma \big(\bar{U} - \bar{V}'/a^2 \big) H_0^2 + \frac{8\pi G}{3} \bar{\rho} \right]^{1/2}, \tag{A.1}$$

where H_0 is the present value of the Hubble parameter and $\bar{U}$ and $\bar{V}$ denote the background values of the auxiliary fields U and V. The derivative of the Hubble parameter is not computed numerically, but rather obtained algebraically from the trace of the (ij) component of Einstein

1. This version is not publicly available, but can been obtained on request (Barreira).
2. Here $\mathcal{H} \equiv a'/a^2$, as used in the background module of CLASS.

equations, in terms of the pressure,

$$H' = -\frac{3}{2}a\left[H^2 + \frac{8\pi G}{3}\bar{p} + \gamma\left(\frac{H}{a}\bar{V} - \bar{U}\right)H_0^2\right]. \tag{A.2}$$

As already mentioned above, in our case, the evolution of the auxiliary fields is dictated by a set of second order differential equations,

$$\bar{U}'' + 2aH\bar{U}' = 6a\big(H' + 2aH^2\big) \quad , \quad \bar{V}'' - a\big(H' + 5aH^2\big)\bar{V} = a^2\bar{U}' \,, \tag{A.3}$$

which needs to be integrated numerically directly within the code, in *background_derivs()*, with initial conditions $\bar{U} = \bar{U}' = \bar{V} = \bar{V}' = 0$, set deep into the radiation era. Once the matter components have been specified, such that their energy density and pressure can be written explicitly (for example by using their separate energy-momentum conservation together with an equation of state, or their unperturbed phase-space distribution functions) the system closes and the background evolution can be integrated.

Concerning the linear scalar perturbations, the set of equations needed includes the conservation equation of each fluid component, along with the evolution equations for the auxiliary fields perturbations and two independent components of the modified Einstein equations. For the latter, in *perturb_einstein()*, the code originally uses the divergence of the $(0i)$ component in order to extract ϕ' algebraically. In our case we have [3],

$$\phi' = -\mathcal{H}\psi + 4\pi G\frac{a^2}{k^2}(\bar{\rho} + \bar{p})\theta + \frac{3}{2}\gamma\left[\mathcal{H}\delta Z - \frac{1}{2}\delta Z' + \frac{1}{2}\psi\bar{V} - \frac{1}{2}\delta V\right]H_0^2 \,. \tag{A.4}$$

The expression of ψ is obtained in terms of ϕ from the longitudinal-traceless part of the (ij) component of Einstein equation,

$$\psi = \phi - 12\pi G\frac{a^2}{k^2}(\bar{\rho} + \bar{p})\sigma + 3\gamma\delta Z H_0^2 \,, \tag{A.5}$$

and ϕ is obtained from (A.4) by numerical integration. The equations governing the dynamics of the auxiliary fields are,

$$\delta U'' + k^2\delta U + 2\mathcal{H}\delta U' = (\psi' + 3\phi')(\bar{U}' - 6\mathcal{H}) + 2k^2(\psi - 2\phi) - 6\phi'', \tag{A.6}$$

$$\delta Z'' - 2(\mathcal{H}' + 2\mathcal{H}^2 - k^2)\delta Z = 2a^2\delta U - 4\mathcal{H}\delta V - \delta V' + 3\bar{V}'\psi + \big(\psi' + 2\phi'\big)\bar{V} \,, \tag{A.7}$$

$$\begin{aligned}\delta V'' - \left(\mathcal{H}' + 4\mathcal{H}^2 - \frac{k^2}{2}\right)\delta V = \\ a^2\delta U' - \frac{1}{2}k^2\delta Z' + 2\mathcal{H}k^2\delta Z + \left[\frac{k^2}{2}\psi - \mathcal{H}(\psi' + 9\phi')\right]\bar{V} + (\psi' + 3\phi')\bar{V}' + a^2\bar{U}'\psi \,,\end{aligned} \tag{A.8}$$

and are implemented into *perturb_derivs()*. We see that they contain ψ' and ϕ'', which can also be extracted algebraically from the equations. In particular, ϕ'' is obtained from the trace of the (ij) component of Einstein equations,

$$\begin{aligned}\phi'' = -\psi(\mathcal{H}^2 + 2\mathcal{H}') - \mathcal{H}(\psi' + 2\phi') + \frac{k^2}{3}(\psi - \phi) \\ - \frac{3}{2}\left[\gamma\left(a^2\delta U + \big(\phi' + \mathcal{H}\psi\big)\bar{V} - \mathcal{H}\delta V - \frac{k^2}{3}\delta Z\right)H_0^2 - \frac{8\pi G}{3}a^2\delta p\right],\end{aligned} \tag{A.9}$$

3. Here we set, $\mathcal{H} \equiv a'/a$.

whereas ψ' is obtained by taking the derivatives of (A.5),

$$\psi' = \phi' - \frac{24\pi G}{k^2}\mathcal{H}a^2(\bar{\rho}+\bar{p})\sigma - 12\pi G\frac{a^2}{k^2}\big[(\bar{\rho}+\bar{p})\sigma\big]' + 3\gamma\delta Z' H_0^2\,. \tag{A.10}$$

Within the version of CLASS that we used, the source term $\big[(\bar{\rho}+\bar{p})\sigma\big]$ decomposes as

$$\big[(\bar{\rho}+\bar{p})\sigma\big] = \frac{4}{3}\big(\rho_\gamma\sigma_\gamma + \rho_{ur}\sigma_{ur}\big) + (\rho+p)_{ncdm}\sigma_{ncdm}\,, \tag{A.11}$$

where γ, ur and $ncdm$ denote the photon, ultra-relativistic particles and non-cold dark matter (NCDM) components, respectively. Therefore to compute its corresponding time derivative one needs,

$$\big[(\bar{\rho}+\bar{p})\sigma\big]' = \frac{4}{3}\big(\rho'_\gamma\sigma_\gamma + \rho'_{ur}\sigma_{ur} + \rho_\gamma\sigma'_\gamma + \rho_{ur}\sigma'_{ur}\big) + \big[(\rho+p)_{ncdm}\sigma_{ncdm}\big]'\,, \tag{A.12}$$

and, since at background level each of the ultra-relativistic particles and photons components is conserved, one can use the background conservation equation, $\bar{\rho}' = -3\mathcal{H}(\bar{\rho}+\bar{p})$ together with the equation of state for ultra-relativistic particle $\bar{p} = (1/3)\bar{\rho}$, to write,

$$\big[(\bar{\rho}+\bar{p})\sigma\big]' = \frac{4}{3}\rho_\gamma\big(\sigma'_\gamma - 4\mathcal{H}\sigma_\gamma\big) + \frac{4}{3}\rho_{ur}\big(\sigma'_{ur} - 4\mathcal{H}\sigma_{ur}\big) + \big[(\rho+p)_{ncdm}\sigma_{ncdm}\big]'\,, \tag{A.13}$$

while the (massive) NCDM components have to be treated separately in terms of their phase-space description. This form is quite convenient for being implemented into the code since the various quantities have already been built into the original version.

A.2 Implementation of the RR model

In the case of the RR model, the general structure is the same as above and we only display the relevant equations needed for the implementation in the code. At the background level, the (00) component of the modified first Friedmann equation reads,

$$H = \left(1-3\gamma\bar{V}\right)^{-1}\left\{\frac{3\gamma}{2a}\bar{V}' + \left[\left(\frac{3\gamma}{2a}\bar{V}'\right)^2 + \left(1-3\gamma\bar{V}\right)\left(\frac{\gamma}{4}\bar{U}^2H_0^2 - \frac{\gamma}{2a^2}\bar{V}'\bar{U}' + \frac{8\pi G}{3}\rho\right)\right]^{1/2}\right\}. \tag{A.14}$$

From the (ij) component one gets,

$$H' = -\frac{3}{2}a\left\{H^2 + \left(1-3\gamma\bar{V}\right)^{-1}\left[\frac{8\pi G}{3}\bar{p} - \gamma\left(\frac{1}{4}\bar{U}^2H_0^2 + \bar{U}H_0^2 - \frac{H}{a}\bar{V}' + \frac{1}{2a^2}\bar{V}'\bar{U}'\right)\right]\right\}. \tag{A.15}$$

The equation of the auxiliary fields are,

$$\bar{U}'' + 2aH\bar{U}' = 6a\big(H' + 2aH^2\big), \qquad \bar{V}'' + 2aH\bar{V}' = a^2\bar{U}H_0^2\,. \tag{A.16}$$

To linear order in the scalar perturbations, the $(0i)$ component of the modified Einstein equations leads to,

$$\phi' = -\mathcal{H}\psi + \frac{3}{2}\left(1-3\gamma\bar{V}\right)^{-1}\left[\frac{8\pi Ga^2}{3k^2}(\bar{\rho}+\bar{p})\theta - \gamma\left(\delta V' - \bar{V}'\psi - \mathcal{H}\delta V + \frac{1}{2}\big(\bar{U}'\delta V + \bar{V}'\delta U\big)\right)\right]. \tag{A.17}$$

The equation sourced by the anisotropic stress gives,

$$\psi = \phi + \left(1 - 3\gamma\bar{V}\right)^{-1}\left[- 12\pi G\frac{a^2}{k^2}(\bar{\rho} + \bar{p})\sigma + 3\gamma\delta V\right], \tag{A.18}$$

while the perturbation of the equations for the auxiliary field equations yields,

$$\delta U'' + 2\mathcal{H}\delta U' + k^2\delta U = \big(\psi' + 3\phi'\big)(\bar{U}' - 6\mathcal{H}) + 2k^2\big(\psi - 2\phi\big) - 6\phi'', \tag{A.19}$$

$$\delta V'' + 2\mathcal{H}\delta V' + k^2\delta V = \big(\psi' + 3\phi'\big)\bar{V}' + 2a^2\psi\bar{U}H_0^2 + a^2\delta U H_0^2\,. \tag{A.20}$$

In order to solve the system, one has also to provide expressions of ψ' and ϕ'' obtained similarly to the case of the RT model. One finds,

$$\psi' = \phi' + \left(1 - 3\gamma\bar{V}\right)^{-1}\left[3\gamma(\psi - \phi)\bar{V}' - \frac{24\pi G}{k^2}\mathcal{H}a^2(\bar{\rho} + \bar{p})\sigma - 12\pi G\frac{a^2}{k^2}\big[(\bar{\rho} + \bar{p})\sigma\big]' + 3\gamma\delta V'\right], \tag{A.21}$$

and,

$$\begin{aligned}\phi'' = &-\psi(\mathcal{H}^2 + 2\mathcal{H}') - \mathcal{H}(\psi' + 2\phi') + \frac{k^2}{3}(\psi - \phi)\\ &- \frac{3}{2}\left(1 - 3\gamma\bar{V}\right)^{-1}\left\{\gamma\left[\frac{1}{2}a^2\bar{U}\delta U H_0^2 - 2a^2\psi\bar{U}H_0^2 - \big(2\phi' - 2\mathcal{H}\psi + \psi' + \psi\bar{U}'\big)\bar{V}'\right.\right.\\ &\left.\left. + \delta V'' + \mathcal{H}\delta V' + \left(\mathcal{H}^2 + 2\mathcal{H}' + \frac{2k^2}{3}\right)\delta V + \frac{1}{2}\big(\bar{U}'\delta V' + \bar{V}'\delta U'\big)\right] - \frac{8\pi G}{3}a^2\delta p\right\}.\end{aligned} \tag{A.22}$$

Bibliography

K. N. Abazajian et al. CMB-S4 Science Book, First Edition. 2016.

B. P. Abbott et al. Observation of Gravitational Waves from a Binary Black Hole Merger. *Phys. Rev. Lett.*, 116(6):061102, 2016a. doi: 10.1103/PhysRevLett.116.061102.

B. P. Abbott et al. GW151226: Observation of Gravitational Waves from a 22-Solar-Mass Binary Black Hole Coalescence. *Phys. Rev. Lett.*, 116(24):241103, 2016b. doi: 10.1103/PhysRevLett.116.241103.

B. P. Abbott et al. Observation of gravitational waves from a binary black hole merger. *Phys. Rev. Lett.*, 116:061102, Feb 2016c. doi: 10.1103/PhysRevLett.116.061102.

B. P. Abbott et al. Binary Black Hole Mergers in the first Advanced LIGO Observing Run. *Phys. Rev.*, X6(4):041015, 2016d. doi: 10.1103/PhysRevX.6.041015.

B. P. Abbott et al. Gw170608: Observation of a 19 solar-mass binary black hole coalescence. *The Astrophysical Journal Letters*, 851(2):L35, 2017a.

B. P. Abbott et al. GW170814: A Three-Detector Observation of Gravitational Waves from a Binary Black Hole Coalescence. *Phys. Rev. Lett.*, 119(14):141101, 2017b. doi: 10.1103/PhysRevLett.119.141101.

B. P. Abbott et al. GW170104: Observation of a 50-Solar-Mass Binary Black Hole Coalescence at Redshift 0.2. *Phys. Rev. Lett.*, 118(22):221101, 2017c. doi: 10.1103/PhysRevLett.118.221101.

B. P. Abbott et al. A gravitational-wave standard siren measurement of the Hubble constant. *Nature*, 551(7678):85–88, 2017d. doi: 10.1038/nature24471.

B. P. Abbott et al. Exploring the Sensitivity of Next Generation Gravitational Wave Detectors. *Class. Quant. Grav.*, 34(4):044001, 2017e. doi: 10.1088/1361-6382/aa51f4.

B. P. Abbott et al. Multi-messenger Observations of a Binary Neutron Star Merger. *Astrophys. J.*, 848(2):L12, 2017f. doi: 10.3847/2041-8213/aa91c9.

B. P. Abbott et al. Gravitational Waves and Gamma-rays from a Binary Neutron Star Merger: GW170817 and GRB 170817A. *Astrophys. J.*, 848:L13, 2017g. doi: 10.3847/2041-8213/aa920c.

B. P. Abbott et al. Gw170817: Observation of gravitational waves from a binary neutron star inspiral. *Phys. Rev. Lett.*, 119:161101, Oct 2017h. doi: 10.1103/PhysRevLett.119.161101.

B.P. Abbott et al. Gw170817: Observation of gravitational waves from a binary neutron star inspiral. *Phys. Rev. Lett.*, 119(16):161101, 2017i. doi: 10.1103/PhysRevLett.119.161101.

T. M. C. Abbott et al. Dark Energy Survey Year 1 Results: Cosmological Constraints from Galaxy Clustering and Weak Lensing. 2017j.

V. Acquaviva, N. Bartolo, S. Matarrese, and A. Riotto. Second order cosmological perturbations from inflation. *Nucl. Phys.*, B667:119–148, 2003. doi: 10.1016/S0550-3213(03)00550-9.

R. Adam et al. Planck 2015 results. I. Overview of products and scientific results. 2015.

R. Adam et al. Planck 2015 results. I. Overview of products and scientific results. *Astron. Astrophys.*, 594:A1, 2016. doi: 10.1051/0004-6361/201527101.

J. Adamek, D. Daverio, R. Durrer, and M. Kunz. gevolution: a cosmological N-body code based on General Relativity. *JCAP*, 1607(07):053, 2016. doi: 10.1088/1475-7516/2016/07/053.

P. A. R. Ade et al. Planck 2013 results. XVI. Cosmological parameters. *Astron. Astrophys.*, 571:A16, 2014a. doi: 10.1051/0004-6361/201321591.

P. A. R. Ade et al. Detection of B-Mode Polarization at Degree Angular Scales by BICEP2. *Phys. Rev. Lett.*, 112(24):241101, 2014b. doi: 10.1103/PhysRevLett.112.241101.

P. A. R. Ade et al. Planck 2013 results. I. Overview of products and scientific results. *Astron. Astrophys.*, 571:A1, 2014c. doi: 10.1051/0004-6361/201321529.

P. A. R. Ade et al. Planck 2013 results. XVI. Cosmological parameters. *Astron.Astrophys.*, 571: A16, 2014d. doi: 10.1051/0004-6361/201321591.

P. A. R. Ade et al. Joint Analysis of BICEP2/$KeckArray$ and $Planck$ Data. *Phys. Rev. Lett.*, 114:101301, 2015a. doi: 10.1103/PhysRevLett.114.101301.

P. A. R. Ade et al. Planck 2015 results. XIII. Cosmological parameters. 2015b.

P. A. R. Ade et al. Joint Analysis of BICEP2 / Keck Array and Planck Data. *Phys.Rev.Lett.*, 114(10):101301, 2015c. doi: 10.1103/PhysRevLett.114.101301.

P. A. R. Ade et al. Planck 2015 results. XIII. Cosmological parameters. 2015d.

P. A. R. Ade et al. Planck 2015 results. XIV. Dark energy and modified gravity. 2015e.

P. A. R. Ade et al. Planck 2015 results. XV. Gravitational lensing. 2015f.

P. A. R. Ade et al. Planck 2015 results. XXIV. Cosmology from Sunyaev-Zeldovich cluster counts. *Astron. Astrophys.*, 594:A24, 2016. doi: 10.1051/0004-6361/201525833.

P. A. R. Ade et al. A Measurement of the Cosmic Microwave Background B-Mode Polarization Power Spectrum at Sub-Degree Scales from 2 years of POLARBEAR Data. *Astrophys. J.*, 848(2):121, 2017. doi: 10.3847/1538-4357/aa8e9f.

N. Afshordi, B. J. H. Chung, M. Doran, and G. Geshnizjani. Cuscuton Cosmology: Dark Energy meets Modified Gravity. *Phys. Rev.*, D75:123509, 2007a. doi: 10.1103/PhysRevD.75.123509.

N. Afshordi, D. J. H. Chung, and G. Geshnizjani. Cuscuton: A Causal Field Theory with an Infinite Speed of Sound. *Phys. Rev.*, D75:083513, 2007b. doi: 10.1103/PhysRevD.75.083513.

N. Aghanim et al. Planck 2016 intermediate results. LI. Features in the cosmic microwave background temperature power spectrum and shifts in cosmological parameters. 2016a.

N. Aghanim et al. Planck intermediate results. XLVI. Reduction of large-scale systematic effects in HFI polarization maps and estimation of the reionization optical depth. *Astron. Astrophys.*, 596:A107, 2016b. doi: 10.1051/0004-6361/201628890.

N. Aghanim et al. Planck 2015 results - xi. cmb power spectra, likelihoods, and robustness of parameters. *A&A*, 594:A11, 2016c. doi: 10.1051/0004-6361/201526926.

N. Aghanim et al. Planck 2018 results. VI. Cosmological parameters. 2018.

S. Alam et al. The clustering of galaxies in the completed SDSS-III Baryon Oscillation Spectroscopic Survey: cosmological analysis of the DR12 galaxy sample. *Submitted to: Mon. Not. Roy. Astron. Soc.*, 2016.

I. Albarran, M. Bouhmadi-Lpez, and J. Morais. Cosmological perturbations in an effective and genuinely phantom dark energy Universe. *Phys. Dark Univ.*, 16:94–108, 2017. doi: 10.1016/j.dark.2017.04.002.

A. Albrecht and J. Magueijo. A Time varying speed of light as a solution to cosmological puzzles. *Phys. Rev.*, D59:043516, 1999. doi: 10.1103/PhysRevD.59.043516.

A. Albrecht et al. Report of the Dark Energy Task Force. 2006.

C. Alcock and B. Paczynski. An evolution free test for non-zero cosmological constant. *Nature*, 281:358, October 1979. doi: 10.1038/281358a0.

G. Aldering et al. In J. A. Tyson and S. Wolff, editors, *Survey and Other Telescope Technologies and Discoveries*, volume 4836 of *Proceedings of the SPIE*, pages 61–72, December 2002. doi: 10.1117/12.458107.

S. W. Allen, R. W. Schmidt, and A. C. Fabian. Cosmological constraints from the X-ray gas mass fraction in relaxed lensing clusters observed with Chandra. *MNRAS*, 334:L11–L15, August 2002. doi: 10.1046/j.1365-8711.2002.05601.x.

S. W. Allen, R. W. Schmidt, H. Ebeling, A. C. Fabian, and L. van Speybroeck. Constraints on dark energy from Chandra observations of the largest relaxed galaxy clusters. *MNRAS*, 353: 457–467, September 2004. doi: 10.1111/j.1365-2966.2004.08080.x.

S. W. Allen, D. A. Rapetti, R. W. Schmidt, H. Ebeling, G. Morris, and A. C. Fabian. Improved constraints on dark energy from Chandra X-ray observations of the largest relaxed galaxy clusters. *Mon. Not. Roy. Astron. Soc.*, 383:879–896, 2008. doi: 10.1111/j.1365-2966.2007.12610.x.

R. A. Alpher and R. Herman. Evolution of the Universe. *Nature*, 162:774–775, November 1948. doi: 10.1038/162774b0.

R. A. Alpher, H. Bethe, and G. Gamow. The origin of chemical elements. *Phys. Rev.*, 73: 803–804, Apr 1948. doi: 10.1103/PhysRev.73.803.

R. Amanullah et al. Spectra and Hubble Space Telescope Light Curves of Six Type Ia Supernovae at $0.511 < z < 1.12$ and the Union2 Compilation. *Astrophys. J.*, 716:712–738, June 2010. doi: 10.1088/0004-637X/716/1/712.

L. Amendola. Coupled quintessence. *Phys. Rev.*, D62:043511, 2000. doi: 10.1103/PhysRevD.62.043511.

L. Amendola and S. Tsujikawa. *Dark Energy: Theory and Observations*. Cambridge University Press, 2010. doi: 10.1017/CBO9780511750823.

L. Amendola, C. Quercellini, and E. Giallongo. Constraints on perfect fluid and scalar field dark energy models from future redshift surveys. *Mon. Not. Roy. Astron. Soc.*, 357:429–439, February 2005. doi: 10.1111/j.1365-2966.2004.08558.x.

L. Amendola, M. Baldi, and C. Wetterich. Quintessence cosmologies with a growing matter component. *Phys. Rev.*, D78:023015, 2008a. doi: 10.1103/PhysRevD.78.023015.

L. Amendola, M. Kunz, and D. Sapone. Measuring the dark side (with weak lensing). *JCAP*, 0804:013, 2008b. doi: 10.1088/1475-7516/2008/04/013.

L. Amendola, N. Burzilla, and H. Nersisyan. Quantum Gravity inspired nonlocal gravity model. *Phys. Rev.*, D96(8):084031, 2017a. doi: 10.1103/PhysRevD.96.084031.

L. Amendola, I. Sawicki, M. Kunz, and I. D. Saltas. Direct detection of gravitational waves can measure the time variation of the Planck mass. 2017b.

L. Amendola, Y. Dirian, S. Park, and H. Nersisyn. *(in preparation)*, 2018.

L. Amendola et al. Cosmology and fundamental physics with the Euclid satellite. *Living Rev. Rel.*, 16:6, 2013. doi: 10.12942/lrr-2013-6.

L. Amendola et al. Cosmology and Fundamental Physics with the Euclid Satellite. *Living Reviews in Relativity*, 16:6, September 2013. doi: 10.12942/lrr-2013-6.

L. Anderson et al. The clustering of galaxies in the SDSS-III Baryon Oscillation Spectroscopic Survey: Baryon Acoustic Oscillations in the Data Release 10 and 11 galaxy samples. *Mon.Not.Roy.Astron.Soc.*, 441(1):24–62, 2014. doi: 10.1093/mnras/stu523.

I. Antoniadis and E. Mottola. Graviton fluctuations in de sitter space. *Journal of Mathematical Physics*, 32(4):1037–1044, 1991. doi: 10.1063/1.529381.

I. Antoniadis, N. Arkani-Hamed, S. Dimopoulos, and G. R. Dvali. New dimensions at a millimeter to a Fermi and superstrings at a TeV. *Phys. Lett.*, B436:257–263, 1998. doi: 10.1016/S0370-2693(98)00860-0.

I. Antoniadis, P. O. Mazur, and E. Mottola. Cosmological dark energy: Prospects for a dynamical theory. *New J. Phys.*, 9:11, 2007. doi: 10.1088/1367-2630/9/1/011.

Ignatios Antoniadis, Pawel O. Mazur, and Emil Mottola. Physical states of the quantum conformal factor. *Phys. Rev.*, D55:4770–4784, 1997. doi: 10.1103/PhysRevD.55.4770.

T. Appelquist and J. Carazzone. Infrared singularities and massive fields. *Phys. Rev. D*, 11: 2856–2861, May 1975. doi: 10.1103/PhysRevD.11.2856.

S. Arai and A. Nishizawa. Generalized framework for testing gravity with gravitational-wave propagation. II. Constraints on Horndeski theory. 2017.

M. Archidiacono, T. Brinckmann, J. Lesgourgues, and V. Poulin. Physical effects involved in the measurements of neutrino masses with future cosmological data. *JCAP*, 1702(02):052, 2017. doi: 10.1088/1475-7516/2017/02/052.

N. Arkani-Hamed, S. Dimopoulos, and G. R. Dvali. The Hierarchy problem and new dimensions at a millimeter. *Phys. Lett.*, B429:263–272, 1998. doi: 10.1016/S0370-2693(98)00466-3.

N. Arkani-Hamed, S. Dimopoulos, G. Dvali, and G. Gabadadze. Nonlocal modification of gravity and the cosmological constant problem. 2002.

N. Arkani-Hamed, H.-C. Cheng, M. A. Luty, and S. Mukohyama. Ghost condensation and a consistent infrared modification of gravity. *JHEP*, 05:074, 2004. doi: 10.1088/1126-6708/2004/05/074.

C. Armendariz-Picon, Viatcheslav F. Mukhanov, and Paul J. Steinhardt. Essentials of k essence. *Phys. Rev.*, D63:103510, 2001. doi: 10.1103/PhysRevD.63.103510.

P. Astier et al. The Supernova legacy survey: Measurement of omega(m), omega(lambda) and W from the first year data set. *Astron. Astrophys.*, 447:31–48, 2006. doi: 10.1051/0004-6361:20054185.

H. Audley et al. Laser Interferometer Space Antenna. 2017.

B. Audren, J. Lesgourgues, K. Benabed, and S. Prunet. Conservative constraints on early cosmology with MONTE PYTHON. *JCAP*, 2:001, February 2013. doi: 10.1088/1475-7516/2013/02/001.

I. G. Avramidi. *Covariant methods for the calculation of the effective action in quantum field theory and investigation of higher derivative quantum gravity.* PhD thesis, Moscow State U., 1986.

E. Babichev, C. Deffayet, and R. Ziour. k-Mouflage gravity. *Int. J. Mod. Phys.*, D18:2147–2154, 2009. doi: 10.1142/S0218271809016107.

E. Babichev, C. Deffayet, and G. Esposito-Farese. Constraints on Shift-Symmetric Scalar-Tensor Theories with a Vainshtein Mechanism from Bounds on the Time Variation of G. *Phys. Rev. Lett.*, 107:251102, 2011. doi: 10.1103/PhysRevLett.107.251102.

N. A. Bahcall and R. Cen. The mass function of clusters of galaxies. *Astrophysical Journal*, 407:L49–L52, April 1993. doi: 10.1086/186803.

T. Baker, E. Bellini, P. G. Ferreira, M. Lagos, J. Noller, and I. Sawicki. Strong constraints on cosmological gravity from GW170817 and GRB 170817A. *Phys. Rev. Lett.*, 119:251301, 2017. doi: 10.1103/PhysRevLett.119.251301.

M. Baldi, F. Villaescusa-Navarro, M. Viel, E. Puchwein, V. Springel, and L. Moscardini. Cosmic degeneracies - I. Joint N-body simulations of modified gravity and massive neutrinos. *Mon. Not. Roy. Astron. Soc.*, 440:75–88, May 2014. doi: 10.1093/mnras/stu259.

W. E. Ballinger, J. A. Peacock, and A. F. Heavens. Measuring the cosmological constant with redshift surveys. *Mon. Not. Roy. Astron. Soc.*, 282:877–888, 1996. doi: 10.1093/mnras/282.3.877.

J. M. Bardeen. Gauge-invariant cosmological perturbations. *Phys. Rev. D*, 22:1882–1905, Oct 1980. doi: 10.1103/PhysRevD.22.1882.

J. M. Bardeen, P. J. Steinhardt, and M. S. Turner. Spontaneous creation of almost scale-free density perturbations in an inflationary universe. *Phys. Rev. D*, 28:679–693, Aug 1983. doi: 10.1103/PhysRevD.28.679.

J. M. Bardeen, J. R. Bond, N. Kaiser, and A. S. Szalay. The statistics of peaks of Gaussian random fields. *Astrophysical Journal*, 304:15–61, May 1986. doi: 10.1086/164143.

A. Barreira. Modified CAMB version with the RR model.

A. Barreira, B. Li, C. M. Baugh, and S. Pascoli. Linear perturbations in Galileon gravity models. *Phys.Rev.*, D86:124016, 2012. doi: 10.1103/PhysRevD.86.124016.

A. Barreira, B. Li, C. M. Baugh, and S. Pascoli. Modified gravity with massive neutrinos as a testable alternative cosmological model. *PRD*, 90(2):023528, July 2014a. doi: 10.1103/PhysRevD.90.023528.

A. Barreira, B. Li, W. A. Hellwing, C. M. Baugh, and S. Pascoli. Nonlinear structure formation in nonlocal gravity. *JCAP*, 9:031, September 2014b. doi: 10.1088/1475-7516/2014/09/031.

A. Barreira, P. Brax, S. Clesse, B. Li, and P. Valageas. Linear perturbations in K-mouflage cosmologies with massive neutrinos. *PRD*, 91(6):063528, March 2015. doi: 10.1103/PhysRevD.91.063528.

A. Barreira, A. G. Sànchez, and F. Schmidt. Validating estimates of the growth rate of structure with modified gravity simulations. *Phys. Rev.*, D94(8):084022, 2016. doi: 10.1103/PhysRevD.94.084022.

Alexandre Barreira, Marius Cautun, Baojiu Li, Carlton Baugh, and Silvia Pascoli. Weak lensing by voids in modified lensing potentials. *JCAP*, 1508:028, 2015a. doi: 10.1088/1475-7516/2015/08/028.

Alexandre Barreira, Baojiu Li, Elise Jennings, Julian Merten, Lindsay King, Carlton Baugh, and Silvia Pascoli. Galaxy cluster lensing masses in modified lensing potentials. *Mon. Not. Roy. Astron. Soc.*, 454(4):4085–4102, 2015b. doi: 10.1093/mnras/stv2211.

B. J. Barros, L. Amendola, T. Barreiro, and N. J. Nunes. Coupled quintessence with a ΛCDM background: removing the σ_8 tension. 2018.

M. Bartelmann and P. Schneider. Weak gravitational lensing. *Phys. Rept.*, 340:291–472, 2001. doi: 10.1016/S0370-1573(00)00082-X.

A. O. Barvinsky. Nonlocal action for long distance modifications of gravity theory. *Phys. Lett.*, B572:109–116, 2003. doi: 10.1016/j.physletb.2003.08.055.

A. O. Barvinsky. Cosmological constant problem and long-distance modifications of Einstein theory. In *Proceedings, 13th International Seminar on High-Energy Physics: Quarks 2004: Pushkinskie Gory, Russia, May 24-30, 2004*, 2004.

A. O. Barvinsky. Serendipitous discoveries in nonlocal gravity theory. *Phys.Rev.*, D85:104018, 2012. doi: 10.1103/PhysRevD.85.104018.

A. O. Barvinsky and Viatcheslav F. Mukhanov. New nonlocal effective action. *Phys. Rev.*, D66:065007, 2002. doi: 10.1103/PhysRevD.66.065007.

A. O. Barvinsky and G. A. Vilkovisky. Beyond the Schwinger-DeWitt technique: Converting loops into trees and in-in currents. *Nuclear Physics B*, 282:163–188, 1987. doi: 10.1016/0550-3213(87)90681-X.

A. O. Barvinsky and G. A. Vilkovisky. Covariant perturbation theory (ii). second order in the curvature. general algorithms. *Nuclear Physics B*, 333(2):471 – 511, 1990. ISSN 0550-3213. doi: http://dx.doi.org/10.1016/0550-3213(90)90047-H.

A. O. Barvinsky, Yu. V. Gusev, G. A. Vilkovisky, and V. V. Zhytnikov. The One loop effective action and trace anomaly in four-dimensions. *Nucl. Phys.*, B439:561–582, 1995. doi: 10.1016/0550-3213(94)00585-3.

B. A. Bassett. Cosmic acceleration vs axion - photon mixing. *Astrophys. J.*, 607:661–664, 2004. doi: 10.1086/383520.

B. A. Bassett and R. Hlozek. Baryon Acoustic Oscillations. 2009.

B. A. Bassett and M. Kunz. Cosmic distance-duality as a probe of exotic physics and acceleration. *Phys. Rev. D*, 69:101305, May 2004. doi: 10.1103/PhysRevD.69.101305.

D. Baumann. Inflation. In *Physics of the large and the small, TASI 09, proceedings of the Theoretical Advanced Study Institute in Elementary Particle Physics, Boulder, Colorado, USA, 1-26 June 2009*, pages 523–686, 2011. doi: 10.1142/9789814327183_0010.

R. H. Becker et al. Evidence for reionization at $z \sim 6$: Detection of a Gunn-Peterson trough in a $z = 6.28$ quasar. *Astron. J.*, 122:2850, 2001. doi: 10.1086/324231.

J. Bekenstein and M. Milgrom. Does the missing mass problem signal the breakdown of Newtonian gravity? *Astrophysical Journal*, 286:7–14, November 1984. doi: 10.1086/162570.

J. D. Bekenstein. Relativistic gravitation theory for the MOND paradigm. *Phys. Rev.*, D70: 083509, 2004. doi: 10.1103/PhysRevD.70.083509,10.1103/PhysRevD.71.069901. [Erratum: Phys. Rev.D71,069901(2005)].

E. Belgacem, Y. Dirian, S. Foffa, and M. Maggiore. The gravitational-wave luminosity distance in modified gravity theories. *To Appear in Phys. Rev. D*, 2017.

E. Belgacem, G. Cusin, S. Foffa, M. Maggiore, and M. Mancarella. Stability issues of nonlocal gravity during primordial inflation. *Int. J. Mod. Phys.*, A33(01):1850007, 2018a. doi: 10.1142/S0217751X18500070.

E. Belgacem, Y. Dirian, S. Foffa, and M. Maggiore. Nonlocal gravity. Conceptual aspects and cosmological predictions. *JCAP*, 1803(03):002, 2018b. doi: 10.1088/1475-7516/2018/03/002.

E. Belgacem, Y. Dirian, S. Foffa, and M. Maggiore. Modified gravitational-wave propagation and standard sirens. 2018c.

E. Bellini et al. Comparison of Einstein-Boltzmann solvers for testing general relativity. *Phys. Rev.*, D97(2):023520, 2018. doi: 10.1103/PhysRevD.97.023520.

N. Bellomo, E. Bellini, B. Hu, R. Jimenez, C. Pena-Garay, and L. Verde. Hiding neutrino mass in modified gravity cosmologies. *JCAP*, 1702(02):043, 2017. doi: 10.1088/1475-7516/2017/02/043.

N. Benitez et al. Measuring Baryon Acoustic Oscillations along the line of sight with photometric redshifs: the PAU survey. *Astrophys. J.*, 691:241–260, 2009. doi: 10.1088/0004-637X/691/1/241.

C. L. Bennett et al. First year Wilkinson Microwave Anisotropy Probe (WMAP) observations: Preliminary maps and basic results. *Astrophys. J. Suppl.*, 148:1–27, 2003. doi: 10.1086/377253.

J. L. Bernal, L. Verde, and A. G. Riess. The trouble with H_0. *JCAP*, 1610(10):019, 2016. doi: 10.1088/1475-7516/2016/10/019.

F. Bernardeau. Lens distortion effects on CMB maps. *Astron. Astrophys.*, 338:767–776, 1998.

E. Berti et al. Testing General Relativity with Present and Future Astrophysical Observations. *Class. Quant. Grav.*, 32:243001, 2015. doi: 10.1088/0264-9381/32/24/243001.

G. Bertone and D. Hooper. A History of Dark Matter. *Submitted to: Rev. Mod. Phys.*, 2016.

E. Bertschinger, A. Dekel, S. M. Faber, A. Dressler, and D. Burstein. Potential, velocity, and density fields from redshift-distance samples: Application - Cosmography within 6000 kilometers per second. *Astrophysical Journal*, 364:370–395, December 1990. doi: 10.1086/169419.

M. Betoule et al. Improved cosmological constraints from a joint analysis of the SDSS-II and SNLS supernova samples. *Astron.Astrophys.*, 568:A22, 2014. doi: 10.1051/0004-6361/201423413.

F. Beutler, C. Blake, M. Colless, D. H. Jones, L. Staveley-Smith, L. Campbell, Q. Parker, W. Saunders, and F. Watson. The 6dF Galaxy Survey: baryon acoustic oscillations and the local Hubble constant. *Mon.Not.Roy.Astron.Soc.*, 416:3017–3032, October 2011. doi: 10.1111/j.1365-2966.2011.19250.x.

F. Beutler, C. Blake, M. Colless, D. H. Jones, L. Staveley-Smith, G. B. Poole, L. Campbell, Q. Parker, W. Saunders, and F. Watson. The 6dF Galaxy Survey: $z \approx 0$ measurements of the growth rate and σ_8. *MNRAS*, 423:3430–3444, July 2012. doi: 10.1111/j.1365-2966.2012.21136.x.

E. Bianchi and C. Rovelli. Why all these prejudices against a constant? 2010.

P. Binetruy. Cosmological constant versus quintessence. In *The primordial universe. Proceedings, Summer School on physics, 71st session, Les Houches, France, June 28-July 23, 1999*, pages 397–422, 2000. doi: 10.1007/3-540-45334-2_8.

N. D. Birrell and P. C. W. Davies. *Quantum Fields in Curved Space*. Cambridge Monographs on Mathematical Physics. Cambridge Univ. Press, Cambridge, UK, 1984.

C. Blake and K. Glazebrook. Probing Dark Energy Using Baryonic Oscillations in the Galaxy Power Spectrum as a Cosmological Ruler. *Astrophys. J.*, 594:665–673, September 2003. doi: 10.1086/376983.

C.and Brough Blake et al. The WiggleZ Dark Energy Survey: Joint measurements of the expansion and growth history at $z < 1$. *Mon.Not.Roy.Astron.Soc.*, 425:405–414, 2012. doi: 10.1111/j.1365-2966.2012.21473.x.

A. Blanchard and J. Schneider. Gravitational lensing effect on the fluctuations of the cosmic background radiation. *A & A*, 184:1–6, October 1987.

D. Blas, J. Lesgourgues, and T. Tram. The Cosmic Linear Anisotropy Solving System (CLASS). Part II: Approximation schemes. *JCAP*, 7:034, July 2011. doi: 10.1088/1475-7516/2011/07/034.

G. R. Blumenthal, S. M. Faber, J. R. Primack, and M. J. Rees. Formation of galaxies and large-scale structure with cold dark matter. *Nature*, 311:517–525, October 1984. doi: 10.1038/311517a0.

B. Bolliet, B. Comis, E. Komatsu, and J. F. Macas-Pérez. Dark Energy from the Thermal Sunyaev Zeldovich Power Spectrum. 2017. doi: 10.1093/mnras/sty823.

J. R. Bond and G. Efstathiou. Cosmic background radiation anisotropies in universes dominated by nonbaryonic dark matter. *The Astrophysical Journal Letters*, 285:L45–L48, October 1984. doi: 10.1086/184362.

J. R. Bond and A. S. Szalay. The collisionless damping of density fluctuations in an expanding universe. *Astrophysical Journal*, 274:443–468, November 1983. doi: 10.1086/161460.

J. R. Bond, G. Efstathiou, and J. Silk. Massive neutrinos and the large-scale structure of the universe. *Phys. Rev. Lett.*, 45:1980–1984, Dec 1980. doi: 10.1103/PhysRevLett.45.1980.

J. R. Bond, A. S. Szalay, and M. S. Turner. Formation of galaxies in a gravitino-dominated universe. *Phys. Rev. Lett.*, 48:1636–1639, Jun 1982. doi: 10.1103/PhysRevLett.48.1636.

J. R. Bond, R. Crittenden, R. L. Davis, G. Efstathiou, and P. J. Steinhardt. Measuring cosmological parameters with cosmic microwave background experiments. *Phys. Rev. Lett.*, 72:13–16, 1994. doi: 10.1103/PhysRevLett.72.13.

J. R. Bond, G. Efstathiou, and M. Tegmark. Forecasting cosmic parameter errors from microwave background anisotropy experiments. *Mon. Not. Roy. Astron. Soc.*, 291:L33–L41, November 1997. doi: 10.1093/mnras/291.1.L33.

J. R. Bond, A. H. Jaffe, and L. Knox. Estimating the power spectrum of the cosmic microwave background. *Phys. Rev.*, D57:2117–2137, 1998. doi: 10.1103/PhysRevD.57.2117.

J. Richard Bond et al. CMB analysis of Boomerang and Maxima and the cosmic parameters Ω_{tot}, $\Omega_b h^2$, $\Omega_{cdm} h^2$, Ω_Λ, n_s. In *IAU Symposium 201: New Cosmological Data and the Value of the Fundamental Parameters Manchester, England, August 7-11, 2000*, 2000.

H. Bondi and T. Gold. The Steady-State Theory of the Expanding Universe. *Mon. Not. Roy. Astron. Soc.*, 108:252, 1948. doi: 10.1093/mnras/108.3.252.

V. Bonvin, F. Courbin, S. H. Suyu, P. J. Marshall, C. E. Rusu, D. Sluse, M. Tewes, K. C. Wong, T. Collett, C. D. Fassnacht, T. Treu, M. W. Auger, S. Hilbert, L. V. E. Koopmans, G. Meylan, N. Rumbaugh, A. Sonnenfeld, and C. Spiniello. H0licow v. new cosmograil time delays of he0435-1223: h_0 to 3.8% precision from strong lensing in a flat λcdm model. *MNRAS*, 465 (4):4914, 2017. doi: 10.1093/mnras/stw3006.

Ph. Boucaud, A. Le Yaouanc, J. P. Leroy, J. Micheli, O. Pene, and J. Rodriguez-Quintero. Testing Landau gauge OPE on the lattice with a $\langle A^2 \rangle$ condensate. *Phys. Rev.*, D63:114003, 2001. doi: 10.1103/PhysRevD.63.114003.

S. P. Boughn, R. G. Crittenden, and N. G. Turok. Correlations between the cosmic X-ray and microwave backgrounds: Constraints on a cosmological constant. *New Astron.*, 3:275–291, 1998. doi: 10.1016/S1384-1076(98)00009-8.

G. Boulware and S. Deser. Can gravitation have a finite range ? *Phys. Rev. D*, 6:3368–3382, (1972). doi: 10.1103/PhysRevD.6.3368.

P. Brax, C. van de Bruck, A.-C. Davis, J. Khoury, and A. Weltman. Detecting dark energy in orbit - The Cosmological chameleon. *Phys. Rev.*, D70:123518, 2004. doi: 10.1103/PhysRevD.70.123518.

M. P. Bronstein. On the expanding universe. *Phys. Z. Sowjetunion*, 3:73, 1933.

I. L. Buchbinder, S. D. Odintsov, and I. L. Shapiro. *Effective action in quantum gravity*. 1992.

T. Buchert and S. Räsänen. Backreaction in late-time cosmology. *Ann. Rev. Nucl. Part. Sci.*, 62:57–79, 2012. doi: 10.1146/annurev.nucl.012809.104435.

K. P. Burnham and D. R. (biologiste) Anderson. *Model selection and multimodel inference : a practical information-theoretic approach*. Springer, New York, 2002. ISBN 0-387-95364-7. Édition revue et corrigée de : Model selection and inference, cop. 1998.

A. Cabre, Enrique Gaztanaga, M. Manera, P. Fosalba, and F. Castander. Cross-correlation of wmap 3rd year and the sdss dr4 galaxy survey: new evidence for dark energy. *Mon. Not. Roy. Astron. Soc.*, 372:L23–L27, 2006. doi: 10.1111/j.1745-3933.2006.00218.x.

R.-G. Cai and T. Yang. Estimating cosmological parameters by the simulated data of gravitational waves from the Einstein Telescope. *Phys. Rev.*, D95:044024, 2017. doi: 10.1103/PhysRevD.95.044024.

E. Calabrese et al. Cosmological parameters from pre-planck cosmic microwave background measurements. *Phys. Rev.*, D87(10):103012, 2013. doi: 10.1103/PhysRevD.87.103012.

E. Calabrese et al. Cosmological Parameters from pre-Planck CMB Measurements: a 2017 Update. *Phys. Rev.*, D95(6):063525, 2017. doi: 10.1103/PhysRevD.95.063525.

R. Caldwell, A. Cooray, and A. Melchiorri. Constraints on a New Post-General Relativity Cosmological Parameter. *Phys. Rev.*, D76:023507, 2007. doi: 10.1103/PhysRevD.76.023507.

R. R. Caldwell. A Phantom menace? *Phys. Lett.*, B545:23–29, 2002. doi: 10.1016/S0370-2693(02)02589-3.

R. R. Caldwell and S. S. Gubser. Brief history of curvature. *Phys. Rev.*, D87(6):063523, 2013. doi: 10.1103/PhysRevD.87.063523.

R. R. Caldwell and M. Kamionkowski. The Physics of Cosmic Acceleration. *Ann. Rev. Nucl. Part. Sci.*, 59:397–429, 2009. doi: 10.1146/annurev-nucl-010709-151330.

R. R. Caldwell, Rahul Dave, and Paul J. Steinhardt. Cosmological imprint of an energy component with general equation of state. *Phys. Rev. Lett.*, 80:1582–1585, 1998. doi: 10.1103/PhysRevLett.80.1582.

R. R. Caldwell, M. Kamionkowski, and N. N. Weinberg. Phantom energy and cosmic doomsday. *Phys. Rev. Lett.*, 91:071301, 2003. doi: 10.1103/PhysRevLett.91.071301.

S. Camera and A. Nishizawa. Beyond Concordance Cosmology with Magnification of Gravitational-Wave Standard Sirens. *Phys. Rev. Lett.*, 110:151103, 2013. doi: 10.1103/PhysRevLett.110.151103.

S. Capozziello, E. Elizalde, S. Nojiri, and S. D. Odintsov. Accelerating cosmologies from non-local higher-derivative gravity. *Phys. Lett.*, B671:193–198, 2009. doi: 10.1016/j.physletb.2008.11.060.

D. M. Capper and M. J. Duff. Trace anomalies in dimensional regularization. *Il Nuovo Cimento A (1965-1970)*, 23(1):173–183, Sep 1974. ISSN 1826-9869. doi: 10.1007/BF02748300.

M. A. L. Capri, D. Dudal, J. A. Gracey, V. E. R. Lemes, R. F. Sobreiro, S. P. Sorella, and H. Verschelde. A Study of the gauge invariant, nonlocal mass operator Tr $\int d^4x F_{\mu\nu}(D^2)^{-1}F_{\mu\nu}$ in Yang-Mills theories. *Phys. Rev.*, D72:105016, 2005. doi: 10.1103/PhysRevD.72.105016.

C. Caprini and N. Tamanini. Constraining early and interacting dark energy with gravitational wave standard sirens: the potential of the eLISA mission. *JCAP*, 1610:006, 2016. doi: 10.1088/1475-7516/2016/10/006.

W. Cardona, M. Kunz, and V. Pettorino. Determining H_0 with Bayesian hyper-parameters. *JCAP*, 1703(03):056, 2017. doi: 10.1088/1475-7516/2017/03/056.

B. J. Carr and S. W. Hawking. Black holes in the early Universe. *Mon. Not. Roy. Astron. Soc.*, 168:399–416, August 1974. doi: 10.1093/mnras/168.2.399.

S. M. Carroll. Why is the universe accelerating? *eConf*, C0307282:TTH09, 2003. doi: 10.1063/1.1848314. [AIP Conf. Proc.743,16(2005)].

S. M. Carroll, V. Duvvuri, M. Trodden, and M. S. Turner. Is cosmic speed-up due to new gravitational physics? *Phys. Rev.*, D70:043528, 2004. doi: 10.1103/PhysRevD.70.043528.

S. M. Carroll, A. De Felice, V. Duvvuri, D. A. Easson, M. Trodden, and M. S. Turner. The Cosmology of generalized modified gravity models. *Phys. Rev.*, D71:063513, 2005. doi: 10.1103/PhysRevD.71.063513.

E. Cartan. Sur les équations de la gravitation d'Einstein. *Journal de Mathématiques Pures et Appliquées*, 1:141–204, 1922.

S. Casas, M. Kunz, M. Martinelli, and V. Pettorino. Linear and non-linear Modified Gravity forecasts with future surveys. *Phys. Dark Univ.*, 18:73–104, 2017. doi: 10.1016/j.dark.2017.09.009.

S. Casas, Y. Dirian, E. Majerotto, M. Kunz, M. Maggiore, and V. Pettorino. Forecasts on nonlocal gravity with future surveys (in preparation). 2018.

C. Charmousis, R. Gregory, N. Kaloper, and A. Padilla. DGP Specteroscopy. *JHEP*, 10:066, 2006. doi: 10.1088/1126-6708/2006/10/066.

H.-Y. Chen, M. Fishbach, and Daniel E. Holz. Precision standard siren cosmology. 2017.

C. Cheung, P. Creminelli, A. L. Fitzpatrick, J. Kaplan, and L. Senatore. The Effective Field Theory of Inflation. *JHEP*, 03:014, 2008. doi: 10.1088/1126-6708/2008/03/014.

M. Chevallier and D. Polarski. Accelerating universes with scaling dark matter. *Int. J. Mod. Phys.*, D10:213–224, 2001. doi: 10.1142/S0218271801000822.

K. Choi. String or M theory axion as a quintessence. *Phys. Rev.*, D62:043509, 2000. doi: 10.1103/PhysRevD.62.043509.

N. Chow and J. Khoury. Galileon Cosmology. *Phys. Rev.*, D80:024037, 2009. doi: 10.1103/PhysRevD.80.024037.

D. Christodoulou and S. Klainerman. The Global nonlinear stability of the Minkowski space. 1993.

Chia-Hsun Chuang et al. The clustering of galaxies in the SDSS-III Baryon Oscillation Spectroscopic Survey: single-probe measurements from CMASS anisotropic galaxy clustering. *MNRAS*, 461(4):3781–3793, 2016. doi: 10.1093/mnras/stw1535.

T. Clifton, P. G. Ferreira, A. Padilla, and C. Skordis. Modified Gravity and Cosmology. *Phys. Rept.*, 513:1–189, 2012. doi: 10.1016/j.physrep.2012.01.001.

K. Coble, S. Dodelson, and J. A. Frieman. Dynamical λ models of structure formation. *Phys. Rev. D*, 55:1851–1859, Feb 1997. doi: 10.1103/PhysRevD.55.1851.

A. Codello and Rajeev K. Jain. On the covariant formalism of the effective field theory of gravity and leading order corrections. *Class. Quant. Grav.*, 33(22):225006, 2016. doi: 10.1088/0264-9381/33/22/225006.

S. Cole and G. Efstathiou. Gravitational lensing of fluctuations in the microwave background radiation. *MNRAS*, 239:195–200, July 1989. doi: 10.1093/mnras/239.1.195.

C. Contreras et al. The Carnegie Supernova Project: First Photometry Data Release of Low-Redshift Type Ia Supernovae. *Astronomical Journal*, 139:519–539, February 2010. doi: 10.1088/0004-6256/139/2/519.

E. J. Copeland, A. R Liddle, and D. Wands. Exponential potentials and cosmological scaling solutions. *Phys. Rev.*, D57:4686–4690, 1998. doi: 10.1103/PhysRevD.57.4686.

E. J. Copeland, M. S., and S. Tsujikawa. Dynamics of dark energy. *Int. J. Mod. Phys.*, D15:1753–1936, 2006. doi: 10.1142/S021827180600942X.

P. Creminelli and F. Vernizzi. Dark Energy after GW170817 and GRB170817A. *Phys. Rev. Lett.*, 119:251302, 2017. doi: 10.1103/PhysRevLett.119.251302.

Neil Crittenden, Robert G.; Turok. Looking for a cosmological constant with the rees-sciama effect. *Physical Review Letters*, 76, 1 1996. doi: 10.1103/PhysRevLett.76.575.

A. J. Cuesta, L. Verde, A. Riess, and R. Jimenez. The cosmic inverse distance ladder: baryon acoustic oscillations and type-Ia supernovae. In A. J. Cenarro, F. Figueras, C. Hernández-Monteagudo, J. Trujillo Bueno, and L. Valdivielso, editors, *Highlights of Spanish Astrophysics VIII*, pages 172–176, May 2015.

A. J. Cuesta, L. Verde, A. Riess, and R. Jimenez. Calibrating the cosmic distance scale ladder: the role of the sound horizon scale and the local expansion rate as distance anchors. *Mon. Not. Roy. Astron. Soc.*, 448(4):3463–3471, 2015. doi: 10.1093/mnras/stv261.

G. Cusin, S. Foffa, M. Maggiore, and M. Mancarella. Conformal symmetry and nonlinear extensions of nonlocal gravity. *Phys. Rev.*, D93(8):083008, 2016a. doi: 10.1103/PhysRevD.93.083008.

G. Cusin, S. Foffa, M. Maggiore, and M. Mancarella. Nonlocal gravity with a Weyl-square term. *Phys. Rev.*, D93(4):043006, 2016b. doi: 10.1103/PhysRevD.93.043006.

G. Cusin, S. Foffa, M. Maggiore, and M. Mancarella. Conformal symmetry and nonlinear extensions of nonlocal gravity. *Phys. Rev.*, D93(8):083008, 2016c. doi: 10.1103/PhysRevD.93.083008.

C. Cutler and D. E. Holz. Ultra-high precision cosmology from gravitational waves. *Phys. Rev.*, D80:104009, 2009. doi: 10.1103/PhysRevD.80.104009.

N. Dalal, D. E. Holz, S. A. Hughes, and B. Jain. Short grb and binary black hole standard sirens as a probe of dark energy. *Phys. Rev.*, D74:063006, 2006. doi: 10.1103/PhysRevD.74.063006.

D. A. R. Dalvit and F. D. Mazzitelli. Running coupling constants, Newtonian potential and nonlocalities in the effective action. *Phys. Rev.*, D50:1001–1009, 1994. doi: 10.1103/PhysRevD.50.1001.

S. F. Daniel, E. V. Linder, T. L. Smith, R. R. Caldwell, A. Cooray, A. Leauthaud, and L. Lombriser. Testing general relativity with current cosmological data. *Phys. Rev. D*, 81(12):123508, June 2010. doi: 10.1103/PhysRevD.81.123508.

S. Das et al. Detection of the power spectrum of cosmic microwave background lensing by the atacama cosmology telescope. *Phys. Rev. Lett.*, 107:021301, Jul 2011. doi: 10.1103/PhysRevLett.107.021301.

M. Davis and P. J. E. Peebles. A survey of galaxy redshifts. V - The two-point position and velocity correlations. *Astrophysical Journal*, 267:465–482, April 1983. doi: 10.1086/160884.

M. Davis, J. Huchra, D. W. Latham, and J. Tonry. A survey of galaxy redshifts. II - The large scale space distribution. *Astrophysical Journal*, 253:423–445, February 1982. doi: 10.1086/159646.

M. Davis, G. Efstathiou, C. S. Frenk, and S. D. M. White. The evolution of large-scale structure in a universe dominated by cold dark matter. *Astrophysical Journal*, 292:371–394, May 1985. doi: 10.1086/163168.

P. de Bernardis, Peter Ade, J J. Bock, J R. Bond, J Borrill, A Boscaleri, K Coble, B P. Crill, Giancarlo de Gasperis, G De Troia, P C. Farese, P G. Ferreira, Ken Ganga, M Giacometti, Eric Hivon, V V. Hristov, A Iacoangeli, A H. Jaffe, A E. Lange, and Nicola Vittorio. First results from the boomerang experiment. 555, 11 2000.

A. De Felice and S. Tsujikawa. Cosmology of a covariant Galileon field. *Phys. Rev. Lett.*, 105: 111301, 2010. doi: 10.1103/PhysRevLett.105.111301.

S. de la Torre, L. Guzzo, J.A. Peacock, E. Branchini, A. Iovino, et al. The VIMOS Public Extragalactic Redshift Survey (VIPERS). Galaxy clustering and redshift-space distortions at $z = 0.8$ in the first data release. *Astron.Astrophys.*, 557:A54, 2013. doi: 10.1051/0004-6361/201321463.

C. de Rham. Massive Gravity. *Living Rev. Rel.*, 17:7, 2014. doi: 10.12942/lrr-2014-7.

C. de Rham and G. Gabadadze. Generalization of the fierz-pauli action. *Phys. Rev. D*, 82: 044020, Aug 2010. doi: 10.1103/PhysRevD.82.044020.

C. de Rham, G. Gabadadze, and A.J. Tolley. Resummation of massive gravity. *Phys. Rev. Lett.*, 106:231101, 2011. doi: 10.1103/PhysRevLett.106.231101.

C. Deffayet. Cosmology on a brane in Minkowski bulk. *Phys. Lett.*, B502:199–208, 2001. doi: 10.1016/S0370-2693(01)00160-5.

C. Deffayet and K. Menou. Probing Gravity with Spacetime Sirens. *Astrophys. J.*, 668:L143–L146, 2007. doi: 10.1086/522931.

C. Deffayet and R. P. Woodard. Reconstructing the Distortion Function for Nonlocal Cosmology. *JCAP*, 0908:023, 2009. doi: 10.1088/1475-7516/2009/08/023.

C. Deffayet, G. R. Dvali, and G. Gabadadze. Accelerated universe from gravity leaking to extra dimensions. *Phys. Rev.*, D65:044023, 2002. doi: 10.1103/PhysRevD.65.044023.

C. Deffayet, S. Deser, and G. Esposito-Farese. Generalized Galileons: All scalar models whose curved background extensions maintain second-order field equations and stress-tensors. *Phys. Rev.*, D80:064015, 2009. doi: 10.1103/PhysRevD.80.064015.

C. Deffayet, G. Esposito-Farèse, and A. Vikman. Covariant Galileon. *PRD*, 79(8):084003, April 2009. doi: 10.1103/PhysRevD.79.084003.

C. Deffayet, X. Gao, D. A. Steer, and G. Zahariade. From k-essence to generalised Galileons. *Phys. Rev.*, D84:064039, 2011. doi: 10.1103/PhysRevD.84.064039.

W. Del Pozzo. Inference of the cosmological parameters from gravitational waves: application to second generation interferometers. *Phys. Rev.*, D86:043011, 2012. doi: 10.1103/PhysRevD.86.043011.

S. Dell'Oro, S. Marcocci, M. Viel, and Francesco Vissani. Neutrinoless double beta decay: 2015 review. *Adv. High Energy Phys.*, 2016:2162659, 2016. doi: 10.1155/2016/2162659.

P. Demarque, C. P. Deliyannis, and A. Sarajedini. *Ages of Globular Clusters*, pages 111–129. Springer Netherlands, Dordrecht, 1991. ISBN 978-94-011-3510-8. doi: 10.1007/978-94-011-3510-8_11.

S. Deser and R. P. Woodard. Nonlocal Cosmology. *Phys. Rev. Lett.*, 99:111301, 2007. doi: 10.1103/PhysRevLett.99.111301.

S. Deser and R. P. Woodard. Observational Viability and Stability of Nonlocal Cosmology. *JCAP*, 1311:036, 2013a. doi: 10.1088/1475-7516/2013/11/036.

S. Deser and R.P. Woodard. Observational Viability and Stability of Nonlocal Cosmology. *JCAP*, 1311:036, 2013b. doi: 10.1088/1475-7516/2013/11/036.

S. Deser, M. J. Duff, and C. J. Isham. Nonlocal Conformal Anomalies. *Nucl. Phys.*, B111: 45–55, 1976. doi: 10.1016/0550-3213(76)90480-6.

DESI Collaboration, A. Aghamousa, J. Aguilar, S. Ahlen, S. Alam, L. E. Allen, C. Allende Prieto, J. Annis, S. Bailey, C. Balland, and et al. The DESI Experiment Part I: Science,Targeting, and Survey Design. *ArXiv e-prints*, October 2016a.

DESI Collaboration, A. Aghamousa, J. Aguilar, S. Ahlen, S. Alam, L. E. Allen, C. Allende Prieto, J. Annis, S. Bailey, C. Balland, and et al. The DESI Experiment Part II: Instrument Design. *ArXiv e-prints*, October 2016b.

V. Desjacques, D. Jeong, and F. Schmidt. Large-Scale Galaxy Bias. 2016.

P. E. Dewdney, P. J. Hall, R. T. Schilizzi, and T. J. L. W. Lazio. The square kilometre array. *Proceedings of the IEEE*, 97(8):1482–1496, 2009. ISSN 0018-9219. doi: 10.1109/JPROC.2009.2021005.

B. S. DeWitt. Quantum theory of gravity. ii. the manifestly covariant theory. *Phys. Rev.*, 162: 1195–1239, Oct 1967. doi: 10.1103/PhysRev.162.1195.

E. Di Valentino, A. Melchiorri, and J. Silk. Reconciling Planck with the local value of H_0 in extended parameter space. *Phys. Lett.*, B761:242–246, 2016. doi: 10.1016/j.physletb.2016.08.043.

Y. Dirian. Changing the Bayesian prior: Absolute neutrino mass constraints in nonlocal gravity. *Phys. Rev.*, D96(8):083513, 2017. doi: 10.1103/PhysRevD.96.083513.

Y. Dirian and E. Mitsou. Stability analysis and future singularity of the $m^2R\Box^{-2}R$ model of non-local gravity. *JCAP*, 10:065, October 2014. doi: 10.1088/1475-7516/2014/10/065.

Y. Dirian, S. Foffa, N. Khosravi, M. Kunz, and M. Maggiore. Cosmological perturbations and structure formation in nonlocal infrared modifications of general relativity. *JCAP*, 1406:033, 2014. doi: 10.1088/1475-7516/2014/06/033.

Y. Dirian, S. Foffa, M. Kunz, M. Maggiore, and V. Pettorino. Non-local gravity and comparison with observational datasets. *JCAP*, 1504(04):044, 2015. doi: 10.1088/1475-7516/2015/04/044.

Y. Dirian, S. Foffa, M. Kunz, M. Maggiore, and V. Pettorino. Non-local gravity and comparison with observational datasets. II. Updated results and Bayesian model comparison with ΛCDM. *JCAP*, 1605(05):068, 2016. doi: 10.1088/1475-7516/2016/05/068.

A. Dobado and A. L. Maroto. Particle production from nonlocal gravitational effective action. *Phys. Rev.*, D60:104045, 1999. doi: 10.1103/PhysRevD.60.104045.

S. Dodelson and S. Park. Nonlocal gravity and structure in the Universe. *PRD*, 90(4):043535, August 2014. doi: 10.1103/PhysRevD.90.043535.

S. Dodelson and L. M. Widrow. Sterile-neutrinos as dark matter. *Phys. Rev. Lett.*, 72:17–20, 1994. doi: 10.1103/PhysRevLett.72.17.

S. Dodelson, E. I. Gates, and M. S. Turner. Cold dark matter models. *Science*, 274:69–75, 1996. doi: 10.1126/science.274.5284.69.

J. F. Donoghue. Leading quantum correction to the Newtonian potential. *Phys. Rev. Lett.*, 72: 2996–2999, 1994. doi: 10.1103/PhysRevLett.72.2996.

M. Doran. Cmbeasy: an object oriented code for the cosmic microwave background. *Journal of Cosmology and Astroparticle Physics*, 2005(10):011, 2005.

A. G. Doroshkevich. Spatial structure of perturbations and origin of galactic rotation in fluctuation theory. *Astrophysics*, 6(4):320–330, Oct 1970. ISSN 1573-8191. doi: 10.1007/BF01001625.

A. G. Doroshkevich, Y. B. Zel'dovich, and R. A. Syunyaev. Fluctuations of the microwave background radiation in the adiabatic and entropic theories of galaxy formation. *Soviet Astronomy*, 22:523–528, October 1978.

A. G. Doroshkevich, E. V. Kotok, I. D. Novikov, A. N. Polyudov, S. F. Shandarin, and Yu. S. Sigov. Two-dimensional simulation of the gravitational system dynamics and formation of the large-scale structure of the universe. *Monthly Notices of the Royal Astronomical Society*, 192(2):321–337, 1980a. doi: 10.1093/mnras/192.2.321.

A. G. Doroshkevich, Y. B. Zeldovich, R. A. Sunyaev, and M. Khlopov. Astrophysical implications of the neutrino rest mass. II. The density-perturbation spectrum and small-scale fluctuations in the microwave background. *Sov. Astron. Lett.*, 6:252–256, 1980b. [Pisma Astron. Zh.6,457(1980)].

G. Drexlin, V. Hannen, S. Mertens, and C. Weinheimer. Current direct neutrino mass experiments. *Adv. High Energy Phys.*, 2013:293986, 2013. doi: 10.1155/2013/293986.

D. Dudal, J. A. Gracey, S. P. Sorella, N. Vandersickel, and H. Verschelde. A Refinement of the Gribov-Zwanziger approach in the Landau gauge: Infrared propagators in harmony with the lattice results. *Phys. Rev.*, D78:065047, 2008. doi: 10.1103/PhysRevD.78.065047.

R. Durrer. *The Cosmic Microwave Background*. Cambridge University Press, 2008. doi: 10.1017/CBO9780511817205.

R. Durrer and T. Kahniashvili. CMB anisotropies caused by gravitational waves: A Parameter study. *Helv. Phys. Acta*, 71:445–457, 1998.

R. Durrer, A. Howard, and Z. Zhou. Microwave anisotropies from texture-seeded structure formation. *Phys. Rev. D*, 49:681–691, Jan 1994. doi: 10.1103/PhysRevD.49.681.

J.-B. Durrive, J. Ooba, K. Ichiki, and N. Sugiyama. Updated observational constraints on quintessence dark energy models. *Phys. Rev.*, D97(4):043503, 2018. doi: 10.1103/PhysRevD.97.043503.

G. Dvali. Predictive Power of Strong Coupling in Theories with Large Distance Modified Gravity. *New J. Phys.*, 8:326, 2006. doi: 10.1088/1367-2630/8/12/326.

G. Dvali, G. Gabadadze, and M. Porrati. 4D gravity on a brane in 5D Minkowski space. *Physics Letters B*, 485:208–214, July 2000. doi: 10.1016/S0370-2693(00)00669-9.

G. Dvali, G. Gabadadze, and M. Shifman. Diluting cosmological constant via large distance modification of gravity. In *PIMS Summer Workshop on Brane World and Supersymmetry (7th Frontiers in Mathematical Physics) Vancouver, British Columbia, Canada, July 22-August 6, 2002*, pages 566–581, 2002. doi: 10.1142/9789812776310_0034. [,566(2002)].

G. Dvali, S. Hofmann, and J. Khoury. Degravitation of the cosmological constant and graviton width. *Phys. Rev.*, D76:084006, 2007. doi: 10.1103/PhysRevD.76.084006.

G. R. Dvali and Gregory Gabadadze. Gravity on a brane in infinite volume extra space. *Phys. Rev.*, D63:065007, 2001. doi: 10.1103/PhysRevD.63.065007.

G. Efstathiou. An anthropic argument for a cosmological constant. *MNRAS*, 274:L73–L76, June 1995. doi: 10.1093/mnras/274.1.L73.

G. Efstathiou. Limitations of Bayesian Evidence Applied to Cosmology. *MNRAS*, 388:1314, 2008. doi: 10.1111/j.1365-2966.2008.13498.x.

G. Efstathiou. H_0 revisited. *Mon. Not. Roy. Astron. Soc.*, 440:1138–1152, May 2014. doi: 10.1093/mnras/stu278.

G. Efstathiou. H_0 Revisited. *Mon.Not.Roy.Astron.Soc.*, 440(2):1138–1152, 2014. doi: 10.1093/mnras/stu278.

G. Efstathiou and J. R. Bond. Cosmic confusion: Degeneracies among cosmological parameters derived from measurements of microwave background anisotropies. *Mon. Not. Roy. Astron. Soc.*, 304:75–97, 1999. doi: 10.1046/j.1365-8711.1999.02274.x.

G. Efstathiou and J. W. Eastwood. On the clustering of particles in an expanding universe. *Mon. Not. Roy. Astron. Soc.*, 194:503–525, February 1981. doi: 10.1093/mnras/194.3.503.

G. Efstathiou, W. J. Sutherland, and S. J. Maddox. The cosmological constant and cold dark matter. *Nature*, 348:705–707, December 1990. doi: 10.1038/348705a0.

G. Efstathiou, J. R. Bond, and S. D. M. White. Cobe background radiation anisotropies and large-scale structure in the universe. *Monthly Notices of the Royal Astronomical Society*, 258 (1):1P–6P, 1992. doi: 10.1093/mnras/258.1.1P.

J. Einasto, A. Kaasik, and E. Saar. Dynamic evidence on massive coronas of galaxies. *Nature*, 250:309–310, July 1974. doi: 10.1038/250309a0.

A. Einstein. Zur Elektrodynamik bewegter Körper. *Annalen der Physik*, 322:891–921, 1905. doi: 10.1002/andp.19053221004.

A. Einstein. Die Feldgleichungen der Gravitation. *Sitzungsberichte der Königlich Preußischen Akademie der Wissenschaften (Berlin), Seite 844-847.*, 1915.

A. Einstein. Die grundlage der allgemeinen relativittstheorie. *Annalen der Physik*, 354(7): 769–822, 1916. doi: 10.1002/andp.19163540702.

A. Einstein. Kosmologische Betrachtungen zur allgemeinen Relativitätstheorie. *Sitzungsberichte der Königlich Preußischen Akademie der Wissenschaften (Berlin), Seite 142-152.*, 1917.

D. Eisenstein. Large scale structure and future surveys. In *Conference on Next Generation Wide-Field Multi-Object Spectroscopy Tuscon, Arizona, October 11-12, 2001*, 2003. [Submitted to: ASP Conf. Ser.(2003)].

D. J. Eisenstein and W. Hu. Baryonic Features in the Matter Transfer Function. *Astrophys. J.*, 496:605–614, March 1998. doi: 10.1086/305424.

D. J. Eisenstein, W. Hu, and M. Tegmark. Cosmic complementarity: H_0 and $Omega_m$ from combining CMB experiments and redshift surveys. *Astrophys. J.*, 504:L57–L61, 1998. doi: 10.1086/311582.

D. J. Eisenstein, W. Hu, and M. Tegmark. Cosmic complementarity: Joint parameter estimation from CMB experiments and redshift surveys. *Astrophys. J.*, 518:2–23, 1999. doi: 10.1086/307261.

D. J. Eisenstein et al. Detection of the Baryon Acoustic Peak in the Large-Scale Correlation Function of SDSS Luminous Red Galaxies. *Astrophys. J.*, 633:560–574, 2005. doi: 10.1086/466512.

J. Ellis, J.S. Hagelin, D.V. Nanopoulos, K. Olive, and M. Srednicki. Supersymmetric relics from the big bang. *Nuclear Physics B*, 238(2):453 – 476, 1984. ISSN 0550-3213. doi: https://doi.org/10.1016/0550-3213(84)90461-9.

J. Engel and J. Menéndez. Status and Future of Nuclear Matrix Elements for Neutrinoless Double-Beta Decay: A Review. *Rept. Prog. Phys.*, 80(4):046301, 2017. doi: 10.1088/1361-6633/aa5bc5.

ESA. Cosmic Microwave Background seen by *Planck*.

D. Espriu, T. Multamaki, and E. C. Vagenas. Cosmological significance of one-loop effective gravity. *Phys. Lett.*, B628:197–205, 2005. doi: 10.1016/j.physletb.2005.09.033.

J. M. Ezquiaga and M. Zumalacárregui. Dark Energy After GW170817: Dead Ends and the Road Ahead. *Phys. Rev. Lett.*, 119:251304, 2017. doi: 10.1103/PhysRevLett.119.251304.

K. Falls. Asymptotic safety and the cosmological constant. *JHEP*, 01:069, 2016. doi: 10.1007/JHEP01(2016)069.

R. Fardon, A. E. Nelson, and N. Weiner. Dark energy from mass varying neutrinos. *JCAP*, 0410:005, 2004. doi: 10.1088/1475-7516/2004/10/005.

S. M. Feeney, D. J. Mortlock, and N. Dalmasso. Clarifying the Hubble constant tension with a Bayesian hierarchical model of the local distance ladder. 2017. doi: 10.1093/mnras/sty418.

S. M. Feeney, H. V. Peiris, A. R. Williamson, S. M. Nissanke, D. J. Mortlock, J. Alsing, and D. Scolnic. Prospects for resolving the Hubble constant tension with standard sirens. 2018.

P. G. Ferreira and M. Joyce. Structure formation with a selftuning scalar field. *Phys. Rev. Lett.*, 79:4740–4743, 1997. doi: 10.1103/PhysRevLett.79.4740.

P. G. Ferreira and M. Joyce. Cosmology with a primordial scaling field. *Phys. Rev. D*, 58:023503, Jun 1998. doi: 10.1103/PhysRevD.58.023503.

P. G. Ferreira and A. L. Maroto. A few cosmological implications of tensor nonlocalities. *Phys. Rev.*, D88(12):123502, 2013. doi: 10.1103/PhysRevD.88.123502.

R.P Feynman and F.L Vernon. The theory of a general quantum system interacting with a linear dissipative system. *Annals of Physics*, 24:118 – 173, 1963. ISSN 0003-4916. doi: https://doi.org/10.1016/0003-4916(63)90068-X.

S. Foffa, M. Maggiore, and E. Mitsou. Apparent ghosts and spurious degrees of freedom in non-local theories. *Phys.Lett.*, B733:76–83, 2014a. doi: 10.1016/j.physletb.2014.04.024.

S. Foffa, M. Maggiore, and E. Mitsou. Cosmological dynamics and dark energy from non-local infrared modifications of gravity. *Int.J.Mod.Phys. A, to appear*, 2014b.

W. L. Freedman and L. L. Feng. Determination of the hubble constant. *Proceedings of the National Academy of Sciences*, 96(20):11063–11064, 1999. ISSN 0027-8424. doi: 10.1073/pnas.96.20.11063.

W. L. Freedman and B. F. Madore. The Hubble Constant. *Ann. Rev. Astron. Astrophys.*, 48: 673–710, 2010. doi: 10.1146/annurev-astro-082708-101829.

W. L. Freedman, B. F. Madore, V. Scowcroft, C. Burns, A. Monson, S. E. Persson, M. Seibert, and J. Rigby. Carnegie Hubble Program: A Mid-infrared Calibration of the Hubble Constant. *Astrophys. J.*, 758:24, October 2012. doi: 10.1088/0004-637X/758/1/24.

W. L. Freedman et al. Final results from the Hubble Space Telescope key project to measure the Hubble constant. *Astrophys. J.*, 553:47–72, 2001. doi: 10.1086/320638.

A. Friedmann. On the curvature of space. *General Relativity and Gravitation*, 31(12):1991–2000, Dec 1922. ISSN 1572-9532. doi: 10.1023/A:1026751225741.

A. Friedmann. Über die Möglichkeit einer Welt mit konstanter negativer Krümmung des Raumes. *Zeitschrift fur Physik*, 21:326–332, December 1924. doi: 10.1007/BF01328280.

J. N. Fry and A. L. Melott. Statistical comparison of galaxy formation models - The bispectrum. *Astrophysical Journal*, 292:395–403, May 1985. doi: 10.1086/163169.

B. Fuks. *Supersymmetry - When Theory Inspires Experimental Searches*. PhD thesis, U. Strasbourg, 2013.

M. Fukugita, C. J. Hogan, and P. J. E. Peebles. The cosmic distance scale and the Hubble constant. *Nature*, 366:309–312, December 1993. doi: 10.1038/366309a0.

C. R. Galley. Classical Mechanics of Nonconservative Systems. *Phys. Rev. Lett.*, 110(17):174301, 2013. doi: 10.1103/PhysRevLett.110.174301.

G. Gamow. The Evolution of the Universe. *Nature*, 162:680–682, October 1948. doi: 10.1038/162680a0.

M. Ganeshalingam, W. Li, and A. V. Filippenko. Constraints on dark energy with the LOSS SN Ia sample. *Mon. Not. Roy. Astron. Soc.*, 433:2240, 2013. doi: 10.1093/mnras/stt893.

A. Gangui, F. Lucchin, S. Matarrese, and S. Mollerach. The Three point correlation function of the cosmic microwave background in inflationary models. *Astrophys. J.*, 430:447–457, 1994. doi: 10.1086/174421.

R. Gannouji and M. Sami. Galileon gravity and its relevance to late time cosmic acceleration. *Phys. Rev.*, D82:024011, 2010. doi: 10.1103/PhysRevD.82.024011.

S. Gary and S. Michael. Cosmological constraints on the properties of weakly interacting massive particles. *Nuclear Physics B*, 253, 1985. doi: 10.1016/0550-3213(85)90537-1.

T. Giannantonio, R. Scranton, R. G. Crittenden, R. C. Nichol, S. P. Boughn, A. D. Myers, and G. T. Richards. Combined analysis of the integrated Sachs-Wolfe effect and cosmological implications. *Phys. Rev.*, D77:123520, 2008. doi: 10.1103/PhysRevD.77.123520.

E. Giusarma, S. Vagnozzi, S. Ho, S. Ferraro, K. Freese, R. Kamen-Rubio, and K.-B. Luk. Scale-dependent galaxy bias, CMB lensing-galaxy cross-correlation, and neutrino masses. 2018.

J. Gleyzes, D. Langlois, F. Piazza, and F. Vernizzi. Essential Building Blocks of Dark Energy. *JCAP*, 1308:025, 2013. doi: 10.1088/1475-7516/2013/08/025.

J. Gleyzes, D. Langlois, F. Piazza, and F. Vernizzi. Healthy theories beyond Horndeski. *Phys. Rev. Lett.*, 114(21):211101, 2015a. doi: 10.1103/PhysRevLett.114.211101.

J. Gleyzes, D. Langlois, and F. Vernizzi. A unifying description of dark energy. *Int. J. Mod. Phys.*, D23(13):1443010, 2015b. doi: 10.1142/S021827181443010X.

A. Goldstein et al. An Ordinary Short Gamma-Ray Burst with Extraordinary Implications: Fermi-GBM Detection of GRB 170817A. *Astrophys. J.*, 848(2):L14, 2017. doi: 10.3847/2041-8213/aa8f41.

A. Goobar and B. Leibundgut. Supernova Cosmology: Legacy and Future. *Annual Review of Nuclear and Particle Science*, 61:251–279, November 2011. doi: 10.1146/annurev-nucl-102010-130434.

A. Goobar and S. Perlmutter. Feasibility of measuring the cosmological constant Lambda and mass density Omega using type Ia supernovae. *Astrophys. J.*, 450:14, 1995. doi: 10.1086/176113.

A. K. Gooding, D. N. Spergel, and N. Turok. The formation of galaxies and quasars in a texture-seeded cold dark matter cosmogony. *Astrophysical Journal*, 372:L5–L8, May 1991. doi: 10.1086/186010.

E. V. Gorbar and I. L. Shapiro. Renormalization group and decoupling in curved space. *JHEP*, 02:021, 2003a. doi: 10.1088/1126-6708/2003/02/021.

E. V. Gorbar and I. L. Shapiro. Renormalization group and decoupling in curved space. 2. The Standard model and beyond. *JHEP*, 06:004, 2003b. doi: 10.1088/1126-6708/2003/06/004.

D. Gorbunov, K. Koyama, and S. Sibiryakov. More on ghosts in DGP model. *Phys. Rev.*, D73: 044016, 2006. doi: 10.1103/PhysRevD.73.044016.

V. Gorini, A. Kamenshchik, U. Moschella, and V. Pasquier. The Chaplygin gas as a model for dark energy. In *On recent developments in theoretical and experimental general relativity, gravitation, and relativistic field theories. Proceedings, 10th Marcel Grossmann Meeting, MG10, Rio de Janeiro, Brazil, July 20-26, 2003. Pt. A-C*, pages 840–859, 2004. doi: 10.1142/9789812704030_0050.

J. R. Gott, III, J. E. Gunn, D. N. Schramm, and B. M. Tinsley. An unbound universe. *Astrophysical Journal*, 194:543–553, December 1974. doi: 10.1086/153273.

J. Richard Gott and Wesley N. Colley. Reanalysis of the BICEP2, Keck and Planck Data: No Evidence for Gravitational Radiation. 2017.

L. Grego, J. Carlstrom, E. Reese, G. Holder, W. Holzapfel, M. Joy, J. Mohr, and S. Patel. Galaxy cluster gas mass fractions from sunyaev-zeldovich effect measurements: Constraints on m. *The Astrophysical Journal*, 552(1):2, 2001.

R. Gregory, V. A. Rubakov, and S. M. Sibiryakov. Opening up extra dimensions at ultra large scales. *Phys. Rev. Lett.*, 84:5928–5931, 2000. doi: 10.1103/PhysRevLett.84.5928.

C. Guidorzi et al. Improved Constraints on H_0 from a Combined Analysis of Gravitational-wave and Electromagnetic Emission from GW170817. *Astrophys. J.*, 851(2):L36, 2017. doi: 10.3847/2041-8213/aaa009.

J. E. Gunn. On the Propagation of Light in Inhomogeneous Cosmologies. I. Mean Effects. *Astrophys. J.*, 150:737, December 1967. doi: 10.1086/149378.

A. H. Guth. Inflationary universe: A possible solution to the horizon and flatness problems. *Phys. Rev. D*, 23:347–356, Jan 1981. doi: 10.1103/PhysRevD.23.347.

L. Guzzo et al. A test of the nature of cosmic acceleration using galaxy redshift distortions. *Nature*, 451:541–545, 2008. doi: 10.1038/nature06555.

Z. Haiman, J. J. Mohr, and G. P. Holder. Constraints on quintessence from future galaxy cluster surveys. *Astrophys. J.*, 553:545, 2000. doi: 10.1086/320939.

H. W. Hamber and R. Toriumi. Scale-Dependent Newton's Constant G in the Conformal Newtonian Gauge. *Phys. Rev.*, D84:103507, 2011. doi: 10.1103/PhysRevD.84.103507.

H. W. Hamber and R. M. Williams. Newtonian potential in quantum Regge gravity. *Nucl. Phys.*, B435:361–398, 1995. doi: 10.1016/0550-3213(94)00495-Z.

H. W. Hamber and R. M. Williams. Nonlocal effective gravitational field equations and the running of Newton's G. *Phys. Rev.*, D72:044026, 2005. doi: 10.1103/PhysRevD.72.044026.

A. J. S. Hamilton. Linear redshift distortions: A Review. In *Ringberg Workshop on Large Scale Structure Ringberg, Germany, September 23-28, 1996*, 1997. doi: 10.1007/978-94-011-4960-0_17.

S. Hanany et al. MAXIMA-1: A Measurement of the cosmic microwave background anisotropy on angular scales of 10 arcminutes to 5 degrees. *Astrophys. J.*, 545:L5, 2000. doi: 10.1086/317322.

S. F. Hassan and R. A. Rosen. Resolving the ghost problem in nonlinear massive gravity. *Phys. Rev. Lett.*, 108:041101, Jan 2012a. doi: 10.1103/PhysRevLett.108.041101.

S. F. Hassan and Rachel A. Rosen. Bimetric Gravity from Ghost-free Massive Gravity. *JHEP*, 02:126, 2012b. doi: 10.1007/JHEP02(2012)126.

S. Hatton and S. Cole. Estimating β from redshift-space distortions in the 2dF galaxy survey. *MNRAS*, 310:1137–1146, December 1999. doi: 10.1046/j.1365-8711.1999.03034.x.

W. Heisenberg and H. Euler. Folgerungen aus der diracschen theorie des positrons. *Zeitschrift für Physik*, 98(11):714–732, Nov 1936. ISSN 0044-3328. doi: 10.1007/BF01343663.

C. Heymans et al. CFHTLenS: the Canada-France-Hawaii Telescope Lensing Survey. *Mon. Not. Roy. Astron. Soc.*, 427:146–166, November 2012. doi: 10.1111/j.1365-2966.2012.21952.x.

M. Hicken et al. CfA3: 185 Type Ia Supernova Light Curves from the CfA. *Astrophys. J.*, 700:331–357, July 2009. doi: 10.1088/0004-637X/700/1/331.

W. Hillebrandt and J. C. Niemeyer. Type Ia supernova explosion models. *Ann. Rev. Astron. Astrophys.*, 38:191–230, 2000. doi: 10.1146/annurev.astro.38.1.191.

G. Hinshaw et al. Nine-year Wilkinson Microwave Anisotropy Probe (WMAP) Observations: Cosmological Parameter Results. *The Astrophysical Journal Supplement*, 208:19, October 2013. doi: 10.1088/0067-0049/208/2/19.

K. Hinterbichler. Theoretical Aspects of Massive Gravity. *Rev. Mod. Phys.*, 84:671–710, 2012. doi: 10.1103/RevModPhys.84.671.

K. Hinterbichler. Cosmology of Massive Gravity and its Extensions. In *Proceedings, 51st Rencontres de Moriond, Cosmology session: La Thuile, Italy, March 19-26, 2016*, pages 223–232, 2016.

K. Hinterbichler and J. Khoury. Symmetron Fields: Screening Long-Range Forces Through Local Symmetry Restoration. *Phys. Rev. Lett.*, 104:231301, 2010. doi: 10.1103/PhysRevLett.104.231301.

K. Hinterbichler, J. Khoury, A. Levy, and A. Matas. Symmetron cosmology. *Phys. Rev. D*, 84: 103521, Nov 2011. doi: 10.1103/PhysRevD.84.103521.

H. Hoekstra, Y. Mellier, L. Van Waerbeke, E. Semboloni, L. Fu, M. J. Hudson, L. C. Parker, I. Tereno, and K. Benabed. First cosmic shear results from the canada-france-hawaii telescope wide synoptic legacy survey. *Astrophys. J.*, 647:116–127, 2006. doi: 10.1086/503249.

J. A. Holtzman and J. R. Primack. Cluster correlations for cold + hot dark matter and other models. *Astrophysical Journal*, 405:428–436, March 1993. doi: 10.1086/172375.

J. A. Holtzman et al. The Sloan Digital Sky Survey-II: Photometry and Supernova IA Light Curves from the 2005 Data. *Astronomical Journal*, 136:2306–2320, December 2008. doi: 10.1088/0004-6256/136/6/2306.

D. E. Holz and S. A. Hughes. Using gravitational-wave standard sirens. *Astrophys. J.*, 629: 15–22, 2005. doi: 10.1086/431341.

G. W. Horndeski. Second-order scalar-tensor field equations in a four-dimensional space. *Int.J.Theor.Phys.*, 10:363–384, 1974. doi: 10.1007/BF01807638.

C. Howlett, A. Ross, L. Samushia, W. Percival, and M. Manera. The Clustering of the SDSS Main Galaxy Sample II: Mock galaxy catalogues and a measurement of the growth of structure from Redshift Space Distortions at $z = 0.15$. 2014.

F. Hoyle. A New Model for the Expanding Universe. *Mon. Not. Roy. Astron. Soc.*, 108:372, 1948. doi: 10.1093/mnras/108.5.372.

B. Hu, M. Raveri, A. Silvestri, and N. Frusciante. Exploring massive neutrinos in dark cosmologies with eftcamb/EFTCosmoMC. *PRD*, 91(6):063524, March 2015. doi: 10.1103/PhysRevD.91.063524.

W. Hu. Dark synergy: Gravitational lensing and the CMB. *Phys. Rev.*, D65:023003, 2002. doi: 10.1103/PhysRevD.65.023003.

W. Hu and D. J. Eisenstein. The Structure of structure formation theories. *Phys. Rev.*, D59: 083509, 1999. doi: 10.1103/PhysRevD.59.083509.

W. Hu and Z. Haiman. Redshifting rings of power. *Phys. Rev. D*, 68:063004, Sep 2003. doi: 10.1103/PhysRevD.68.063004.

W. Hu and B. Jain. Joint galaxy - lensing observables and the dark energy. *Phys. Rev.*, D70: 043009, 2004. doi: 10.1103/PhysRevD.70.043009.

W. Hu and I. Sawicki. A Parameterized Post-Friedmann Framework for Modified Gravity. *Phys. Rev.*, D76:104043, 2007. doi: 10.1103/PhysRevD.76.104043.

W. Hu and N. Sugiyama. Small scale cosmological perturbations: An Analytic approach. *Astrophys. J.*, 471:542–570, 1996. doi: 10.1086/177989.

W. Hu and M. Tegmark. Weak lensing: Prospects for measuring cosmological parameters. *The Astrophysical Journal Letters*, 514(2):L65, 1999.

W. Hu and M. J. White. The Damping tail of CMB anisotropies. *Astrophys. J.*, 479:568, 1997a. doi: 10.1086/303928.

W. Hu and M. J. White. CMB anisotropies: Total angular momentum method. *Phys. Rev.*, D56:596–615, 1997b. doi: 10.1103/PhysRevD.56.596.

W. Hu and M. J. White. A CMB polarization primer. *New Astron.*, 2:323, 1997c. doi: 10.1016/S1384-1076(97)00022-5.

W. Hu, N. Sugiyama, and J. Silk. The Physics of microwave background anisotropies. *Nature*, 386:37–43, 1997. doi: 10.1038/386037a0.

W. Hu, D. J. Eisenstein, and M. Tegmark. Weighing neutrinos with galaxy surveys. *Phys. Rev. Lett.*, 80:5255–5258, 1998. doi: 10.1103/PhysRevLett.80.5255.

E. Hubble. A relation between distance and radial velocity among extra-galactic nebulae. *Proceedings of the National Academy of Sciences*, 15(3):168–173, 1929. ISSN 0027-8424. doi: 10.1073/pnas.15.3.168.

E. M. L. Humphreys, M. J. Reid, J. M. Moran, L. J. Greenhill, and A. L. Argon. Toward a New Geometric Distance to the Active Galaxy NGC 4258. III. Final Results and the Hubble Constant. *APJ*, 775:13, September 2013. doi: 10.1088/0004-637X/775/1/13.

G. Hurier and F. Lacasa. Combined analysis of galaxy cluster number count, thermal Sunyaev-Zel'dovich power spectrum, and bispectrum. *Astron.Astrophys.*, 604(604):A71, 2017. doi: 10.1051/0004-6361/201630041.

D. Huterer and E. V. Linder. Separating Dark Physics from Physical Darkness: Minimalist Modified Gravity vs. Dark Energy. *Phys. Rev.*, D75:023519, 2007. doi: 10.1103/PhysRevD.75.023519.

D. Huterer and M. S. Turner. Probing the dark energy: Methods and strategies. *Phys. Rev.*, D64:123527, 2001. doi: 10.1103/PhysRevD.64.123527.

D. Inman and U.-L. Pen. Cosmic neutrinos: dispersive and non-linear. *Phys. Rev.*, D95:063535, 2017. doi: 10.1103/PhysRevD.95.063535.

J. Ipser and P. Sikivie. Can galactic halos be made of axions? *Phys. Rev. Lett.*, 50:925–927, Mar 1983. doi: 10.1103/PhysRevLett.50.925.

M. J. Irwin, R. L. Webster, P. C. Hewett, R. T. Corrigan, and R. I. Jedrzejewski. Photometric variations in the Q2237 + 0305 system - First detection of a microlensing event. *Astrophysical Journal*, 98:1989–1994, December 1989. doi: 10.1086/115272.

Y. Isawaki. Linearized gravitation theory and the graviton mass. *Phys. Rev. D*, 2:2255–2256, 1970.

M. Ishak, A. Upadhye, and D. N. Spergel. Probing cosmic acceleration beyond the equation of state: Distinguishing between dark energy and modified gravity models. *Phys. Rev.*, D74: 043513, 2006. doi: 10.1103/PhysRevD.74.043513.

C. Itzykson and J. B. Zuber. *Quantum Field Theory*. International Series In Pure and Applied Physics. McGraw-Hill, New York, 1980.

K. Izumi, K. Koyama, and T. Tanaka. Unexorcized ghost in DGP brane world. *JHEP*, 04:053, 2007. doi: 10.1088/1126-6708/2007/04/053.

M. Jaccard, M. Maggiore, and E. Mitsou. Nonlocal theory of massive gravity. *Phys. Rev.*, D88 (4):044033, 2013. doi: 10.1103/PhysRevD.88.044033.

J. C. Jackson. A critique of Rees's theory of primordial gravitational radiation. *Mon. Not. Roy. Astron. Soc.*, 156:1P, 1972. doi: 10.1093/mnras/156.1.1P.

N. Jackson. The Hubble Constant. *Living Reviews in Relativity*, 10:4, September 2007. doi: 10.12942/lrr-2007-4.

Andrew H. Jaffe et al. Cosmology from MAXIMA-1, BOOMERANG and COBE / DMR CMB observations. *Phys. Rev. Lett.*, 86:3475–3479, 2001. doi: 10.1103/PhysRevLett.86.3475.

A. Johnson, C. Blake, J. Koda, Y.-Z. Ma, M. Colless, M. Crocce, T. M. Davis, H. Jones, C. Magoulas, J. R. Lucey, J. Mould, M. I. Scrimgeour, and C. M. Springob. The 6dF Galaxy Survey: cosmological constraints from the velocity power spectrum. *MNRAS*, 444:3926–3947, November 2014. doi: 10.1093/mnras/stu1615.

R. D. Jordan. Effective Field Equations for Expectation Values. *Phys. Rev.*, D33:444–454, 1986. doi: 10.1103/PhysRevD.33.444.

S. Joudaki et al. KiDS-450: Testing extensions to the standard cosmological model. 2016.

A. Joyce, B. Jain, J. Khoury, and M. Trodden. Beyond the Cosmological Standard Model. *Phys. Rept.*, 568:1–98, 2015. doi: 10.1016/j.physrep.2014.12.002.

A. Joyce, L. Lombriser, and F. Schmidt. Dark Energy Versus Modified Gravity. *Ann. Rev. Nucl. Part. Sci.*, 66:95–122, 2016. doi: 10.1146/annurev-nucl-102115-044553.

G. Jungman, M. Kamionkowski, and K. Griest. Supersymmetric dark matter. *Phys. Rept.*, 267: 195–373, 1996a. doi: 10.1016/0370-1573(95)00058-5.

G. Jungman, M. Kamionkowski, A. Kosowsky, and D. N. Spergel. Cosmological-parameter determination with microwave background maps. *Phys. Rev. D*, 54:1332–1344, Jul 1996b. doi: 10.1103/PhysRevD.54.1332.

G. Jungman, M. Kamionkowski, A. Kosowsky, and D. N. Spergel. Weighing the universe with the cosmic microwave background. *Phys. Rev. Lett.*, 76:1007–1010, Feb 1996c. doi: 10.1103/PhysRevLett.76.1007.

N. Kaiser. On the spatial correlations of Abell clusters. *Astrophysical Journal*, 284:L9–L12, September 1984. doi: 10.1086/184341.

N. Kaiser. Clustering in real space and in redshift space. *MNRAS*, 227:1–21, July 1987. doi: 10.1093/mnras/227.1.1.

A. Y.. Kamenshchik, U. Moschella, and V. Pasquier. An Alternative to quintessence. *Phys. Lett.*, B511:265–268, 2001. doi: 10.1016/S0370-2693(01)00571-8.

M. Kamionkowski and D. N. Spergel. Large-angle cosmic microwave background anisotropies in an open universe. *Astrophysical Journal*, 432:7–16, September 1994. doi: 10.1086/174543.

M. Kamionkowski, A. Kosowsky, and A. Stebbins. Statistics of cosmic microwave background polarization. *Phys. Rev.*, D55:7368–7388, 1997a. doi: 10.1103/PhysRevD.55.7368.

M. Kamionkowski, A. Kosowsky, and A. Stebbins. A Probe of primordial gravity waves and vorticity. *Phys. Rev. Lett.*, 78:2058–2061, 1997b. doi: 10.1103/PhysRevLett.78.2058.

A. Kehagias and M. Maggiore. Spherically symmetric static solutions in a nonlocal infrared modification of General Relativity. *JHEP*, 08:029, 2014. doi: 10.1007/JHEP08(2014)029.

L. V. Keldysh. Diagram technique for nonequilibrium processes. *Zh. Eksp. Teor. Fiz.*, 47: 1515–1527, 1964. [Sov. Phys. JETP20,1018(1965)].

B. Kelvin. Baltimore lectures on molecular dynamics and the wave theory of light. *https://archive.org/details/baltimorelecture00kelviala*, 1904.

J. Khoury and A. Weltman. Chameleon fields: Awaiting surprises for tests of gravity in space. *Phys. Rev. Lett.*, 93:171104, 2004. doi: 10.1103/PhysRevLett.93.171104.

T. W. B. Kibble. Topology of Cosmic Domains and Strings. *J. Phys.*, A9:1387–1398, 1976. doi: 10.1088/0305-4470/9/8/029.

M. Kilbinger. Cosmology with cosmic shear observations: a review. *Rept. Prog. Phys.*, 78: 086901, 2015. doi: 10.1088/0034-4885/78/8/086901.

J. E. Kim and H. P. Nilles. A Quintessential axion. *Phys. Lett.*, B553:1–6, 2003. doi: 10.1016/S0370-2693(02)03148-9.

R. P. Kirshner, A. Oemler, Jr., and P. L. Schechter. A study of field galaxies. II - The luminosity function and space distribution of galaxies. *Astron. J.*, 84:951–959, July 1979. doi: 10.1086/112498.

A. Klypin, J. Holtzman, J. Primack, and E. Regos. Structure formation with cold plus hot dark matter. *Astrophysical Journal*, 416:1–16, 1993. doi: 10.1086/173210.

A. A. Klypin and A. I. Kopylov. The Spatial Covariance Function for Rich Clusters of Galaxies. *Soviet Astronomy Letters*, 9:41–44, February 1983.

A. A. Klypin, I. A. Strukov, and D. P. Skulachev. The relikt missions: results and prospects for detection of the microwave background anisotropy. *Monthly Notices of the Royal Astronomical Society*, 258(1):71–81, 1992. doi: 10.1093/mnras/258.1.71.

R. A. Knop et al. New Constraints on Ω_M, Ω, and w from an Independent Set of 11 High-Redshift Supernovae Observed with the Hubble Space Telescope. *Astrophys. J.*, 598:102–137, November 2003. doi: 10.1086/378560.

B. Knorr and F. Saueressig. Towards reconstructing the quantum effective action of gravity. 2018.

L. Knox, Y.-S. Song, and J. A. Tyson. Distance-redshift and growth-redshift relations as two windows on acceleration and gravitation: Dark energy or new gravity? *Phys. Rev.*, D74: 023512, 2006. doi: 10.1103/PhysRevD.74.023512.

H. Kodama and M. Sasaki. Cosmological perturbation theory. *Progress of Theoretical Physics Supplement*, 78:1–166, 1984. doi: 10.1143/PTPS.78.1.

L. A. Kofman and A. A. Starobinskii. Effect of the Cosmological Constant on Largescale Anisotropies in the Microwave Background. *Soviet Astronomy Letters*, 11:271–274, September 1985.

L. A. Kofman, N. Y. Gnedin, and N. A. Bahcall. Cosmological constant, COBE cosmic microwave background anisotropy, and large-scale clustering. *Astrophysical Journal*, 413:1–9, August 1993. doi: 10.1086/172970.

I. I. Kogan and G. G. Ross. Brane universe and multigravity: Modification of gravity at large and small distances. *Phys. Lett.*, B485:255–262, 2000. doi: 10.1016/S0370-2693(00)00687-0. [,2274(2000)].

A. Kogut et al. Wilkinson Microwave Anisotropy Probe (WMAP) first year observations: TE polarization. *Astrophys. J. Suppl.*, 148:161, 2003. doi: 10.1086/377219.

T. Koivisto. Dynamics of Nonlocal Cosmology. *Phys. Rev.*, D77:123513, 2008a. doi: 10.1103/PhysRevD.77.123513.

T. S. Koivisto. Newtonian limit of nonlocal cosmology. *Phys. Rev.*, D78:123505, 2008b. doi: 10.1103/PhysRevD.78.123505.

T. S. Koivisto. Cosmology of modified (but second order) gravity. *AIP Conf.Proc.*, 1206:79–96, 2010. doi: 10.1063/1.3292516.

E. Komatsu and U. Seljak. Universal gas density and temperature profile. *MNRAS*, 327: 1353–1366, November 2001. doi: 10.1046/j.1365-8711.2001.04838.x.

E. Komatsu and U. Seljak. The Sunyaev-Zel'dovich angular power spectrum as a probe of cosmological parameters. *Mon. Not. Roy. Astron. Soc.*, 336:1256, 2002. doi: 10.1046/j.1365-8711.2002.05889.x.

E. Komatsu and D. N. Spergel. Acoustic signatures in the primary microwave background bispectrum. *Phys. Rev.*, D63:063002, 2001. doi: 10.1103/PhysRevD.63.063002.

E. Komatsu et al. Five-Year Wilkinson Microwave Anisotropy Probe (WMAP) Observations: Cosmological Interpretation. *Astrophys. J. Suppl.*, 180:330–376, 2009. doi: 10.1088/0067-0049/180/2/330.

E. Komatsu et al. Seven-year Wilkinson Microwave Anisotropy Probe (WMAP) Observations: Cosmological Interpretation. *The Astrophysical Journal Supplement*, 192:18, February 2011. doi: 10.1088/0067-0049/192/2/18.

A. Koshelev. Comments on scalar-tensor representation of nonlocally corrected gravity. *Grav.Cosmol.*, 15:220–223, 2009. doi: 10.1134/S0202289309030049.

J. Kovac, E. M. Leitch, C Pryke, J. E. Carlstrom, N. W. Halverson, and W. L. Holzapfel. Detection of polarization in the cosmic microwave background using DASI. *Nature*, 420: 772–787, 2002. doi: 10.1038/nature01269.

M. Kowalski et al. Improved Cosmological Constraints from New, Old and Combined Supernova Datasets. *Astrophys. J.*, 686:749–778, 2008. doi: 10.1086/589937.

K. Koyama. Ghosts in the self-accelerating universe. *Class. Quant. Grav.*, 24(24):R231–R253, 2007. doi: 10.1088/0264-9381/24/24/R01.

K. Koyama. Cosmological Tests of Modified Gravity. *Rept. Prog. Phys.*, 79(4):046902, 2016. doi: 10.1088/0034-4885/79/4/046902.

K. Koyama and R. Maartens. Structure formation in the DGP cosmological model. *JCAP*, 0601:016, 2006. doi: 10.1088/1475-7516/2006/01/016.

K. Kuijken et al. Gravitational Lensing Analysis of the Kilo Degree Survey. *MNRAS*, 454(4): 3500–3532, 2015. doi: 10.1093/mnras/stv2140.

M. Kunz. The phenomenological approach to modeling the dark energy. *Comptes Rendus Physique*, 13:539–565, July 2012. doi: 10.1016/j.crhy.2012.04.007.

M. Kunz and D. Sapone. Dark Energy versus Modified Gravity. *Phys. Rev. Lett.*, 98:121301, 2007. doi: 10.1103/PhysRevLett.98.121301.

A. E. Lange et al. Cosmological parameters from the first results of BOOMERANG. *Phys. Rev.*, D63:042001, 2001. doi: 10.1103/PhysRevD.63.042001.

D. Langlois and K. Noui. Degenerate higher derivative theories beyond Horndeski: evading the Ostrogradski instability. *JCAP*, 1602(02):034, 2016. doi: 10.1088/1475-7516/2016/02/034.

R. Laureijs, J. Amiaux, S. Arduini, J. . Augueres, J. Brinchmann, R. Cole, M. Cropper, C. Dabin, L. Duvet, A. Ealet, and et al. Euclid Definition Study Report. *ArXiv e-prints*, October 2011.

G. Lemaître. Un Univers homogène de masse constante et de rayon croissant rendant compte de la vitesse radiale des nébuleuses extra-galactiques. *Annales de la Société Scientifique de Bruxelles*, 47:49–59, 1927.

J. Lesgourgues. *Inflationary Cosmology*. Troisième cycle de la physique en Suisse romande. vente: M.D. Reymond, Ecole polytechnique fédérale de Lausanne, Bâtiment des sciences physiques, 2006.

J. Lesgourgues and S. Pastor. Massive neutrinos and cosmology. *PHYSREP*, 429:307–379, July 2006. doi: 10.1016/j.physrep.2006.04.001.

J. Lesgourgues and S. Pastor. Neutrino cosmology and Planck. *New Journal of Physics*, 16(6): 065002, June 2014. doi: 10.1088/1367-2630/16/6/065002.

J. Lesgourgues, G. Mangano, G. Miele, and S. Pastor. *Neutrino cosmology*. Cambridge University Press, 2013.

M. Levi et al. The DESI Experiment, a whitepaper for Snowmass 2013. 2013.

A. Lewis. CAMB Notes. `http://cosmologist.info/notes/CAMB.pdf`.

A. Lewis and A. Challinor. Weak gravitational lensing of the cmb. *Phys. Rept.*, 429:1–65, 2006. doi: 10.1016/j.physrep.2006.03.002.

A. Lewis, A. Challinor, and A. Lasenby. Efficient computation of CMB anisotropies in closed FRW models. *Astrophys. J.*, 538:473–476, 2000. doi: 10.1086/309179.

A. R. Liddle and D. H. Lyth. The Cold dark matter density perturbation. *Phys. Rept.*, 231: 1–105, 1993. doi: 10.1016/0370-1573(93)90114-S.

E. Lifshitz. Republication of: On the gravitational stability of the expanding universe. *J. Phys.(USSR)*, 10:116, 1946. doi: 10.1007/s10714-016-2165-8. [Gen. Rel. Grav.49,no.2,18(2017)].

A.D. Linde. A new inflationary universe scenario: A possible solution of the horizon, flatness, homogeneity, isotropy and primordial monopole problems. *Physics Letters B*, 108(6):389 – 393, 1982. ISSN 0370-2693. doi: https://doi.org/10.1016/0370-2693(82)91219-9.

E. V. Linder. Analysis of gravitationally lensed microwave background anisotropies. *MNRAS*, 243:353–361, April 1990.

E. V. Linder. Exploring the expansion history of the universe. *Phys. Rev. Lett.*, 90:091301, 2003. doi: 10.1103/PhysRevLett.90.091301.

E. V. Linder. No Slip Gravity. 2018.

L. Lombriser and A. Taylor. Breaking a Dark Degeneracy with Gravitational Waves. *JCAP*, 1603:031, 2016. doi: 10.1088/1475-7516/2016/03/031.

D. Lovelock. The Einstein tensor and its generalizations. *J. Math. Phys.*, 12:498–501, 1971. doi: 10.1063/1.1665613.

D. Lovelock. The four-dimensionality of space and the Einstein tensor. *J. Math. Phys.*, 13: 874–876, 1972. doi: 10.1063/1.1666069.

LSST Science Collaboration, P. A. Abell, et al. LSST Science Book, Version 2.0. *ArXiv e-prints*, December 2009.

V. V. Lukovi\'c, R. D'Agostino, and N. Vittorio. Is there a concordance value for H_0? *Astron. Astrophys.*, 595:A109, 2016. doi: 10.1051/0004-6361/201628217.

M. A. Luty, M. Porrati, and R. Rattazzi. Strong interactions and stability in the DGP model. *JHEP*, 09:029, 2003. doi: 10.1088/1126-6708/2003/09/029.

D. H. Lyth. What would we learn by detecting a gravitational wave signal in the cosmic microwave background anisotropy? *Phys. Rev. Lett.*, 78:1861–1863, Mar 1997. doi: 10.1103/PhysRevLett.78.1861.

C.-P. Ma and E. Bertschinger. Cosmological perturbation theory in the synchronous and conformal Newtonian gauges. *Astrophys. J.*, 455:7–25, 1995. doi: 10.1086/176550.

C. L. MacLeod and C. J. Hogan. Precision of Hubble constant derived using black hole binary absolute distances and statistical redshift information. *Phys. Rev.*, D77:043512, 2008. doi: 10.1103/PhysRevD.77.043512.

S. J. Maddox, G. Efstathiou, W. J. Sutherland, and J. Loveday. Galaxy correlations on large scales. *Mon. Not. Roy. Astron. Soc.*, 242:43P–47P, January 1990. doi: 10.1093/mnras/242.1.43P.

M. Maggiore. *A modern introduction to quantum field theory*. Oxford Master Series in Statistical, Computational, and Theoretical Physics. Oxford Univ., Oxford, 2005.

M. Maggiore. *Gravitational Waves. Vol. 1. Theory and Experiments*. Oxford University Press, 574 p, 2007.

M. Maggiore. Phantom dark energy from non-local infrared modifications of General Relativity. *Phys.Rev.*, D89:043008, 2014. doi: 10.1103/PhysRevD.89.043008.

M. Maggiore. Dark energy and dimensional transmutation in R^2 gravity. 2015.

M. Maggiore. Nonlocal Infrared Modifications of Gravity. A Review. *Fundam. Theor. Phys.*, 187:221–281, 2017. doi: 10.1007/978-3-319-51700-1_16.

M. Maggiore. *Gravitational Waves. Vol. 2. Astrophysics and Cosmology*. Oxford University Press, 848 p, 2018.

M. Maggiore and M. Mancarella. Non-local gravity and dark energy. *Phys.Rev.*, D90:023005, 2014. doi: 10.1103/PhysRevD.90.023005.

J. Magueijo. New varying speed of light theories. *Rept. Prog. Phys.*, 66:2025, 2003. doi: 10.1088/0034-4885/66/11/R04.

E. Majerotto, L. Guzzo, L. Samushia, W. J. Percival, Y. Wang, S. de la Torre, B. Garilli, P. Franzetti, E. Rossetti, A. Cimatti, C. Carbone, N. Roche, and G. Zamorani. Probing deviations from general relativity with the Euclid spectroscopic survey. *MNRAS*, 424:1392–1408, August 2012. doi: 10.1111/j.1365-2966.2012.21323.x.

S. Majumdar and J. J. Mohr. Self calibration in cluster studies of dark energy: Combining the cluster redshift distribution, the power spectrum and mass measurements. *Astrophys. J.*, 613:41–50, 2004. doi: 10.1086/422829.

J. M. Maldacena. Non-Gaussian features of primordial fluctuations in single field inflationary models. *JHEP*, 05:013, 2003. doi: 10.1088/1126-6708/2003/05/013.

G. Mangano, G. Miele, S. Pastor, T. Pinto, O. Pisanti, and P. D. Serpico. Relic neutrino decoupling including flavor oscillations. *Nucl. Phys.*, B729:221–234, 2005. doi: 10.1016/j.nuclphysb.2005.09.041.

A. V. Manohar. Effective field theories. *Lect.Notes Phys.*, 479:311–362, 1997. doi: 10.1007/BFb0104294.

S. P. Martin. A Supersymmetry primer. pages 1–98, 1997. doi: 10.1142/9789812839657_0001, 10.1142/9789814307505_0001. [Adv. Ser. Direct. High Energy Phys.18,1(1998)].

J. C. Mather et al. Measurement of the cosmic microwave background spectrum by the COBE FIRAS instrument. *Astrophysical Journal*, 420:439–444, January 1994. doi: 10.1086/173574.

T. Matsubara. Correlation function in deep redshift space as a cosmological probe. *The Astrophysical Journal*, 615(2):573, 2004.

A. Meiksin and M. White. The growth of correlations in the matter power spectrum. *MNRAS*, 308:1179–1184, October 1999. doi: 10.1046/j.1365-8711.1999.02825.x.

A. Melchiorri et al. A measurement of ω from the north american test flight of boomerang. *The Astrophysical Journal Letters*, 536(2):L63, 2000.

C. Messenger and J. Read. Measuring a cosmological distance-redshift relationship using only gravitational wave observations of binary neutron star coalescences. *Phys. Rev. Lett.*, 108: 091101, 2012. doi: 10.1103/PhysRevLett.108.091101.

M. Milgrom. A modification of the Newtonian dynamics as a possible alternative to the hidden mass hypothesis. *Astrophysical Journal*, 270:365–370, July 1983. doi: 10.1086/161130.

E.A. Milne. *Relativity, Gravitation and World-structure*. International series of monographs on physics. At the Clarendon Press, 1935.

C.W. Misner, K.S. Thorne, and J.A. Wheeler. *Gravitation*. Number ptie. 3 in Gravitation. W. H. Freeman, 1973.

E. Mitsou. *Aspects of Infrared Non-local Modifications of General Relativity*. PhD thesis, Geneva U., 2015.

L. Modesto and S. Tsujikawa. Non-local massive gravity. *Phys. Lett.*, B727:48–56, 2013. doi: 10.1016/j.physletb.2013.10.037.

E. Mottola. New Horizons in Gravity: The Trace Anomaly, Dark Energy and Condensate Stars. *Acta Phys. Polon.*, B41:2031–2162, 2010.

E. Mottola. Scalar Gravitational Waves in the Effective Theory of Gravity. *JHEP*, 07:043, 2017. doi: 10.1007/JHEP07(2017)043,10.1007/JHEP09(2017)107. [Erratum: JHEP09,107(2017)].

V. F. Mukhanov and S. Winitzki. *Introduction to quantum effects in gravity*. Cambridge Univ. Press, Cambridge, 2007.

V. F. Mukhanov, H. A. Feldman, and R. H. Brandenberger. Theory of cosmological perturbations. *Phys. Rep.*, 215:203–333, June 1992. doi: 10.1016/0370-1573(92)90044-Z.

P. Mukherjee, J. Urrestilla, M. Kunz, A. R. Liddle, N. Bevis, and M. Hindmarsh. Detecting and distinguishing topological defects in future data from the CMBPol satellite. *Phys. Rev. D*, 83(4):043003, February 2011. doi: 10.1103/PhysRevD.83.043003.

D. Munshi, P. Valageas, Ludovic Van Waerbeke, and A. Heavens. Cosmology with Weak Lensing Surveys. *Phys. Rept.*, 462:67–121, 2008. doi: 10.1016/j.physrep.2008.02.003.

G. Narain and T. Li. Ultraviolet complete dark energy model. *Phys. Rev.*, D97(8):083523, 2018. doi: 10.1103/PhysRevD.97.083523.

H. Nersisyan, Y. Akrami, L. Amendola, T. S. Koivisto, and J. Rubio. Dynamical analysis of $R\Box^{-2}R$ cosmology: Impact of initial conditions and constraints from supernovae. *Phys. Rev.*, D94(4):043531, 2016. doi: 10.1103/PhysRevD.94.043531.

H. Nersisyan, Y. Akrami, L. Amendola, T. S. Koivisto, J. Rubio, and A. R. Solomon. Instabilities in tensorial nonlocal gravity. *Phys. Rev.*, D95(4):043539, 2017a. doi: 10.1103/PhysRevD.95.043539.

H. Nersisyan, A. Cid, and L. Amendola. Structure formation in the Deser-Woodard nonlocal gravity model: a reappraisal. *JCAP*, 1704(04):046, 2017b. doi: 10.1088/1475-7516/2017/04/046.

S. Nesseris and J. Garcia-Bellido. Is the Jeffreys' scale a reliable tool for Bayesian model comparison in cosmology? *JCAP*, 1308:036, 2013. doi: 10.1088/1475-7516/2013/08/036.

S. Nesseris and S. Tsujikawa. Cosmological perturbations and observational constraints on nonlocal massive gravity. *Phys. Rev.*, D90(2):024070, 2014. doi: 10.1103/PhysRevD.90.024070.

C. B. Netterfield, M. J. Devlin, N. Jarosik, L. Page, and E. J. Wollack. A Measurement of the Angular Power Spectrum of the Anisotropy in the Cosmic Microwave Background. *Astrophys. J.*, 474:47–66, January 1997. doi: 10.1086/303438.

A. Nicolis and R. Rattazzi. Classical and quantum consistency of the DGP model. *JHEP*, 06:059, 2004. doi: 10.1088/1126-6708/2004/06/059.

A. Nicolis, R. Rattazzi, and E. Trincherini. The Galileon as a local modification of gravity. *Phys. Rev.*, D79:064036, 2009. doi: 10.1103/PhysRevD.79.064036.

A. Nishizawa. Generalized framework for testing gravity with gravitational-wave propagation. I. Formulation. 2017.

A. Nishizawa, K. Yagi, A. Taruya, and T. Tanaka. Cosmology with space-based gravitational-wave detectors — dark energy and primordial gravitational waves —. *Phys. Rev.*, D85:044047, 2012. doi: 10.1103/PhysRevD.85.044047.

S. Nissanke, D. E. Holz, S.A. Hughes, N. Dalal, and J. L. Sievers. Exploring short gamma-ray bursts as gravitational-wave standard sirens. *Astrophys. J.*, 725:496–514, 2010. doi: 10.1088/0004-637X/725/1/496.

S. Nojiri and S. D. Odintsov. Unified cosmic history in modified gravity: from F(R) theory to Lorentz non-invariant models. *Phys. Rept.*, 505:59–144, 2011. doi: 10.1016/j.physrep.2011.04.001.

A. Oka, S. Saito, T. Nishimichi, A. Taruya, and K. Yamamoto. Simultaneous constraints on the growth of structure and cosmic expansion from the multipole power spectra of the SDSS DR7 LRG sample. *MNRAS*, 439:2515–2530, 2014. doi: 10.1093/mnras/stu111.

T. Okamoto and W. Hu. CMB lensing reconstruction on the full sky. *Phys. Rev.*, D67:083002, 2003. doi: 10.1103/PhysRevD.67.083002.

K. A. Olive and M. S. Turner. Cosmological bounds on the masses of stable, right-handed neutrinos. *Phys. Rev. D*, 25:213–216, Jan 1982. doi: 10.1103/PhysRevD.25.213.

J. P. Ostriker and Paul J. Steinhardt. Cosmic concordance. *arXiv:astro-ph/9505066*, 1995.

J.P. Ostriker, P.J.E. Peebles, and A. Yahil. The size and mass of galaxies, and the mass of the universe. *Astrophysical Journal*, 193:L1–L4, October 1974. doi: 10.1086/181617.

M. Ostrogradsky. Mémoires sur les équations différentielles, relatives au problème des isopérimètres. *Mem. Acad. St. Petersbourg*, 6(4):385–517, 1850.

T. Padmanabhan. Cosmological constant: The Weight of the vacuum. *Phys. Rept.*, 380:235–320, 2003. doi: 10.1016/S0370-1573(03)00120-0.

T. Padmanabhan. Dark energy: mystery of the millennium. *AIP Conf. Proc.*, 861:179–196, 2006. doi: 10.1063/1.2399577. [,179(2006)].

H. Pagels and J. R. Primack. Supersymmetry, cosmology, and new physics at teraelectronvolt energies. *Phys. Rev. Lett.*, 48:223–226, Jan 1982. doi: 10.1103/PhysRevLett.48.223.

S. M. Paneitz. A Quartic Conformally Covariant Differential Operator for Arbitrary Pseudo-Riemannian Manifolds (Summary). *SIGMA*, 4:036, March 2008. doi: 10.3842/SIGMA.2008.036.

K. Pardo, M. Fishbach, D. E. Holz, and D. N. Spergel. Limits on the number of spacetime dimensions from GW170817. 2018.

M. K. Parikh and S. N. Solodukhin. De Sitter brane gravity: From close-up to panorama. *Phys. Lett.*, B503:384–393, 2001. doi: 10.1016/S0370-2693(01)00233-7.

C. Park, J. R. Gott, III, and L. N. da Costa. Large-scale structure in the Southern Sky Redshift Survey. *Astrophysical Journal*, 392:L51–L54, June 1992. doi: 10.1086/186423.

S. Park. Revival of the Deser-Woodard nonlocal gravity model: Comparison of the original nonlocal form and a localized formulation. *Phys. Rev.*, D97(4):044006, 2018. doi: 10.1103/PhysRevD.97.044006.

S. Park and A. Shafieloo. Growth of perturbations in nonlocal gravity with non-ΛCDM background. *Phys. Rev.*, D95(6):064061, 2017. doi: 10.1103/PhysRevD.95.064061.

D. J. Parker, L.; Toms. Renormalization group and nonlocal terms in the curved-spacetime effective action: Weak-field results. *Physical Review D*, 32, 9 1985. doi: 10.1103/physrevd.32.1409.

S. P. Patil. Degravitation, Inflation and the Cosmological Constant as an Afterglow. *JCAP*, 0901:017, 2009. doi: 10.1088/1475-7516/2009/01/017.

W. Pauli and M. Fierz. On relativistic wave-equations for particles of arbitrary spin in an electromagnetic field. *Proc. Roy. Soc.*, A 173:221, 1939.

J. A. Peacock et al. A Measurement of the cosmological mass density from clustering in the 2dF Galaxy Redshift Survey. *Nature*, 410:169–173, 2001. doi: 10.1038/35065528.

R. D. Peccei. Neutrino models of dark energy. *Phys. Rev.*, D71:023527, 2005. doi: 10.1103/PhysRevD.71.023527.

P. J. E. Peebles. The Gravitational Instability of the Universe. *Astrophysical Journal*, 147:859, March 1967. doi: 10.1086/149077.

P. J. E. Peebles. Statistical Analysis of Catalogs of Extragalactic Objects. I. Theory. *Astrophysical Journal*, 185:413–440, October 1973. doi: 10.1086/152431.

P. J. E. Peebles. Large-scale background temperature and mass fluctuations due to scale-invariant primeval perturbations. *Astrophysical Journal*, 263:L1–L5, December 1982. doi: 10.1086/183911.

P. J. E. Peebles and B. Ratra. The Cosmological constant and dark energy. *Rev. Mod. Phys.*, 75:559–606, 2003. doi: 10.1103/RevModPhys.75.559.

P. J. E. Peebles and J. T. Yu. Primeval Adiabatic Perturbation in an Expanding Universe. *Astrophys. J.*, 162:815, December 1970. doi: 10.1086/150713.

H. V. Peiris and D. N. Spergel. Cross-correlating the Sloan Digital Sky Survey with the microwave sky. *Astrophys. J.*, 540:605, 2000. doi: 10.1086/309373.

U.-L. Pen. Measuring the universal deceleration using angular diameter distances to clusters of galaxies. *New Astronomy*, 2:309–317, October 1997. doi: 10.1016/S1384-1076(97)00021-3.

A. A. Penzias and R. W. Wilson. A Measurement of Excess Antenna Temperature at 4080 Mc/s. *Astrophysical Journal*, 142:419–421, July 1965. doi: 10.1086/148307.

R. Percacci. Asymptotic Safety. *Oriti, D. (ed.): Approaches to quantum gravity*, pages 111–128, 2007.

W. J Percival and M. White. Testing cosmological structure formation using redshift-space distortions. *Mon. Not. Roy. Astron. Soc.*, 393:297, 2009. doi: 10.1111/j.1365-2966.2008.14211.x.

W. J. Percival, L. Samushia, A. J. Ross, C. Shapiro, and A. Raccanelli. Redshift-space distortions. *Philosophical Transactions of the Royal Society of London A: Mathematical, Physical and Engineering Sciences*, 369(1957):5058–5067, 2011. ISSN 1364-503X. doi: 10.1098/rsta.2011.0370.

S. Perlmutter et al. Measurements of Omega and Lambda from 42 high redshift supernovae. *Astrophys. J.*, 517:565–586, 1999. doi: 10.1086/307221.

Planck Wiki. Planck 2015 release explanatory supplement. 2015.

M. Porrati. Fully covariant van Dam-Veltman-Zakharov discontinuity, and absence thereof. *Phys. Lett.*, B534:209–215, 2002. doi: 10.1016/S0370-2693(02)01656-8.

A. Proca. Sur la théorie ondulatoire des électrons positifs et négatifs. *J. Phys. Radium*, 7:347 – 353, (1936). doi: 10.1051/jphysrad:0193600708034700.

L. Randall and R. Sundrum. A Large mass hierarchy from a small extra dimension. *Phys. Rev. Lett.*, 83:3370–3373, 1999. doi: 10.1103/PhysRevLett.83.3370.

B. Ratra and P. J. E. Peebles. Cosmological consequences of a rolling homogeneous scalar field. *Phys. Rev. D*, 37:3406–3427, Jun 1988. doi: 10.1103/PhysRevD.37.3406.

H. Reeves, J. Audouze, W. A. Fowler, and D. N. Schramm. On the Origin of Light Elements. *Astrophysical Journal*, 179:909–930, February 1973. doi: 10.1086/151928.

T. Regimbau, K. Siellez, D. Meacher, B. Gendre, and M. Boër. Revisiting coincidence rate between Gravitational Wave detection and short Gamma-Ray Burst for the Advanced and third generation. *Astrophys. J.*, 799(1):69, 2015. doi: 10.1088/0004-637X/799/1/69.

C. L. Reichardt et al. A Measurement of Secondary Cosmic Microwave Background Anisotropies with Two Years of South Pole Telescope Observations. *Astrophys. J.*, 755:70, August 2012. doi: 10.1088/0004-637X/755/1/70.

M. J. Reid, J. A. Braatz, J. J. Condon, K. Y. Lo, C. Y. Kuo, C. M. V. Impellizzeri, and C. Henkel. The Megamaser Cosmology Project. IV. A Direct Measurement of the Hubble Constant from UGC 3789. *Astrophys. J.*, 767:154, April 2013. doi: 10.1088/0004-637X/767/2/154.

A. Rest et al. Cosmological Constraints from Measurements of Type Ia Supernovae discovered during the first 1.5 yr of the Pan-STARRS1 Survey. *Astrophys. J.*, 795(1):44, 2014. doi: 10.1088/0004-637X/795/1/44.

R. J. Riegert. A non-local action for the trace anomaly. *Physics Letters B*, 134(1):56 – 60, 1984. ISSN 0370-2693. doi: https://doi.org/10.1016/0370-2693(84)90983-3.

A. G. Riess, L. Macri, S. Casertano, M. Sosey, H. Lampeitl, H. C. Ferguson, A. V. Filippenko, S. W. Jha, W. Li, R. Chornock, and D. Sarkar. A Redetermination of the Hubble Constant with the Hubble Space Telescope from a Differential Distance Ladder. *Astrophys. J.*, 699:539–563, July 2009. doi: 10.1088/0004-637X/699/1/539.

A. G. Riess, L. Macri, S. Casertano, H. Lampeitl, H. C. Ferguson, A. V. Filippenko, S. W. Jha, W. Li, and R. Chornock. A 3% Solution: Determination of the Hubble Constant with the Hubble Space Telescope and Wide Field Camera 3. *Astrophys.J.*, 730:119, April 2011. doi: 10.1088/0004-637X/730/2/119.

A. G. Riess et al. Observational evidence from supernovae for an accelerating universe and a cosmological constant. *Astron. J.*, 116:1009–1038, 1998. doi: 10.1086/300499.

A. G. Riess et al. A 2.4% Determination of the Local Value of the Hubble Constant. *Astrophys. J.*, 826(1):56, 2016. doi: 10.3847/0004-637X/826/1/56.

A. G. Riess et al. New Parallaxes of Galactic Cepheids from Spatially Scanning the Hubble Space Telescope: Implications for the Hubble Constant. *Astro. Phys. Journal*, 855:136, March 2018. doi: 10.3847/1538-4357/aaadb7.

H. P. Robertson. Kinematics and World-Structure. *Astrophysical Journal*, 82:284, November 1935. doi: 10.1086/143681.

A. J. Ross, L. Samushia, C. Howlett, W. J. Percival, A. Burden, and M. Manera. The clustering of the SDSS DR7 main Galaxy sample - I. A 4 per cent distance measure at z = 0.15. *Mon. Not. Roy. Astron. Soc.*, 449:835–847, May 2015. doi: 10.1093/mnras/stv154.

V. C. Rubin and W. K. Ford, Jr. Rotation of the Andromeda Nebula from a Spectroscopic Survey of Emission Regions. *Astrophysical Journal*, 159:379, February 1970. doi: 10.1086/150317.

V. C. Rubin, W. K. Ford, Jr., and N. Thonnard. Extended rotation curves of high-luminosity spiral galaxies. IV - Systematic dynamical properties, SA through SC. *Astrophysical Journal*, 225:L107–L111, November 1978. doi: 10.1086/182804.

V. C. Rubin, W. K. Ford, Jr., and N. Thonnard. Rotational properties of 21 SC galaxies with a large range of luminosities and radii, from NGC 4605 /R = 4kpc/ to UGC 2885 /R = 122 kpc/. *Astrophysical Journal*, 238:471–487, June 1980. doi: 10.1086/158003.

P. Ruiz-Lapuente. *Dark Energy: Observational and Theoretical Approaches*. Cambridge University Press, 2010. doi: 10.1017/CBO9781139193627.

R. K. Sachs and A. M. Wolfe. Perturbations of a Cosmological Model and Angular Variations of the Microwave Background. *Astrophysical Journal*, 147:73, January 1967. doi: 10.1086/148982.

V. Sahni and A. A. Starobinsky. The Case for a positive cosmological Lambda term. *Int. J. Mod. Phys.*, D9:373–444, 2000. doi: 10.1142/S0218271800000542.

J. Sakstein and B. Jain. Implications of the Neutron Star Merger GW170817 for Cosmological Scalar-Tensor Theories. *Phys. Rev. Lett.*, 119:251303, 2017. doi: 10.1103/PhysRevLett.119.251303.

I. D. Saltas, I. Sawicki, L. Amendola, and M. Kunz. Anisotropic Stress as a Signature of Nonstandard Propagation of Gravitational Waves. *Phys. Rev. Lett.*, 113:191101, 2014. doi: 10.1103/PhysRevLett.113.191101.

L. Salvati, M. Douspis, and N. Aghanim. Constraints from thermal Sunyaev-Zeldovich cluster counts and power spectrum combined with CMB. 2017. doi: 10.1051/0004-6361/201731990.

L. Samushia et al. *Mon.Not.Roy.Astron.Soc.*, 439:3504–3519, 2014. doi: 10.1093/mnras/stu197.

A. Sandage and G. A. Tammann. Steps toward the Hubble constant. V - The Hubble constant from nearby galaxies and the regularity of the local velocity field. *Astrophysical Journal*, 196:313–328, March 1975. doi: 10.1086/153413.

D. Sapone and M. Kunz. Fingerprinting Dark Energy. *Phys. Rev.*, D80:083519, 2009. doi: 10.1103/PhysRevD.80.083519.

S. Sasaki. A New Method to Estimate Cosmological Parameters Using the Baryon Fraction of Clusters of Galaxies. *Publications of the Astronomical Society of Japan*, 48:L119–L122, December 1996. doi: 10.1093/pasj/48.6.L119.

B. Sathyaprakash et al. Scientific Objectives of Einstein Telescope. *Class. Quant. Grav.*, 29:124013, 2012. doi: 10.1088/0264-9381/29/12/124013,10.1088/0264-9381/30/7/079501. [Erratum: Class. Quant. Grav.30,079501(2013)].

B. S. Sathyaprakash, B. F. Schutz, and C. Van Den Broeck. Cosmography with the Einstein Telescope. *Class. Quant. Grav.*, 27:215006, 2010. doi: 10.1088/0264-9381/27/21/215006.

W. Saunders, C. Frenk, M. Rowan-Robinson, G. Efstathiou, A. Lawrence, N. Kaiser, R. Ellis, J. Crawford, X.-Y. Xia, and I. Parry. The density field of the local universe. *Nature*, 349:32–38, January 1991. doi: 10.1038/349032a0.

V. Savchenko et al. INTEGRAL Detection of the First Prompt Gamma-Ray Signal Coincident with the Gravitational-wave Event GW170817. *Astrophys. J.*, 848(2):L15, 2017. doi: 10.3847/2041-8213/aa8f94.

R. K. Schaefer and Q. Shafi. Inflation and large-scale structure formation after the cosmic background explorer. *Phys. Rev. D*, 47:1333–1338, Feb 1993. doi: 10.1103/PhysRevD.47.1333.

R. K. Schaefer, Q. Shafi, and F. W. Stecker. Large-scale structure formation and cosmic microwave anisotropy in a cold plus hot dark matter universe. *Astrophysical Journal*, 347:575–589, December 1989. doi: 10.1086/168150.

F. Schmidt. Weak Lensing Probes of Modified Gravity. *Phys. Rev.*, D78:043002, 2008. doi: 10.1103/PhysRevD.78.043002.

R. Schneider, V. Ferrari, S. Matarrese, and S. F. Portegies Zwart. Gravitational waves from cosmological compact binaries. *Mon. Not. Roy. Astron. Soc.*, 324:797, 2001. doi: 10.1046/j.1365-8711.2001.04217.x.

D. N. Schramm and G. Steigman. Relic Neutrinos and the Density of the Universe. *Astrophysical Journal*, 243:1, January 1981. doi: 10.1086/158559.

B. F. Schutz. Determining the Hubble Constant from Gravitational Wave Observations. *Nature*, 323:310–311, 1986. doi: 10.1038/323310a0.

B. F. Schutz. Lighthouses of gravitational wave astronomy. In *Proceedings, MPA / ESO / MPE / USM Conference on Lighthouses of the Universe: The Most Luminous Celestial Objects and their use for Cosmology: Garching, Munich, Germany, August 6-9, 2001*, 2001. doi: 10.1007/10856495_29.

J. Schwinger. Brownian Motion of a Quantum Oscillator. *Journal of Mathematical Physics*, 2:407–432, May 1961. doi: 10.1063/1.1703727.

D. M. Scolnic et al. The Complete Light-curve Sample of Spectroscopically Confirmed Type Ia Supernovae from Pan-STARRS1 and Cosmological Constraints from The Combined Pantheon Sample. 2017. doi: 10.17909/T95Q4X.

P. F. Scott., R. Saunders, G. Pooley, C. O'Sullivan, A. N. Lasenby, M. Jones, M. P. Hobson, P. J. Duffett-Smith, and J. Baker. Measurements of structure in the cosmic background radiation with the cambridge cosmic anisotropy telescope. *The Astrophysical Journal Letters*, 461(1):L1, 1996.

C. Sealfon, L. Verde, and R. Jimenez. Limits on deviations from the inverse-square law on megaparsec scales. *Phys. Rev. D*, 71:083004, Apr 2005. doi: 10.1103/PhysRevD.71.083004.

U. Seljak. Gravitational lensing effect on cosmic microwave background anisotropies: A Power spectrum approach. *Astrophys. J.*, 463:1, 1996. doi: 10.1086/177218.

U. Seljak and E. Bertschinger. Amplitude of primeval fluctuations from cosmological mass density reconstructions. *Astrophysical Journal*, 427:523–526, June 1994. doi: 10.1086/174163.

U. Seljak and M. Zaldarriaga. A Line of sight integration approach to cosmic microwave background anisotropies. *Astrophysical Journal*, 469:437–444, 1996. doi: 10.1086/177793.

U. Seljak and M. Zaldarriaga. Signature of gravity waves in polarization of the microwave background. *Phys. Rev. Lett.*, 78:2054–2057, 1997. doi: 10.1103/PhysRevLett.78.2054.

E. Semboloni et al. Cosmic shear analysis with cfhtls deep data. *Astron. Astrophys.*, 452:51, 2006. doi: 10.1051/0004-6361:20054479.

H.-J. Seo and D. J. Eisenstein. Probing Dark Energy with Baryonic Acoustic Oscillations from Future Large Galaxy Redshift Surveys. *Astrophys. J.*, 598:720–740, December 2003. doi: 10.1086/379122.

D. L. Shafer and D. Huterer. Chasing the phantom: A closer look at Type Ia supernovae and the dark energy equation of state. *Phys. Rev.*, D89(6):063510, 2014. doi: 10.1103/PhysRevD.89.063510.

T. Shanks, R. Fong, B. J. Boyle, and B. A. Peterson. The spatial clustering of QSOs. *Mon. Not. Roy. Astron. Soc.*, 227:739–748, August 1987. doi: 10.1093/mnras/227.3.739.

E. P. S. Shellard. *Topological Defects in Cosmology*, pages 129–177. Springer Netherlands, Dordrecht, 1995. ISBN 978-94-011-0095-3. doi: 10.1007/978-94-011-0095-3_4.

J. L. Sievers et al. The Atacama Cosmology Telescope: Cosmological parameters from three seasons of data. *JCAP*, 1310:060, 2013. doi: 10.1088/1475-7516/2013/10/060.

J. Silk. Cosmic Black-Body Radiation and Galaxy Formation. *Astrophysical Journal*, 151:459, February 1968. doi: 10.1086/149449.

V. Silveira and I. Waga. Cosmological properties of a class of λ decaying cosmologies. *Phys. Rev. D*, 56:4625–4632, Oct 1997. doi: 10.1103/PhysRevD.56.4625.

A. Silvestri and M. Trodden. Approaches to Understanding Cosmic Acceleration. *Rept. Prog. Phys.*, 72:096901, 2009. doi: 10.1088/0034-4885/72/9/096901.

C. Skordis, D. F. Mota, P. G. Ferreira, and C. Boehm. Large Scale Structure in Bekenstein's theory of relativistic Modified Newtonian Dynamics. *Phys. Rev. Lett.*, 96:011301, 2006. doi: 10.1103/PhysRevLett.96.011301.

S. Smith. The Mass of the Virgo Cluster. *Astrophysical Journal*, 83:23, January 1936. doi: 10.1086/143697.

G. F. Smoot et al. Structure in the COBE differential microwave radiometer first-year maps. *Astrophysical Journal*, 396:L1–L5, September 1992. doi: 10.1086/186504.

Y.-S. Song and K. Koyama. Consistency test of general relativity from large scale structure of the Universe. *JCAP*, 0901:048, 2009. doi: 10.1088/1475-7516/2009/01/048.

Y.-S. Song and W. J. Percival. Reconstructing the history of structure formation using Redshift Distortions. *JCAP*, 0910:004, 2009. doi: 10.1088/1475-7516/2009/10/004.

Y.-S. Song, W. Hu, and I. Sawicki. The Large Scale Structure of f(R) Gravity. *Phys. Rev.*, D75: 044004, 2007. doi: 10.1103/PhysRevD.75.044004.

Y.-S. Song, G.-B. Zhao, D. Bacon, K. Koyama, R. C. Nichol, and L. Pogosian. Complementarity of weak lensing and peculiar velocity measurements in testing general relativity. *Phys. Rev. D*, 84(8):083523, October 2011. doi: 10.1103/PhysRevD.84.083523.

T. P. Sotiriou. f(R) gravity and scalar-tensor theory. *Class. Quant. Grav.*, 23:5117–5128, 2006. doi: 10.1088/0264-9381/23/17/003.

M. E. Soussa and Richard P. Woodard. A Nonlocal metric formulation of MOND. *Class. Quant. Grav.*, 20:2737–2752, 2003. doi: 10.1088/0264-9381/20/13/321.

D. N. Spergel et al. First year Wilkinson Microwave Anisotropy Probe (WMAP) observations: Determination of cosmological parameters. *Astrophys. J. Suppl.*, 148:175–194, 2003. doi: 10.1086/377226.

D. N. Spergel et al. Wilkinson Microwave Anisotropy Probe (WMAP) three year results: implications for cosmology. *Astrophys. J. Suppl.*, 170:377, 2007. doi: 10.1086/513700.

V. Springel, C. S. Frenk, and C. D. M. White. The large-scale structure of the Universe. *Nature*, 440:1137, 2006. doi: 10.1038/nature04805.

A. A. Starobinsky. Dynamics of phase transition in the new inflationary universe scenario and generation of perturbations. *Physics Letters B*, 117(3):175 – 178, 1982. ISSN 0370-2693. doi: https://doi.org/10.1016/0370-2693(82)90541-X.

P. J. Steinhardt. Missing energy and cosmic expansion. *Nature*, 382, 1996. doi: 10.1038/382768a0.

K. S. Stelle. Classical Gravity with Higher Derivatives. *Gen. Rel. Grav.*, 9:353–371, 1978. doi: 10.1007/BF00760427.

N. Straumann. *General relativity and relativistic astrophysics*. Texts and monographs in physics. Springer, Berlin, 1984. German version available : Allgemeine Relativittstheorie und relativistische Astrophysik - Berlin, Springer, 1981.

M. A. Strauss and J. A. Willick. The Density and peculiar velocity fields of nearby galaxies. *Phys. Rept.*, 261:271–431, 1995. doi: 10.1016/0370-1573(95)00013-7.

M. A. Strauss, M. Davis, A. Yahil, and J. P. Huchra. A redshift survey of IRAS galaxies. I - Sample selection. *Astrophysical Journal*, 361:49–62, September 1990. doi: 10.1086/169166.

E. Stueckelberg. Die wechselwirkungskrfte in der elektrodynamik und in der feldtheorie der krfte. *Helv. Phys. Acta.*, 11, 1938.

R. A. Sunyaev and Y. B. Zeldovich. Small-Scale Fluctuations of Relic Radiation. *Astrophysics and Space Science*, 7:3–19, April 1970. doi: 10.1007/BF00653471.

R. A. Sunyaev and Y. B. Zeldovich. The Observations of Relic Radiation as a Test of the Nature of X-Ray Radiation from the Clusters of Galaxies. *Comments on Astrophysics and Space Physics*, 4:173, November 1972.

N. Suzuki et al. The Hubble Space Telescope Cluster Supernova Survey. V. Improving the Dark-energy Constraints above z $>$ 1 and Building an Early-type-hosted Supernova Sample. *Astrophys. J.*, 746:85, February 2012. doi: 10.1088/0004-637X/746/1/85.

G. 't Hooft. Naturalness, chiral symmetry, and spontaneous chiral symmetry breaking. *NATO Sci. Ser. B*, 59:135–157, 1980. doi: 10.1007/978-1-4684-7571-5_9.

H. Tadros et al. Spherical harmonic analysis of the pscz galaxy catalogue: redshift distortions and the real-space power spectrum. *Mon. Not. Roy. Astron. Soc.*, 305:527–546, 1999. doi: 10.1046/j.1365-8711.1999.02409.x.

Y. D. Takahashi et al. Characterization of the BICEP Telescope for High-precision Cosmic Microwave Background Polarimetry. *Astrophys. J.*, 711:1141–1156, March 2010. doi: 10.1088/0004-637X/711/2/1141.

N. Tamanini, C. Caprini, E. Barausse, A. Sesana, A. Klein, and A. Petiteau. Science with the space-based interferometer eLISA. III: Probing the expansion of the Universe using gravitational wave standard sirens. *JCAP*, 1604:002, 2016. doi: 10.1088/1475-7516/2016/04/002.

S. R. Taylor and J. R. Gair. Cosmology with the lights off: standard sirens in the Einstein Telescope era. *Phys. Rev.*, D86:023502, 2012. doi: 10.1103/PhysRevD.86.023502.

M. Tegmark, D. J. Eisenstein, W. Hu, and R. G. Kron. Cosmic complementarity: Probing the acceleration of the universe. 1998.

M. Tegmark et al. Cosmological parameters from SDSS and WMAP. *Phys. Rev.*, D69:103501, 2004a. doi: 10.1103/PhysRevD.69.103501.

M. Tegmark et al. The 3-D power spectrum of galaxies from the SDSS. *Astrophys. J.*, 606: 702–740, 2004b. doi: 10.1086/382125.

J. Tonry and M. Davis. A survey of galaxy redshifts. I - Data reduction techniques. *Astronomoical Journal*, 84:1511–1525, October 1979. doi: 10.1086/112569.

R. Trotta. Applications of Bayesian model selection to cosmological parameters. *MNRAS*, 378: 72–82, 2007. doi: 10.1111/j.1365-2966.2007.11738.x.

R. Trotta. Bayes in the sky: Bayesian inference and model selection in cosmology. *Contemp. Phys.*, 49:71–104, 2008. doi: 10.1080/00107510802066753.

M. A. Troxel et al. Survey geometry and the internal consistency of recent cosmic shear measurements. *Submitted to: Mon. Not. Roy. Astron. Soc.*, 2018.

N. C. Tsamis and R. P. Woodard. The Quantum gravitational back reaction on inflation. *Annals Phys.*, 253:1–54, 1997. doi: 10.1006/aphy.1997.5613.

N. C. Tsamis and R. P. Woodard. A Caveat on Building Nonlocal Models of Cosmology. *JCAP*, 1409:008, 2014. doi: 10.1088/1475-7516/2014/09/008.

S. Tsujikawa. Modified gravity models of dark energy. *Lect. Notes Phys.*, 800:99–145, 2010. doi: 10.1007/978-3-642-10598-2_3.

S. Tsujikawa. Quintessence: A Review. *Class. Quant. Grav.*, 30:214003, 2013. doi: 10.1088/0264-9381/30/21/214003.

E. L. Turner. Gravitational lensing limits on the cosmological constant in a flat universe. *Astrophysical Journal*, 365:L43–L46, December 1990. doi: 10.1086/185884.

M. S. Turner and M. J. White. CDM models with a smooth component. *Phys. Rev.*, D56(8): R4439, 1997. doi: 10.1103/PhysRevD.56.R4439.

M. S. Turner, M. J. White, and J. E. Lidsey. Tensor perturbations in inflationary models as a probe of cosmology. *Phys. Rev.*, D48:4613–4622, 1993. doi: 10.1103/PhysRevD.48.4613.

H. Ueda, M. Itoh, and Y. Suto. Clusters and groups of galaxies as cosmological probes. *Astrophysical Journal*, 408:3–16, May 1993. doi: 10.1086/172564.

URL. `https://github.com/dirian/class_public/tree/nonlocal`.

J. M. Uson and D. T. Wilkinson. Improved limits on small-scale anisotropy in cosmic microwave background. *Nature*, 312:427–429, November 1984. doi: 10.1038/312427a0.

J.-P. Uzan. Variation of the constants in the late and early universe. *AIP Conf. Proc.*, 736: 3–20, 2005. doi: 10.1063/1.1835171. [,3(2004)].

J.-P. Uzan. The acceleration of the universe and the physics behind it. *Gen. Rel. Grav.*, 39: 307–342, 2007. doi: 10.1007/s10714-006-0385-z.

J.-P. Uzan. Dark energy, gravitation and the Copernican principle. 2009.

S. Vagnozzi, E. Giusarma, O. Mena, K. Freese, M. Gerbino, S. Ho, and M. Lattanzi. Unveiling ν secrets with cosmological data: neutrino masses and mass hierarchy. 2017.

S. Vagnozzi, S. Dhawan, M. Gerbino, K. Freese, A. Goobar, and O. Mena. Constraints on the sum of the neutrino masses in dynamical dark energy models with $w(z) \geq -1$ are tighter than those obtained in ΛCDM. 2018.

A.I. Vainshtein. To the problem of nonvanishing gravitation mass. *Physics Letters B*, 39(3):393 – 394, 1972. ISSN 0370-2693. doi: https://doi.org/10.1016/0370-2693(72)90147-5.

H. van Dam and M. Veltman. *Nucl. Phys. B*, 22:397, 1970.

A. van Engelen et al. A Measurement of Gravitational Lensing of the Microwave Background Using South Pole Telescope Data. *Atrophys. J.*, 756:142, September 2012. doi: 10.1088/0004-637X/756/2/142.

V. Vardanyan, Y. Akrami, L. Amendola, and A. Silvestri. On nonlocally interacting metrics, and a simple proposal for cosmic acceleration. *JCAP*, 1803(03):048, 2018. doi: 10.1088/1475-7516/2018/03/048.

D. V. Vassilevich. Heat kernel expansion: User's manual. *Phys. Rept.*, 388:279–360, 2003. doi: 10.1016/j.physrep.2003.09.002.

L. Verde, Z. Haiman, and D. N. Spergel. Are Clusters Standard Candles? Using Galaxy Cluster Scaling Relations for Cosmology. In N. Metcalfe and T. Shanks, editors, *A New Era in Cosmology*, volume 283 of *Astronomical Society of the Pacific Conference Series*, page 214, 2002.

L. Verde et al. First year Wilkinson Microwave Anisotropy Probe (WMAP) observations: Parameter estimation methodology. *Astrophys. J. Suppl.*, 148:195, 2003. doi: 10.1086/377335.

J. D. Vergados, H. Ejiri, and F. Simkovic. Neutrinoless double beta decay and neutrino mass. *Int. J. Mod. Phys.*, E25(11):1630007, 2016. doi: 10.1142/S0218301316300071.

H. Vermeil. *Nachr. Ges. Wiss. Gottingen*, page 334, 1917.

M. S. Vogeley, C. Park, M. J. Geller, and J. P. Huchra. Large-scale clustering of galaxies in the CfA Redshift Survey. *Astrophysical Journal*, 391:L5–L8, May 1992. doi: 10.1086/186385.

E.-J. Wagenmakers, T. Lodewyckx, H. Kuriyal, and Grasman R. Bayesian hypothesis testing for psychologists: a tutorial on the Savage-Dickey method. *Cogn, Psychol.*, 60(3):158?189, 2010. doi: doi:10.1016/j.cogpsych.2009.12.001.

A. G. Walker. On milne's theory of world-structure. *Proceedings of the London Mathematical Society*, s2-42(1):90–127, 1937. doi: 10.1112/plms/s2-42.1.90.

L.-M. Wang, R. R. Caldwell, J. P. Ostriker, and P. J. Steinhardt. Cosmic concordance and quintessence. *Astrophys. J.*, 530:17–35, 2000. doi: 10.1086/308331.

D. H. Weinberg, M. J. Mortonson, D. J. Eisenstein, C. Hirata, A. G. Riess, and E. Rozo. Observational probes of cosmic acceleration. *Phys. Rep.*, 530:87–255, September 2013. doi: 10.1016/j.physrep.2013.05.001.

S. Weinberg. *Gravitation and Cosmology: Principles and Applications of the General Theory of Relativity.* Wiley, New York, NY, 1972.

S. Weinberg. A new light boson? *Phys. Rev. Lett.*, 40:223–226, Jan 1978. doi: 10.1103/PhysRevLett.40.223.

S. Weinberg. *in General Relativity: An Einstein Centenary Survey*, pages 790–831, 1980.

S. Weinberg. The cosmological constant problem. *Rev. Mod. Phys.*, 61:1–23, Jan 1989. doi: 10.1103/RevModPhys.61.1.

S. Weinberg. The Cosmological constant problems. In *Sources and detection of dark matter and dark energy in the universe. Proceedings, 4th International Symposium, DM 2000, Marina del Rey, USA, February 23-25, 2000*, pages 18–26, 2000.

S. Weinberg. Damping of tensor modes in cosmology. *Phys. Rev.*, D69:023503, 2004. doi: 10.1103/PhysRevD.69.023503.

N. Weiss. Possible origins of a small, nonzero cosmological constant. *Physics Letters B*, 197, 1987. doi: 10.1016/0370-2693(87)90338-8.

C. Wetterich. Cosmology and the fate of dilatation symmetry. *Nuclear Physics B*, 302:668–696, June 1988. doi: 10.1016/0550-3213(88)90193-9.

C. Wetterich. Effective nonlocal Euclidean gravity. *Gen. Rel. Grav.*, 30:159–172, 1998. doi: 10.1023/A:1018837319976.

C. Wetterich. Growing neutrinos and cosmological selection. *Phys. Lett.*, B655:201–208, 2007. doi: 10.1016/j.physletb.2007.08.060.

C. Wetterich. Graviton fluctuations erase the cosmological constant. *Phys. Lett.*, B773:6–19, 2017. doi: 10.1016/j.physletb.2017.08.002.

H. Weyl. *Space, Time, Matter.* Dover Books on Advanced Mathematics. Dover, 1922.

M. J. White. Complementary measures of the mass density and cosmological constant. *Astrophys. J.*, 506:495, 1998. doi: 10.1086/306278.

M. J. White, D. Scott, and J. Silk. Anisotropies in the Cosmic Microwave Background. *Annu. Rev. Astron. Astrophys.*, 32:319–370, 1994. doi: 10.1146/annurev.astro.32.1.319.

S. D. M. White, C. S. Frenk, and M. Davis. Clustering in a neutrino-dominated universe. *Astrophysical Journal*, 274:L1–L5, November 1983. doi: 10.1086/184139.

S. D. M. White, M. Davis, G. Efstathiou, and C. S. Frenk. Galaxy distribution in a cold dark matter universe. *Nature*, 330:451–453, December 1987a. doi: 10.1038/330451a0.

S. D. M. White, C. S. Frenk, M. Davis, and G. Efstathiou. Clusters, filaments, and voids in a universe dominated by cold dark matter. *Astrophysical Journal*, 313:505–516, February 1987b. doi: 10.1086/164990.

S. D. M. White, J. F. Navarro, A. E. Evrard, and C. S. Frenk. The Baryon content of galaxy clusters: A Challenge to cosmological orthodoxy. *Nature*, 366:429–433, 1993. doi: 10.1038/366429a0.

R. N. Whitehurst and M. S. Roberts. High-Velocity Neutral Hydrogen in the Central Region of the Andromeda Galaxy. *Astrophysical Journal*, 175:347, July 1972. doi: 10.1086/151562.

F. Wilczek. Problem of strong p and t invariance in the presence of instantons. *Phys. Rev. Lett.*, 40:279–282, Jan 1978. doi: 10.1103/PhysRevLett.40.279.

C. M. Will. The Confrontation between General Relativity and Experiment. *Living Rev. Rel.*, 17:4, 2014. doi: 10.12942/lrr-2014-4.

J. G. Williams, S. G. Turyshev, and D. H. Boggs. Progress in lunar laser ranging tests of relativistic gravity. *Phys. Rev. Lett.*, 93:261101, 2004. doi: 10.1103/PhysRevLett.93.261101.

Wolfram. Mathematica 8.0, 2010.

W. Michael Wood-Vasey et al. Observational Constraints on the Nature of the Dark Energy: First Cosmological Results from the ESSENCE Supernova Survey. *Astrophys. J.*, 666:694–715, 2007. doi: 10.1086/518642.

E. L. Wright et al. Interpretation of the cosmic microwave background radiation anisotropy detected by the COBE Differential Microwave Radiometer. *Astrophysical Journal*, 396:L13–L18, September 1992. doi: 10.1086/186506.

S. Yahya, P. Bull, M. G. Santos, M. Silva, R. Maartens, P. Okouma, and B. Bassett. Cosmological performance of SKA H I galaxy surveys. *Monthly Notices of the Royal Astronomical Society*, 450:2251–2260, July 2015. doi: 10.1093/mnras/stv695.

J. Yoo. Complete Treatment of Galaxy Two-Point Statistics: Gravitational Lensing Effects and Redshift-Space Distortions. *Phys. Rev.*, D79:023517, 2009. doi: 10.1103/PhysRevD.79.023517.

V. Zahkarov. Linearized gravitation theory and the graviton mass. *ZhETF Pis. Red.*, 12: 447–449, 1970.

M. Zaldarriaga. Polarization of the microwave background in reionized models. *Phys. Rev.*, D55:1822–1829, 1997. doi: 10.1103/PhysRevD.55.1822.

M. Zaldarriaga and U. Seljak. An all sky analysis of polarization in the microwave background. *Phys. Rev.*, D55:1830–1840, 1997. doi: 10.1103/PhysRevD.55.1830.

M. Zaldarriaga and U. Seljak. Gravitational lensing effect on cosmic microwave background polarization. *Phys. Rev.*, D58:023003, 1998. doi: 10.1103/PhysRevD.58.023003.

M. Zaldarriaga and U. Seljak. Reconstructing projected matter density from cosmic microwave background. *Phys. Rev.*, D59:123507, 1999. doi: 10.1103/PhysRevD.59.123507.

M. Zaldarriaga, D. N. Spergel, and U. Seljak. Microwave background constraints on cosmological parameters. *Astrophys. J.*, 488:1–13, 1997. doi: 10.1086/304692.

I. B. Zeldovich, J. Einasto, and S. F. Shandarin. Giant voids in the universe. *Nature*, 300: 407–413, December 1982. doi: 10.1038/300407a0.

P. Zhang, M. Liguori, R. Bean, and S. Dodelson. Probing Gravity at Cosmological Scales by Measurements which Test the Relationship between Gravitational Lensing and Matter Overdensity. *Phys. Rev. Lett.*, 99:141302, 2007. doi: 10.1103/PhysRevLett.99.141302.

W. Zhao, C. Van Den Broeck, D. Baskaran, and T. G. F. Li. Determination of Dark Energy by the Einstein Telescope: Comparing with CMB, BAO and SNIa Observations. *Phys. Rev.*, D83:023005, 2011. doi: 10.1103/PhysRevD.83.023005.

J. Zinn-Justin. Quantum Field Theory and Critical Phenomena, 2002. International Series of Monographs on Physics 113, 1054 pp. (2002), Fourth Edition.

I. Zlatev, L. Wang, and P. J. Steinhardt. Quintessence, cosmic coincidence, and the cosmological constant. *Phys. Rev. Lett.*, 82:896–899, Feb 1999. doi: 10.1103/PhysRevLett.82.896.

F. Zwicky. On the redshift of spectral lines through interstellar space. *Proceedings of the National Academy of Sciences*, 15(10):773–779, 1929. ISSN 0027-8424. doi: 10.1073/pnas.15.10.773.

F. Zwicky. Die Rotverschiebung von extragalaktischen Nebeln. *Helvetica Physica Acta*, 6: 110–127, 1933.

F. Zwicky. On the Masses of Nebulae and of Clusters of Nebulae. *Astrophysical Journal*, 86: 217, October 1937. doi: 10.1086/143864.